Electronic Dynamics of Monomers, Dimers and Oligomers of Purine Nucleobases Studied by Femtosecond Time-Resolved Spectroscopy

Dissertation
zur Erlangung des Doktorgrades
Dr. rer. nat.
der Mathematisch-Naturwissenschaftlichen Fakultät
der Christian-Albrechts-Universität zu Kiel

vorgelegt von
Uta Corinna Stange

Institut für Physikalische Chemie,
Christian-Albrechts-Universität zu Kiel

Oktober 2018

Erster Gutachter: Prof. Dr. Friedrich Temps

Zweiter Gutachter: Prof. Dr. Gernot Friedrichs

Tag der mündlichen Prüfung: 21.11.2018

Erklärung

Hiermit erkläre ich, dass die vorliegende Abhandlung – abgesehen von der Beratung durch meinen Betreuer Herrn Prof. Dr. Friedrich Temps – nach Inhalt und Form meine eigene Arbeit ist und dass keine anderen als die angegebenen Quellen genutzt wurden. Diese Arbeit hat weder in Auszügen noch in ganzer Form einer anderen Stelle im Rahmen eines Promotionsverfahrens vorgelegen. Sie wurde in ihrer Gesamtheit nicht veröffentlicht und auch nicht zur Veröffentlichung eingereicht. Teile dieser Arbeit wurden in fachwissenschaftlichen Zeitschriften veröffentlicht. Dies bezieht sich auf das folgende Kapitel:

Kapitel 3
U. C. Stange, F. Temps, 'Ultrafast electronic deactivation of UV-excited adenine and its ribo- and deoxyribonucleosides and -nucleotides: A comparative study', *Chem. Phys.* **2018**, doi: 10.1016/j.chemphys.2018.08.031

Die Arbeit ist unter Einhaltung der Regeln guter wissenschaftlicher Praxis der Deutschen Forschungsgemeinschaft entstanden. Ein akademischer Grad wurde mir nicht entzogen.

Lörrach, 28. November 2018

Uta Corinna Stange

Abstract

The electronic deactivation dynamics of selected mono-, di- and oligonucleotides of adenine and guanine were investigated by means of aqueous-phase femtosecond time-resolved transient electronic absorption and fluorescence spectroscopy in order to assign deactivation pathways and to experimentally characterize molecular deactivation mechanisms.

The investigation of the single purine nucleobases 9H-adenine, 7H-adenine and guanine yielded diverging electronic lifetimes, although the deactivation processes is thought to take place on the $\pi\pi^*$ L_a excited state for all samples and also thought to be facilitated by similar puckering deformations. The deactivation pathway of 9H-adenine was concluded to be barrierless based on the observed ultrafast and temperature-independent excited-state lifetime. The mechanism most probably involves a C^2-puckering with out-of-plane motion of the C^2–H bond as predicted by quantum chemical studies and consistent with the absence of a kinetic isotope effect in D_2O. Virtually identical excited-state dynamics were observed for the adenine nucleosides and nucleotides. For the decay dynamics of 7H-adenine, temperature-dependent measurements revealed a thermal activation process in the excited state. This was assigned to a crucial potential energy barrier along the relaxation pathway. The electronic deactivation of deoxyguanosine monophosphate was also found to be impeded by a small potential energy barrier that may be induced by the out-of-plane motion of the amino group placed at the C^2-position in guanine.

The investigation of the stacked di- and tri- and tetranucleotides of adenine yielded drastically increased overall electronic lifetimes compared to the monomer. The temporal components span four orders of magnitude, indicating a stepwise evolution of the excited-state character from excitons to excimer-like states. An intermediate excimer was proposed to be directly populated after relaxation within the exciton stack and to decay to a stabilized excimer. Both excimer states were found to lie at similar energy levels and to show pronounced barriers for the decay. Measurements in D_2O suggest that the molecular mechanism for internal conversion to the ground state involves at least one of the amino groups located at the C^6-position of the adenine units. In the longer oligonucleotides, the increased stacking interaction seemed to slightly destabilize excimer formation and to lower the potential energy barrier for internal conversion. An increased lifetime was also seen for the guanine dinucleotide in comparison with its monomer. In analogy to the other results, this was assigned to formation of an excimer-like state.

Kurzzusammenfassung

In dieser Dissertation wurde die elektronische Desaktivierungsdynamik ausgewählter Mono-, Di- und Oligonukleotide von Adenin und Guanin mittels Femtosekunden-zeitaufgelöster elektronischer Absorptions- und Fluoreszenzspektroskopie in wässriger Lösung untersucht, um Desaktivierungspfade zuzuordnen und um die molekularen Desaktivierungsmechanismen experimentell zu charakterisieren.

Die Untersuchung der einzelnen Purin-Nukleobasen 9H-Adenin, 7H-Adenin und Guanin ergab unterschiedliche elektronische Lebensdauern, obwohl angenommen wird, dass der Desaktivierungsprozess in allen Proben auf dem $\pi\pi^*$ L_a-angeregten Zustand erfolgt und dabei eine ähnliche Ringfaltungsstruktur ausgebildet wird. Die Desaktivierung von 9H-Adenin wurde anhand der Beobachtung einer ultraschnellen und temperaturunabhängigen Lebensdauer einem barrierelosen Pfad zugeordnet. Für den Mechanismus kommt eine an der C^2-Position zentrierte Ringfaltung und die Bewegung der C^2–H Bindung aus der Ebene heraus in Frage, wie sie durch quanten-chemische Studien beschrieben wurde. Das Ausbleiben eines kinetischen Isotopeneffekts in D_2O unterstützt diese Interpretation. Die Adeninnukleoside und -nukleotide zeigten eine praktisch identische elektronische Dynamik. Die temperaturabhängige Desaktivierungsdynamik von 7H-Adenin offenbarte einen thermischen Aktivierungsprozess im angeregten Zustand, welcher einer maßgeblichen Potentialbarriere auf dem Desaktivierungspfad zugeordnet wurde. Es wurde beobachtet, dass auch die elektronische Desaktivierung des Desoxyguanosinmonophosphats durch eine Potentialbarriere gehemmt ist. Diese wird vermutlich durch eine Bewegung der Aminogruppe aus der Ebene heraus hervorgerufen, die im Guanin an der C^2-Position sitzt.

Die Untersuchungen der gestapelten Di-, Tri- und Tetranukleotide des Adenin zeigten im Vergleich zum Monomer drastisch verlängerte elektronische Gesamtlebensdauern. Die einzelnen Zeitkomponenten erstrecken sich über vier Größenordnungen und weisen auf eine schrittweise Änderung des Charakters des angeregten Zustands vom Exziton zu Excimer-ähnlichen Zuständen hin. Es wird angenommen, dass eine Excimerzwischenstufe direkt nach der Relaxation innerhalb der Exzitonenleiter erreicht wird und anschließend zu einem stabilen Excimer-Zustand relaxiert. Den experimentellen Daten zufolge liegen die Excimer-Zustände auf ähnlichen Energieniveaus und zeigen deutliche Barrieren für die Desaktivierung auf. Messungen in D_2O legen nahe, dass der Desaktivierungsmechanismus mindestens eine der Aminogruppen an den C^6-Positionen der Adeninuntereinheiten involviert. Die stärkere Stapelwechselwirkung in den längeren Oligonukleotiden scheint die Excimerausbildung leicht zu destabilisieren und die Potentialbarriere für die Desaktivierung zu verringern. Eine verlängerte Lebensdauer wurde auch für das Guanosindinukleotid im Vergleich mit seinem Monomer beobachtet. Auch dies wurde einer Excimerausbildung zugeordnet.

TO THE UNIVERSE

Contents

1 Introduction **1**
1.1 Structural and Electronic Properties of DNA . . . 3
1.1.1 Molecular Structure of DNA . . . 3
1.1.2 Electronic Deactivation via Conical Intersections . . . 5
1.2 Structural and Electronic Properties of Single Purine Nucleobases . . . 9
1.2.1 Adenine . . . 9
1.2.2 Guanine . . . 12
1.3 Structural and Electronic Properties of Stacked Purine Nucleobases . . . 14
1.3.1 π-Stacking Interactions . . . 15
1.3.2 Delocalization of Excitation Energy . . . 16
1.3.3 Electronic Deactivation Mechanisms . . . 25
1.4 Aim and Content of this Thesis . . . 26
References . . . 28

2 Experimental Methods **45**
2.1 Setup and Data Acquisition . . . 45
2.1.1 Transient Electronic Absorption Spectrometer . . . 45
2.1.2 Wire-Guided Liquid Sample Film Device . . . 50
2.1.3 Transient Fluorescence Spectrometer . . . 53
2.2 Data Analysis . . . 54
2.2.1 Data Handling . . . 54
2.2.2 Exponential Modeling . . . 54
2.2.3 Band Fit Analysis . . . 55
2.2.4 Singular Value Decomposition . . . 55
2.2.5 Arrhenius Analysis . . . 56
2.3 Other Devices and Materials . . . 57
References . . . 57

3 Electronic Deactivation of Adenine, Adenosine and Adenosine Monophosphate **61**
3.1 Introduction . . . 62
3.2 Experimental Section . . . 65
3.3 Results . . . 66
3.3.1 Excited-State Dynamics . . . 66
3.3.2 Ground-State Recovery Dynamics . . . 72
3.4 Discussion . . . 73
3.4.1 Comparison of the Results . . . 74
3.4.2 Time Constants and Electronic Deactivation Mechanism . . . 74

3.5 Conclusions . . . 80
References and Notes . . . 81

4 Temperature-Dependent Electronic Deactivation of 7H-Adenine 89
4.1 Introduction . . . 90
4.2 Experimental Methods . . . 92
4.3 Results and Discussion . . . 92
4.3.1 Experimental Results . . . 92
4.3.2 Electronic Deactivation Mechanisms . . . 94
4.3.3 Master Equation Modeling . . . 96
4.4 Conclusion . . . 101
References . . . 102
Additional Information . . . 107
4.A Additional Experimental Details . . . 107
4.B Additional Experimental Data . . . 107
4.C Additional Master Equation Modeling Details and Results . . . 109

5 Electronic Deactivation Dynamics of the Adenine Dinucleotide 113
5.1 Introduction and Motivation . . . 114
5.2 Experimental Details . . . 117
5.3 Results in H_2O at Room Temperature . . . 119
5.3.1 Transient Electronic Absorption . . . 119
5.4 Results in H_2O at Lowered Temperature . . . 125
5.4.1 Static Absorption and Static Fluorescence . . . 125
5.4.2 Transient Electronic Absorption . . . 126
5.5 Results in D_2O at Room Temperature . . . 130
5.5.1 Transient Electronic Absorption . . . 130
5.6 Discussion . . . 133
5.6.1 Comparison to dAMP . . . 134
5.6.2 Effect of Temperature . . . 138
5.6.3 Effect of D_2O . . . 140
5.6.4 Electronic Deactivation Mechanisms . . . 141
5.7 Conclusion . . . 144
References . . . 145
Additional Information . . . 153
5.B Comparison with Previous Results for d(ApA) in H_2O . . . 153
5.C Additional Results for dAMP in H_2O . . . 156
5.D Additional Results for dAMP in D_2O . . . 164
5.E Electronic Deactivation Mechanism of dAMP . . . 167

6 Electronic Deactivation Dynamics of the Adenine Tri- and Tetranucleotide 173
6.1 Introduction and Motivation . . . 173
6.2 Experimental Details . . . 175

6.3 Results . . . 176
6.3.1 Static Absorption and Static Fluorescence . . . 176
6.3.2 Transient Electronic Absorption . . . 177
6.4 Discussion . . . 184
6.5 Conclusion . . . 187
References . . . 187

7 Electronic Deactivation Dynamics of the Guanine Dinucleotide and dGMP 191
7.1 Introduction and Motivation . . . 192
7.2 Experimental Details . . . 193
7.3 Results . . . 194
7.3.1 Static Absorption and Static Fluorescence . . . 194
7.3.2 Transient Electronic Absorption of d(GpG) in comparison to dGMP 196
7.3.3 Transient Electronic Absorption of dGMP at $T = 278$ K . . . 200
7.4 Discussion . . . 202
7.4.1 Electronic Decay Dynamics of d(GpG) . . . 202
7.4.2 Electronic Decay Dynamics of dGMP . . . 203
7.5 Conclusion . . . 205
References . . . 206

8 Summary and Outlook 213
8.1 Electronic Deactivation Dynamics of Single Purine Nucleobases . . . 213
8.1.1 9H-Adenine . . . 213
8.1.2 7H-Adenine . . . 214
8.1.3 Guanine . . . 214
8.2 Electronic Deactivation Dynamics of Stacked Purine Nucleobases . . . 215
8.2.1 Adenine Dinucleotide . . . 215
8.2.2 Adenine Tri- and Tetranucleotide . . . 216
8.2.3 Guanine Dinucleotide . . . 216
8.3 Concluding Remarks . . . 216
8.4 Ongoing Studies . . . 217

List of Figures 221

List of Tables 225

1 Introduction

The structural stability of deoxyribonucleic acid (DNA) is of utmost importance for life on Earth because it serves as the carrier of genetic information for every organism. Its exceptional double helical structure is stabilized by hydrogen bonding between the constituting nucleobases of the complementing strands and by π-stacking interactions within a strand. The entwined strands are compact and firmly bound, yet flexible enough to adapt to different environmental effects without losing their integrity.

The high stability of the DNA macromolecule finds an additional technical application in a promising data storage method.[1] When one bit is stored per nucleobase, an extremely high data density can be achieved. This way, the human body already stores $150 \cdot 10^{21}$ Bytes of data within the DNA of 10^{14} cells. Recording and reading of data stored in DNA is performed by sequencing and synthesis with up to 99 % coupling efficiency. So far, however, DNA data storage is only useful for long-time storage and not for high data throughput. Another use of the stable DNA structure is the famous DNA origami.[2] Targeted superordinate 3D-structures can be built up by self-assembling DNA double strands of matched sequences. This way, nanostructures of arbitrary shape can be achieved that may act as molds for other materials, as substrates for site-specific binding of ligands, or as vaults for carrying and releasing reactive substances.[3]

The strong interactions that stabilize the helical DNA structure rely on the close vicinity of aromatic molecules. Within the single strands, overlap of the electron densities of the moieties enhances the interactions but makes them prone to reactions. Photoproduct formation of nucleobases is known to occur under UV-light irradiation. Irradiation products are cyclobutane pyrimidine dimers (CPD) and 6,4-photoproducts involving adjacent thymine bases of the same strand. Other minor photoreactions are dimer formation of adenine with another adenine or a thymine molecule, the methylation of cytosine, and the generation of 8-oxo-7,8-dihydroguanine (8-oxo-G).[4,5]

In complex organisms, DNA is protected from light by the natural sunscreen melanin and is kept functional by intracellular repair mechanisms reducing the risk of

light-induced mutagenesis and skin cancer. If photolesion occurs, nucleotide excision repair enzymes use the undamaged strand as a template. The discovery of the mechanism of this crucial process was recently awarded with the Nobel prize in chemistry.[6] Under certain circumstances, photolesions can also be fixed by self-repair mechanisms. Most intriguingly, the oxidation product 8-oxo-G is able to repair CPDs by excited-state proton-coupled electron transfer.[7–9] Also, a charge transfer state, as found for the stacked adenine–guanine exciplex, can act as an electron donor for CPD repair.[10]

However, the enzymatic and self-repair mechanisms would be completely overburdened without the intrinsic UV stability of the DNA molecule. Ultrafast radiationless transitions to the ground state of the intact molecule compete with the photo-induced cycloaddition within the first picosecond and thereby inhibit photodegradation. The ultrashort excited-state lifetime of DNA is attributed to its building blocks, the canonical nucleobases. The photostability presumably is a consequence of evolution under high UV exposition.

Studying the electronic dynamics of DNA building blocks is indispensable because they showcase how photophysics successfully competes with photochemistry. In this context, it is remarkable that the molecular interactions of the nucleobases, namely base stacking and pairing, both drastically increase the electronic lifetimes of DNA building blocks.[11] Base stacking and its excited-state effects influence the structural stability and recognition of DNA strands,[12–14] e. g. by a recently found charge-transfer mediated base-pairing mechanism involving two pairs of stacked nucleobases.[15] In stacked bases, the excitation energy is trapped in so-called excimers, but the molecular mechanism for the impeded electronic deactivation is so far unclear. The decay mechanism in base pairs of guanine and cytosine is an electron-driven proton transfer (EDPT) that was first directly observed in a collaboration between Kiel and Bristol.[16] As can be inferred, the structural and photochemical stability of the DNA molecule is directly connected to its electronic properties.

In this Thesis, the electronic deactivation processes of DNA building blocks are probed by means of time-resolved spectroscopy. By careful analysis, major relaxation pathways are identified that lead the molecule back to the ground state. This introduction gives an overview of the unique structural and electronic properties of the DNA molecule. In this context, the concept of conical intersections of potential energy hypersurfaces which facilitate ultrafast internal conversion processes is explained and serves as a theoretical background for the following literature survey on the electronic deactivation dynamics of single purine nucleobases. Special attention

is paid to adenine and guanine, because they show the shortest excited-state lifetimes and the strongest stacking interactions. The third part of the introduction presents the characteristics of stacking-induced effects and the current state of research on the electronic deactivation mechanisms of stacked nucleobases.

1.1 Structural and Electronic Properties of DNA

1.1.1 Molecular Structure of DNA

The molecular structure of DNA is a combination of two complementary polynucleotide strands forming a double helix. The strands are made up of a deoxyribose phosphate backbone with nucleobases attached to each sugar moiety. The single building blocks are called nucleosides for the nucleobase and the sugar, and nucleotides including the phosphate group. The nucleotides are periodically connected by the phosphates at the 5'- and the 3'-position of the deoxyribose. An exemplary DNA double strand is shown in Fig. 1.1 together with the canonical DNA bases adenine (Ade), guanine (Gua), cytosine (Cyt) and thymine (Thy). The nucleobases are purine and pyrimidine derivatives, i. e. planar and heteroaromatic molecules. The specific sequence of the bases encodes the genetic information.

Due to the polar sugar-phosphate backbone and hydrophobic effects of the aromatics, the nucleobases are oriented into the middle of the helix, where they form hydrogen bonds between the strands according to the Watson–Crick pattern, i. e. base pairs of Ade–Thy and Gua–Cyt form.[18,19] The helical structure of DNA is stabilized by the sequence of the polynucleotides,[20,21] the base pairing,[18,19] and the stacking interactions between the nucleobases.[12–14]

The structure shown is that of a natural right-handed B-DNA. The nucleobases are stacked with a distance of 3.4 Å and with a twist angle of 36° between the bases. One full turn of the helix is completed after 10.5 bases which corresponds to a length of 34 Å. The diameter of the double helix is 10 Å. The structure shows minor and major grooves which, under physiological conditions, are filled with water molecules. Counterions are situated close to the deprotonated phosphate groups. The three-dimensional structure of DNA is mostly determined by environmental effects. The compact, right-handed A-DNA, for example, can be achieved by dehydration, and the left-handed Z-DNA forms at high salt concentrations.

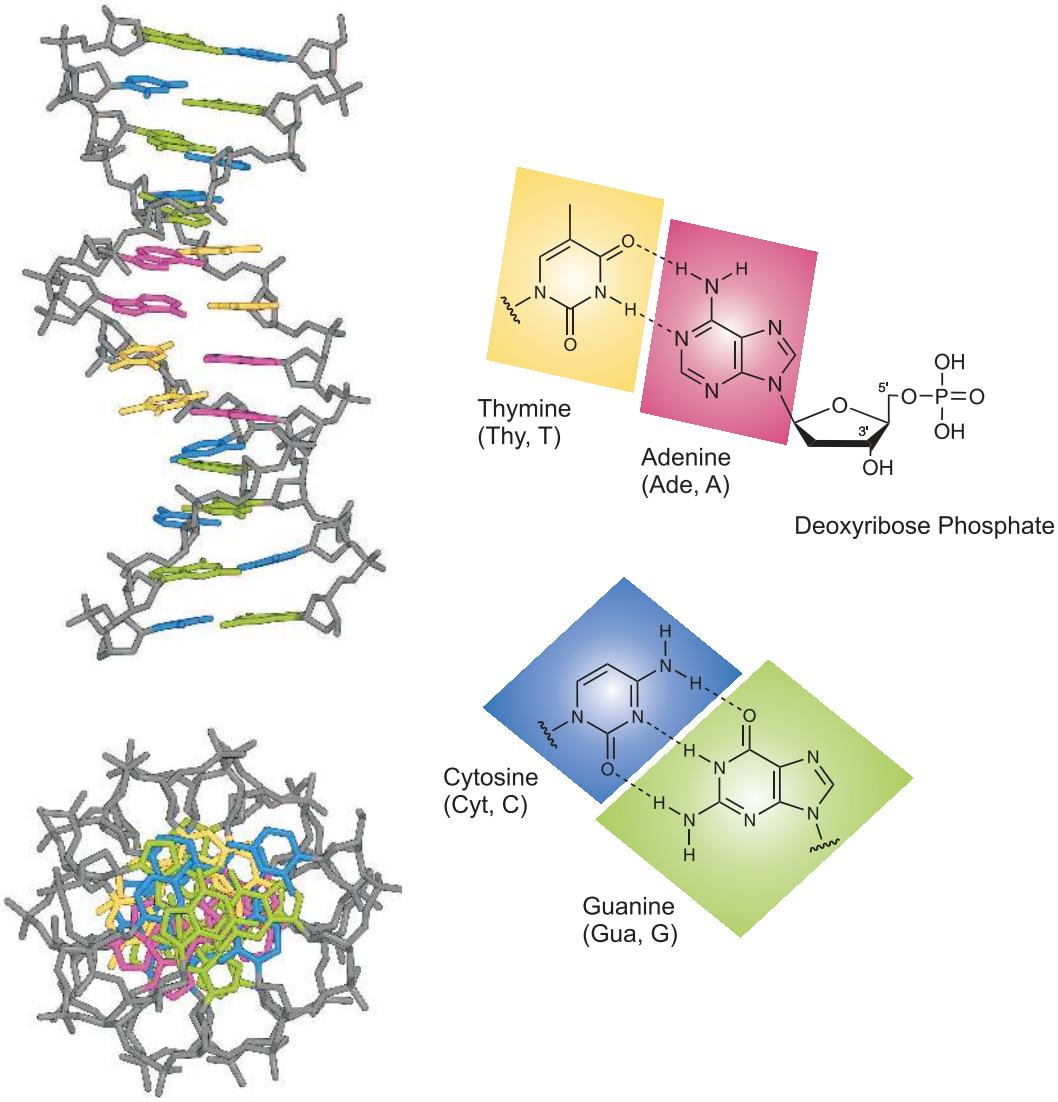

Figure 1.1: Molecular structure of DNA and Watson–Crick base pairing of the canonical nucleobases. Left: An example DNA double strand with B-DNA conformation is shown in side and top view. The crystal structure was taken from the Protein Data Bank[17] and the water molecules were removed for clarity. The sequence of the two identical complementary strands is 5'-d(CGCGAATTCGCG)-3'. Right: Shown are the Watson–Crick nucleobase pairs. For adenine, the nucleotide with the deoxyribosephosphate backbone is depicted exemplarily, for the other bases the bond to the backbone is indicated. Under physiological conditions, the phosphate groups are deprotonated and their charge is compensated by Na^+ counterions.

1.1.2 Electronic Deactivation via Conical Intersections

The UV-vis absorption spectrum of any DNA strand is predominated by the absorptions of the nucleobases at $\lambda_{max} = 250 - 280$ nm because the backbone shows no absorbance in this wavelength range. The fluorescence quantum yield of natural purified DNA is very low ($\phi_{fl}(\text{DNA}) \approx 3 \cdot 10^{-4}$).[22] This can be attributed to effective non-radiative transitions which involve internal conversion processes beyond Fermi's Golden Rule.

The deactivation of electronically excited molecules is driven by the excess energy and the energy gradient of the excited state. Potential energy minima may pose barriers impeding the relaxation depending on the internal energy of the system. The effects are determined by three basic theories: i) Thermodynamics determine the excess energy in the excited state. The stationary population of potential energy minima is balanced by the relative energies of potential energy wells. ii) Kinetics determine how fast the energy is converted. Stationary states or internal conversion points are reached by energy transfer, e. g. by collisions between sample and solute molecules or by vibrational relaxation, in dependence of temperature and pressure. Thereby, the population may pass through multiple wells and surmount barriers. That the framework of kinetics is actually applicable to excited-state deactivation processes will be shown in Chapter 4. iii) Dynamics determine the effectively taken deactivation route guided by the minimum energy path. On the deactivation pathway, the molecules adopt intermediate conformations allowing for the formation of potential wells or state crossings. Strong structural deformations can lift the ground state energy and give rise to the formation of conical intersections (CIs). The movement of wavepackets on steep or shallow potential energy hypersurfaces (PEHS) and the detailed shape of CIs determine at which point in time the molecule is converted to the ground state.

For a mathematical description of the PEHS, we need to solve the Schrödinger equation (SE) for the molecule

$$\hat{H}\Psi(\mathbf{r},\mathbf{R}) = \varepsilon\Psi(\mathbf{r},\mathbf{R}), \tag{1.1}$$

where ε is the energy eigenvalue for the molecular wavefunction $\Psi(\mathbf{r},\mathbf{R})$ that is a function of the electronic coordinates $\mathbf{r}$ and the nuclear coordinates $\mathbf{R}$, and the Hamiltonian $\hat{H}$ is composed of

$$\hat{H} = \hat{H}_{el} + \hat{T}_N = \hat{T}_{el}(\mathbf{r}) + V(\mathbf{r},\mathbf{R}) + \hat{T}_N(\mathbf{R}). \tag{1.2}$$

In a perturbation ansatz, the nuclear kinetic energy operator $\hat{T}_N$ and the electronic

Hamiltonian $\hat{H}_{\mathrm{el}}$, which contains the electronic kinetic energy $\hat{T}_{\mathrm{el}}$ and the complete potential energy V, are treated separately. The separation is based on the idea that the electrons instantaneously follow the nuclear motion because of the huge mass difference of the particles which is also the foundation for the Franck–Condon (FC) principle (stating that the nuclear coordinates of a molecule are preserved during electronic excitation). However, ultrafast electronic deactivation takes place on coupled electronic states, thus, the result from the separation ansatz is a set of two coupled Schrödinger equations.[23–26] The first is the electronic SE

$$\hat{H}_{\mathrm{el}}\,\phi_n^{\mathrm{el}}(\mathbf{r};\mathbf{R}) = E_n(\mathbf{R})\,\phi_n^{\mathrm{el}}(\mathbf{r};\mathbf{R}) \tag{1.3}$$

that acts only on the electronic wavefunctions ϕ_n^{el}. These are functions of the electronic coordinates $\mathbf{r}$ but are only parametrically dependent on the nuclear coordinates $\mathbf{R}$. Since the ϕ_n^{el} are eigenfunctions of the SE, they form a complete orthonormal system and the molecular wavefunction can be expanded in the basis of the electronic wavefunctions

$$\Psi(\mathbf{r},\mathbf{R}) = \sum_n \chi_n(\mathbf{R})\,\phi_n^{\mathrm{el}}(\mathbf{r};\mathbf{R}). \tag{1.4}$$

The expansion coefficients χ_n depend only on $\mathbf{R}$ and are interpreted as the nuclear wavefunctions. Inserting this into the molecular SE (Eq. 1.1), yields the second SE, the coupled system of nuclear Schrödinger equations

$$\hat{T}_{\mathrm{N}}\,\chi_n(\mathbf{R}) - \sum_m \Lambda_{nm}\,\chi_m(\mathbf{R}) = (\epsilon - E_n(\mathbf{R}))\;\chi_n(\mathbf{R}). \tag{1.5}$$

The potential energy $E_n(\mathbf{R})$ is interpreted as the unperturbed PEHS that is changed by the nonadiabatic coupling Λ_{nm} depending on the nuclear motion. The nonadiabatic coupling matrix elements are given by

$$\Lambda_{nm} = \langle\phi_n^{\mathrm{el}}|\,\hat{T}_{\mathrm{N}}(\mathbf{R})\,|\phi_m^{\mathrm{el}}\rangle - \hbar^2\,\langle\phi_n^{\mathrm{el}}|\,\nabla_{\mathrm{R}}\,|\phi_m^{\mathrm{el}}\rangle\,\nabla_{\mathrm{R}} \tag{1.6}$$

where ∇_{R} is the derivative operator with respect to the nuclear coordinates $\mathbf{R}$. The nonadiabatic coupling describes the correlation between the nuclear and the electronic motion.[27] It is split into a scalar and a derivative coupling term, respectively.

The often useful Born–Oppenheimer approximation neglects the nonadiabatic coupling to give sufficiently reliable results for well-separated electronic states.[28,29] In this Thesis, however, we are interested in excited-state dynamics including electronic relaxation and transfer between electronic states. In these cases, electronic and nuclear relaxation occur simultaneously and the nonadiabatic coupling cannot be neglected.

This is referred to as the breakdown of the Born–Oppenheimer approximation. The above given coupled Schrödinger equations yield correct results for state crossings and internal conversion processes, but the coupling terms are not easily obtained.

In an N-atomic molecule with $s = 3N - 6$ independent nuclear coordinates, the degeneracy of two electronic states creates an $(s-2)$-dimensional hyperpoint of degeneracy on an $(s-1)$-dimensional hyperline of intersection. The intersection surface resembles a double cone. Hence, this state crossing is called a conical intersection and here the transition from one state to another is most probable, i. e. CIs mediate ultrafast non-radiative electronic transitions by funneling the excited-state wavepacket from one PEHS to the other. A schematic representation of a conical intersection is shown in Fig. 1.2 and the figure caption gives a description of the corresponding wavepacket dynamics.

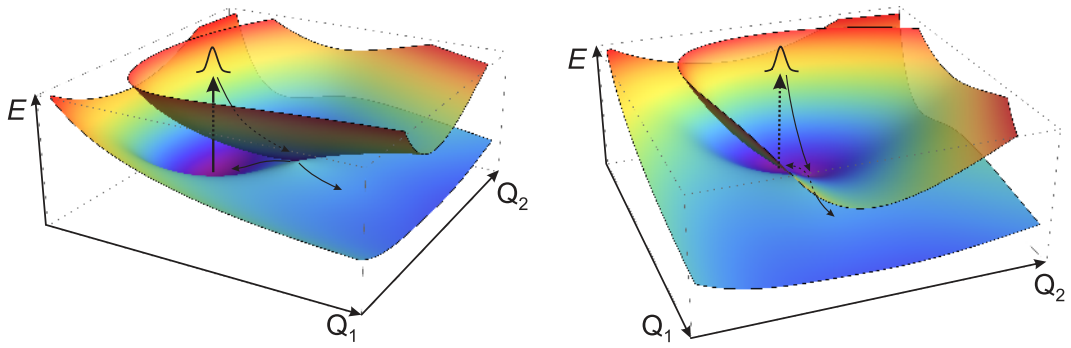

Figure 1.2: Schematic 3D representation of a conical intersection calculated between two arbitrary adiabatic states shown from two different viewing points. The $(s-2)$-dimensional intersection surface is projected on two coordinates Q_1 and Q_2. Electronic excitation from the ground state minimum prepares an excited-state wavepacket. In the Franck–Condon region, the excited state shows a strong gradient. By relaxation on the excited-state PEHS, the wavepacket is transferred towards the region of conical intersection with the ground state where the transition probability is greatest. At the intersection, the wavepacket is funneled to the ground state where it can either relax back to the initial ground state or towards a product configuration as indicated by the arrows.

The nonadiabatic derivative coupling (the second term in Eq. 1.6) diverges right around the CI because the states approach each other and the electronic wavefunctions are no longer independent from the nuclear motion. This divergence makes a mathematical solution very difficult. The coupled Schrödinger equations (Eq. 1.3 and 1.5) can be solved with a mathematical trick. A unitary transformation

from the adiabatic picture to the so-called diabatic picture transfers the coupling terms from the kinetic to the potential energy operator. A detailed mathematical description of this procedure can be found in standard textbooks.[23–26] In the diabatic representation, the derivative coupling is chosen to be zero at the CI and the PEHS are constructed to be smooth which facilitates the calculations. In practice, however, the diabatic solution needs approximations regarding the number of included adiabatic electronic states.

The transition probability of an excited-state wavepacket in regions of strong nonadiabatic coupling can be approximated in the simplest model by the Landau-Zener equation

$$p_{\mathrm{LZ}} = 1 - \exp\left(-\frac{4\pi^2|W_{12}|^2}{h v_x |\Delta F_x|}\right), \tag{1.7}$$

where v_x is the velocity of the wavepacket and ΔF_x is the difference of the slopes of the two potential curves at position x on the deactivation pathway. The equation shows that a transition may occur not only directly at the crossing but also in its immediate vicinity since the energy difference of the states is not factored in. In the presented case of a symmetric CI with respect to the energy axis ($\Delta F_x \approx 0$, Fig. 1.2), the transition probability mostly depends on the velocity of the wavepacket, i. e. on the gradient in the FC region and on the excess energy. After transition to the electronic ground state, either relaxation to the initial minimum or photo-induced product formation is possible. The essential role of CIs in organic photochemistry and photophysics was reviewed in textbooks and book series.[30–32]

The relevant CI is the point where the deactivation pathway crosses the seam. This is not necessarily at the minimum of seam, i. e. the energetic accessibility of a CI plays a crucial role. Variations of excitation energy in the experiment can open or close deactivation pathways due to the different energetic positions of CIs.[33,34] Elevated temperature may accelerate electronic decay and can reveal barriers along the deactivation pathways as will be shown in Chapters 4 and 5 of this Thesis. The time scale for the relaxation and the exact pathway of the wavepacket depend on the topography of the PEHS and the CI and can be assessed by quantum chemical dynamics simulations, which often using Tully's surface hopping method.[35] Explicit wavepacket dynamics needs solving the time-dependent SE, e. g. with the MCTDH algorithm, which is time consuming for reaction times of many picoseconds.[36]

In nucleobases, CIs are found at high energies with respect to the ground state minimum. However, the excess energy deposited in the ground state at interconversion

is mostly harmless: thermal reactions of nucleobases are rarely observed because the heat is dissipated quickly, e. g. by vibrational energy transfer via hydrogen bonds, and almost always a full ground-state recovery is observed. The molecular structure of the nucleobases is decisive in this context because it influences the order and character of the electronic states and becomes deformed during electronic deactivation as will be outlined in the next Section.

1.2 Structural and Electronic Properties of Single Purine Nucleobases

1.2.1 Adenine

1.2.1.1 9H-Adenine

The canonical form of the nucleobase Ade is the 9H-tautomer which will be investigated in Chapters 3 and 5 of this Thesis. Its structure is shown in Fig. 1.3. Time-resolved measurements of the electronic deactivation after photoexcitation yield two time components for the sub-picosecond electronic decay of 9H-Ade. The first component with $0.04-0.2$ ps is usually close to or below the experimental temporal resolution and is commonly assigned to FC relaxation.[37] For the subsequent internal conversion to the ground state, different lifetimes were observed in gas and liquid phase experiments. While lifetimes between $0.75-1.3$ ps were found in the gas phase,[33,38–43] 9H-Ade shows shorter lifetimes of $0.18-0.43$ ps in aqueous solution.[34,44,45] Ade nucleosides and nucleotides are reported with similar electronic decay dynamics as the free base 9H-Ade.[37,44,46,47]

Quantum chemical calculations on 9H-Ade identified two $\pi\pi^*$ and one $n\pi^*$ excited states in the FC region.[48–66] All three states are close in energy and vibronically coupled. The energetic sequence of states is not agreed upon because it depends on the minimum structure[57,60,65,67,68] and on the computational method,[52,53,55,59,69] as well as on fluctuations of the molecular environment.[65,70–72] The three states are connected by CIs and mutual inter-state population transfer was found possible.[52,53,56,63,67,73–75]

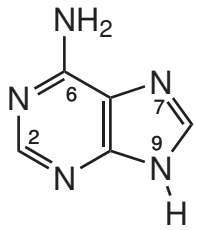

Figure 1.3: Molecular structure of the canonical nucleobase 9H-Ade with important atom numbers.

The $\pi\pi^*$ excited states are labeled L_a and L_b according to Platt's nomenclature[76] due to the orientation of their transition dipole moments parallel and perpendicular (in-plane) to the molecular axes, respectively.[47] The $\pi\pi^*$ L_a excited state can be described mainly by HOMO $\rightarrow$ LUMO excitation, whereas the $\pi\pi^*$ L_b excited state is a linear combination of HOMO $\rightarrow$ LUMO + 1 and HOMO $-$ 1 $\rightarrow$ LUMO transitions.[54] A HOMO is the highest occupied molecular orbital, a LUMO is the lowest unoccupied molecular orbital.

The energetically higher-lying $\pi\pi^*$ excited state is the L_a state and has a substantially higher oscillator strength than L_b.[52,65,69] Thus, mainly this one is excited by UV radiation although the $\pi\pi^*$ excited states are spectrally hardly separated. The $\pi\pi^*$ L_a excited PEHS was either described as barrierless for internal conversion to the ground state[52,54,55,58] or a stationary point was predicted[53,57,63,67] inducing a small barrier for deactivation of $\approx$ 0.1 eV.[52,67,77] Deactivation of 9H-Ade is facilitated by C^2-puckering and the out-of-plane motion of the C^2–H bond leads to a CI with S_0.[52–54,56–61,63,65,67,69,72,74,77,78] The structure at the CI is shown on the left-hand side in Fig. 1.4.

For the $\pi\pi^*$ L_b excited PEHS, a minimum was predicted and no decay pathway to the ground state was found from there.[52–54,56,57] Thus, some authors state that the $\pi\pi^*$ L_b excited state is the state emitting the observed fluorescence.[50,51,54] However, conversion to the $\pi\pi^*$ L_a excited PEHS is possible over a shallow barrier.[53,54,56] Recent experimental results confirm ultrafast conversion from $\pi\pi^*$ L_b to L_a within 0.1 ps directly after excitation.[47] The $n\pi^*$ excitation is optically nearly forbidden.[52] On the $n\pi^*$ excited PEHS, a minimum was found and poses a barrier of 0.08 eV[54] for internal conversion to the ground state.[50,52–54,56,57,60,65,69] At the CI, the structure shows C^6-puckering and out-of-plane bending of the amino group.[50,52–54,56,60,63–65,74,77,78] This structure is shown on the right-hand side in Fig. 1.4.

Figure 1.4: Molecular structure of the characteristic CIs of 9H-Ade formed during electronic deactivation. The puckering at the C^2- (left) and C^6-position (right) is accompanied by the out-of-plane bending of the respective substituent. Coordinates were taken from Ref. 54.

In many theoretical publications, the C^2-puckering pathway is assigned to the $\pi\pi^*$ L_a excited state and the C^6-puckering is attributed exclusively to the $n\pi^*$ excited state.[52–54,56,61,63,65,71,78] On the route to the CI, however, the PEHS is described to acquire mixed character[50,67,69] and unimpeded back transfer from the $n\pi^*$ excited to the $\pi\pi^*$ L_a excited PEHS is possible.[52,53,56,63,67,69,73–75] The experimental and theoretical results of Prokhorenko et al.[79], for example, are in favor of electronic decay via a dark state. Other, more recent studies even state that both puckered CI structures are accessible in water because both are formed by the $\pi\pi^*$ L_a excited-state PEHS.[74,80] The C^6-puckered CI, however, seems to have a lower accessibility and the wavepacket motion towards this point is more time-demanding.[80] In surface-hopping dynamics simulations, both pathways contribute to the electronic deactivation of 9H-Ade within $\Delta t = 1$ ps and the dominating mechanism depends directly on the applied theoretical method.[71] The highest-level ab inito methods used to-date predict the puckering centered at C^2 to dominate during the deactivation process,[71,74,81] especially in water.[72,80] The experimental results may reflect a mixture of the two participating deactivation pathways.

Solvation in water stabilizes the $\pi\pi^*$ excited states with respect to the $n\pi^*$ excited states.[51,57,62,64,65,82,83] The longer lifetime of 9H-Ade in the gas phase was assigned to the $n\pi^*$ excited state PEHS deactivation pathway[40,41] that becomes energetically available in the gas phase, but takes more time because of the motion of the sterically demanding amino group and the inhibition by a barrier. Another explanation approach is reduced vibrational relaxation.[84]

At high excitation energies, an optically dark $\pi\sigma^*$ excited state was found localized at the N^9–H bond of the free base 9H-Ade.[34,57,61,63,67,69,85,86] Incomplete dissociation of the bond leads to formation of a CI with S_0. The pathway is hindered by a barrier of ≤ 1 eV.[61,67,69] The mechanism is thought to be available only at $\lambda_{exc} < 250$ nm[34,87] and it is controversially discussed because of contradictory experimental results.[45,87–91]

1.2.1.2 7H-Adenine

The free base adenine tautomerizes in aqueous solution. A mixture of 80 % 9H-Ade and 20 % 7H-Ade[92] is generated immediately due to their different dipole moments.[51] The non-canonical tautomer is shown in Fig. 1.5 and is the subject of Chapter 4 of this Thesis.

The 7H-tautomer was found to have an excited-state lifetime on a different timescale than 9H-Ade, namely ≈ 8 ps,[34,45,93] making it easy to distinguish between

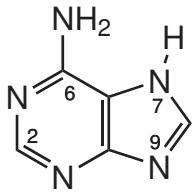

Figure 1.5: Molecular structure of the non-canonical nucleobase 7H-Ade.

the species in the experiment in solution. Consequently, 7H-Ade predominates in the static fluorescence spectrum,[94] but shows lower contributions in time-resolved experiments. The electronic origin of 7H-Ade lies below 9H-Ade.[34,95]

In 7H-Ade, the amino group is pyramidalized and rotated due to steric interactions with the N^7–H bond.[54] In the $\pi\pi^*$ L_a excited state of the molecule, a puckering deformation centered at the C^2-position and an out-of-plane motion of the C^2–H bond leads to a CI with the ground state.[54,68] The CI lies at or slightly above the energy level of excitation[68] and is thus not easily reached. Another explanation for the increased lifetime is a changed PEHS topography. The $\pi\pi^*$ L_a excited PEHS forms a shallow minimum,[51,54] where the CIs with the $\pi\pi^*$ L_b and $n\pi^*$ excited PEHS can be found. All three PEHS were predicted to have minima and mutual interconversion was found possible. Similar to 9H-Ade, C^2- and C^6-puckered structures were found for the points of internal conversion. So far it is unclear to what extent the three electronic states take part in the deactivation of 7H-Ade.

1.2.2 Guanine

The 9H-tautomer of guanine is stabilized in polar solvents.[96] Thus, only the canonical form is present in aqueous solution experiments. The molecular structure is shown in Fig. 1.6. Gua will be investigated in Chapter 7 of this Thesis.

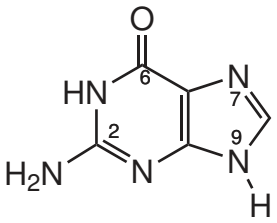

Figure 1.6: Molecular structure of the canonical nucleobase Gua with important atom numbers.

The experimental excited-state lifetimes of Gua, its nucleosides or nucleotides in aqueous solution are ≈ 0.2 ps, ≈ 0.9 ps and $\gtrsim 2$ ps, as found in time-resolved

fluorescence[97] and transient absorption experiments,[98] and confirmed by gas phase experiments, where the intermediate time constant is missing.[99,100] The shortest component was assigned to ultrafast S_2–S_1 interconversion. The other lifetime components were associated with internal conversion to the ground state.[37,38,46,101,102] The 2 ps–decay was only recently found as a very weak contribution in the red part of the fluorescence spectrum[97,98] and had earlier been assigned to vibrational cooling.[103] A dark state was invoked for its occurrence[79,98] or it was attributed to non-canoncial tautomers.[99] Lastly, this component was assigned to an out-of-plane motion of the amino group.[98,104] This is supported by a kinetic isotope effect of the lifetime component in D_2O[98] where the amino group is deuterated. Studies on NH_2-bridged Gua derivatives[105] and on Gua-containing base pairs[106] showed highly increased lifetimes due to constraining of the C^2-puckering. The deactivation of Gua slows down in methanol and in glycerol[104] which also indicates that large-amplitude motions are required for the process. The non-canonical nucleobase hypoxanthine shows excellent agreement of lifetimes with Gua for the first two components, but lacks the third[107] which may be due to the missing amino group.

The electronic structure of Gua is quite similar to that of Ade. The two $\pi\pi^*$ excited states are clearly separated in Gua, with L_a at lower energies than L_b, but with similar oscillator strengths. The sequence of states is not affected by solvation.[66] They have nearly perpendicular transition dipole moments[108] that are parallel to the short molecular axis for the L_a transition, and parallel to the long molecular axis for the L_b transition.[48,98,103] The $\pi\pi^*$ L_a excited state results from HOMO $\rightarrow$ LUMO excitation whereas the $\pi\pi^*$ L_b excited state is composed of HOMO $\rightarrow$ LUMO + 1 and HOMO − 1 $\rightarrow$ LUMO transitions.[109] Ultrafast interconversion from L_b to L_a within 0.1 ps is possible.[98,103,110]

Two structures for $\pi\pi^*$ L_a/S_0 CIs with C^2-puckering and different degrees of NH_2 out-of-plane bending were found.[78,81,106,109–118] The two molecular structures at such CIs are shown on the left-hand side in Fig. 1.7. The $\pi\pi^*$ L_a excited PEHS was predicted to be barrierless[81,103,109,115–117] or to have a shallow minimum.[113,114,118] The spectrally broad transient signals observed in experiments[101] may be a sign of a widely spread wavepacket on this rather flat PEHS.

An $n_O\pi^*$ excited state is reached by excitation of a non-bonding orbital at the oxygen atom. Its CI with S_0 was predicted to form by ring puckering at the C^6-position and out-of-plane motion of the carbonyl bond.[78,109,114,116–118] The structure is shown on the right-hand side in Fig. 1.7. This pathway is inhibited by a pronounced barrier[109,119] and the $n_O\pi^*$ excited state is destabilized by solvation in water.[48,118]

Back-transfer to the $\pi\pi^*$ excited state was found possible and leads to a mixing of the states.[109] The out-of-plane motion of the carbonyl group was also predicted for the decay of the $\pi\pi^*$ L_a excited state.[110]

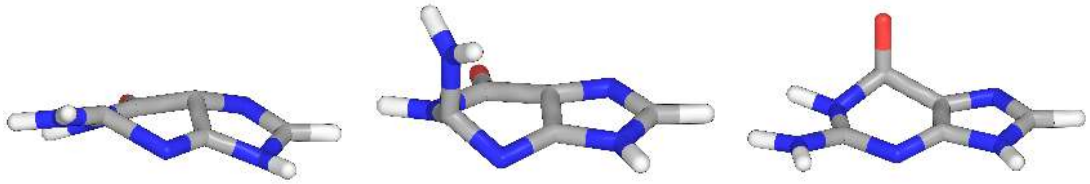

Figure 1.7: Molecular structure of Gua at the characteristic CIs formed during electronic deactivation. The structure on the left-hand side shows C^2-puckering, the middle shows C^2-puckering with out-of-plane motion of the amino group and the right-hand side shows a structure with puckering centered at the C^6-position and out-of-plane motion of the carbonyl oxygen. Coordinates were taken from Ref. 110.

Surface-hopping dynamics simulations indicate that both puckering deformations play a role in the electronic deactivation of Gua. The deformation with (partial) out-of-plane motion of the amino group was found to dominate the calculated trajectories in the gas phase,[116] in water,[117,118] and in a DNA double strand.[106] Still, it is not unlikely that the experimental results reflect a mixture of the predicted deactivation routes.

Additionally, a triplet mechanism was proposed for the deactivation of Gua with intersystem crossing occurring in the region of the $\pi\pi^*$ L_a/S_0 CI and subsequent population of a triplet potential energy minimum that decays via a singlet-triplet crossing with the ground state.[120] A $\pi\sigma^*$ excited state, discussed for facilitating excited-state tautomerism,[121,122] is not expected to be involved in the electronic deactivation of Gua.[113,115]

1.3 Structural and Electronic Properties of Stacked Purine Nucleobases

In contrast to mononucleotides, the electronic deactivation dynamics of oligo- and polynucleotides are influenced by stacking interactions. In stacked nucleobases, vertical excitation mostly populates excitonically coupled states. Subsequent energetic relaxation is proposed to generate excimers, which give rise to long electronic lifetimes.[123–126] The involved phenomena were observed experimentally, but the terms are poorly defined. This Section explains the occurrence of stacking interactions and delocalized electronic states in the context of the present Thesis reflecting the most common use of the terms in literature.

1.3.1 π-Stacking Interactions

Stacking is a ground-state phenomenon that results in a minimum energy conformation of co-planar molecular units, thus also for adjacent nucleobases in a DNA strand. A nucleobase stack is defined as the near-parallel alignment of two or more bases with van der Waals contact of the orbitals of the adjacent aromatic ring systems.[127] The distance of the bases is below 4.5 Å[128–130] and no solvent molecules or ions can be found in-between. The stack is stabilized by hydrophobic interactions.[131,132] Neat nucleobase stacks can be seen in the DNA structure depicted in Fig. 1.1.

Unstacking can be induced by decreasing the pH value of the solution or by increasing the temperature.[133] A higher stacking yield was observed at low temperatures, because stacking is exothermic and entropically disfavoured.[127] The twist angle between the bases seems to be moderately variable for stacking interactions. Most oligonucleotides show stacks with a twist angle of about $\alpha = 30°$, allowing for the helical B-DNA structure,[129,134,135] but face-to-back configurations with low twist angles are also energetically favorable for homostacks of free purine bases.[136]

Base stacking in the gas phase is determined by dispersion attraction, short-range exchange repulsion and Coulombic interaction.[137] Although often referred to as π-stacking, no specific π–π orbital interaction was found to play a role.[15,136,137] The mutual orientation of the bases is regulated by dipole–dipole interaction.[137a,138] Dispersion attraction is anti-proportional to the twist angle between the bases and by interplay with repulsion controls the interbase distance which is often lowered below DNA configuration. Note that the extent of orbital overlap is frequently used to characterize the quality of stacked systems and describes the twist angle as well as the interbase distance. In water, dispersion interaction predominates[139] and hydrophobic effects play a role.

The stabilization energy by base stacking is biggest in purine stacks.[134,136,140,141] The base-stacking energy among adenine polymers was determined to be $0.14 - 0.17$ eV per base ($13.5 - 16.4$ kJ/mol)[142–147] and explains the observed self-association of free Ade molecules to vertical stacks in aqueous solution.[148–152] This association is also likely for Gua molecules and most certainly initiated the first stacked structures in the primordial “soup” that will have led to the development of the DNA macromolecule.

The theoretical description of nucleobase stacks is challenging, because explicit intermolecular interaction must be included. Accurately predicting the excited-state behavior of nucleobase stacks is especially difficult because of the important phenomena of exciton and excimer formation.

1.3.2 Delocalization of Excitation Energy

The stacking-induced behavior of nucleobases in the excited state shows a delocalization of excitation energy and is described by the concepts of excitons and excimers. The localized or delocalized nature of wavefunctions is of great importance. In the context of this Thesis, the term delocalized means the excited state spans more than one base, while a localized state means only one base is excited. Accordingly, both excitons and excimers are considered delocalized states. By some authors, however, short-lived excimer populations in PEHS minima are referred to as "localized" because here the excitation energy occupies a certain molecular site in the observed time window. Reading and comparing literature on the topic thus requires careful inspection of the used terms.

1.3.2.1 Frenkel Excitons

In solid-state physics, an exciton is an electron–hole pair that is generated by UV-light absorption and behaves like a single particle. In crystals and other periodic structures, it can dissociate and mediate charge transport processes.

The concept of Frenkel excitons describes non-dissociated electron–hole pairs. It can be applied to the electronic excitation of molecular aggregates like polynucleotides and explains the formation of delocalized excited states. As described by Kasha,[153,154] delocalized states are generated by mixing of degenerate or close-lying bright states and allow for coherent collective excitation. This so-called excitonic coupling is determined by dipolar interaction between the transition dipole moments of two or more molecules and, thus, depends on the oscillator strengths of the transitions. It is independent of whether the interacting units are connected by a non-conducting backbone or not. For two molecules within interaction distance, but with marginal orbital overlap, the excitons can be described by perturbation theory. The Hamilton operator

$$\hat{H} = \hat{H}_\mathrm{a} + \hat{H}_\mathrm{b} + \hat{V}_\mathrm{ab} \tag{1.8}$$

is composed of the Hamiltonians of the isolated molecules a and b, of which the eigenstates are known, and the intermolecular perturbation potential $\hat{V}_\mathrm{ab}$, which is a Coulombic potential. Solving the Schrödinger equation for the excitonically coupled states of the dimer gives two orthogonal exciton wavefunctions

$$\Psi'_\mathrm{E} = \frac{1}{\sqrt{2}}(\psi^*_\mathrm{a}\psi_\mathrm{b} - \psi_\mathrm{a}\psi^*_\mathrm{b}), \tag{1.9a}$$

$$\Psi''_{\mathrm{E}} = \frac{1}{\sqrt{2}}(\psi^*_{\mathrm{a}}\psi_{\mathrm{b}} + \psi_{\mathrm{a}}\psi^*_{\mathrm{b}}), \tag{1.9b}$$

and the corresponding exciton energies

$$E^-_{\mathrm{E}} = E^*_{\mathrm{a}} + E_{\mathrm{b}} + D' - \epsilon, \tag{1.10a}$$

$$E^+_{\mathrm{E}} = E^*_{\mathrm{a}} + E_{\mathrm{b}} + D' + \epsilon, \tag{1.10b}$$

which are composed of the excited-state energy E^*_{a} of molecule a, the ground-state energy E_{b} of molecule b, the van der Waals interaction energy D' between the excited state of molecule a and the ground state of molecule b (or vice versa), and the exciton splitting term ϵ. Note that the + or − sign in the exciton wavefunctions is not related to the exciton energy. Fig. 1.8 shows an energy scheme for the formation of excitons in a molecular dimer. The resulting excitonic states are separated by $\Delta E = 2\epsilon$.

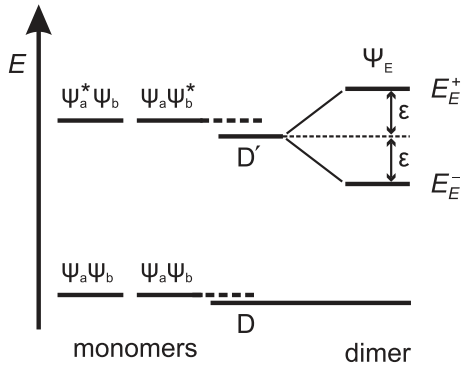

Figure 1.8: Energy scheme for the formation of excitons in a molecular dimer. Van der Waals interaction lowers the ground and excited state energy of the molecular aggregate by D and D′, respectively. Exciton coupling of the transition dipole moments disrupts the degeneracy of the excited states of the monomers. The resulting excitons Ψ_{E} are separated by $\Delta E = 2\epsilon$.

In theory, a random mutual orientation of the two interacting molecules, like in a liquid, leads to symmetric exciton splitting because both excitonic transitions are similarly allowed. For the two limiting cases of molecular H and J aggregates, which are vertical stacks and side-by-side arrays, respectively, the exciton coupling leads to distinct spectroscopic signatures. The excitonic states and their transition probabilities are shown in Fig. 1.9 for three conformations of the aggregates. The exciton energies $E^{\pm}_{\mathrm{E}}$ can be assigned to the molecular conformations by inspecting the dipole–dipole interactions of the momentary phases of the transition dipole moments μ_i. Due to attraction or repulsion of the partial charges, the interaction is either

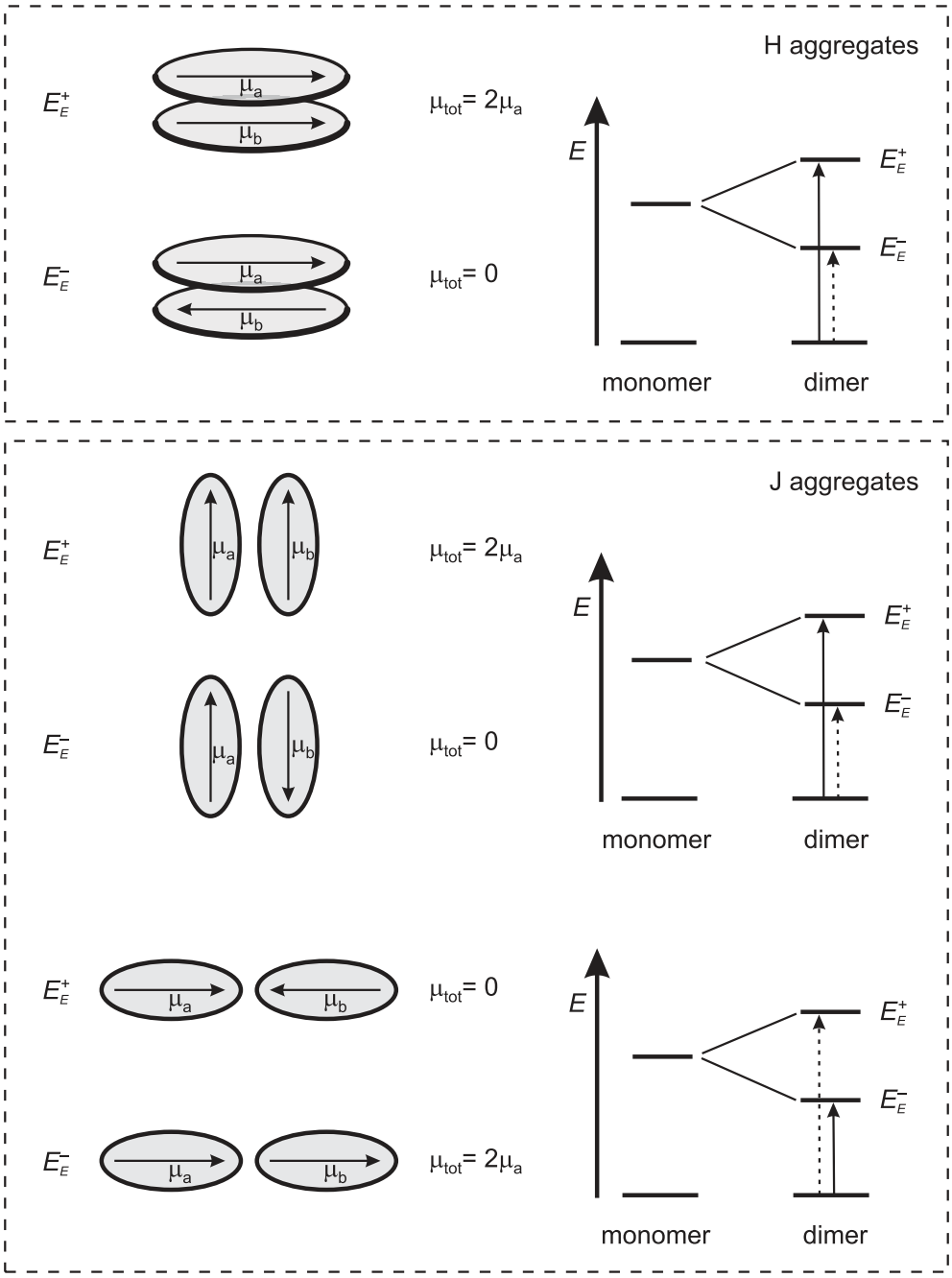

Figure 1.9: Schematic presentation of exciton splitting in H aggregates (in side view) and J aggregates (in top view). Which aggregate conformation is energetically favorable, E_{E}^-, or unfavorable, E_{E}^+, is given by the dipolar interaction of the momentary phase of the transition dipole moments. The sum of the dipole moment vectors determines the transition probability, which is proportional to $|\mu_{\mathrm{tot}}|^2$. Exciton coupling leads to blue-shifted absorption in H aggregates, while J aggregates show blue- and red-shifted absorption, depending on their conformation (indicated by solid and dashed arrows).

energetically favorable or unfavorable and determines which excitonic transition is found at increased or decreased energy compared to the monomer transitions. The oscillator strength of the transition is determined by the total transition dipole moment μ_{tot} which is the sum of the two transition dipole moment vectors. These either add up or cancel out and, thus, generate optically bright and dark states, respectively. Consequently, H aggregates generally show blue-shifted absorption spectra, while J aggregates can have blue- or red-shifted absorption depending on their molecular conformation.

The case of the vertically stacked nucleobase dimer with co-planar molecules is a twisted H aggregate. The exciton splitting energy directly depends on the twist angle α between the transition dipole moments and can be approximated by[153,154]

$$2\epsilon = E_{\mathrm{E}}^{+} - E_{\mathrm{E}}^{-} = \frac{2|\mu_{\mathrm{a}}|^2}{r_{\mathrm{ab}}^3} \cos\alpha, \tag{1.11}$$

where μ_{a} is the transition dipole moment of the individual molecule and r_{ab} is the distance between the molecular centers in the stack. As shown schematically in Fig. 1.10, reducing the angle towards $\alpha = 0°$ parallelly aligns the transition dipole moments of the molecules, enhances the oscillator strength of the transition, and also raises the exciton energy of the dimer. Antiparallel alignment causes the transition

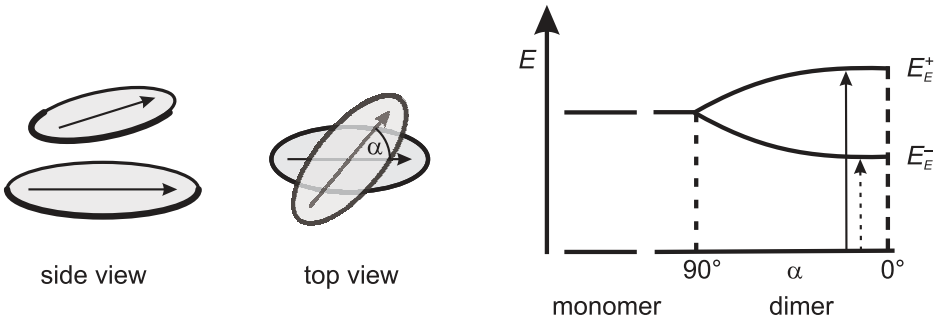

Figure 1.10: Exciton energy angle dependence. In the case of the H aggregate, the excitonic splitting depends on the twist angle α between the transition dipole moments μ_i of the interacting molecules and follows Eq. 1.11. A stack with a twist angle of $\alpha = 0°$ generates the strongest exciton splitting where the upper state is the optically bright state (indicated by a solid arrow).

dipole moments to cancel out and renders the transition optically dark. This is accompanied by energetic lowering.

In this light it becomes clear that, in a nucleobase stack, the oscillator strength of excitons and their splitting energy depend on the conformation of the stack and the relative orientation of the bases.[153,155] Where a clear blue-shift of the

absorption can be expected, a splitting of the absorption band is observed with weakly allowed transitions in the red-wing of the spectrum. It was shown that this arises predominantly from the helical structure of an oligonucleotide, where the twist angle is $\alpha \approx 36°$.[156,157]

In a purine dinucleotide, two bright $\pi\pi^*$ states interact and split to excitons (see left-hand side of Fig. 1.11). The L_b states are known to have a lower oscillator strength and thus the exciton splitting here is smaller. In a polynucleotide and in DNA single and double strands, a large number of bright states is mixed to yield the same number of exciton states (see right-hand side of Fig. 1.11). Since this delocalization is induced by long-range electrostatic interaction, and not by π-orbital overlap, excitons are delocalized even over defect sites and their existence is insensitive to structural fluctuations.[155,158,159] In a polymer, the number of interacting states increases the exciton band width to roughly twice the value of the dimer ($2 \cdot \Delta E = 2 \cdot 2\epsilon$) . This may be explained by nearest-neighbor interactions of which a molecule in a stacked polymer has two. Additional long-range dipole interaction increases the exciton splitting energy by a factor of 2.39 in a theoretical 17-mer compared to its dimer.[154]

In the model DNA double strand $dA_{20}{\cdot}dT_{20}$, the excitonic eigenstates were found to contain contributions from all bases which is referred to as delocalization over the complete strand length.[160] However, the contribution of the single bases to the excitons is limited. It is often found that excitation only involves two bases[125,161,162] or slightly more than two bases.[159,163–165] This "exciton length" seems to depend on

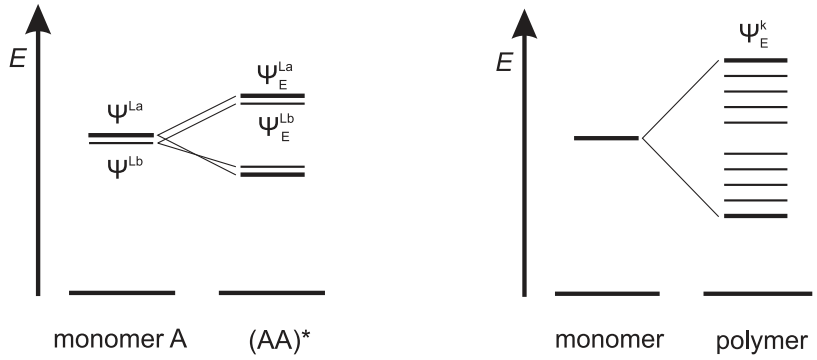

Figure 1.11: Energy scheme of the formation of excitons in a dinucleotide of A and in an arbitrary polymer. The degenerate excited states of close-lying chromophores are split by exciton coupling of the transition dipole moments. In the dinucleotide, each base A contributes two bright states. The $\pi\pi^*$ L_b states experience lower excitonic coupling than L_a due to their lower oscillator strength. In a polymer, a multitude of bright states forms an exciton stack.

the structural flexibility of the molecule.[159]

Excitonic coupling is only one aspect of nucleobase interactions. Base stacks do not only show splitting of the absorption bands, but also hypochromism. This may be attributed to the occurrence of charge transfer (CT) states which are naturally optically dark.[11] In these, an electron from one base is fully or partially transferred to another base. The formation of CT states is mediated by the orbital overlap in well-stacked bases,[166] but is favored for dynamically slightly deformed conformations.[159] Direct absorption to CT states is predicted for the red wing of the absorption spectrum.[167] The probability for CT states increases with the absorption wavelength and the oxidation potential difference of the interacting bases, e. g. the dinucleotide d(ApG) has a high chance for direct excitation to CT states.[167] It must be noted, however, that the hypochromism cannot be fully explained by CT states, either, and other authors explain it by long-range environmental perturbations.[159,168]

Another example for the limits of exciton theory is the fluorescence of nucleobase stacks. Following excitonic coupling, the lower exciton should be dark. Internal conversion from the upper state is quick and the fluorescence, thus, is expected to be quenched.[153] In nucleobase stacks, however, other processes lead to the enhancement of fluorescence as will be described in the following Section. In fact, exciton theory as described above only applies for strong dipolar coupling. For an overview of the applicability of exciton theory and discrimination between strongly and weakly coupled cases see Refs. 154 and 169.

Directly after excitation, excitons in nucleobase stacks may undergo relaxation processes. Internal conversion within the exciton stack is called intraband scattering and is supposed to be ultrafast, i. e. it occurs well within one picosecond.[170] Monitoring this decay in an experiment needs a temporal solution < 100 fs. Excitons then are thought to decay to states localized at single bases[70,124,167,170–172] or to excimers.[123–125,159,167,170,171,173–175]

1.3.2.2 Excimers

An excimer (or exciplex) is a complex of a ground-state molecule with an identical (or different) excited-state molecule that leads to an energetic stabilization.[176] Originally only described for independent chromophores, the concept was applied to DNA strands, where the nucleobases are covalently linked by the backbone. The term excimer is widely established for describing excited-state nucleobase interactions today. A critical discussion of the use of the term in the context of stacked nucleobases can be found in Ref. 82.

The theoretical electronic configuration of an excimer state is a mixture of an exciton state with a charge transfer state as depicted in Fig. 1.12. This results in a high electron density between the bases which weakly binds the π-stacked units.

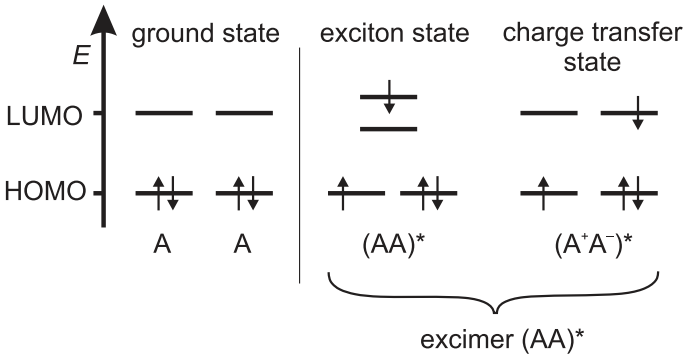

Figure 1.12: Energy scheme of a homodimer. The electronic interaction of the chromophores A gives rise to the formation of excimer states which are a mixture of exciton states and charge transfer states. Excitation to an exciton transfers an electron from one of the highest occupied molecular orbitals (HOMO) of the separate molecules to one of the coupled lowest unoccupied molecular orbitals (LUMO). A charge transfer state is reached by transfer of an electron from the HOMO of one molecule to the LUMO of the other resulting in charge separation.

In comparison to their monomers, red-shifted and amplified emission spectra were found for stacked homo- and heterodinucleotides which demonstrate an energetic stabilization in the excited state.[177–187] The emission of all stacks of purine bases was found to have long picosecond lifetimes.[188,189] These long-lived states with red-shifted emission were assigned to excimers.

It was initially suggested that exciton-like states are responsible for the characteristic spectroscopic features observed in UV-excited purine homodinucleotides.[190,191] However, most recent computational and experimental studies favor the formation of excimer states by electronic relaxation.[124,125,127,192,193] Excimer formation is mediated not only by excitonic coupling and Coulombic interaction, but becomes possible only by short-range interaction of the adjacent π-orbitals of stacked nucleobases, i. e. by orbital overlap.[194] Minimum structures on the excited state PEHS were predicted for excimers[193–195] and account for the experimentally observed high fluorescence quantum yields and the prolonged fluorescence lifetimes.[82,127]

In comparison with excitons, excimer formation is more sensitive to environmental factors like solvation with water, approaching of ionic species, and stack conformation.[11] While the monomer fluorescence is largely independent of temperature, the fluorescence quantum yield of the excimer decreases with increasing

temperature[180,196] and hints that excimer formation is dependent on the quality of the stack.[184,185,196,197] Later experiments and calculations could show that the electronic lifetime of excimers depends on the orbital interaction between the bases.[83,127,198,199] At room temperature, 79 % of bases are stacked in an oligonucleotide,[143] but only 65 % of bases were found to yield a long electronic lifetime.[200] Thus, every excimer has a stacked structure, but not every stacked structure may lead to an excimer.

The concept of excimers is usually only applied to dimers, but there is a possibility that the excimer spans more than two bases. However, in spite of the strong stacking observed in nucleobase polymers, excimers were only found between $2-3$ bases.[199,201]

The identification and description of excimer states, apart from the unambiguous fluorescence shift, becomes especially difficult because the excited-state electronic structure of stacked bases is not clear.[127] Excimers with various degree of charge transfer character were predicted, so-called neutral, CT and mixed excimers.[167,171,172,192,193,202] Moreover, a new class of bonded excimers was recently introduced and is characterized by approaching of two specific molecular sites by deformation of both adjacent bases.[195,203–206] In an QM/MM (quantum mechanics/molecular mechanics) approach of an Ade stack within a solvated DNA double strand, Spata et al.[206] predicted four different possible excimer states. An overview of the molecular structures, their natural transition orbitals and their difference dipole moments is shown in Fig. 1.13 to facilitate visualization of the concept of excimers.

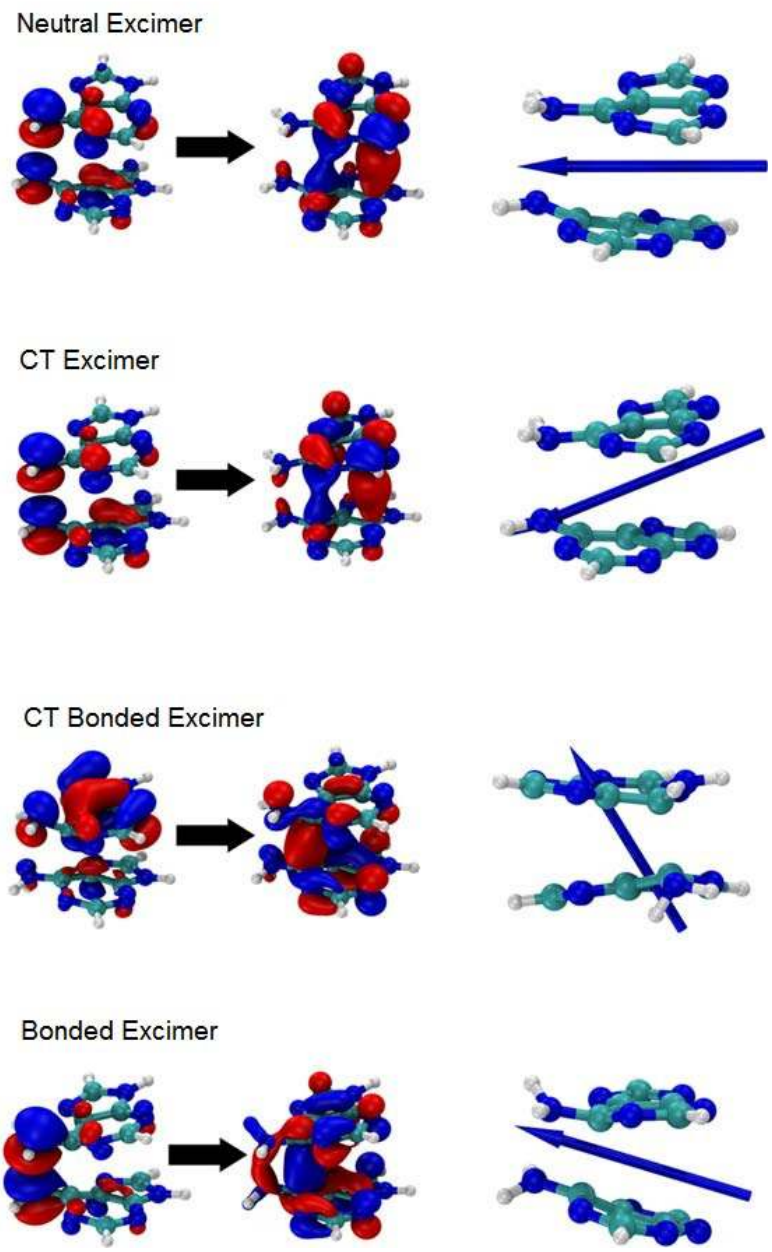

Figure 1.13: Natural transition orbitals (left) and difference dipole moments (right) for the excimers found in Ade stacks within the double strand $dA_{20}{\cdot}dT_{20}$. Figure adapted and republished with permission of the Royal Society of Chemistry, from Ref. 206; permission conveyed through Copyright Clearance Center, Inc.

The following experimental observations are in favor of a strong CT character of excimer states. The long-lived states in nucleobase stacks have around three times the fluorescence quantum yields of their monomers (e. g. $\phi_f(\mathrm{ApA}) \approx 1.6 \cdot 10^{-4}$ and $\phi_f(\mathrm{dAMP}) \approx 0.5 \cdot 10^{-4}$)[184,207] in spite of an up to 1000-fold lifetime. The emissive state thus must be comparatively dark, which is the case for states with CT character.[127] Different Ade dimers with varying backbones were found to exhibit nearly the same lifetime. This was attributed to formation of CT excimers rather than neutral excimers[175] since CT coupling is strong and only moderately sensitive to stacking fluctuations.[208] CT excimers were predicted to evolve from excitons and to have lifetimes of more than 100 ps, especially in polar solvents, and thus they can act as trap states.[124,209,210]

Excimer formation in nucleobase stacks was found to be fast and to need no or only small geometry changes.[127,175] Long-lived excited states are potentially harmful,[211] but the short time-scale for excimer formation makes this process competitive with the equally rapid photoproduct formation. Since, additionally, excimers were so far reported as non-reactive Nielsen et al.[212] coined their formation as the "self-protection excimer process."

1.3.3 Electronic Deactivation Mechanisms

The excimer state is a potential energy minimum, thus, deactivation pathways of stacked nucleobase systems are difficult to calculate.[194,213] Several deactivation mechanisms were proposed to explain the molecular processes behind the experimentally observed long lifetimes:

- Charge recombination.[125,167]
- Monomer-like deformation:[65,77,106,165,171,209,214,215] Puckering and out-of-plane deformations are sterically hindered in stacked systems and thus take more time. This effect is enhanced in double strands due to hydrogen bonding.[70]
- Relocalization to monomers:[70,77,124,172,216] Overcoming the stacking interaction is only possible after a long dwelling in the potential energy minimum. CT states act as a reservoir for monomer deactivation.[11]
- Shortening of the interbase distance:[83,106,167,202,209,211,217] This is possibly accompanied by a face-to-back orientation.[171] Decay from this conformation takes a long time because of the necessary structural rearrangement.
- Intermediate bond-formation:[195,203–206] The structure resembles an intermediate in a stepwise cycloaddition between the C^6-atoms, but the process is fully

reversible.[195] The bonded excimer facilitates deactivation but slows down the process because the new bond sterically hinders ring puckering.[203] Nanosecond lifetimes were predicted.[206]

Many of these predictions have in common that the conical intersections where interconversion to the ground state occurs show structures very similar to those of monomer deactivation, i. e. ring puckering with out-of-plane bending of the C^2- or C^6-substituents. Often only one of the bases is deformed like this and the distance between the bases plays a big role for the deactivation.

One has to keep in mind that a parallel pathway exists in stacked systems. Localization of the excitation energy to one of the monomers allows for ultrafast deactivation[11,22,125,164,173,206] with the well-known mechanisms described in Section 1.2. This mechanism was found to predominate in unstacked systems,[175,218] but was also found for end-linked polydA·polydT double strands that cannot unstack,[219] and in dynamics calculations of well-stacked adenines.[83]

The molecular mechanism of the electronic deactivation process is quite well understood for nucleobase monomers. For stacked structures, many different excited-state structures were predicted and mechanisms were proposed. However, the direct connection between structural deformation and electronic decay remains obscure. So far it has been difficult to pin down the molecular mechanism leading to the electronic deactivation of excimers.

1.4 Aim and Content of this Thesis

This Thesis aims at further uncovering the complex electronic deactivation dynamics of selected mono-, di- and oligonucleotides of adenine and guanine by means of femtosecond time-resolved transient electronic absorption and fluorescence spectroscopy. The analysis is focused on the discrimination between barrierless and hindered electronic deactivation processes. Three approaches are adopted in order to characterize molecular deactivation mechanisms: i) comparative studies of structurally related molecules, ii) temperature-dependent measurements, iii) comparison of measurements in H_2O and D_2O.

The first approach is used for studying adenine and the influence of the sugar-phosphate backbone to its electronic decay dynamics. The results unambiguously demonstrate chromophore-governed dynamics as will be seen in Chapter 3.

The second approach is employed first in Chapter 4 for studying the tautomeric mixture of the free base adenine using time-resolved fluorescence spectroscopy.

The canonical 9H-adenine shows a temperature-independent ultrafast excited-state lifetime consistent with a barrierless deactivation pathway. The longer fluorescence lifetime of 7H-adenine, in contrast, drastically decreases with temperature and indicates a thermal activation process in the excited state. As will be discussed, the results are in agreement with a potential energy barrier on the deactivation pathway which can be quantified via Arrhenius analysis. To the best of our knowledge, this procedure is unprecedented.

In Chapter 5, the stacking interactions of adenine are exhaustively investigated by applying all three experimental approaches. The adenine dinucleotide poses a good example for the stacking-induced phenomena presented earlier in this introduction: excitonic coupling is clearly visible in the static absorption spectrum and characteristics of excimers were found in static fluorescence and in transient spectroscopy.[125,164,198,220–223] Comparison with the adenine monomer exposes a striking increase of electronic lifetime of the dimer as it was seen before[220–222] and consistent with the proposed stepwise excimer formation mechanism. The change of these lifetimes with temperature can again be assigned to potential energy barriers impeding the deactivation, especially for well-stabilized structures. Most intriguingly, measurements in D_2O show a drastic temporal prolongation of the excited-state signal which may be caused by the fully deuterated amino group. Implications for the molecular deactivation mechanisms will be discussed.

Based on the results of the adenine dinucleotide, the adenine tri- and tetranucleotide are studied in Chapter 6 as to whether the same decay mechanism is in place. It will be shown that the results are consistent with a stepwise excimer formation, but that the energetics seem to change.

Finally, the guanine dinucleotide is studied in Chapter 7. To the best of our knowledge, the transient electronic absorption results are the first of their kind. Direct comparison to the mononucleotide exposes exciton characteristics in static absorption and, in transient spectroscopy, a nearly tenfold increase of the electronic lifetime is observed which may be assigned to the formation of an excimer state. Additionally, the electronic dynamics of the guanine monomer will be discussed on the basis of the new measurements.

The used experimental setups for the time-resolved spectroscopy are highly sensitive and can cover broad spectral ranges. Particularly low excitation energies are chosen to monitor the photophysics of unscathed molecules with reduced unwanted signal. Careful analyses of the data provide a firm basis for interpretation. The experiments and analysis methods are described in Chapter 2. At the end of this

Thesis, Chapter 8 gives a summary and an outlook.

References

[1] J. Bornholt, R. Lopez, D. M. Carmean, L. Ceze, G. Seelig, K. Strauss, 'A DNA-Based Archival Storage System' in *Proceedings of the Twenty-First International Conference on Architectural Support for Programming Languages and Operating Systems (ASPLOS '16)*, ACM, New York, NY, USA, **2016**, 637–649.

[2] P. W. K. Rothemund, 'Folding DNA to create nanoscale shapes and patterns', *Nature* **2006**, *440*, 297–302.

[3] A. A. Arora, C. de Silva, 'Beyond the smiley face: applications of structural DNA nanotechnology', *Nano Rev. Exp.* **2018**, *9*, 1430976.

[4] J.-L. Ravanat, T. Douki, J. Cadet, 'Direct and indirect effects of UV radiation on DNA and its components', *J. Photochem. Photobiol. B* **2001**, *63*, 88–102.

[5] J. Cadet, T. Douki, 'Formation of UV-induced DNA damage contributing to skin cancer development', *Photochem. Photobiol. Sci.* **2018**, Advance Article, DOI 10.1039/C7PP00395A.

[6] A. Sancar, 'Mechanisms of DNA Repair by Photolyase and Excision Nuclease (Nobel Lecture)', *Angew. Chem. Int. Ed.* **2016**, *55*, 8502–8527.

[7] K. Van Nguyen, C. J. Burrows, 'A Prebiotic Role for 8-Oxoguanosine as a Flavin Mimic in Pyrimidine Dimer Photorepair', *J. Am. Chem. Soc.* **2011**, *133*, 14586–14589.

[8] Y. Zhang, J. Dood, A. A. Beckstead, X.-B. Li, K. V. Nguyen, C. J. Burrows, R. Improta, B. Kohler, 'Efficient UV-induced charge separation and recombination in an 8-oxoguanine-containing dinucleotide', *Proc. Natl. Acad. Sci. U.S.A.* **2014**, *111*, 11612–11617.

[9] A. Kumar, M. D. Sevilla, 'Excited state proton-coupled electron transfer in 8-oxoG-C and 8-oxoG-A base pairs: A time dependent density functional theory (TD-DFT) study', *Photochem. Photobiol. Sci.* **2013**, 1328–1340.

[10] D. B. Bucher, C. L. Kufner, A. Schlueter, T. Carell, W. Zinth, 'UV-Induced Charge Transfer States in DNA Promote Sequence Selective Self-Repair', *J. Am. Chem. Soc.* **2016**, *138*, 186–190.

[11] D. Markovitsi, 'UV-induced DNA Damage: The Role of Electronic Excited States', *Photochem. Photobiol.* **2016**, *92*, 45–51.

[12] K. Kleinermanns, D. Nachtigallová, M. S. de Vries, 'Excited State Dynamics of DNA Bases', *Int. Rev. Phys. Chem.* **2013**, *32*, 308–342.

[13] V. R. Cooper, T. Thonhauser, A. Puzder, E. Schröder, B. I. Lundqvist, D. C. Langreth, 'Stacking Interactions and the Twist of DNA', *J. Am. Chem. Soc.* **2008**, *130*, 1304–1308.

[14] C. F. Matta, N. Castillo, R. J. Boyd, 'Extended Weak Bonding Interactions in DNA: π-Stacking (Base–Base), Base–Backbone, and Backbone–Backbone Interactions', *J. Phys. Chem. B* **2006**, *110*, 563–578.

[15] H. Karabiyik, R. Sevinçek, H. Karabiyik, 'π-Cooperativity effect on the base stacking interactions in DNA: is there a novel stabilization factor coupled with base pairing H-bonds?', *Phys. Chem. Chem. Phys.* **2014**, *16*, 15527–15538.

[16] K. Röttger, H. Marroux, M. Grubb, P. Coulter, H. Böhnke, A. Henderson, M. Galan, F. Temps, A. Orr-Ewing, G. Roberts, 'Ultraviolet Absorption Induces Hydrogen-Atom Transfer in G·C Watson–Crick DNA Base Pairs in Solution', *Angew. Chem.* **2015**, *127*, 14932–14935.

[17] H. R. Drew, R. M. Wing, T. Takano, C. Broka, S. Tanaka, K. Itakura, R. E. Dickerson, 'Structure of a B-DNA Dodecamer: Confomation and Dynamics', *Proc. Natl. Acad. Sci. U. S. A.* **1981**, *78*, 2179–2183.

[18] J. D. Watson, F. H. C. Crick, 'Molecular structure of nucleic acids. A structure for deoxyribose nucleic acid', *Nature* **1953**, *171*, 737–738.

[19] F. H. C. Crick, J. D. Watson, 'The complementary structure of deoxyribonucleic acid (DNA)', *Proc. R. Soc. London Ser. A* **1954**, *223*, 80–96.

[20] S. Mukherjee, S. Kailasam, M. Bansal, D. Bhattacharyya, 'Stacking interactions in RNA and DNA: Roll-slide energy hyperspace for ten unique dinucleotide steps', *Biopolymers* **2015**, *103*, 134–147.

[21] C. R. Cantor, M. M. Warshaw, H. Shapiro, 'Oligonucleotide Interactions. III. Circular Dichroism Studies of the Conformation of Deoxyoligonucleotides', *Biopolymers* **1970**, *9*, 1059–1077.

[22] I. Vayá, T. Gustavsson, F.-A. Miannay, T. Douki, D. Markovitsi, 'Fluorescence of Natural DNA: From the Femtosecond to the Nanosecond Time Scales', *J. Am. Chem. Soc.* **2010**, *132*, 11834–11835.

[23] V. May, O. Kühn, *Charge and Energy Transfer Dynamics in Molecular Systems*, 3rd ed., WILEY-VCH Verlag GmbH & Co. KGaA, Weinheim, Germany, **2011**.

[24] M. Baer, *Beyond Born–Oppenheimer: Elelctronic Nonadiabatic Coupling Terms and Conical Intersections*, John Wiley & Sons, Inc., Hoboken, New Jersey, **2006**.

[25] H. Nakamura, *Nonadiabatic Transition: Concepts, Basic Theories and Applications*, 2nd ed., World Scientific Publishing Co. Pte. Ltd., Singapore, **2012**.

[26] G. Fisher, *Vibronic Coupling—The Interaction between Electronic and Nuclear Motion*, Academic Press, London, England, **1984**.

[27] G. A. Worth, L. S. Cederbaum, 'Beyond Born–Oppenheimer: Molecular Dynamics Through a Conical Intersection', *Annu. Rev. Phys. Chem.* **2004**, *55*, 127–158.

[28] M. Born, R. Oppenheimer, 'Zur Quantentheorie der Molekeln', *Ann. Phys.* **1927**, *389*, 457–484.

[29] M. Born, K. Huang, *Dynamical Theory of Crystal Lattices*, Oxford University Press, Oxford, England, **1954**.

[30] S. Matsika, 'Conical Intersections in Molecular Systems' in *Reviews in Computational Chemistry, Vol. 23*, (Eds.: K. B. Lipkowitz, T. R. Cundari, D. B. Boyd), John Wiley & Sons, Inc., Hoboken, New Jersey, **2007**, Chapter 2, 83–124.

[31] W. Domcke, D. R. Yarkony, H. Köppel, Eds., 'Conical Intersections: Theory, Computation and Experiment', *Advanced Series in Physical Chemistry, Vol. 17*, World Scientific Publishing Co. Pte. Ltd., Singapore, USA, UK, **2011**.

[32] M. Klessinger, J. Michl, *Excited States and Photochemistry of Organic Molecules*, VCH Verlagsgesellschaft, Weinheim, Germany, **1995**.

[33] N. L. Evans, S. Ullrich, 'Wavelength Dependence of Electronic Relaxation in Isolated Adenine Using UV Femtosecond Time-Resolved Photoelectron Spectroscopy', *J. Phys. Chem. A* **2010**, *114*, 11225–11230.

[34] T. Pancur, N. K. Schwalb, F. Renth, F. Temps, 'Femtosecond fluorescence upconversion spectroscopy of adenine and adenosine: Experimental evidence for the $\pi\sigma^*$ state?', *Chem. Phys.* **2005**, *313*, 199–212.

[35] J. C. Tully, 'Molecular dynamics with electronic transitions', *J. Chem. Phys.* **1990**, *93*, 1061–1071.

[36] M. H. Beck, A. Jäckle, G. A. Worth, H.-D. Meyer, 'The multiconfiguration time-dependent Hartree (MCTDH) method: a highly efficient algorithm for propagating wavepackets', *Physics Reports* **2000**, *324*, 1–105.

[37] D. Onidas, D. Markovitsi, S. Marguet, A. Sharonov, T. Gustavsson, 'Fluorescence Properties of DNA Nucleosides and Nucleotides: A Refined Steady-State and Femtosecond Investigation', *J. Phys. Chem. B* **2002**, *106*, 11367–11374.

[38] H. Kang, K. T. Lee, B. Jung, Y. J. Ko, S. K. Kim, 'Intrinsic Lifetimes of the Excited State of DNA and RNA Bases', *J. Am. Chem. Soc.* **2002**, *124*, 12958–12959.

[39] C. Canuel, M. Mons, F. Piuzzi, B. Tardivel, I. Dimicoli, M. Elhanine, 'Excited States Dynamics of DNA and RNA Bases: Characterization of a Stepwise Deactivation Pathway in the Gas Phase', *J. Chem. Phys.* **2005**, *122*, 074316.

[40] H. Satzger, D. Townsend, M. Z. Zgierski, S. Patchkovski, S. Ullrich, A. Stolow, 'Primary processes underlying the photostability of isolated DNA bases: Adenine', *Proc. Natl. Acad. Sci. U. S. A.* **2006**, *103*, 10196–10201.

[41] S. Ullrich, T. Schultz, M. Z. Zgierski, A. Stolow, 'Direct Observation of Electronic Relaxation Dynamics in Adenine via Time-Resolved Photoelectron Spectroscopy', *J. Am. Chem. Soc.* **2004**, *126*, 2262–2263.

[42] V. R. Smith, E. Samoylova, H.-H. Ritze, W. Radloff, T. Schultz, 'Excimer states in microhydrated adenine clusters', *Phys. Chem. Chem. Phys.* **2010**, *12*, 9632–9636.

[43] F. Buchner, H.-H. Ritze, J. Lahl, A. Lübcke, 'Time-resolved photoelectron spectroscopy of adenine and adenosine in aqueous solution', *Phys. Chem. Chem. Phys.* **2013**, *15*, 11402–11408.

[44] T. Gustavsson, A. Sharonov, D. Onidas, D. Markovitsi, 'Adenine, deoxyadenosine and deoxyadenosine 5'-monophosphate studied by femtosecond fluorescence upconversion spectroscopy', *Chem. Phys. Lett.* **2002**, *356*, 49–54.

[45] B. Cohen, P. M. Hare, B. Kohler, 'Ultrafast Excited-State Dynamics of Adenine and Monomethylated Adenines in Solution: Implications for the Nonradiative Decay Mechanism', *J. Am. Chem. Soc.* **2003**, *125*, 13594–13601.

[46] J. Peon, A. H. Zewail, 'DNA/RNA nucleotides and nucleosides: Direct measurement of excited-state lifetimes by femtosecond fluorescence up-conversion', *Chem. Phys. Lett.* **2001**, *348*, 255–262.

[47] T. Gustavsson, N. Sarkar, I. Vayá, M. C. Jilménez, D. Markovitsi, R. Improta, 'A joint experimental/theoretical study of the ultrafast excited state deactivation of deoxyadenosine and 9-methyladenine in water and acetonitrile', *Photochem. Photobiol. Sci.* **2013**, *12*, 1375–1386.

[48] M. P. Fülscher, L. Serrano-Andrés, B. O. Roos, 'A Theoretical Study of the Electronic Spectra of Adenine and Guanine', *J. Am. Chem. Soc.* **1997**, *119*, 6168–6176.

[49] A. Holmén, A. Broo, B. Albinsson, B. Nordén, 'Assignment of Electronic Transition Moment Directions of Adenine from Linear Dichroism Measurements', *J. Am. Chem. Soc.* **1997**, *119*, 12240–12250.

[50] A. Broo, 'A Theoretical Investigation of the Physical Reason for the Very Different Luminescence Properties of the Two Isomers Adenine and 2-Aminopurine', *J. Phys. Chem. A* **1998**, *102*, 526–531.

[51] B. Mennucci, A. Toninolo, J. Tomasi, 'Theoretical Study of the Photophysics of Adenine in Solution: Tautomerism, Deactivation Mechanisms, and Comparison with the 2-Aminopurine Fluorescent Isomer', *J. Phys. Chem. A* **2001**, *105*, 4749–4757.

[52] S. Perun, A. L. Sobolewski, W. Domcke, 'Ab Initio Studies on the Radiationless Decay Mechanisms of the Lowest Excited Singlet States of 9H-Adenine', *J. Am. Chem. Soc.* **2005**, *127*, 6257–6265.

[53] H. Chen, S. Li, 'Theoretical Study toward Understanding Ultrafast Internal Conversion of Excited 9H-Adenine', *J. Phys. Chem. A* **2005**, *109*, 8443–8446.

[54] L. Serrano-Andrés, M. Merchán, A. C. Borin, 'A Three-State Model for the Photophysics of Adenine', *Chem. Eur. J.* **2006**, *12*, 6559–6571.

[55] L. Serrano-Andrés, M. Merchán, A. C. Borin, 'Adenine and 2-aminopurine: Paradigms of modern theoretical photochemistry', *Proc. Natl. Acad. Sci. U. S. A.* **2006**, *103*, 8691–8696.

[56] L. Blancafort, 'Excited-State Potential Energy Surface for the Photophysics of Adenine', *J. Am. Chem. Soc.* **2006**, *128*, 210–219.

[57] S. Yamazaki, S. Kato, 'Solvent Effect on Conical Intersections in Excited-State 9H-Adenine: Radiationless Decay Mechanism in Polar Solvent', *J. Am. Chem. Soc.* **2007**, *129*, 2901–2909.

[58] M. Z. Zgierski, S. Patchkovski, E. Lim, 'Biradical radiationless decay channel in adenine and its derivatives', *Can. J. Chem.* **2007**, *85*, 124–134.

[59] M. Barbatti, H. Lischka, 'Nonadiabatic Deactivation of 9H-Adenine: A Comprehensive Picture Based on Mixed Quantum-Classical Dynamics', *J. Am. Chem. Soc.* **2008**, *130*, 6831–6839.

[60] E. Fabiano, W. Thiel, 'Nonradiative Deexcitation Dynamics of 9H-Adenine: An OM2 Surface Hopping Study', *J. Phys. Chem. A* **2008**, *112*, 6859–6863.

[61] I. Conti, M. Garavelli, G. Orlandi, 'Deciphering Low Energy Deactivation Channels in Adenine', *J. Am. Chem. Soc.* **2009**, *131*, 16108–16118.

[62] S. K. Mishra, M. K. Shukla, P. Mishra, 'Electronic spectra of adenine and 2-aminopurine: an ab initio study of energy level diagrams of different tautomers in gas phase and aqueous solution', *Spectrochim. Acta Part A* **2000**, *56*, 1355–1384.

[63] W. M. I. Hassan, W. C. Chung, N. Shimakura, S. Koseki, H. Kono, Y. Fujimura, 'Ultrafast radiationless transition pathways through conical intersections in photo-excited 9H-adenine', *Phys. Chem. Chem. Phys.* **2010**, *12*, 5317–5328.

[64] V. Ludwig, Z. M. da Costa, M. S. do Amaral, A. C. Borin, S. Canuto, L. Serrano-Andrés, 'Photophysics and photostability of adenine in aqueous solution: A theoretical study', *Chem. Phys. Lett.* **2010**, *492*, 164–169.

[65] Z. Lan, Y. Lu, E. Fabiano, W. Thiel, 'QM/MM Nonadiabatic Decay Dynamics of 9H-Adenine in Aqueous Solution', *ChemPhysChem* **2011**, *12*, 1989–1998.

[66] F. Santoro, R. Improta, T. Fahleson, J. Kauczor, P. Norman, S. Coriani, 'Relative Stability of the L_a and L_b Excited States in Adenine and Guanine: Direct Evidence from TD-DFT Calculations of MCD Spectra', *J. Phys. Chem. Lett.* **2014**, *5*, 1806–1811.

[67] C. M. Marian, 'A new pathway for the rapid decay of electronically excited adenine', *J. Chem. Phys.* **2005**, *122*, 104314.

[68] C. M. Marian, M. Kleinschmidt, J. Tatchen, 'The photophysics of 7H-adenine: A quantum chemical investigation including spin–orbit effects', *Chem. Phys.* **2008**, *347*, 346–359.

[69] S. Perun, A. L. Sobolewski, W. Domcke, 'Photostability of 9H-Adenine: Mechanisms of the Radiationless Deactivation of the Lowest Excited Singlet States', *Chem. Phys.* **2005**, *313*, 107–112.

[70] Y. Lu, Z.-G. Lan, W. Thiel, 'Hydrogen Bonding Regulates the Monomeric Non-radiative Decay of Adenine in DNA Strands', *Angew. Chem.* **2011**, *123*, 6996–6999.

[71] M. Barbatti, Z. Lan, R. Crespo-Otero, J. J. Szymczak, H. Lischka, W. Thiel, 'Critical appraisal of excited state nonadiabatic dynamics simulations of 9H-adenine', *J. Chem. Phys.* **2012**, *137*, 22A503.

[72] M. Barbatti, 'Photorelaxation Induced by Water-Chromophore Electron Transfer', *J. Am. Chem. Soc.* **2014**, *136*, 10246–10249.

[73] S. Matsika, 'Three-State Conical Intersections in Nucleic Acid Bases', *J. Phys. Chem. A* **2005**, *109*, 7538–7545.

[74] Y. Lei, S. Yuan, Y. Dou, Y. Wang, Z. Wen, 'Detailed Dynamics of the Nonradiative Deactivation of Adenine: A Semiclassical Dynamics Study', *J. Phys. Chem. A* **2008**, *112*, 8497–8504.

[75] Z. Benda, P. G. Szalay, 'Details of the Excited State Potential Energy Surfaces of Adenine by Coupled-Cluster Techniques', *J. Phys. Chem. A* **2014**, *118*, 6197–6207.

[76] J. R. Platt, 'Classification of Spectra of Cata-Condensed Hydrocarbons', *J. Chem. Phys.* **1949**, *17*, 484–495.

[77] X. Chen, W. Fang, H. Wang, 'Slow deactivation channels in UV-photoexcited adenine DNA', *Phys. Chem. Chem. Phys.* **2014**, *16*, 4210–4219.

[78] S. Mai, M. Richter, P. Marquetand, L. González, 'Excitation of Nucleobases from a Computational Perspective II: Dynamics' in *Photoinduced Phenomena in Nucleic Acids I. Nucleobases in the Gas Phase and in Solvents*, (Eds.: M. Barbatti, A. C. Borin, S. Ullrich), *Topics in Current Chemistry, Vol. 355*, Springer, Heidelberg, Germany, **2014**, 99–153.

[79] V. Prokhorenko, A. Picchiotti, M. Pola, A. Dijkstra, R. Miller, 'New Insights into the Photophysics of DNA Nucleobases', *J. Phys. Chem. Lett.* **2016**, *7*, 4445–4450.

[80] J. W. Park, T. Shiozaki, 'On-the-Fly CASPT2 Surface-Hopping Dynamics', *J. Chem. Theory Comput.* **2017**, *13*, 3676–3683.

[81] M. Barbatti, A. J. A. Aquino, J. J. Szymczak, D. Nachtigallová, P. Hobza, H. Lischka, 'Relaxation mechanisms of UV-photoexcited DNA and RNA nucleobases', *Proc. Natl. Acad. Sci. U. S. A.* **2010**, *107*, 21453–21458.

[82] C. E. Crespo-Hernández, B. Cohen, P. M. Hare, B. Kohler, 'Ultrafast Excited-State Dynamics in Nucleic Acids', *Chem. Rev.* **2004**, *104*, 1977–2019.

[83] F. Plasser, H. Lischka, 'Electronic excitation and structural relaxation of the adenine dinucleotide in gas phase and solution', *Photochem. Photobiol.* **2013**, *12*, 1440–1452.

[84] D. C. Lührs, J. Viallon, I. Fischer, 'Excited state spectroscopy and dynamics of isolated adenine and 9-methyladenine', *Phys. Chem. Chem. Phys.* **2001**, *3*, 1827–1831.

[85] A. L. Sobolewski, W. Domcke, C. Dedonder-Lardeux, C. Jouvet, 'Excited-state hydrogen detachment and hydrogen transfer driven by repulsive $^1\pi\sigma^*$ states: A new paradigm for nonradiative decay in aromatic biomolecules', *Phys. Chem. Chem. Phys.* **2002**, *4*, 1093–1100.

[86] G. M. Roberts, H. J. B. Marroux, M. P. Grubb, M. N. R. Ashfold, A. J. Orr-Ewing, 'On the Participation of Photoinduced N–H Bond Fission in Aqueous Adenine at 266 and 220 nm: A Combined Ultrafast Transient Electronic and Vibrational Absorption Spectroscopy Study', *J. Phys. Chem. A* **2014**, *118*, 11211–11225.

[87] M. G. D. Nix, A. Devine, B. Cronin, M. N. R. Ashfold, 'Ultraviolet photolysis of adenine: Dissociation via the $^1\pi\sigma^*$ state', *J. Chem. Phys.* **2007**, *126*, 124312.

[88] I. Hünig, C. Plützer, K. A. Seefeld, D. Löwenich, M. Nispel, K. Kleinermanns, 'Photostability of Isolated and Paired Nucleobases: N–H Dissociation of Adenine and Hydrogen Transfer in its Base Pairs Examined by Laser Spectroscopy', *ChemPhysChem* **2004**, *5*, 1427–1431.

[89] M. Zierhut, W. Roth, I. Fischer, 'Dynamics of H-Atom Loss in Adenine', *Phys. Chem. Chem. Phys.* **2004**, *6*, 5178–5183.

[90] K. L. Wells, D. J. Hadden, M. G. D. Nix, V. G. Stavros, 'Competing $\pi\sigma^*$ States in the Photodissociation of Adenine', *J. Phys. Chem. Lett.* **2010**, *1*, 993–996.

[91] H. Kang, B. Jung, S. K. Kim, 'Mechanism for Ultrafast Internal Conversion of Adenine', *J. Chem. Phys.* **2003**, *118*, 6717–6719.

[92] M. Dreyfus, G. Dodin, O. Bensaude, J. E. Dubois, 'Tautomerism of Purines. I. N(7)H ⇌ N(9)H Equilibrium in Adenine', *J. Am. Chem. Soc.* **1975**, *97*, 2369–2376.

[93] T. Häupl, C. Windolph, T. Jochum, O. Brede, R. Hermann, 'Picosecond fluorescence of nucleic acid bases', *Chem. Phys. Lett.* **1997**, *280*, 520–524.

[94] J. W. Eastman, 'Fluorescence and tautomerism of adenine', *Ber. Bunsenges. Phys. Chem.* **1969**, *73*, 407–412.

[95] E. Nir, C. Plützer, K. Kleinermanns, M. de Vries, 'Properties of isolated DNA bases, base pairs and nucleosides examined by laser spectroscopy', *Eur. Phys. J. D* **2002**, *20*, 317–329.

[96] J. Leszczynski, 'The Potential Energy Surface of Guanine Is Not Flat: An ab Initio Study with Large Basis Sets and Higher Order Electron Correlation Contributions', *J. Phys. Chem. A* **1998**, *102*, 2357–2362.

[97] F.-A. Miannay, T. Gustavsson, A. Bányász, D. Markovitsi, 'Excited-State Dynamics of dGMP Measured by Steady-State and Femtosecond Fluorescence Spectroscopy', *J. Phys. Chem. A* **2010**, *114*, 3256–3263.

[98] C. Cheng, C. Ma, C. Chan, K. Ho, W. Kwok, 'The solvent effect and identification of a weakly emissive state in nonradiative dynamics of guanine nucleosides and nucleotides—a combined femtosecond broadband time-resolved fluorescence and transient absorption study', *Photochem. Photobiol. Sci.* **2013**, *12*, 1351–1365.

[99] S. D. Camillis, J. Miles, G. Alexander, O. Ghafur, I. Williams, D. Townsend, J. Greenwood, 'Ultrafast non-radiative decay of gas-phase nucleosides', *Phys. Chem. Chem. Phys.* **2015**, *17*, 23643–23650.

[100] F. Buchner, B. Heggen, H. Ritze, W. Thiel, A. Lübcke, 'Excited-state dynamics of guanosine in aqueous solution revealed by time-resolved photoelectron spectroscopy: experiment and theory', *Phys. Chem. Chem. Phys.* **2015**, *17*, 31978–31987.

[101] M. C. Stuhldreier, F. Temps, 'Ultrafast photo-initiated molecular quantum dynamics in the DNA dinucleotide d(ApG) revealed by broadband transient absorption spectroscopy', *Faraday Discuss.* **2013**, *163*, 173–188.

[102] A. Chatterley, C. West, V. Stavros, J. Verlet, 'Time-resolved photoelectron imaging of the isolated deprotonated nucleotides', *Chem. Sci.* **2014**, *5*, 3963–3975.

[103] V. Karunakaran, K. Kleinermanns, R. Improta, S. A. Kovalenko, 'Photoinduced Dynamics of Guanosine Monophosphate in Water from Broad-Band Transient Absorption Spectroscopy and Quantum-Chemical Calculations', *J. Am. Chem. Soc.* **2009**, *131*, 5839–5850.

[104] J. Lee, J. R. Challa, D. W. McCamant, 'Ultraviolet Light Makes dGMP Floppy: Femtosecond Stimulated Raman Spectroscopy of 2'-Deoxyguanosine 5'-Monophosphate', *J. Phys. Chem. B* **2017**, *121*, 4722–4732.

[105] M. Zgierski, S. Patchkovskii, T. Fujiwara, E. C. Lim, 'The Role of Out-of-Plane Deformations in Subpicosecond Internal Conversion of Photoexcited Purine Bases: Absence of the Ultrafast Decay Channel in Propanodeoxyguanosine', *Chem. Phys. Lett.* **2007**, *440*, 145–149.

[106] T. Zelený, M. Ruckenbauer, A. J. Aquino, T. Müller, F. Lankaš, T. Dřsata, W. L. Hase, D. Nachtigallova, H. Lischka, 'Strikingly Different Effects of Hydrogen Bonding on the Photodynamics of Individual Nucleobases in DNA: Comparison of Guanine and Cytosine', *J. Am. Chem. Soc.* **2012**, *134*, 13662–13669.

[107] K. Röttger, R. Stellmacher, M. Stuhldreier, F. Temps, 'Ultrafast Electronic Deactivation Dynamics of Xanthosine Monophosphate', *Molecules* **2017**, *22*, 160.

[108] R. W. Wilson, P. R. Callis, 'Excitons, Energy Transfer, and Charge Resonance in Excited Dinucleotides and Polynucleotides. A Photoselection Study', *J. Phys. Chem.* **1976**, *80*, 2280–2288.

[109] L. Serrano-Andrés, M. Merchán, A. C. Borin, 'A Three-State Model for the Photophysics of Guanine', *J. Am. Chem. Soc.* **2008**, *130*, 2473–2484.

[110] B. Heggen, Z. Lan, W. Thiel, 'Nonadiabatic decay dynamics of 9H-guanine in aqueous solution', *Phys. Chem. Chem. Phys.* **2012**, *14*, 8137–8146.

[111] M. K. Shukla, J. Leszczynski, 'Effect of Hydration on the Lowest Singlet $\pi\pi^*$ Excited-State Geometry of Guanine: A Theoretical Study', *J. Phys. Chem. B* **2005**, *109*, 17333–17339.

[112] I. Pugliesi, K. Müller-Dethlefs, 'Excited-State Ab Initio Calculations and Multidimensional Franck-Condon Simulations on Guanine', *J. Phys. Chem. A* **2006**, *110*, 13045–13057.

[113] H. Chen, S. Lia, 'Ab initio study on deactivation pathways of excited 9H-guanine', *J. Chem. Phys.* **2006**, *124*, 154315.

[114] C. M. Marian, 'The Guanine Tautomer Puzzle: Quantum Chemical Investigation of Ground and Excited States', *J. Phys. Chem. A* **2007**, *111*, 1545–1553.

[115] S. Yamazaki, W. Domcke, A. L. Sobolewski, 'Nonradiative Decay Mechanisms of the Biologically Relevant Tautomer of Guanine', *J. Phys. Chem. A* **2008**, *112*, 11965–11968.

[116] Z. Lan, E. Fabiano, W. Thiel, 'Photoinduced Nonadiabatic Dynamics of 9H-Guanine.', *ChemPhysChem* **2009**, *10*, 1225–1229.

[117] M. Barbatti, J. J. Szymczak, A. J. A. Aquino, D. Nachtigallová, H. Lischka, 'The decay mechanism of photoexcited guanine—A nonadiabatic dynamics study', *J. Chem. Phys.* **2011**, *134*, 014304.

[118] S. F. Altavilla, J. Segarra-Martí, A. Nenov, I. Conti, I. Rivalta, M. Garavelli, 'Deciphering the photochemical mechanisms describing the UV-induced processes occurring in solvated guanine monophosphate', *Front. Chem.* **2015**, *3*, 29.

[119] A. Giussani, J. Segarra-Martí, D. Roca-Sanjuán, M. Merchán, 'Excitation of Nucleobases from a Computational Perspective I: Reaction Paths' in *Photoinduced Phenomena in Nucleic Acids I. Nucleobases in the Gas Phase and in Solvents*, (Eds.: M. Barbatti, A. C. Borin, S. Ullrich), *Topics in Current Chemistry, Vol. 355*, Springer, Heidelberg, Germany, **2014**, 57–97.

[120] R. González-Luque, T. Climent, I. González-Ramírez, M. Merchán, L. Serrano-Andrés, 'Singlet-Triplet States Interaction Regions in DNA/RNA Nucleobase Hypersurfaces', *J. Chem. Theory Comput.* **2010**, *6*, 2103–2114.

[121] H. Langer, N. Doltsinis, D. Marx, 'Excited-State Dynamics and Coupled Proton–Electron Transfer of Guanine', *ChemPhysChem* **2005**, *6*, 1734–1737.

[122] B. Mennucci, A. Toninolo, J. Tomasi, 'Theoretical Study of Guanine from Gas Phase to Aqueous Solution: Role of Tautomerism and Its Implications in Absorption and Emission Spectra', *J. Phys. Chem. A* **2001**, *105*, 7126–7134.

[123] E. R. Bittner, 'Lattice theory of ultrafast excitonic and charge-transfer dynamics in DNA', *J. Chem. Phys.* **2006**, *125*, 094909.

[124] F. Santoro, V. V. Barone, R. Improta, 'Influence of base stacking on excited-state behavior of polyadenine in water, based on time-dependent density functional calculations', *Proc. Natl. Acad. Sci. U.S.A.* **2007**, *104*, 9931–9936.

[125] T. Takaya, C. Su, K. de La Harpe, C. E. Crespo-Hernández, B. Kohler, 'UV excitation of single DNA and RNA strands produces high yields of exciplex states between two stacked bases', *Proc. Natl. Acad. Sci. U. S. A.* **2008**, *105*, 10285–10290.

[126] M. Barbatti, A. C. Borin, S. Ullrich, Eds., 'Photoinduced Phenomena in Nucleic Acids II. DNA Fragments and Phenomenological Aspects', *Topics in Current Chemistry, Vol. 356*, Springer, Heidelberg, Germany, **2014**.

[127] J. Chen, Y. Zhang, B. Kohler, 'Excited States in DNA Strands Investigated by Ultrafast Laser Spectroscopy' in *Photoinduced Phenomena in Nucleic Acids II. DNA Fragments and Phenomenological Aspects*, (Eds.: M. Barbatti, A. C. Borin, S. Ullrich), *Topics in Current Chemistry, Vol. 356*, Springer, Heidelberg, Germany, **2014**, 39–87.

[128] J. Norberg, L. Nilsson, 'Stacking Free Energy Profiles for All 16 Natural Ribodinucleoside Monophosphates in Aqueous Solution', *J. Am. Chem. Soc.* **1995**, *117*, 10832–10840.

[129] K. Murata, Y. Sugita, Y. Okamoto, 'Molecular dynamics simulations of DNA dimers based on replica-exchange umbrella sampling. II. Free Energy analysis', *J. Theor. Comput. Chem.* **2005**, *4*, 433–448.

[130] R. Di Felice, A. Calzolari, E. Molinari, 'Ab initio study of model guanine assemblies: The role of $\pi - \pi$ coupling and band transport', *Phys. Rev. B* **2001**, *65*, 045404.

[131] P. Hobza, J. Šponer, 'Toward True DNA Base-Stacking Energies: MP2, CCSD(T), and Complete Basis Set Calculations', *J. Am. Chem. Soc.* **2002**, *124*, 11802–11808.

[132] J. Norberg, L. Nilsson, 'Solvent Influence on Base Stacking', *Biophys. J.* **1998**, *74*, 394–402.

[133] H. Simpkins, E. G. Richards, 'Titration Properties of Some Dinucleotides', *Biochemistry* **1967**, *6*, 2513–2520.

[134] J. Florián, J. Šponer, A. Warshel, 'Thermodynamic Parameters for Stacking and Hydrogen Bonding of Nucleic Acid Bases in Aqueous Solution: Ab Initio/Langevin Dipoles Study', *J. Phys. Chem. B* **1999**, *103*, 884–892.

[135] A. W. Lange, M. A. Rohrdanz, J. M. Herbert, 'Charge-Transfer Excited States in a π-Stacked Adenine Dimer, As Predicted Using Long-Range-Corrected Time-Dependent Density Functional Theory', *J. Phys. Chem. B* **2008**, *112*, 6304–6306.

[136] S. Jafilan, L. Klein, C. Hyun, J. Florián, 'Intramolecular Base Stacking of Dinucleoside Monophosphate Anions in Aqueous Solution', *J. Chem. Phys. B* **2012**, *116*, 3613–3618.

[137] (a) J. Šponer, J. Leszczynski, V. Vetter, P. Hobza, 'Base Stacking and Hydrogen Bonding in Protonated Cytosine Dimer: The Role of Molecular Ion-Dipole and Induction Interactions', *J. Biomol. Struct. Dyn.* **1996**, *13*, 695–705; (b) J. Šponer, H. Gabb, J. Leszczynski, P. Hobza, 'Base-Base and Deoxyribose-Base Stacking Interactions in B-DNA and Z-DNA: A Quantum-Chemical Study', *Biophys. J.* **1997**, *73*, 76–87; (c) J. Šponer, J. Leszczynski, P. Hobza, 'Hydrogen Bonding, Stacking and Cation Binding of DNA Bases', *J. Mol. Struct.: THEOCHEM* **2001**, *573*, 43–53; (d) J. Šponer, J. Leszczynski, P. Hobza, 'Electronic Properties, Hydrogen Bonding, Stacking, and Cation Binding of DNA and RNA Bases', *Biopolymers* **2002**, *61*, 3–31; (e) J. Šponer, K. E. Riley, P. Hobza, 'Nature and magnitude of aromatic stacking of nucleic acid bases', *Phys. Chem. Chem. Phys.* **2008**, *10*, 2595–2610; (f) J. E. Šponer, Á. Vázquez-Mayagoitia, B. G. Sumpter, J. Leszczynski, J. Šponer, M. Otyepka, P. Banáš, M. Fuentes-Cabrera, 'Theoretical Studies on the Intermolecular Interactions of Potentially Primordial Base-Pair Analogues', *Chem. Eur. J.* **2010**, *16*, 3057–3065; (g) J. Šponer, J. E. Šponer, A. Mládek, P. Jurečka, P. Banáš, M. Otyepka, 'Nature and magnitude of aromatic base stacking in DNA and RNA: Quantum chemistry, molecular mechanics, and experiment', *Biopolymers* **2013**, *99*, 978–988.

[138] V. I. Poltev, N. V. Shulyupina, 'Simulation of Interactions between Nucleic Acid Bases by Refined Atom-Atom Potential Functions', *J. Biomol. Struct. Dyn.* **1986**, *3*, 739–765.

[139] P. Cysewski, Ż. Czyżnikowska, R. Zaleśny, P. Czeleń, 'The post-SCF quantum chemistry characteristics of the guanine–guanine stacking in B-DNA', *Phys. Chem. Chem. Phys.* **2008**, *10*, 2665–2672.

[140] J. Norberg, L. Nilsson, 'Influence of Adjacent Bases on the Stacking-Unstacking Process of Single-Stranded Oligonucleotides', *Biopolymers* **1996**, *39*, 765–768.

[141] R. Brown, C. Andrews, A. Elock, 'Stacking Free Energies of All DNA and RNA Nucleoside Pairs and Dinucleoside-Monophosphates Computed Using Recently Revised AMBER Parameters and Compared with Experiment', *J. Chem. Theory Comput.* **2015**, *11*, 2315–2328.

[142] K. J. Breslauer, J. M. Sturtevant, 'A Calorimetric Investigation of Single Stranded Base Stacking in the Ribo-Oligonucleotide A_7', *Biophys. Chem.* **1977**, *7*, 205–209.

[143] T. G. Dewey, D. H. Turner, 'Laser temperature-jump study of stacking in adenylic acid polymers.', *Biochem-US* **1979**, *18*, 5757–5762.

[144] N. L. Goddard, G. Bonnet, O. Krichevsky, A. Libchaber, 'Sequence Dependent Rigidity of Single Stranded DNA', *Phys. Rev. Lett.* **2000**, *85*, 2400–2403.

[145] R. Luo, H. S. R. Gilson, M. J. Potter, M. K. Gilson, 'The Physical Basis of Nucleic Acid Base Stacking in Water', *Biophys. J.* **2001**, *80*, 140–148.

[146] A. Sain, B.-Y. Ha, H.-K. Tsao, J. Z. Y. Chen, 'Chain persistency in single-stranded DNA', *Phys. Rev.* **2004**, *69*, 061913.

[147] C. Ke, M. Humeniuk, H. S-Gracz, P. E. Marszalek, 'Direct Measurements of Base Stacking Interactions in DNA by Single-Molecule Atomic-Force Spectroscopy', *Phys. Rev. Lett.* **2007**, *99*, 018302.

[148] V. L. Rapoport, B. M. Malkin, S. V. Zorina, 'Luminescence Detection of Tightly Bound Stacking Aggregates of Adenine and Adenosine in Aqueous Solutions—the Candidates for the Role of the First Genetic Templates', *Dokl. Biochem. Biophys.* **2006**, *406*, 23–26.

[149] V. L. Rapoport, V. M. Malkin, A. V. Savina, E. A. Safargaleyeva, V. V. Goryuchko, 'Luminescence of Stable Stacking Aggregates of Adenine and Uracil in Water', *Biophysics* **2012**, *57*, 9–13.

[150] M. P. Schweizer, A. D. Broom, P. O. P. Ts'o, D. P. Hollis, 'Studies of Inter- and Intramolecular Interaction in Mononucleotides by Proton Magnetic Resonance', *J. Am. Chem. Soc.* **1968**, *90*, 1042–1055.

[151] A. D. Broom, M. P. Schweizer, P. O. P. Ts'o, 'Interaction and Association of Bases and Nucleosides in Aqueous Solutions. V. Studies of the Association of Purine Nucleosides by Vapor Pressure Osmometry and by Proton Magnetic Resonance', *J. Am. Chem. Soc.* **1967**, *89*, 3612–3622.

[152] R. Tribolet, H. Sigel, 'Self-association of adenosine 5'-monophosphate (5'-AMP) as a function of pH and in comparison with adenosine, 2'-AMP and 3'-AMP', *Biophys. Chem.* **1987**, *27*, 119–130.

[153] M. Kasha, H. R. Rawls, M. Ashraf El-Bayoumi, 'The Exciton Model in Molecular Spectroscopy', *Pure Appl. Chem.* **1965**, *11*, 371–392.

[154] M. Kasha, 'Molecular Excitons in Small Aggregates' in *Spectroscopy of the Excited State*, (Eds.: B. Di Bartolo, D. Pacheco, V. Goldberg), *Nato Advanced Study Institutes Series: Series B, Physics, Vol. 12*, Plenum Press, New York and London, **1976**, 337–380.

[155] B. Bouvier, J.-P. Dognon, R. Lavery, D. Markovitsi, P. Millié, D. Onidas, K. Zakrzewska, 'Influence of Conformational Dynamics on the Exciton States of DNA Oligomers Benjamin Bouvier', *J. Phys. Chem. B* **2003**, *107*, 13512–13522.

[156] L. M. Nielsen, S. Ø. Pedersen, M.-B. S. Kirketerp, S. Brøndsted Nielsen, 'Absorption by DNA single strands of adenine isolated in vacuo: The role of multiple chromophores', *J. Chem. Phys.* **2012**, *136*, 064302.

[157] L. Hu, Y. Zhao, F. Wang, G. Chen, C. Ma, W. Kwok, D. L. Phillips, 'Are Adenine Strands Helical H-Aggregates?', *J. Phys. Chem. B* **2007**, *111*, 11812–11816.

[158] D. Nachtigallová, P. Hobza, H.-H. Ritze, 'Electronic splitting in the excited states of DNA base homodimers and -trimers: an evaluation of short-range and Coulombic interactions', *Phys. Chem. Chem. Phys.* **2008**, *10*, 5689–5697.

[159] J. J. Nogueira, F. Plasser, L. González, 'Electronic delocalization, charge transfer and hypochromism in the UV absorption spectrum of polyadenine unravelled by multiscale computations and quantitative wavefunction analysis', *Chem. Sci.* **2017**, *8*, 5682–5691.

[160] B. Bouvier, T. Gustavsson, D. Markovitsi, P. Millié, 'Dipolar Coupling Between Electronic Transitions of the DNA Bases and its Relevance to Exciton States in Double Helices', *Chem. Phys.* **2002**, *275*, 75–92.

[161] A. I. Kononov, V. M. Bakulev, V. Rapoport, 'Exciton effects in dinucleotides and polynucleotides', *J. Photochem. Photobiol. B: Biol.* **1993**, *19*, 139–144.

[162] F. Plasser, A. J. A. Aquino, W. L. Hase, H. Lischka, 'UV Absorption Spectrum of Alternating DNA Duplexes. Analysis of Excitonic and Charge Transfer Interactions', *J. Phys. Chem. A* **2012**, *116*, 11151–11160.

[163] E. Emanuele, D. Markovitsi, P. Millié, K. Zakrewska, 'UV Spectra and Excitation Delocalization in DNA: Influence of the Spectral Width', *ChemPhysChem* **2005**, *6*, 1387–1392.

[164] I. Buchvarov, Q. Wang, M. Raytchev, A. Trifonov, T. Fiebig, 'Electronic energy delocalization and dissipation in single- and double-stranded DNA', *Proc. Natl. Acad. Sci. U. S. A.* **2007**, *104*, 4794–4797.

[165] S. O. Konorov, H. G. Schulze, C. J. Addison, C. A. Haynes, M. W. Blades, R. F. B. Turner, 'Base stacking configuration is a major determinant of excited state dynamics in A·T DNA and LNA.', *Open Spectrosc. J.* **2009**, *3*, 9–20.

[166] N. J. Hestand, F. C. Spano, 'Molecular Aggregate Photophysics beyond the Kasha Model: Novel Design Principles for Organic Materials', *Acc. Chem. Res.* **2017**, *50*, 341–350.

[167] R. Improta, V. Barone, 'Interplay between "Neutral" and "Charge-Transfer" Excimers Rules the Excited State Decay in Adenine-Rich Polynucleotides', *Angew. Chem. Int. Ed.* **2011**, *50*, 12016–12019.

[168] W. Rhodes, 'Hypochromism and Other Spectral Properties of Helical Polynucleotides', *J. Am. Chem. Soc.* **1961**, *83*, 3609–3617.

[169] M. Kasha, 'Energy Transfer Mechanisms and the Molecular Exciton Model for Molecular Aggregates', *Radiat. Res.* **1963**, *20*, 55–71.

[170] R. Improta, F. Santoro, V. Barone, A. Lami, 'Vibronic Model for the Quantum Dynamical Study of the Competition between Bright and Charge-Transfer Excited States in Single-Strand Polynucleotides: The Adenine Dimer Case', *J. Phys. Chem. A* **2009**, *113*, 15346–15354.

[171] G. Olaso-González, M. Merchán, L. Serrano-Andrés, 'The Role of Adenine Excimers in the Photophysics of Oligonucleotides', *J. Am. Chem. Soc.* **2009**, *131*, 4368–4377.

[172] I. Conti, P. Altoé, M. Stenta, M. Garavelli, G. Orlandi, 'Adenine deactivation in DNA resolved at the CASPT2//CASSCF/AMBER level', *Phys. Chem. Chem. Phys.* **2010**, *12*, 5016–5023.

[173] R. Improta, 'The excited states of π-stacked 9-methyladenine oligomers: a TD-DFT study in aqueous solution', *Phys. Chem. Chem. Phys.* **2008**, *10*, 2656–2664.

[174] F. Santoro, V. Barone, R. Improta, 'Excited States Decay of the A–T DNA: A PCM/TD-DFT Study in Aqueous Solution of the (9-Methyl-Adenine)$_2$·(1-Methyl-Thymine)$_2$ Stacked Tetramer', *J. Am. Chem. Soc.* **2009**, *131*, 15232–15245.

[175] J. Chen, B. Kohler, 'Base Stacking in Adenosine Dimers Revealed by Femtosecond Transient Absorption Spectroscopy', *J. Am. Chem. Soc.* **2014**, *136*, 6362–6372.

[176] J. B. Birks, 'Excimers', *Rep. Prog. Phys.* **1975**, *38*, 903–974.

[177] J. Eisinger, M. Guéron, R. G. Shulman, T. Yamane, 'Excimer fluorescence of dinucleotides, polynucleotides, and DNA.', *Proc. Natl. Acad. Sci. U. S. A.* **1966**, *55*, 1015–1020.

[178] J. Eisinger, 'The excited states of nucleic acids', *Photochem. Photobiol.* **1968**, *7*, 597–612.

[179] J. Eisinger, R. G. Shulman, 'Excited Electronic States of DNA', *Science* **1968**, *161*, 1311–1319.

[180] P. Vigny, J. P. Ballini, 'Excited states of nucleic acids at 300 K and electronic energy transfer' in *Excited States in Organic Chemistry and Biochemistry*, (Eds.: B. Pullman, N. Goldblum), Reidel, Dordrecht, Holland, **1977**, 1–13.

[181] M. Daniels, J. P. Morgan, 'Polarization spectroscopy of room temperature emissions from CpC (cytidylyl-3',5'-cytidine) and CMP (cytidine monophosphate) in aqueous solution.', *Chem. Phys. Lett.* **1978**, *58*, 283–286.

[182] M. Daniels, J. P. Morgan, 'Polarization spectroscopy of homo-dinucleoside phosphate and homo-polynucleotides: evidence for excimer phosphorescence', *J. Luminescence* **1979**, *18/19*, 593–597.

[183] J. P. Morgan, P. R. Callis, 'Photochemistry and Photophysics of Guanine-Containing Dinucleotides', *Photochem. Photobiol.* **1979**, *29*, 1107–1113.

[184] J. P. Morgan, M. Daniels, 'Excited states of DNA and its components at room temperature. III. Spectra polarization, and quantum yields of emissions from ApA and poly rA.', *Photochem. Photobiol.* **1979**, *31*, 101–113.

[185] J. P. Morgan, M. Daniels, 'Excited states of DNA and its components at room temperature. IV. Spectral, polarization, and quantum yield studies of emissions from CpC and poly rC.', *Photochem. Photobiol.* **1980**, *31*, 207–213.

[186] C. S. Shaar, J. P. Morgan, M. Daniels, 'Excited states of DNA and its components at room temperature-V. Spectral, polarization and quantum yield studies of cytidylyl-(3',5')-adenosine.', *Photochem. Photobiol.* **1984**, *39*, 747–753.

[187] M. Daniels, C. S. Shaar, J. P. Morgan, 'Sequence-dependent emission from stacked forms of ApC and CpA. Evidence for stacked base ('dimer') absorption and left-handed stacked conformation.', *Biophys. Chem.* **1988**, *32*, 229–237.

[188] N. K. Schwalb, F. Temps, 'Base Sequence and Higher-Order Structure Induce the Complex Excited-State Dynamics in DNA', *Science* **2008**, *322*, 243–245.

[189] K. de La Harpe, B. Kohler, 'Observation of Long-Lived Excited States in DNA Oligonucleotides with Significant Base Sequence Disorder', *J. Phys. Chem. Lett.* **2011**, *2*, 133–138.

[190] D. Markovitsi, T. Gustavsson, F. Talbot, 'Excited states and energy transfer among DNA bases in double helices', *Photochem. Photobiol. Sci.* **2007**, *6*, 717–724.

[191] D. Markovitsi, T. Gustavsson, A. Bányász, 'Absorption of UV radiation by DNA: Spatial and temporal features', *Mutat. Res. Rev.* **2010**, *704*, 21–28.

[192] M. Barbatti, A. C. Borin, S. Ullrich, 'Photoinduced Processes in Nucleic Acids' in *Photoinduced Phenomena in Nucleic Acids I. Nucleobases in the Gas Phase and in Solvents*, (Eds.: M. Barbatti, A. C. Borin, S. Ullrich), *Topics in Current Chemistry, Vol. 355*, Springer, Heidelberg, **2014**, 1–32.

[193] R. Improta, F. Santoro, L. Blancafort, 'Quantum Mechanical Studies on the Photophysics and the Photochemistry of Nucleic Acids and Nucleobases', *Chem. Rev.* **2016**, *116*, 3540–3593.

[194] F. Plasser, A. Aquino, H. Lischka, D. Nachtigallová, 'Electronic Excitation Processes in Single-Strand and Double-Strand DNA: A Computational Approach' in *Photoinduced Phenomena in Nucleic Acids II. DNA Fragments and Phenomenological Aspects*, (Eds.: M. Barbatti, A. Borin, S. Ullrich), *Topics in Current Chemistry, Vol. 356*, Springer, Heidelberg, Germany, **2014**, 1–37.

[195] V. A. Spata, W. Lee, S. Matsika, 'Excimers and Exciplexes in Photoinitiated Processes of Oligonucleotides', *J. Phys. Chem. Lett.* **2016**, *7*, 976–984.

[196] P. R. Callis, 'Electronic States and Luminescence of Nucleic Acid Systems', *Annu. Rev. Phys. Chem.* **1983**, *34*, 329–352.

[197] K. Imakubo, 'Luminescence of Dinucleotides at 77 K', *J. Phys. Soc. Jpn.* **1968**, *24*, 1124–1132.

[198] C. Su, 'Femtosecond Transient Absorption Study of the Excited-State Dynamics of Single-Stranded Adenine-Containing Multinucleotides and Steady-State Absorption Spectroscopy of Mononucleotides in Cryogenic Water/Ethylene Glycol Matrices', Dissertation, Graduate School of The Ohio State University, **2010**.

[199] C. Su, C. T. Middleton, B. Kohler, 'Base-Stacking Disorder and Excited-State Dynamics in Single-Stranded Adenine Homo-Oligonucleotides', *J. Phys. Chem. B* **2012**, *116*, 10266–10274.

[200] C. E. Crespo-Hernández, B. Cohen, B. Kohler, 'Base Stacking Controls Excited-State Dynamics in A·T DNA', *Nature* **2005**, *436*, 1141–1144.

[201] S. Tonzani, G. C. Schatz, 'Electronic Excitations and Spectra in Single-Stranded DNA', *J. Am. Chem. Soc.* **2008**, *130*, 7607–7612.

[202] Á. Bányász, T. Gustavsson, D. Onidas, P. Changenet-Barret, D. Markovitsi, R. Improta, 'Multi-pathway excited state relaxation of adenine oligomers in aqueous solution: A joint theoretical and experimental study', *Chem. Eur. J.* **2013**, *19*, 3762–3774.

[203] Y. Dou, W. Zhao, S. Yuan, W. Zhang, H. Tang, 'Bonded excimer in stacked adenines: Semiclassical simulations', *Sci. China. Chem.* **2012**, *55*, 1377–1383.

[204] Y. Dou, Z. Liu, S. Yuan, W. Zhang, H. Tang, J. Zhao, W. Fang, G. V. Lo, 'Dynamics of laser-excited stacked adenines: Semiclassical simulations', *Int. J. Biol. Macromol.* **2012**, *52*, 358–367.

[205] V. A. Spata, S. Matsika, 'Role of Excitonic Coupling and Charge-Transfer States in the Absorption and CD Spectra of Adenine-Based Oligonucleotides Investigated through QM/MM Simulations', *J. Phys. Chem. A* **2014**, *118*, 12021–12030.

[206] V. A. Spata, S. Matsika, 'Photophysical deactivation pathways in adenine oligonucleotides', *Phys. Chem. Chem. Phys.* **2015**, *17*, 31073–31083.

[207] P. Vigny, M. Duquesne, *Organic Molecular Photophysics*, (Ed.: J. B. Birks), Wiley, New York, **1976**, 167–177.

[208] K. de La Harpe, C. E. Crespo-Hernández, B. Kohler, 'Deuterium Isotope Effect on Excited-State Dynamics in an Alternating GC Oligonucleotide', *J. Am. Chem. Soc.* **2009**, *131*, 17557–17559.

[209] I. Conti, A. Nenov, S. Höfinger, S. F. Altavilla, I. Rivalta, E. Dumont, G. Orlandi, M. Garavelli, 'Excited state evolution of DNA stacked adenines resolved at the CASPT2//CASSCF/Amber level: From the bright to the excimer state and back', *Phys. Chem. Chem. Phys.* **2015**, *17*, 7291–7302.

[210] F. Santoro, R. Improta, F. Avila, M. Segado, A. Lami, 'The interplay between neutral exciton and charge transfer states in single-strand polyadenine: A quantum dynamical investigation', *Photochem. Photobiol. Sci.* **2013**, *12*, 1527–1543.

[211] R. R. Ramazanov, D. A. Maksimov, A. I. Kononov, 'Noncanonical Stacking Geometries of Nucleobases as a Preferred Target for Solar Radiation', *J. Am. Chem. Soc.* **2015**, *137*, 11656–11665.

[212] J. B. Nielsen, J. Thøgersen, S. K. Jensen, S. B. Nielsen, S. R. Keiding, 'Vibrational dynamics of deoxyguanosine 5'-monophosphate following UV excitation', *Phys. Chem. Chem. Phys.* **2011**, *13*, 13821–13826.

[213] M. K. Shukla, J. Leszczynski, 'Computational Study of UV-Induced Excitations of DNA Fragments' in *Radiation Induced Molecular Phenomena in Nucleic Acids*, (Eds.: M. K. Shukla, J. Leszczynski), Springer Science+Business Media B.V., **2008**, 369–393.

[214] M. Z. Zgierski, T. Fujiwara, E. C. Lim, 'Non-Adiabatic Photoprocesses of Fundamental Importance to Chemistry: From Electronic Relaxation of DNA Bases to Intramolecular Charge Transfer in Electron Donor-Acceptor Molecules' in *Radiation Induced Molecular Phenomena in Nucleic Acids*, (Eds.: M. Shukla, J. Leszczynski), Springer Science+Business Media B.V., **2008**, 395–433.

[215] S. O. Konorov, H. G. Schulze, C. J. Addison, C. A. Haynes, R. F. Turner, M. W. Blades, 'Temperature-Dependent Excited State Absorption in DNA and LNA Oligomers Supports an Emerging Model of Excited State Dynamics in DNA', *Open Spectrosc. J.* **2009**, *3*, 43–51.

[216] Á. Bányász, I. Vayá, P. Changenet-Barret, T. Gustavsson, T. Douki, D. Markovitsi, 'Base Pairing Enhances Fluorescence and Favors Cyclobutane Dimer Formation Induced upon Absorption of UVA Radiation by DNA', *J. Am. Chem. Soc.* **2011**, *133*, 5163–5165.

[217] W. Zhang, S. Yuan, Z. Wang, Z. Qi, J. Zhao, Y. Dou, G. V. Lo, 'A Semiclassical Dynamics Simulation for a Long-Lived Excimer State of π-Stacked Adenines', *Chem. Phys. Lett.* **2011**, *506*, 303–308.

[218] A. Chatterley, C. West, G. Roberts, V. Stavros, J. Verlet, 'Mapping the Ultrafast Dynamics of Adenine onto Its Nucleotide and Oligonucleotides by Time-Resolved Photoelectron Imaging', *J. Phys. Chem. Lett.* **2014**, *5*, 843–848.

[219] J. Chen, A. K. Thazhathveetil, F. D. Lewis, B. Kohler, 'Ultrafast Excited-State Dynamics in Hexaethyleneglycol-Linked DNA Homoduplexes Made of A·T Base Pairs', *J. Am. Chem. Soc.* **2013**, *135*, 10290–10293.

[220] M. C. Stuhldreier, 'Electronic Deactivation Dynamics of DNA Model Systems and Solvation Dynamics of a Natural Antioxidant by Femtosecond Fluorescence and Absorption Spectroscopy', Dissertation, Christian-Albrechts-Universität zu Kiel, **2013**.

[221] M. C. Stuhldreier, C. Schüler, J. Kleber, F. Temps, 'Femtosecond Fluorescence Measurements of the Adenine Dinucleotide: Direct Observation of the Excimer State' in *Ultrafast Phenomena XVII*, (Eds.: M. Chergui, D. M. Jonas, E. Riedle, R. W. Schoenlein, A. J. Taylor), Oxford, **2011**, 553–555.

[222] M. C. Stuhldreier, K. Röttger, F. Temps, 'Distinctive Spectral Features of Exciton and Excimer States in the Ultrafast Electronic Deactivation of the Adenine Dinucleotide' in *Ultrafast Phenomena XIX*, Vol. 162, (Eds.: K. Yamanouchi, S. Cundiff, R. de Vivie-Riedle, M. Kuwata-Gonokami, L. DiMauro), **2015**, 452–454.

[223] U. C. Stange, 'Untersuchung der Temperaturabhängigkeit der ultraschnellen elektronischen Desaktivierung von Adenin und dem Adenindinukleotid', Masterarbeit, Christian-Albrechts-Universität zu Kiel, **2012**.

2 Experimental Methods

The deactivation of electronically excited molecules is driven by the excess energy and the energy gradient of the excited state. The movement of wavepackets on the multidimensional potential energy hypersurfaces (PEHS) and the detailed shape of conical intersections determine at which point in time the molecule is converted to the ground state. These processes occur over a wide range of timescales covering femtoseconds to more than a nanosecond. However, this scale is still so short that it is not attainable with classic experiments using electronic devices because of their too long response time. Ultrafast molecular dynamics calls for a pump–probe experimental setup. This technique is widely applied and has become the best available technology for femtosecond laser-assisted experiments such as transient absorption and fluorescence spectroscopy, time-resolved mass spectrometry, and photoelectron or photofragment imaging spectroscopy.

Mono-, di- and oligomers of DNA building blocks were investigated by femtosecond time-resolved electronic absorption and fluorescence spectroscopy towards understanding their excited-state decay mechanisms. The spectro-temporal behavior of the corresponding experimental signal allows tracking the fate of the excited state. This was helped by comparing interrelated samples, with particular interest on the influence of the DNA backbone, stacking-induced effects and the implications of temperature changes. Careful data acquisition and a subsequent thorough data analysis with respect to signal decay times, the spectral positions of the transient signals and their temporal shifts, and temperature- and solvent-induced changes, allowed for assignments of the transient signals to molecular deactivation processes. The employed methods for measurement and analysis will be described in the following.

2.1 Setup and Data Acquisition

2.1.1 Transient Electronic Absorption Spectrometer

The setup of the femtosecond time-resolved transient electronic absorption spectrometer (TEAS) for simultaneous broadband and single-color detection was devised and described in detail by K. Röttger.[1,2] The used pump–probe experiment is shown in Fig. 2.1 was set up with a Ti:Sa laser (Clark MXR, CPA 2001) providing pulses at

$\lambda = 775$ nm with durations of 190 fs (fwhm) at a repetition rate of 1 kHz.

Pump and Probe Pulse Generation

UV pump pulses were generated in a three-stage process employing a variety of non-linear optical processes. A theoretical description of these can be found in appropriate optics textbooks.[3–5] A home-built NOPA (non-collinear optical parametric amplifier) was adjusted to deliver spectrally broad pulses centered at $\lambda = 520$ nm. The pulses were temporally compressed by a prism compressor and frequency doubled in a β-bariumborate (BBO) crystal to yield pump pulses at $\lambda_{\mathrm{pump}} = 260$ nm with pulse durations down to 35 fs (fwhm) under magic angle polarization with respect to the probe pulse polarizations. The excitation energy was attenuated to $100-220$ nJ per pulse to keep the sample intact.

Broadband probe pulses were generated from the laser fundamental in a CaF_2 crystal by careful adjustment of the pump energy to yield a spectrum between $\lambda_{\mathrm{probe}} = 310 - 600$ nm. The resulting white light beam was split into probe and reference by a 5 mm glass plate.

Single-color probe pulses were generated in a second home-built frequency-doubled NOPA at $\lambda_{\mathrm{probe}} = 255$ nm with pulse durations of 50 fs (fwhm), and split into probe and reference beams by a glass wedge (30') or a planar glass plate (5 mm).

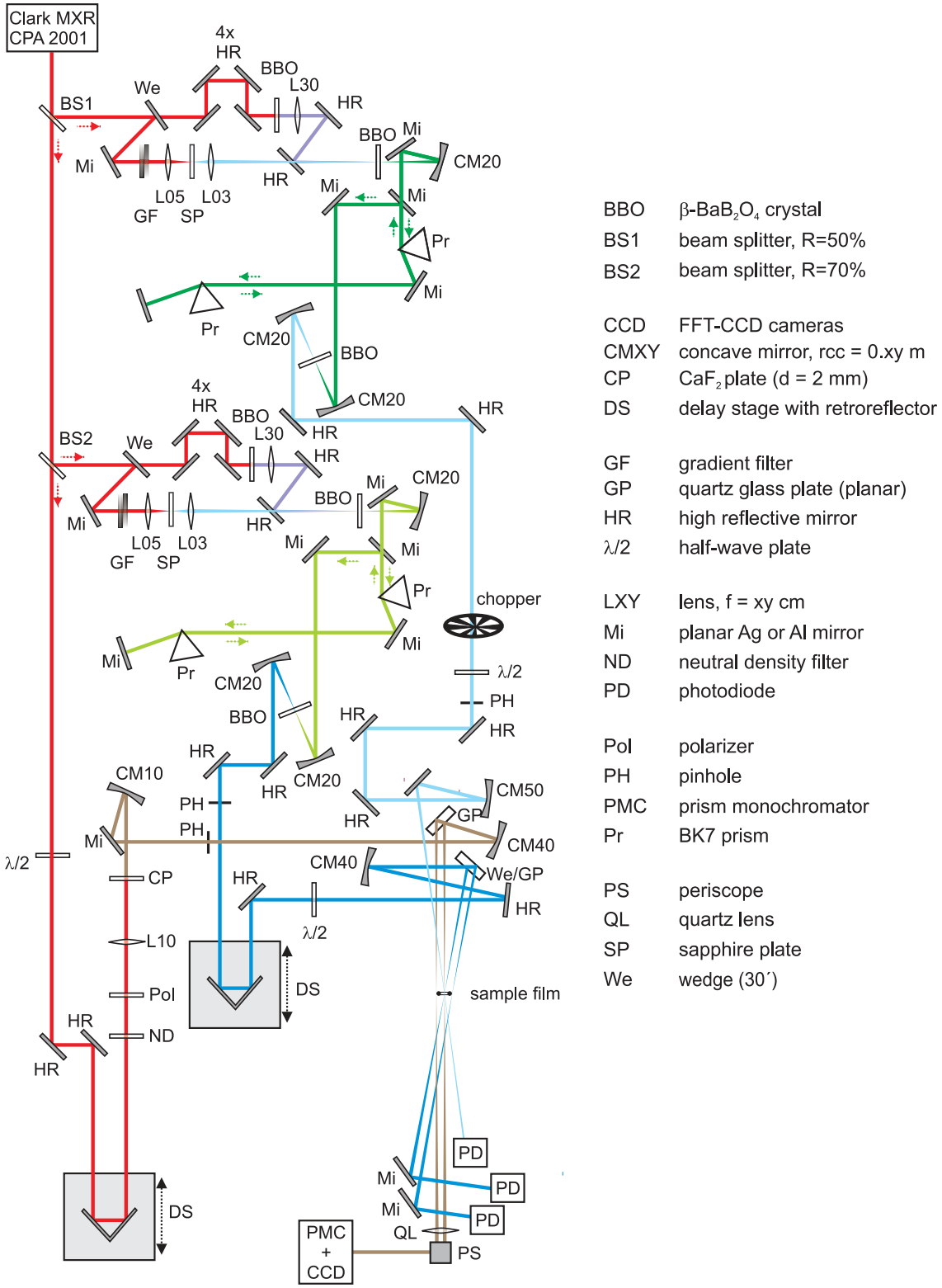

BBO	β-BaB_2O_4 crystal
BS1	beam splitter, R=50%
BS2	beam splitter, R=70%
CCD	FFT-CCD cameras
CMXY	concave mirror, rcc = 0.xy m
CP	CaF_2 plate (d = 2 mm)
DS	delay stage with retroreflector
GF	gradient filter
GP	quartz glass plate (planar)
HR	high reflective mirror
λ/2	half-wave plate
LXY	lens, f = xy cm
Mi	planar Ag or Al mirror
ND	neutral density filter
PD	photodiode
Pol	polarizer
PH	pinhole
PMC	prism monochromator
Pr	BK7 prism
PS	periscope
QL	quartz lens
SP	sapphire plate
We	wedge (30´)

Figure 2.1: Schematic representation of the experimental setup of the femtosecond broadband and single-color transient electronic absorption experiment. The beam colors indicate wavelength conversion processes but do not necessarily reflect the real wavelengths.

Beam Arrangement at the Sample

The sample solutions were flowed through a home-built wire-guided gravity-driven liquid sample film providing a sample film of 100 µm thickness. The film is described in detail below. The beam positions at the film are shown in Fig. 2.2. UV pump and both probe beams were focused onto the same spot in the sample near the center of the film. The size of the pump beam in the sample was adjusted to a diameter of $\approx$ 350 µm, while the probe beam diameters were set significantly smaller with $100 - 200$ µm. The hard foci of all beams lay behind the sample. The broadband reference beam was sent through a horizontally adjacent spot outside the sample film. The single-color reference beam also ran outside the sample film for measurements in Chapter 3, but was sent through a spot in the sample film diagonally above the pump beam for all other measurements.

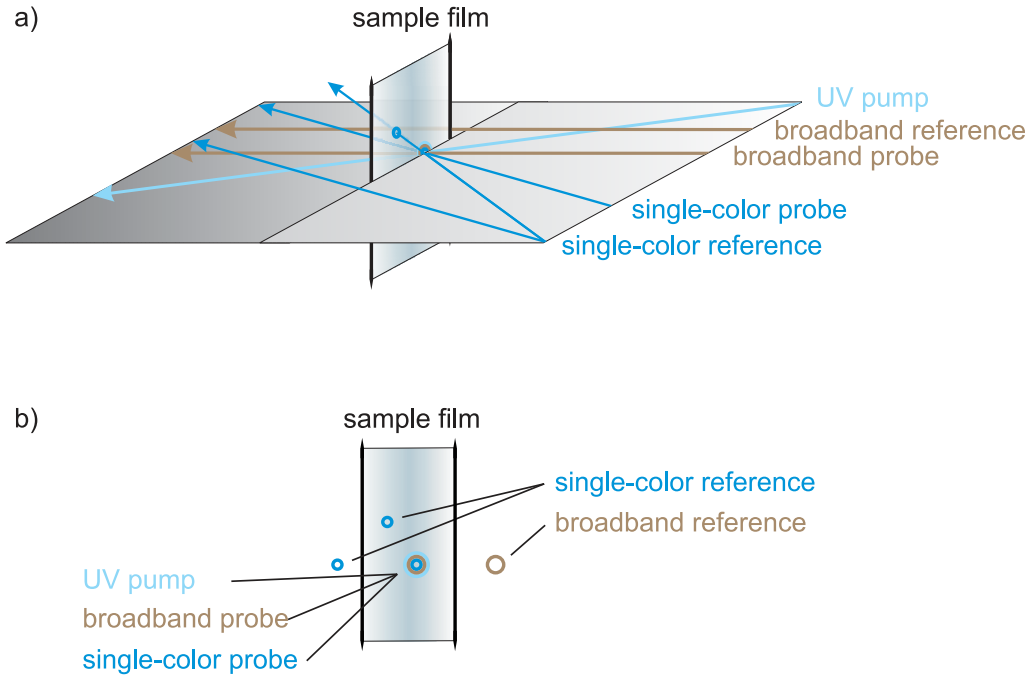

Figure 2.2: Pump and probe beam positions at the sample film in side view (a) and front view (b). The UV pump beam was overlapped with the broadband probe and the single-color probe beam in the sample film. The broadband reference ran through air. The single-color reference beam ran through air for measurements in Chapter 3 and through a spot on the sample film diagonally above the pump beam for all other measurements.

Measurement of the Transient Electronic Absorption Signal

For detection, the broadband probe and reference beams were spectrally dispersed by a prism and focused separately on two fast frame transfer (FFT) CCD camera arrays (Entwicklungsbüro Stresing). The high-intensity part of the spectrum in the red was cut off at $\lambda_{\mathrm{probe}} \approx 600$ nm using a knife edge in order to avoid overexposure. The projection of the white light probe spectrum onto the cameras was carefully adjusted as to cover the same pixel range on both devices. The single-color probe beams were detected by matched photodiodes.

For measurements, the probe pulses were delayed with respect to the pump pulses by a delay stage covering $\Delta t = 2$ ns for the broadband and $\Delta t = 0.7$ ns for the single-color pulses. A chopper was used to block every second pump pulse in order to take a background measurement of unexcited sample. At every delay step, 10 000 pulses were averaged.

The time- and wavelength-dependent transient electronic absorption signal is the difference of absorption ΔOD of the excited and the unexcited sample. It is obtained by the logarithmic difference of the excited and unexcited sample transmissions, T^* and T^0, each calculated from the ratio of probe and reference intensities.

$$\begin{aligned}
\Delta\mathrm{OD}(\lambda,\Delta t) &= -\log T^*(\lambda,\Delta t) - (-\log T^0(\lambda)) \\
&= -\log\left(\frac{I^*_{\mathrm{pr}}(\lambda,\Delta t)}{I^*_{\mathrm{ref}}(\lambda,\Delta t)}\right) - \left(-\log\left(\frac{I^0_{\mathrm{pr}}(\lambda)}{I^0_{\mathrm{ref}}(\lambda)}\right)\right) \\
&= -\log\left(\frac{I^*_{\mathrm{pr}}(\lambda,\Delta t)}{I^*_{\mathrm{ref}}(\lambda,\Delta t)} \cdot \frac{I^0_{\mathrm{ref}}(\lambda)}{I^0_{\mathrm{pr}}(\lambda)}\right)
\end{aligned} \tag{2.1}$$

This procedure was developed to reduce the background signal and to prevent noise from pulse-to-pulse fluctuations.[1,2] Taking the references twice is necessary because I^*_{ref} and I^0_{ref} stem from two consecutive pulses which are not truly identical and thus do not cancel out.

Low-noise data are obtained if the probe and reference intensities at the detection devices are similar, i. e. the noise levels are similar because they are proportional to $\sqrt{I}$. In the measurements for Chapter 3, the single-color beam intensities differed substantially, because the reference beam experienced no absorbance in air but the probe beam was attenuated by the absorbance of the sample. This lead to a high noise of the measured single-color time profiles. For the measurements in all other Chapters, the reference beam was sent through the sample and the beam intensities were similarly decreased yielding low-noise signals. Lens effects or other deflections

by the sample compared to air that could impair the measurement quality were not observed.

Sample volumes of 20 – 25 mL and a high flow speed ensured an exchange of probed molecules between two excitation pulses and an overall excitation of the sample below 1 %. All samples were measured back-to-back with measurements of the neat solvent. After every cycle, the absorption spectrum of the sample was examined for integrity. For each sample, three successive measurements were checked for consistency and averaged.

The transient electronic absorption signal measured after UV excitation is mostly composed of excited-state absorption (ESA) to higher lying electronic states, assumedly a continuum of states. In the Franck–Condon region, the excited state gives another signal via stimulated emission (SE), which has a negative amplitude. Other contributions come from the ground state that is repopulated after internal conversion from the excited state. Hot ground state absorption (HGSA) yields a positive signal, while the ground state recovery (GSR) signal is observed after the initial bleach, which has a negative amplitude. In samples, where intersystem crossing or photoproduct formation occurs, additional positive transient absorption signals can be observed. The spectral and temporal evolution of all these signals gives information about the electronic decay dynamics of the sample.

2.1.2 Wire-Guided Liquid Sample Film Device

For transient electronic absorption measurements, the sample solutions were flowed through a home-built wire-guided gravity-driven liquid film device based on Ref. 6. The device provided a thin and stable liquid film that makes using sample cells with expensive glass windows futile. Quartz glass has the disadvantage that it generates an artificial signal when hit simultaneously by pump and probe pulses and that it stretches the pulses due to group velocity dispersion. Also, windows can be clouded by precipitation or condensation. With application of the film, artificial signals are limited to the used solvent and the adjustment of the signal becomes easier.

The film housing shown in Fig. 2.3 consisted of an aluminum frame with two tungsten wires (Jacques Allemann SA, ⌀ 100 µm ± 2 %) tightened vertically within a distance of 4 mm. The nozzle opened between the wires and was connected to the upper reservoir by a tube. The solution was flowed through by gravity and formed a liquid film between the wires. The liquid was collected in the lower reservoir and pumped to the upper reservoir by a peristaltic pump. The device was tested for water and several organic solvents. In the latter case, wetting of the housing surface

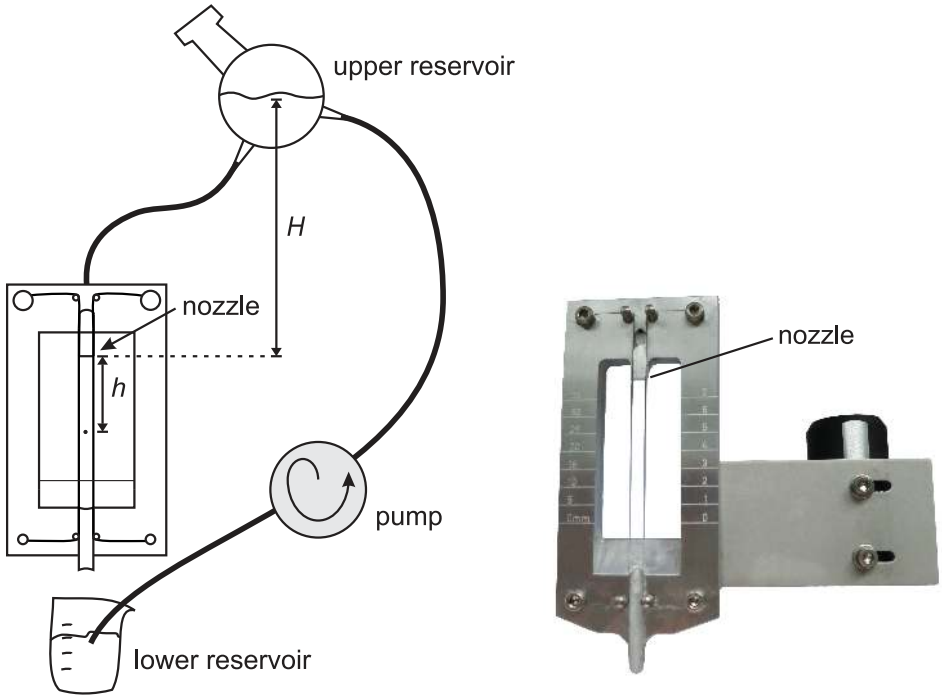

Figure 2.3: Schematic drawing and picture of the home-built wire-guided gravity-driven liquid sample film device used for measurements at room temperature. H: Height difference between the nozzle and the liquid level in the upper reservoir. h: Distance from nozzle.

is a problem and solvent evaporation must be contained.

To secure a steady water film, thickness and flow speed were adjusted. A liquid sample film device with a permanently fixed small nozzle was examined for film thickness by transmission of an aqueous adenine solution in a static absorption spectrometer. The results are shown in Fig. 2.4 and demonstrate a smooth dependence of the film thickness on the distance from the nozzle (a) and on the height difference between the nozzle and the liquid level in the upper reservoir (b). The latter determines the flow speed of the liquid, which is directly proportional to the film thickness. Measurements at different horizontal positions in the film (Fig. 2.4 c) show a practically negligible increase of the film thickness close to the wires.

The wire-guided liquid sample film was used for transient electronic absorption measurements with a film thickness of 100 µm at $h = 2.5$ cm and a flow speed of roughly 50 mL/min. The wires had to be exceptionally clean. Precipitation of the buffer and dust particles would clog the nozzle and prevent a smooth sample flow. Whenever this happened, the film was purged with clean water and the sample solutions were pressed through a syringe filter.

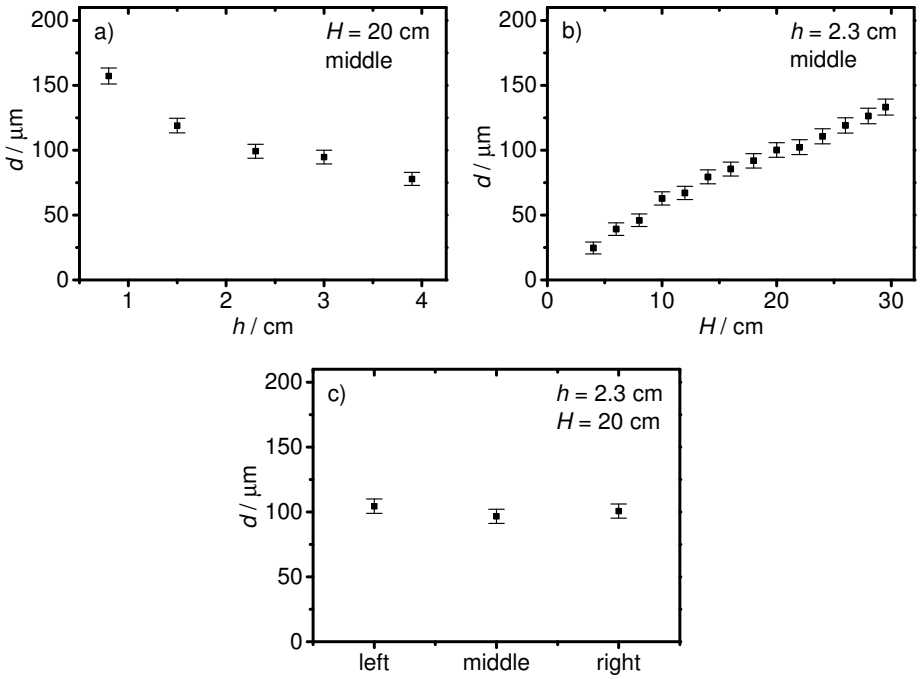

Figure 2.4: Film thickness of the wire-guided gravity-driven liquid sample film depending on a) the distance h from the nozzle, b) the height difference H between the nozzle and the liquid level in the upper reservoir, and c) the horizontal position in the film.

Cooling

For some measurements, the film housing and the sample reservoir were cooled below room temperature. For this purpose, a second liquid film device was built that is shown in Fig. 2.5. The film housing was made of steel. In this device, the upper reservoir and the nozzle were connected by a small pipe at a fixed distance. These parts were made of brass. The upper reservoir had two hollow chambers. One chamber contained the sample solution. The other chamber was joined to a hollow copper body that was attached to the film frame and both were connected to a cryostatic temperature regulator.

It was observed that the sample viscosity changed the film steadiness dependent on temperature, concentration, and the used solvent. The nozzle opening was adjusted to meet sample viscosity by exchanging pins with boreholes of different sizes. A pin with an opening of ∅ 0.6 mm was used for measurements at lowered temperatures and generated a film with a thickness of 100 µm at $T = 278$ K. The same setup would have given a film thickness of 77 µm at $T = 295$ K.

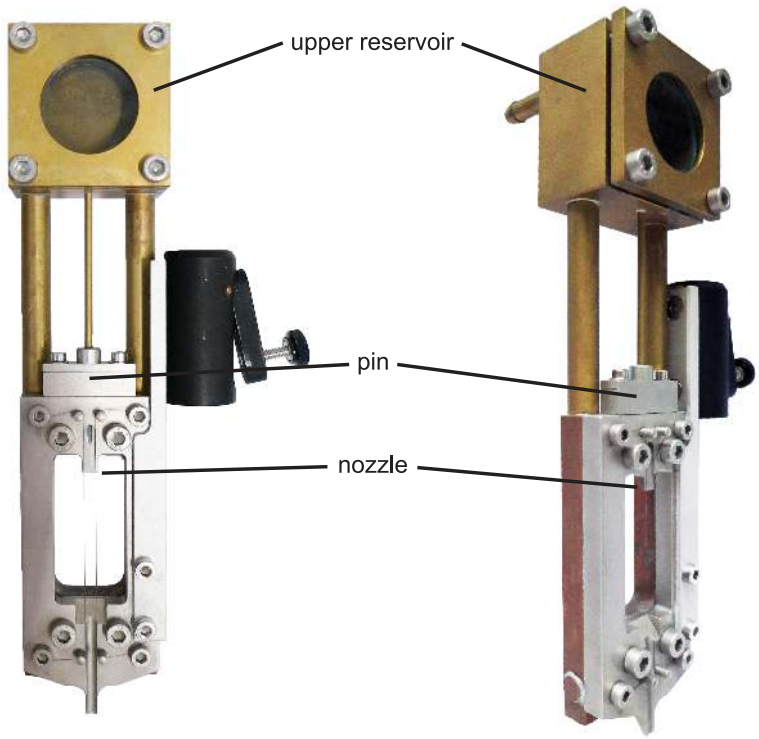

Figure 2.5: Picture of the home-built wire-guided gravity-driven liquid sample film device used for measurements at lowered temperatures in front and side view.

2.1.3 Transient Fluorescence Spectrometer

A transient fluorescence spectrometer (TFLS) with femtosecond time resolution based on the method of fluorescence up-conversion was used for the measurements shown in Chapter 4 as described in Ref. 7. The particular setup was described before since the measurements were part of a Master's Thesis.[8] In short, the sample was excited by UV pump pulses with durations of 90 fs (fwhm) at $\lambda_{\text{pump}} = 260$ nm under magic angle polarization that were generated in a home-built frequency-doubled NOPA. The excitation energy was attenuated to 50 – 100 nJ. The resulting fluorescence was collected and up-converted by the laser fundamental at $\lambda = 775$ nm in a BBO crystal. The up-converted light was run through a monochromator and detected by single photon counting at single probe wavelengths. For each sample, three successive measurements were checked for consistency and averaged. The transient fluorescence signal monitors the electronic decay dynamics of the optically bright states.

Heating

Special sample cells were used for time-resolved fluorescence measurements at elevated temperatures. The body of the cell was heated by heating rods and the sample

reservoir was kept at the same temperature. For measurements above boiling point, a pressure-resistant sample cell was borrowed from D. Schwarzer, MPI for Biophysical Chemistry, Göttingen. A high pressure pump and a fine-adjustable nozzle provided the high pressure and the necessary sample flow. The temporal resolution of the experiment was decreased by using thick, pressure-resistant windows. Further details can be found elsewhere.[8]

2.2 Data Analysis

2.2.1 Data Handling

The transient fluorescence data needed no correction procedures and were analyzed as measured.

The transient electronic absorption data were corrected for chirp, noise and coherent artifacts by procedures programmed and described in detail by K. Röttger.[1] The chirp of the broadband probe pulses was corrected for with the help of narrow band interference filters that matched the camera pixels to the wavelengths by their transmission curves. Artificial signals in transient electronic absorption spectra are generated in the solvent by the high-intensity short laser pulses and are linearly dependent on the excitation energy. They comprise stimulated Raman amplification (SRA), cross-phase modulation (XPM) and two-photon absorption (2PA) of pump and probe pulses.[9–11] In water, an additional artifact results from solvated electrons generated by 2PA of the pump pulse[12] and is observed as a build-up of a constant signal that does not decay within the measurement time frame. Neat solvent measurements that contain all of these artifacts were subtracted from the sample measurements after multiplication with an empirical factor to give clean transient signals. However, long-lived low-amplitude signal components are masked by this procedure. Both 2PA and XPM signals increase with decreasing probe wavelength. Thus, the spectra were cut off in the UV probe range at the maximum of the solvent signal which marks the white light break-off ($\lambda_{\mathrm{probe}} \approx 310$ nm).

2.2.2 Exponential Modeling

The time-resolved fluorescence experiment directly yielded time profiles. For analysis of the transient electronic absorption data, time profiles had to be extracted from the measured two-dimensional maps by spectral integration over broad or narrow probe ranges.

The data sets were simultaneously modeled by Gaussian-convoluted multi-exponential decay functions in a nonlinear least squares Levenberg–Marquardt

algorithm implemented in Mathematica,[13] when similar kinetics were expected. The used analysis routine was written by R. Siewertsen in 2009 and has been continuously improved by successive PhD students.

The temporal resolution of the experiment is determined by the pump–probe pulse convolution, which is retrieved from the standard deviation of the Gaussian width parameter σ_{IRF}. The exponential functions yielded decay components over four orders of magnitude, i. e. between 0.1 and 1000 ps. Many time profiles had to be described by an additional several-nanosecond contribution with an amplitude $< 5\,\%$ not accurately determined due to the limited delay range. This component may be an artifact from overlap with the solvated electron signal and was not further interpreted.

It must be noted, that an exponential analysis is a pure mathematical description of the transient data. It can only be interpreted with help from a realistic model for the electronic dynamics. Sequential multi-step kinetics can be described by exponential functions without approximations, but transient signals may not follow these. The shape of the decay time profiles depends critically on the steps in the deactivation mechanism and the rate at which an excited-state wavepacket approaches and departs from regions of conical intersections.[14]

2.2.3 Band Fit Analysis

The transient spectra directly measured at each delay step in the TEAS experiment were modeled by log-normal functions in a nonlinear least squares Levenberg–Marquardt algorithm implemented in Mathematica[13] in a band fit analysis program written by M. C. Stuhldreier in 2012. Subsequently, the peak positions and integrated areas of the functions were plotted against delay time. The plots finally helped to illustrate the spectral shifts and temporal decays of single transient electronic absorption bands. Exponential fits to these plots quantified the observed behavior.

2.2.4 Singular Value Decomposition

The method of singular value decomposition (SVD)[15–18] facilitates the global analysis of two-dimensional transient electronic absorption data matrices. SVD gives the number of linearly independent transient species without bias by a molecular deactivation model. The method was established in the workgroup by R. Marschan and R. Stellmacher.[19–21] The SVD analysis routine used here was written by F. Renth.[22]

In short, SVD decomposes the data matrix A into three new matrices containing the temporal (matrix U) and the spectral information (matrix V transposed), and

the singular values connecting them (matrix S). The latter is a diagonal matrix with the values ordered in a decreasing fashion.

$$A = USV^T \tag{2.2}$$

Since only singular values of significant size contribute significant information, the number of components n to be included in the analysis is adapted to the particular relative contribution of the singular values.

$$\tilde{A} = \sum_{i=1}^{n} u_{:i} s_i v_{i,:} = \tilde{U}\tilde{S}\tilde{V}^T = \tilde{T}(t)\tilde{V}^T \tag{2.3}$$

This considerably reduces the data sets, i. e. the rank of the matrices, and may correct for noise and low-amplitude artifacts. The spectral matrix $\tilde{V}$ contains the spectra corresponding to the significant singular values. The singular-value-weighted temporal matrix $\tilde{T}(t)$ contains the time traces that were modeled by suitable functions in the next step.

For the analysis, fully corrected data sets were used. The number of components were already known from exponential modeling of time profiles. The number of significant singular values was found matching and to give satisfactory results, i. e. low-residual matrices and easy-to-fit time traces. The time traces were modeled by Gaussian-convoluted multi-exponential functions in a nonlinear least squares Levenberg–Marquardt algorithm to give the electronic decay components. An additional step function and a Gaussian function at the signal start accounted for residuals from solvent and coherent signal, and made the routine powerful and fast. At times, fitting variables had to be kept fixed for the sake of computational convergence and comparability with the previously obtained results. Finally, decay-associated difference spectra (DADS) were calculated from the spectral matrix $\tilde{V}$ by multiplication with the amplitude matrix of the decay components. The DADS illustrate the spectral contribution of the lifetime components to the transient signal.

2.2.5 Arrhenius Analysis

The temperature dependence of chemical reaction rates $k(T)$ is described by the famous Arrhenius equation and relates it to an activation energy E_A (Eq. 2.4a). This empirical relation was suggested by S. Arrhenius in 1889.[23]

$$\tau^{-1} = k(T) = A\, e^{-E_\mathrm{A}/RT} \tag{2.4a}$$

$$\ln(\tau^{-1}) = \ln k = \ln A - (E_\mathrm{A}/R)\left(\frac{1}{T}\right) \tag{2.4b}$$

The rate k is written as the inverse of the reaction time τ, R is the universal gas constant. A and E_A are the Arrhenius parameters that can be determined by linear regression to the experimental data following Eq. 2.4b.

2.3 Other Devices and Materials

Static absorption spectra were taken on a Shimadzu Corporation UV-2401 PC spectrometer in the range $\lambda_{probe} = 190 - 500$ nm with quartz cuvettes of 1 mm optical path length and with neat solvent as a reference.

Static fluorescence spectra were collected on a HORIBA Jobin Yvon FluoroMax-4 spectrometer in the range $\lambda_{probe} = 275 - 505$ nm after excitation at $\lambda_{exc} = 260$ nm with quartz cuvettes of 10 mm optical path length. The measurement software was set to automatically correct the measured data for excitation energy fluctuations and to apply a fluorometric correction.

Sample solutions were prepared with ultrapure water and a pH 7.0 phosphate buffer containing 16 mM NaH_2PO_4, 34 mM Na_2HPO_4, and 117 mM NaCl. Solutions in D_2O bought from Deutero were set to pD 7.4 with the same buffer. All glassware and equipment used for the sample preparation was checked for scrupulous cleanliness by rinsing with ultrapure water and measuring fluorescence spectra of the washings. In these spectra, the background signal amplitude was less than 1/10 of the water Raman signal amplitude. The nucleobase monomers were purchased at Sigma-Aldrich. All oligonucleotides were bought from metabion international AG, where they were synthesized, purified by HPLC and lyophilized. The purities were checked by ESI mass spectrometry. The samples were diluted by agitating at room temperature. If necessary, the solutions were passed through a syringe filter. The sample concentrations were set to an optical density of OD ≈ 0.5 at 260 nm at an optical path length of 100 µm. The solutions were diluted 10-fold or 100-fold for static measurements with the help of a micropipette.

References

[1] K. Röttger, 'Ultrafast Deactivation Dynamics of Structurally Modified and Hydrogen-Bonded DNA and RNA Building Blocks', Dissertation, Christian-Albrechts-Universität zu Kiel, **2013**.

[2] K. Röttger, R. Siewertsen, F. Temps, 'Ultrafast Electronic Deactivation Dynamics of the Rare Natural Nucleobase Hypoxanthine', *Chem. Phys. Lett.* **2012**, *536*, 140–146.

[3] L. Bergmann, C. Schaefer, *Lehrbuch der Experimentalphysik. Band 3: Optik*, Walter de Gruyter, Berlin, Deutschland, 9. Aufl., **1993**.

[4] R. W. Boyd, *Nonlinear Optics Third Edition*, Elsevier Inc., **2008**.

[5] J.-C. Diels, W. Rudolph, *Ultrashort Laser Pulse Phenomena*, 2nd ed., Academic Press, Elsevier, Burlington, USA, **2006**.

[6] M. J. Tauber, R. A. Mathies, X. Chen, S. E. Bradforth, 'Flowing liquid sample jet for resonance Raman and ultrafast optical spectroscopy', *Rev. Sci. Instrum.* **2003**, *74*, 4958–4960.

[7] N. K. Schwalb, 'Ultrafast Electronic Deactivation Dynamics in DNA Model Systems by Femtosecond UV Fluorescence Spectroscopy', Dissertation, Christian-Albrechts-Universität zu Kiel, **2009**.

[8] U. C. Stange, 'Untersuchung der Temperaturabhängigkeit der ultraschnellen elektronischen Desaktivierung von Adenin und dem Adenindinukleotid', Masterarbeit, Christian-Albrechts-Universität zu Kiel, **2012**.

[9] M. Lorenc, M. Ziolek, R. Naskrecki, J. Karolczak, J. Kubicki, A. Maciejewski, 'Artifacts in femtosecond transient absorption spectroscopy', *Appl. Phys. B* **2002**, *74*, 19–27.

[10] A. L. Dobryakov, S. A. Kovalenko, N. P. Ernsting, 'Electronic and vibrational coherence effects in broadband transient absorption spectroscopy with chirped supercontinuum probing.', *J. Chem. Phys.* **2003**, *119*, 988–1002.

[11] A. L. Dobryakov, S. A. Kovalenko, N. P. Ernsting, 'Coherent and sequential contributions to femtosecond transient absorption spectra of a rhodamine dye in solution.', *J. Chem. Phys.* **2005**, *123*, 044502.

[12] K. R. Siefermann, B. Abel, 'The Hydrated Electron: A Seemingly Familiar Chemical and Biological Transient', *Angew. Chem. Int. Ed.* **2011**, *50*, 5264–5272.

[13] Mathematica, Version 8.0, Wolfram Research, Inc., Champaign, IL, U.S.A. Champaign, Illinois, **2010**.

[14] B. P. Molesky, A. M. Moran, 'Fourth-Order Perturbative Model for Photoinduced Internal Conversion Processes', *J. Phys. Chem. A* **2013**, *117*, 13954–13966.

[15] I. van Stokkum, D. S. Larsen, R. van Grondelle, 'Global and Target Analysis of Time-Resolved Spectra', *Biochim. Biophys. Acta* **2004**, *1657*, 82–104.

[16] N. Mouton, A. de Juan, M. Sliwa, C. Ruckebusch, 'Hybrid Hard- and Soft-Modeling Approach for the Resolution of Convoluted Femtosecond Spectrokinetic Data', *Chemom. Intell. Lab. Syst.* **2011**, *105*, 74–82.

[17] C. Ruckebusch, M. Sliwa, P. Pernot, A. de Juan, R. Tauler, 'Comprehensive data analysis of femtosecond transient absorption spectra: A review', *J. Photochem. Photobiol. C* **2012**, *13*, 1–27.

[18] *Essential Numerical Computer Methods*, (Ed.: M. Johnson), Academic Press, Elsevier, Burlington, USA, **2010**.

[19] R. Marschan, 'Globale Analyse von femtosekunden-zeitaufgelösten transienten Absorptionsdaten in MATLAB mittels Singulärwertzerlegung', Masterarbeit, Christian-Albrechts-Universität zu Kiel, **2015**.

[20] R. Stellmacher, 'Globale Analyse transienter Absorptionsdaten für das seltene RNA-Nukleotid Xanthosinmonophosphat', Masterarbeit, Christian-Albrechts-Universität zu Kiel, **2016**.

[21] K. Röttger, R. Stellmacher, M. Stuhldreier, F. Temps, 'Ultrafast Electronic Deactivation Dynamics of Xanthosine Monophosphate', *Molecules* **2017**, *22*, 160.

[22] F. Renth, Unpublished results.

[23] S. A. Arrhenius, 'Über die Reaktionsgeschwindigkeit bei der Inversion von Rohrzucker durch Säuren', *Z. Physik. Chem.* **1889**, *4*, 226–248.

3 Ultrafast electronic deactivation of UV-excited adenine and its ribo- and deoxyribonucleosides and -nucleotides: A comparative study

Uta C. Stange, and Friedrich Temps[1]

Institute of Physical Chemistry, Christian-Albrechts-University Kiel, Olshausen-str. 40, 24098 Kiel, Germany

U. C. Stange, F. Temps, 'Ultrafast electronic deactivation of UV-excited adenine and its ribo- and deoxyribonucleosides and -nucleotides: A comparative study', *Chem. Phys.* **2018**, doi: 10.1016/j.chemphys.2018.08.031.

Own contributions:

- static spectroscopy
- transient electronic absorption spectroscopy
- data analysis
- writing the draft

1 Author to whom correspondence should be addressed. Email: temps@phc.uni-kiel.de

Abstract

The high stability of the DNA bases after UV photoexcitation is generally ascribed to their intrinsic ability to dissipate the supplied electronic energy on ultrafast time scales. The sugar-phosphate backbone of the related nucleosides and nucleotides may modulate the efficiency of these relaxation processes by hydrogen bonding and/or intramolecular energy transfer. To elucidate these effects, we performed a comparative study of the excited-state lifetimes of 9H-adenine, its nucleosides adenosine and deoxyadenosine, and its nucleotides adenosine monophosphate and deoxyadenosine monophosphate by transient electronic absorption spectroscopy under otherwise constant experimental conditions. All five adenine derivatives were found to exhibit virtually identical spectro-temporal behavior with uniform excited-state lifetimes of $\tau_1 = 0.19 \pm 0.03$ ps and $\tau_2 = 0.45 \pm 0.05$ ps. The results support a common deactivation mechanism within the adenine unit that leaves the DNA sugar-phosphate backbone groups idle.

Keywords: Adenine; conical intersections; femtosecond transient absorption; radiationless transitions

3.1 Introduction

Of the five canonical nucleic acid bases, the purine base adenine (Ade) appears to have the shortest excited electronic state lifetime after absorption of ultraviolet (UV) light in aqueous solution.[1–11] The ensuing ultrafast internal conversion is mediated by structural deformations that lower the energy of the excited state and lead to distinct conical intersections (CIs), through which the molecules are funneled back to their ground electronic state. This rapid electronic energy dissipation is a well established property of all canonical nucleobases[12–14] that protects the molecules and their polymeric deoxyribonucleic acids (DNA) against photodamage and sustains the stability of the genomic information of life on Earth.

A fundamental question that has been raised in several recent theoretical papers[15–19] is whether the deoxyribose-phosphate DNA backbone can in any way contribute to the ultrafast electronic deactivation of the nucleobases. As the backbone itself does not absorb at wavelengths above 200 nm, it cannot be directly photoexcited in the near-UV. It may, however, affect the electronic relaxation pathways and energies of the CIs by hydrogen bonding[18,19] or inter- and intramolecular vibra-

tional energy transfer.[20] For example, Domcke and co-workers recently predicted a deactivation pathway in adenosine, where an intramolecular hydrogen bond between the chromophore and the sugar facilitates internal conversion to the S_0 ground state (GS).[18,19] Such a mechanism might not appear likely in aqueous solution because of ubiquitous H-bonding with surrounding water molecules. Intriguingly, however, a systematic study of the excited electronic state lifetime of the Ade chromophore in dependence of the sugar-phosphate units still seems to be missing to date, to the best of our knowledge.

The molecular structures of the canonical nucleobase 9H-Ade, its nucleosides adenosine (Ado) and 2'-deoxyadenosine (dAdo), and its nucleotides adenosine 5'-monophosphate (AMP) and 2'-deoxyadenosine 5'-monophosphate (dAMP) are depicted in Fig. 3.1, together with the structure of the minor 7H-Ade tautomer that contributes in aqueous solution of Ade at room temperature with a fraction of about 22 %.[21]

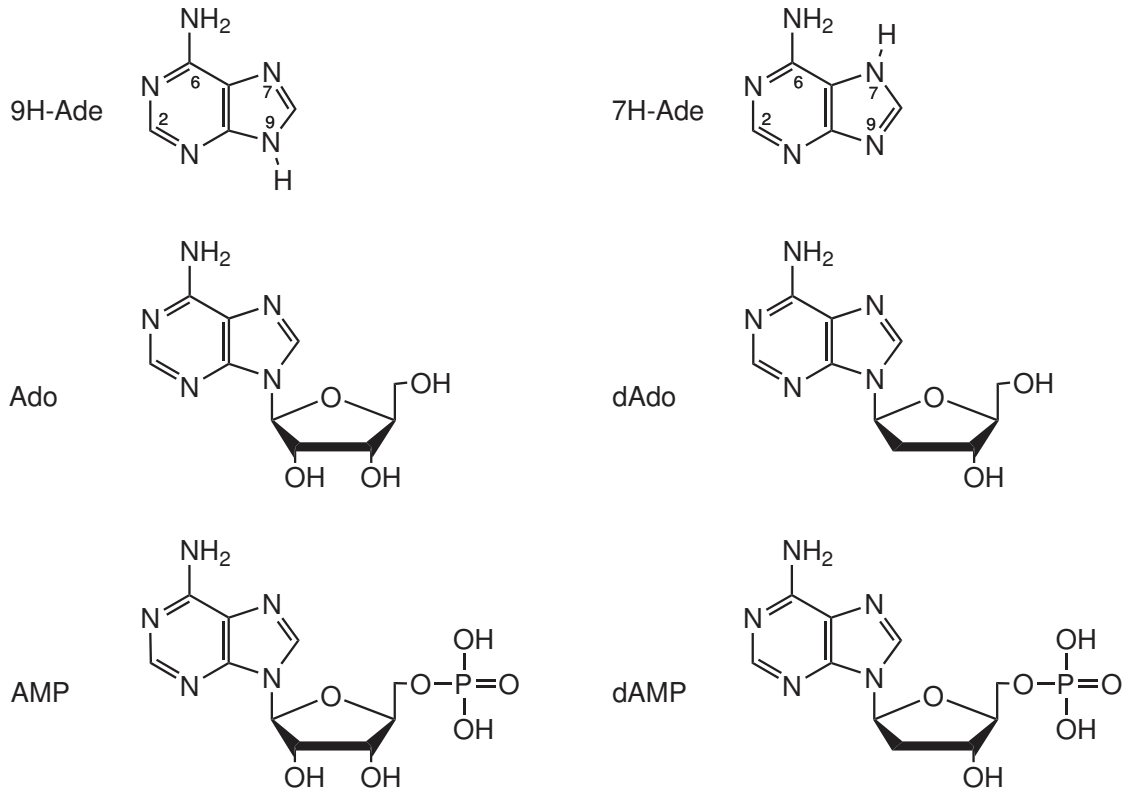

Figure 3.1: Molecular structures of the free nucleobase adenine in its 9H and 7H tautomeric forms (9H-Ade and 7H-Ade), the nucleosides adenosine (Ado) and 2'-deoxyadenosine (dAdo), and the nucleotides adenosine 5'-monophosphate (AMP) and 2'-deoxyadenosine 5'-monophosphate (dAMP).

Figure 3.2 compares the static UV absorption spectrum of the molecules in water at pH 7.0. The spectrum of free Ade exhibits an asymmetric peak at $\lambda = 261$ nm and a shoulder at $\lambda = 270$ nm, and is an overlay of the spectra of the two tautomers. The shoulder can be assigned to 7H-Ade, which has a red-shifted absorption compared to 9H-Ade.[22] The UV spectra of the canonical Ade nucleosides and nucleotides exhibit symmetric maxima at $\lambda = 260$ nm with virtually identical band shapes. The lowest energy absorption band in all cases results from $\pi\pi^*$ excitation of the Ade unit.

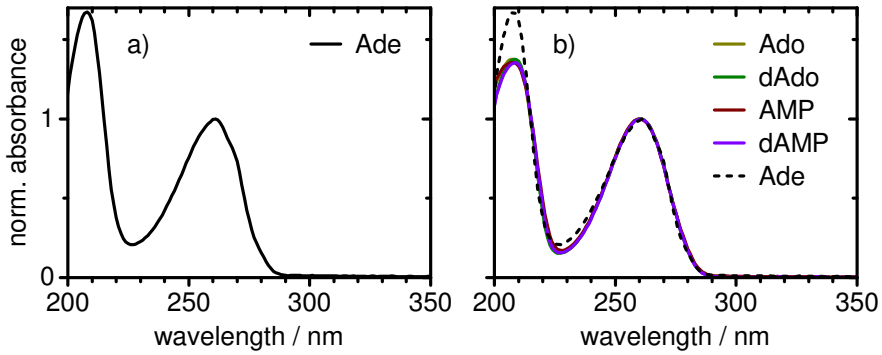

Figure 3.2: Static UV absorption spectrum of (a) the free base Ade in natural tautomeric composition in comparison with (b) the UV absorption spectra of the nucleosides Ado and dAdo and the nucleotides AMP and dAMP in buffered aqueous solution (pH 7.0). The vertical scales were normalized to the absorption maxima at $\lambda = 260$ nm. The spectra of Ado, dAdo, AMP, and dAMP are virtually indistinguishable, while that of Ade differs due to the presence of the minor 7H besides the major 9H tautomer.

Time-resolved measurements of 9H-Ade and its N^9-derivatives Ado, dAdo, AMP and dAMP in water after $\pi\pi^*$ excitation established bi-exponential decay kinetics with sub-picosecond lifetimes.[1–11] A fast component of $\tau \sim 0.1$ ps is usually attributed to the initial departure of the excited wavepacket from the Franck-Condon (FC) region, while somewhat scattered longer lifetime values in the range of $\tau = 0.2 - 0.5$ ps are generally assigned to the actual nonadiabatic deactivation step back to the GS. Theoretical calculations suggested two major relaxation pathways, one through a CI involving ring puckering at the C^2–H position, the other through a CI reached by out-of-plane motion of the NH_2 group.[10,17,23–35] More recently, the $n\pi^*$ state has been brought into play again as an optically dark intermediate state in the mechanism.[36] In the gas phase, the ~ 1 ps excited-state lifetime of 9H-Ade has indeed been attributed to this $n\pi^*$ state.[37–45] The non-canonical minor 7H-Ade tautomer, on the other hand, that coexists in aqueous solution besides 9H-Ade

shows an excited-state lifetime of $\tau \sim 8$ ps, indicating distinctively different decay dynamics.[4,7,8,11] The slow-down is believed to be connected to the proximity of the NH_2 and N^7–H groups, which modifies the potential energy hypersurface (PEHS) and impedes relaxation.[29,46]

In experimental studies of the excited-state dynamics of adenine-containing DNA oligonucleotides,[6,9,47–57] the nucleosides and nucleotides Ado, dAdo, AMP or dAMP have often been adopted as references for the dynamics of the monomeric chromophore. Quantum chemical excited-state dynamics calculations of DNA systems, on the other hand, usually considered only stacks of two or several 9H-Ade molecules without the sugar-phosphate backbone to reduce the size and complexity of the systems.[55,58–66] In this way, however, intramolecular hydrogen bonding contributions or effects by energy transfer to the sugar-phosphate moieties in the backbone modulating the intrinsic photophysical properties of the Ade chromophore may be overlooked. In the DNA double helix, in particular, the nucleobases are shielded from bulk water molecules, such that distinct H-bonding sites become accessible. Taking the pyrimidine bases, moreover, the lifetimes of the nucleosides or nucleotides are known to differ substantially from those of the free bases.[3,5,20,67,68]

Stimulated by the above questions, we initiated a series of systematic back-to-back measurements of the excited electronic state lifetimes of the free nucleobase 9H-Ade, its nucleosides Ado and dAdo, and its nucleotides AMP and dAMP under otherwise identical conditions in aqueous solution at pH 7.0. All experiments were carried out by femtosecond transient electronic absorption spectroscopy following photoexcitation at $\lambda_{pump} = 260$ nm. A critical comparison of the results after global data analyses indicates common electronic deactivation pathways within the adenine unit for all five molecules.

3.2 Experimental section

Our femtosecond transient electronic absorption spectrometer for simultaneous broadband and single-color detection has been described in some detail before.[69] For the present measurements, the previous flow sample cell was replaced by a windowless wire-guided liquid jet with ~ 100 µm optical path length similar to the design of Refs. 70, 71. A high flow speed ensured an exchange of the probe volume between successive excitation pulses, while a large (25 mL) reservoir volume limited the overall excitation of sample molecules to $\leq 1\,\%$ for the duration of an experimental run. The data acquisition times were short enough to ensure constant sample concentrations by negligible evaporation of solvent water during a measurement.

All samples (Ade, 99 %; Ado, ≤ 99 %; dAdo, ≤ 99 %; AMP, ≤ 100 % and dAMP, 98 − 100 %; all Sigma–Aldrich) were investigated at concentrations of $c = 3.7$ mM in ultra-pure water at pH 7.0 set by phosphate buffer (16 mM NaH_2PO_4, 34 mM Na_2HPO_4, 117 mM NaCl). The applied excitation pulses at $\lambda_{pump} = 260$ nm with pulse durations of $\Delta t = 35$ fs (full width at half maximum) were generated in a home-built frequency-doubled non-collinear optical parametric amplifier (NOPA) and focused into the sample under magic-angle polarization. The pulse energies were attenuated to 100 nJ. Broadband detection pulses were generated in CaF_2 by careful adjustment of the Ti:Sa fundamental pump pulse energy to yield stable white-light intensity over a spectral range between $\lambda_{probe} = 310 - 570$ nm. Additional single-color detection pulses at $\lambda_{probe} = 255$ nm with pulse durations of $\Delta t = 50$ fs full width at half maximum (fwhm) were generated in a second frequency-doubled NOPA.

For each sample, three successive measurements were done to check for consistency and averaged for final analysis. All runs were done back-to-back with measurements of the neat solvent. After each run, the static UV absorption spectrum was checked for sample integrity. The recorded transient electronic absorption maps and the single color absorption–time profiles were corrected for cross-phase modulation (XPM), solvent contributions and white-light chirp as described in the literature.[69,72] The maps were cut off at the maximum of the solvent signal in the UV part of the probe spectrum to avoid distortions by white-light break-off.

The obtained data were analyzed first at single wavelengths using a non-linear least-squares fitting routine based on the Marquardt–Levenberg algorithm. Final results were then provided by a systematic global analysis based on singular value decomposition (SVD).[73–75] All routines were implemented using Mathematica.[76] Error limits given below refer to 2σ standard deviations.

3.3 Results

3.3.1 Excited-state dynamics

Fig. 3.3 presents the measured two-dimensional (2D) spectro-temporal electronic absorption maps of the change in optical density ΔOD caused by the 260 nm pump pulses as a function of pump–probe delay and probe wavelength for all five sample molecules. As can be seen, all ΔOD maps show spectrally broad initial excited-state absorption bands (ESA) expanding over practically the entire probe wavelength range. The bands shift towards the UV edge of the probe spectrum within a few hundred fs and decay on very similar time scales. Corresponding transient spectra

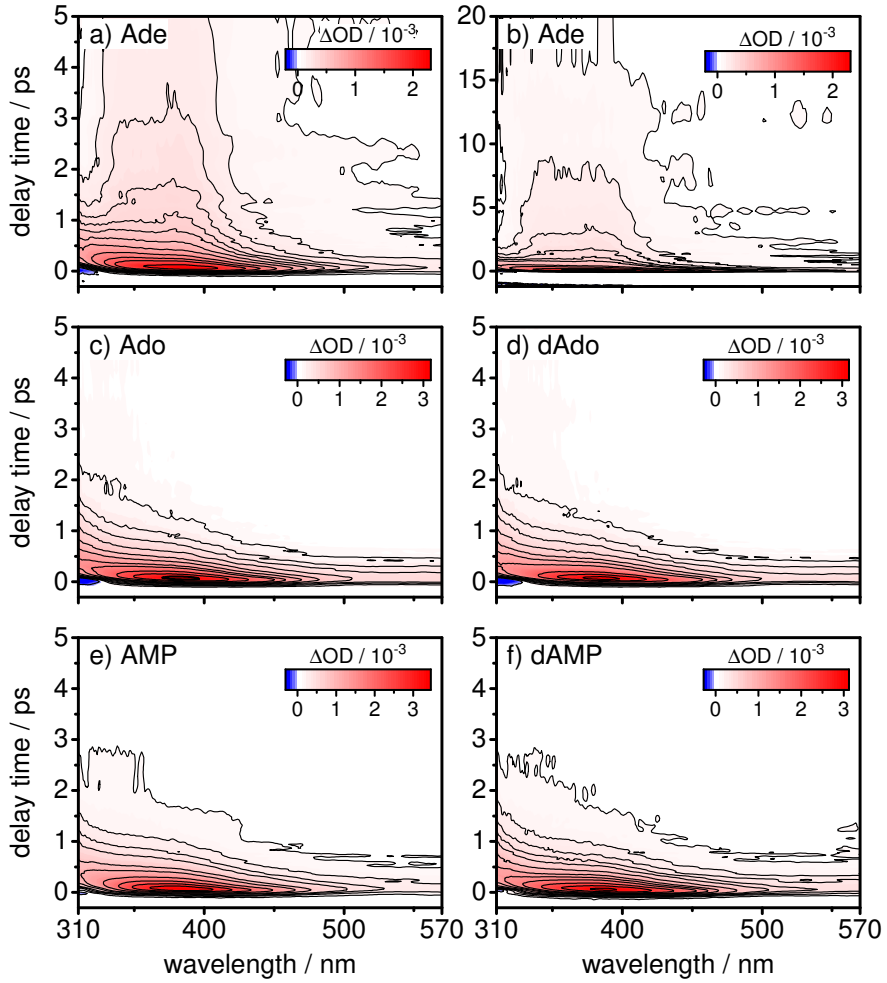

Figure 3.3: Two-dimensional spectro-temporal electronic absorption maps of the change in optical density ΔOD after excitation at $\lambda_{pump} = 260$ nm for (a) Ade (b on an extended time scale), (c) Ado, (d) dAdo, (e) AMP and (f) dAMP. The data are plotted only up to $\Delta t = 5$ ps (20 ps for Ade), but were recorded up to $\Delta t = 600$ ps.

at selected pump–probe delay times illustrating the spectro-temporal evolution are displayed in Fig. 3.4. The short-lived ESA belongs to 9H-Ade and its N^9-substituted derivatives on the grounds that the transient absorption maps for free Ade and the nucleosides and nucleotides show very similar broad and short-lived ESA. An additional weak transient absorption between $\lambda_{probe} = 330$ and 400 nm in the map for the free Ade base (cf. Fig. 3.3b) that decays to near zero within $\Delta t \sim 15$ ps and is absent in the nucleoside and nucleotide cases can be assigned to the minor 7H-Ade tautomer. By a weak absorption maximum near $\lambda_{probe} = 390$ nm at delay times of $\Delta t > 0.75$ ps, Fig. 3.3a indicates that the longer-lived ESA of the 7H-Ade tautomer is

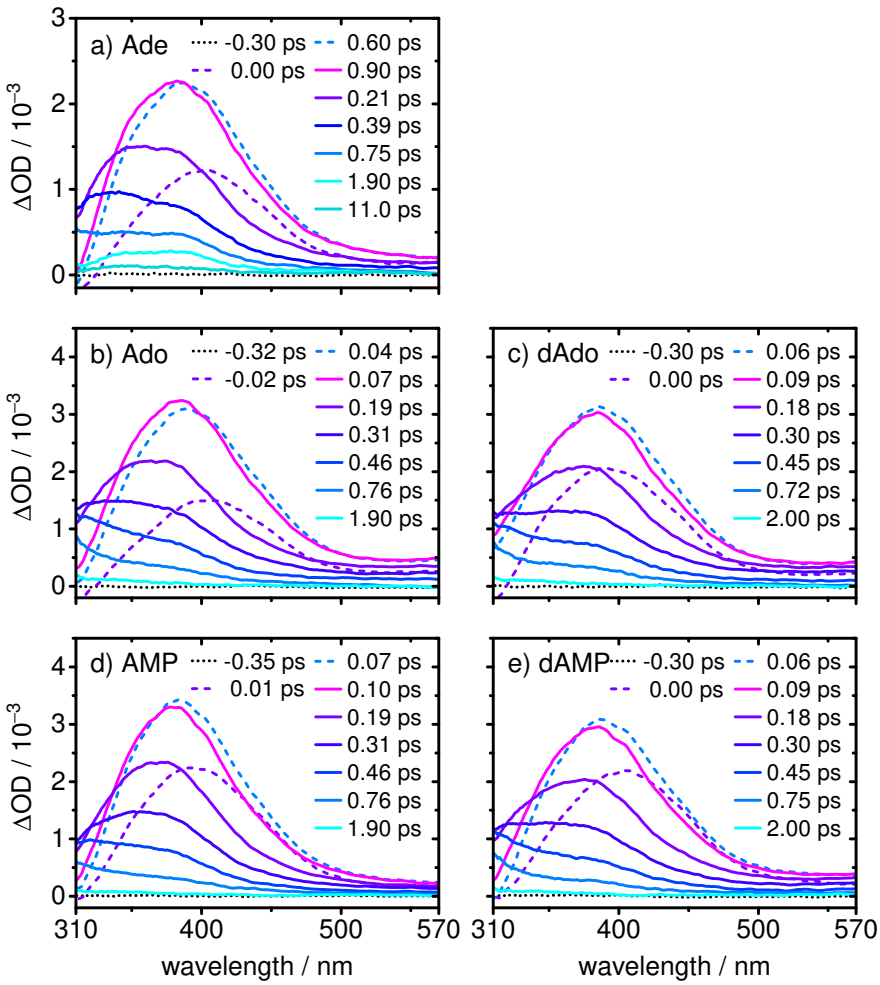

Figure 3.4: Transient spectra of (a) Ade, (b) Ado, (c) dAdo, (d) AMP and (e) dAMP after excitation at $\lambda_{\text{pump}} = 260$ nm at selected pump–probe delay times. Dashed lines indicate delay times during the rise of the signal.

red-shifted compared to that of 9H-Ade. For all samples, furthermore, the transient signals around $\lambda_{\text{probe}} = 315$ nm are negative at short delay times, before showing a delayed rise and subsequent decay to near zero within $\Delta t \sim 3$ ps. This behavior is interpreted as an overlay of stimulated emission (SE, negative), ESA (positive), and hot ground state absorption (HGSA, positive). The latter can be observed after internal conversion of the excited state to the ground electronic state, and is known to decay within a few picoseconds.[2,57,69,77,78]

3.3.1.1 Single-wavelength analysis

The quantitative analysis of the measured spectro-temporal absorption maps was carried out in three steps: First, time profiles were taken from each data set at

nine selected wavelengths distributed over the broadband probe spectrum and modeled independently by nonlinear least squares fitting using multi-exponential decay functions convoluted with Gaussians to account for the instrument response function (IRF). All five Ade derivatives were found to yield similar decay dynamics hinting at similar electronic deactivation processes. Second, the time profiles for all samples at $\lambda_{\text{probe}} = 380$ nm were selected for a combined analysis. The 380 nm probe wavelength was chosen because it corresponds to the maximum of the transient signals and contains mainly contributions from ESA. The respective time profiles could be nicely modeled with multi-exponential decay functions with simultaneously fitted time constants. The experimental and the fitted time profiles are compared in Fig. 3.5. The simultaneous fit yielded two time constant values,

$$\tau_1 = 0.17 \pm 0.01 \text{ ps},$$

$$\tau_2 = 0.51 \pm 0.04 \text{ ps},$$

with an amplitude ratio of about $4-1$ and an IRF width parameter of $\sigma_{\text{IRF}} = 0.047 \pm 0.001$ ps. An additional third decay component of

$$\tau_3 = 6.7 \pm 0.7 \text{ ps}$$

was required to describe the contribution from 7H-Ade in the time profile of free Ade.

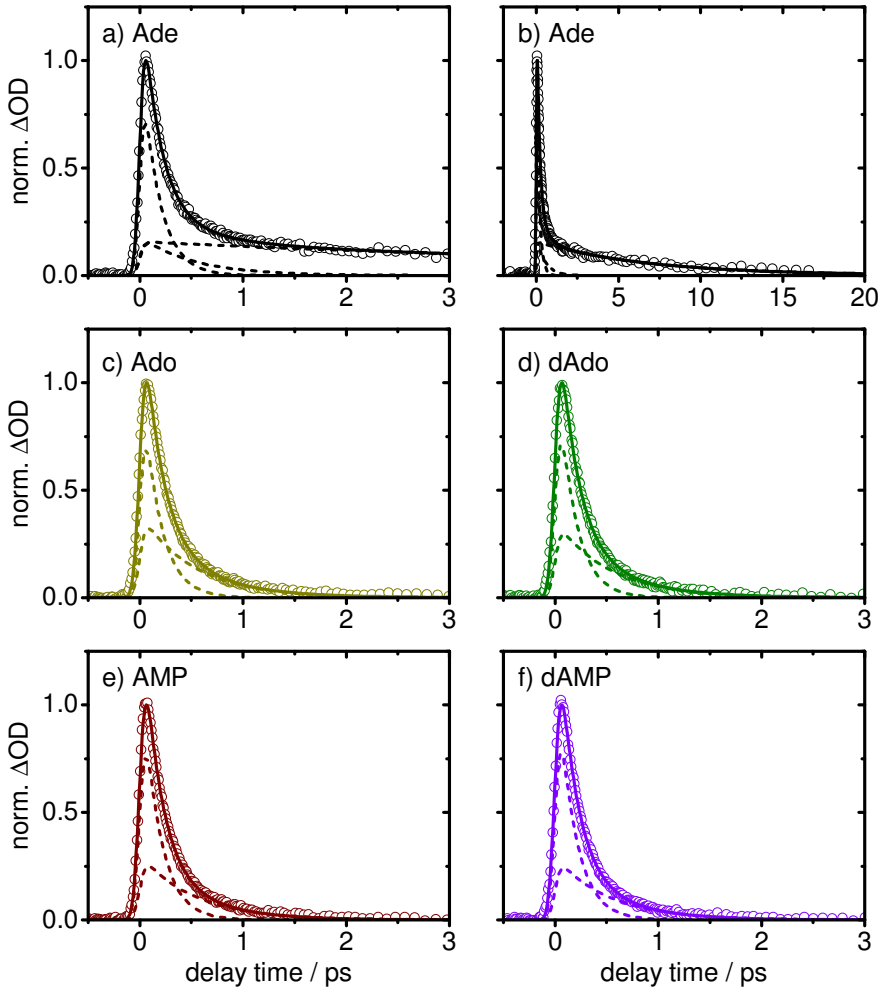

Figure 3.5: Transient absorption–time profiles at $\lambda_{probe} = 380$ nm after excitation at $\lambda_{pump} = 260$ nm for (a) Ade (b for Ade on an extended time scale), (c) Ado, (d) dAdo, (e) AMP and (f) dAMP. Open circles represent data points, solid lines show the best fit curves from a combined simultaneous fit to all five decay curves, and dashed lines indicate the contributions of the different time constant components, which are given in the text.

3.3.1.2 Global analysis

The final analysis of the measured spectro-temporal absorption matrices for the different adenine sample compounds was performed by SVD to derive a bias-free global model for the data over the full probe wavelength spectrum and pump–probe delay time range. The method separates the spectral from the temporal information by giving independent SVD time traces and decay-associated difference spectra (DADS) as displayed in Fig. 3.6.

The SVD time traces are multi-peak functions that can be described by multi-

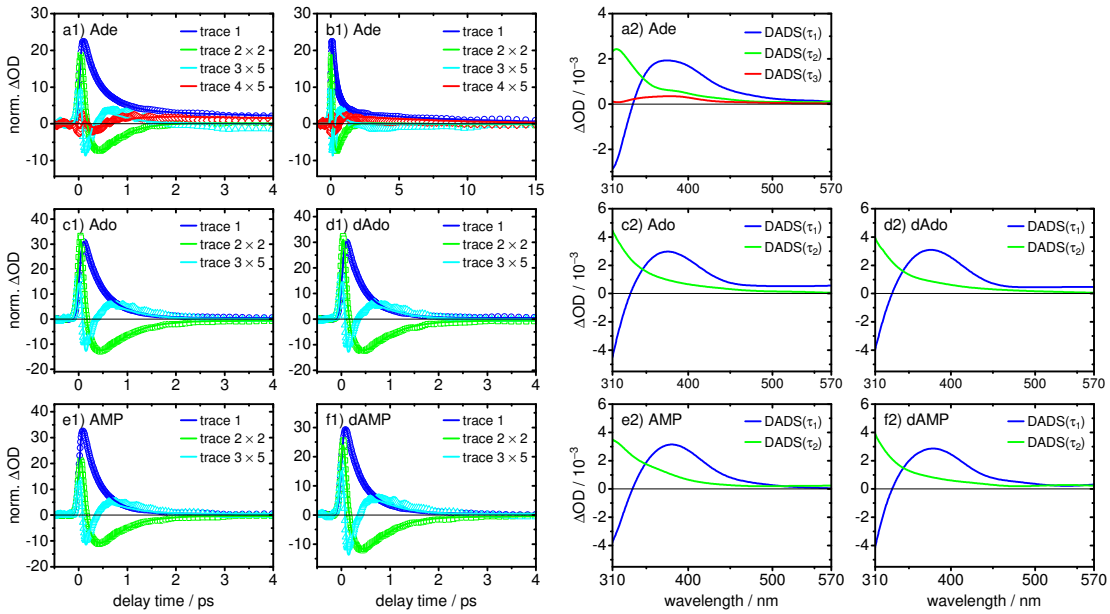

Figure 3.6: SVD time traces (left) and decay-associated difference spectra (DADS, right) from the global analysis of the spectro-temporal transient electronic absorption data of the free base Ade plotted on time scales up to $\Delta t = 4$ ps (a) and 20 ps (b), the nucleosides Ado (c) and dAdo (d), and the nucleotides AMP (e) and dAMP (f). Time traces 2 – 4 were scaled by the given factors for visibility. The third component (red), which shows up in the data for free Ade only, belongs to 7H-Ade.

exponential decay functions convoluted with a Gaussian for the IRF. As shown in Fig. 3.6, they converged to zero within error limits after $\Delta t \sim 15$ ps for free Ade (Fig. 3.6a1, b1) and $\Delta t \sim 3$ ps for the Ade nucleosides and nucleotides (Fig. 3.6c1–f1). Small amplitude oscillations observable for the nucleosides and nucleotides were assumed to be residues from the chirp corrections and experimental noise and therefore not modeled. The time constant parameters derived from this global analysis are listed in Table 3.1. They are virtually identical within experimental errors for the five adenine derivatives and in good agreement with the above results from the simultaneous single-wavelength analysis of the absorption–time profiles at $\lambda_{\text{probe}} = 380$ nm.

The decay-associated difference spectra from the SVD analysis for the five samples are given in Fig. 3.6a2–f2. The DADS are virtually identical for the first two time components. The first time component features a negative contribution in the range 310 nm $\leq \lambda_{\text{probe}} \leq$ 330 nm, which is due to short-lived initial SE and a slightly delayed rise of the ESA signal. The spectrum then turns positive and exhibits a pronounced maximum around $\lambda_{\text{probe}} \sim 375$ nm, corresponding to fast ESA

Table 3.1: Lifetime parameters for the electronic deactivation of Ade, Ado, dAdo, AMP and dAMP from the global SVD analyses of the respective data. Values in parentheses are 2σ standard deviations of the last decimal digit. IRF width parameter from SVD: $\sigma_{\mathrm{IRF}} = 0.055 \pm 0.006$ ps.

Ade derivative	τ_1 / ps	τ_2 / ps	τ_3 / ps
Ade	0.16(1)	0.42(1)	7.2(5)
Ado	0.21(1)	0.47(1)	-
dAdo	0.20(1)	0.48(1)	-
AMP	0.19(1)	0.43(1)	-
dAMP	0.19(1)	0.46(1)	-
$\langle$av.$\rangle$	$\langle$0.19(3)$\rangle$	$\langle$0.45(5)$\rangle$	$\langle$7.2(5)$\rangle$

from the initial excited state, with an extended red wing all the way to $\lambda_{\mathrm{probe}} = 570$ nm. The second DADS component has its maximal amplitude at $\lambda_{\mathrm{probe}} = 310$ nm and decreases steadily with increasing wavelength. This hints at HGSA near the UV edge of the probe spectrum ($\lambda_{\mathrm{probe}} < 350$ nm), but will be assigned (see Discussion) mainly to ESA at $\lambda_{\mathrm{probe}} > 350$ nm. The value of τ_2 from the SVD time trace analysis thus reflects a mixture of ESA and HSGA decay. The third component is the additional ESA band for the 7H-Ade tautomer, which shows a symmetric spectrum with maximum at $\lambda_{\mathrm{probe}} \sim 380$ nm. Thus, the transients for 9H- and 7H-Ade are well separated by the SVD analysis.

3.3.2 Ground-state recovery dynamics

Single-color measurements of the transient ΔOD signals in the deep-UV at $\lambda_{\mathrm{probe}} = 255$ nm gave the time profiles displayed in Fig. 3.7. The observed negative amplitudes are the net result of the initial ground state bleach (GSB) of the UV absorption caused by the 260 nm pump pulses and ESA contributions at the 255 nm probe wavelength, while the measured time evolution is attributed to the slower subsequent ground state recovery (GSR) dynamics. As shown, the time profiles could be nicely modeled using two exponentials convoluted with the Gaussian IRF using time constant values of

$$\tau_1' = 0.25 \pm 0.04 \text{ ps},$$
$$\tau_2' = 2.00 \pm 0.20 \text{ ps}.$$

As will be further discussed below, the 2 ps second component (τ_2') will be identified as the vibrational cooling time τ_c for the "internally hot" molecules returned by the

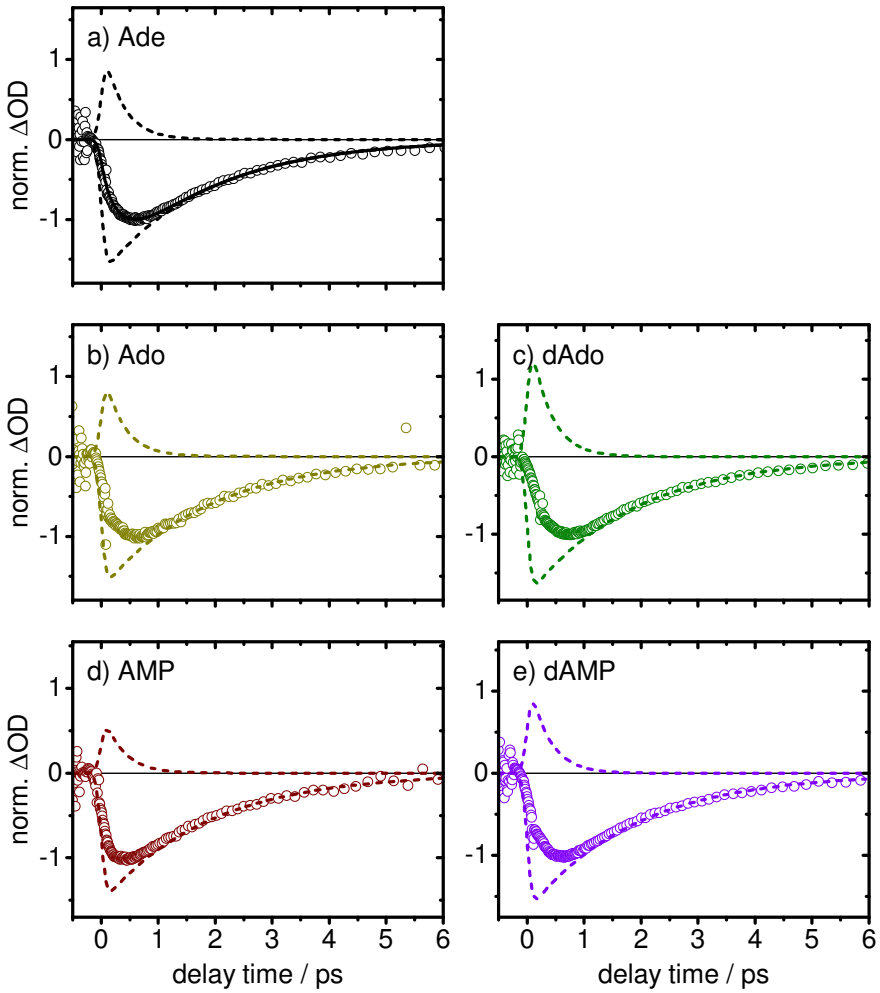

Figure 3.7: Ground state recovery time profiles at $\lambda_{probe} = 255$ nm for (a) Ade, (b) Ado, (c) dAdo, (d) AMP and (e) dAMP after excitation at $\lambda_{pump} = 260$ nm. Open circles are data, solid lines best fit curves from a combined simultaneous fit, dashed lines show the contributing single time components. The high noise at negative delay times is due to an experimental artifact Ref. 79.

internal conversion step from the excited to the ground electronic state. A third GSR component that might be expected for the 7H-Ade tautomer could not be identified in the 255 nm probe profiles, probably because of a low amplitude.

reference beam vertically and steering it through the unexcited film above than the pump beam, rather than horizontally displaced through air.

3.4 Discussion

The above systematic investigation of the transient electronic absorption maps after photoexcitation of the free nucleobase Ade, the nucleosides Ado and dAdo, and

the nucleotides AMP and dAMP at $\lambda_{pump} = 260$ nm showed virtually identical excited-state lifetimes for all five canonical (i.e. N^9-substituted) Ade derivatives.

3.4.1 Comparison of the experimental results for Ade and the N^9-Ade derivatives

The excellent agreement between the observed data is demonstrated by the direct comparison of the observed transient absorption–time profiles at $\lambda_{probe} = 380$ nm in Fig. 3.8a, where the only outlier in the series reflects the (known) contribution by the minor 7H-Ade tautomer in the Ade measurement. Subtraction of this contribution would give virtually perfect agreement for all five N^9-Ade derivatives. The same nearly perfect agreement within experimental errors is illustrated by the superimposed decay-associated difference spectra belonging to time constants τ_1 and τ_2 in Fig. 3.8b, where only the Ade measurement showed the extra (substantially longer) τ_3 component due to the presence of the 7H-Ade tautomer.

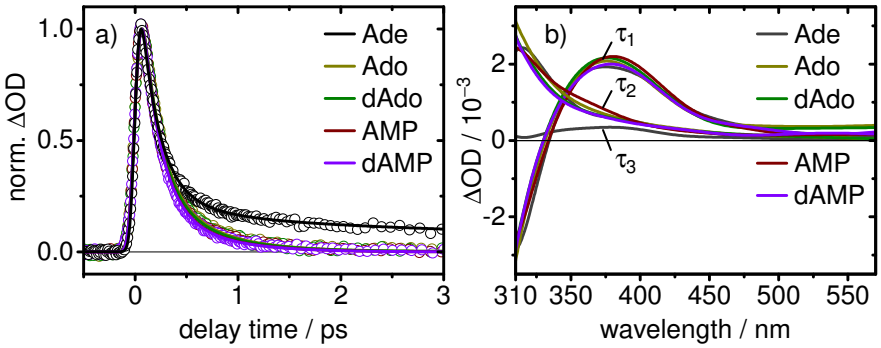

Figure 3.8: Comparison of the obtained main experimental results for Ade, Ado, dAdo, AMP and dAMP. (a) Transient absorption-time profiles at $\lambda_{probe} = 380$ nm; (b) decay-associated difference spectra belonging to the time constant parameters τ_1, τ_2 and (7H-Ade only) τ_3.

3.4.2 Time constants and electronic deactivation mechanism

With the above comparison of our five N^9-Ade derivatives as firm experimental basis, the assignment of the different time constant parameters comes into view. Taking into account our global SVD results, the deep-UV GSR measurements at $\lambda_{probe} = 255$ nm, and complementing evidence from the literature, the following terms have to be discussed:

$$\tau_{FC} < 100 \text{ fs},$$
$$\tau_1 = 0.19 \pm 0.03 \text{ ps},$$
$$\tau_2 = 0.45 \pm 0.05 \text{ ps},$$

$\tau_c = 2.00 \pm 0.20$ ps,

$\tau_3 = 7.20 \pm 0.50$ ps.

3.4.2.1 Excited electronic states of the Ade chromophore

9H-Ade and its N^9-derivatives are known to have two optically bright $^1\pi\pi^*$ excited states, commonly referred to as L_a and L_b using Platt's notation,[80] and one optically dark $^1n\pi^*$ state within reach in the mid-UV spectral range. A weak band at 35 497 cm^{-1} identified in the measured gas phase vibronic spectra has been assigned to the electronic origin of the $^1n\pi^*$ state (S_1), a stronger one at 36 105 cm^{-1} marks the origin of the first $^1\pi\pi^*$ state (S_2).[81,82] Of the two $^1\pi\pi^*$ configurations, the L_a state stands out for the highest oscillator strength, so that it determines the mid-UV absorption spectrum of the molecule. At vertical excitation from the GS, the majority of the reported theoretical calculations placed the $^1\pi\pi^*$ (L_a) state as S_3 in gas phase Ade, while the orderings for the computed $^1n\pi^*$ and $^1\pi\pi^*$ (L_b) vertical energies vary between S_1 and S_2.[10,17,23–29,32–35] However, all three excited states are close in energy, especially near the $^1n\pi^*$ and $^1\pi\pi^*$ (L_b) minimum energy configurations, and connected by various CIs such that fast population transfer between them is possible.[10,17,23–35,83–89]

The prediction of the correct vertical and adiabatic energetic orderings of these excited states under different conditions has indeed been found to be an extremely difficult task.[17,30,83,87,88] In aqueous solution, in particular, the $^1\pi\pi^*$ (L_a) state is energetically stabilized, the $^1n\pi^*$ is destabilized, and only the $^1\pi\pi^*$ (L_b) state remains more or less unchanged with respect to the GS. Thus, the S_1, S_2, and S_3 electronic states resulting from the two $^1\pi\pi^*$ and the $^1n\pi^*$ configurations become strongly mixed in their electronic characters.[87] Furthermore, they are affected by the conformational and H-bonding disorder in the hydration shell. Exploring the consequences of these effects for the electronic relaxation pathways and lifetimes of UV-excited Ade molecules requires at minimum highly elaborate dynamics calculations with conformational sampling,[83–90] which are only just becoming possible (see, especially, Refs. 87–89). An adequate discussion of this area is far beyond the scope of the present paper and shall not be attempted here. Nevertheless, a number of conclusions related to the experimental time constants above can be drawn.

3.4.2.2 The UV-excited $^1\pi\pi^*$ (L_a) Franck–Condon state

The ultrashort < 100 fs component referred to as τ_{FC} above was not clearly resolved in our present transient absorption measurements, but a respective short-lived term

in emission is indicated by the negative amplitudes near $\lambda_{\mathrm{probe}} = 310$ nm in the transient spectra in Fig. 3.4 at the earliest pump–probe delay times ($\Delta t \lesssim 60$ fs). Moreover, it has been identified in transient fluorescence measurements,[53,77] where it was attributed to emission directly from the optically excited FC state. At our 260 nm excitation wavelength, where the $^1\pi\pi^*$ (L_a) configuration carries the bulk of the oscillator strength from the GS, the femtosecond UV pump pulse projects a wavepacket from the GS into the FC window of the $^1\pi\pi^*$ (L_a) state. Considering the predicted downhill slope of the PEHS from the initial FC point towards the CIs that have been calculated among the different excited states and between the excited state(s) and the GS at energies below FC excitation in theoretical investigations,[23,25,27–29,85,87,88] τ_{FC} is attributed with some confidence to the ultrafast immediate departure of the excited wavepacket from its region of birth. Experimentally, this wavepacket movement is nicely reflected in the transient absorption spectra of Fig. 3.4 by the rapid blue-shift that is seen in the first $\sim$60 fs. Within this time, the excited wavepacket reaches a conformationally relaxed region on the $^1\pi\pi^*$ (L_a) PEHS, from where a variety of nonadiabatic electronic deactivation processes may start. Thereafter, Fig. 3.4 indicates a continuing, though less pronounced blue-shift up to $\sim$300 fs, which is at least partially explained as HGSA by the first vibrationally highly excited S_0 molecules that have returned through the CI to the GS (see discussion further below).

3.4.2.3 The relaxed $^1\pi\pi^*$ (L_a) excited state

Time constant $\tau_1 = 0.19 \pm 0.03$ ps provided by our global SVD analysis is associated by the DADS (cf. Figs. 3.6 and 3.8) with an SE component (negative contribution to the DADS at $\lambda < 330$ nm) and an ESA component (positive contribution to the DADS at $\lambda \sim 330 - 500$ nm). Both signals could not be separated by the SVD, suggesting that they arise from the same state. Considering the strong SE intensity, this must be the $^1\pi\pi^*$ (L_a) excited state. Nevertheless, the SE contribution to the DADS may also be ascribed to the last stage of the ultrafast ($\tau_{\mathrm{FC}} < 100$ fs) initial departure of the excited wavepacket from the FC window discussed in the preceding paragraph—the present measurements are at the limits of their time resolution here. For the ESA decay with τ_1, on the other hand, several channels have to be considered:

(*i*) The excited wavepacket may continue its descent on the $^1\pi\pi^*$ (L_a) PEHS to a direct CI with the GS involving an out-of-plane ring puckering motion of the C^2–H moiety. This pathway has been predicted by excited-state calculations early on[23,25,27–34] and has been highlighted again by the recent time-dependent surface hopping quantum dynamics calculations.[83,84,86,88–91]

(*ii*) Ring puckering at C^6 lowers the PEHS towards a CI with the GS, where the NH_2 group stands almost perpendicular to the puckered ring system.[23,27–29,32–34,87,88] While the C^2–H puckering route has been predicted as the preferred pathway for internal conversion at low excitation energies, the C^6 puckering route is supposed to become more important at slightly higher excitation.[84,89] Moreover, it has mostly been attributed to the $^1n\pi^*$ state as transient intermediate excited state (lifetime τ_2, see below), which can be reached via a CI from the $^1\pi\pi^*$ (L_a) state.

(*iii*) From fluorescence anisotropy measurements, Gustavsson et al.[10] proposed a transition between the $^1\pi\pi^*$ (L_b) and $^1\pi\pi^*$ (L_a) states, which are both excited at their $\lambda_{pump} = 267$ nm, to explain the observed bi-exponential decay dynamics with τ_1 and τ_2. However, the $^1\pi\pi^*$ (L_b) PEHS does not seem to form a CI for direct internal conversion to the GS according to most calculations.[23,27–30]

To conclude this paragraph, $\tau_1 = 0.19$ ps corresponds to the lifetime of the optically bright $^1\pi\pi^*$ (L_a) state, but likely encodes nonadiabatic transitions directly to the GS via the C^2–H puckering pathway, possibly also via the C^6 puckering channel, and to the optically dark $^1n\pi^*$ state, which is the topic in the following paragraph. The branching ratio(s) cannot be obtained from our present experiments.

3.4.2.4 The $^1n\pi^*$ state as a transient intermediate

Decay time $\tau_2 = 0.45 \pm 0.05$ ps provided by our global SVD analysis is associated with a DADS that continuously descends in amplitude from the near-UV towards green probe wavelengths (Figs. 3.6 and 3.8). The transient absorption in the visible part of the DADS ($\lambda_{probe} > 400$ nm) clearly hints at a slightly longer lived ESA component compared to τ_1, i.e. a transient intermediate excited state en route from the $^1\pi\pi^*$ (L_a) state to the GS. The prime candidate of interest here is the $^1n\pi^*$ state,[25–27,30,83,84,88,92] or some sort of mixed $^1\pi\pi^*/^1n\pi^*$ state in a flat region of the PEHS.

The $^1n\pi^*$ excited state is optically dark in fluorescence and in excited-state absorption in the relevant probe wavelength ranges, but may become involved when the molecule distorts along out-of-plane directions and the $^1\pi\pi^*$ and $^1n\pi^*$ characters start to mix.[25] A stepwise internal conversion via the $^1n\pi^*$ state indeed has been accepted for isolated 9H-Ade as a rationale for the "long" $\sim$1 ps lifetime component found in gas phase molecular beam experiments.[37–45] For Ade and several N^9-derivatives of Ade in water, time-resolved two-dimensional electronic spectra by

Prokhorenko et al. produced direct experimental evidence for the involvement of an optically dark state, believed to be the $^1n\pi^*$ state, as a transient intermediate in the electronic relaxation in condensed phases as well.[36] However, the reported lifetime of $\tau = 1.5$ ps[36] for this "dark intermediate" state is profoundly different from the present and practically all earlier experimental results. Nevertheless, the $^1n\pi^*$ state has been proposed as the bottleneck in the electronic deactivation of UV-excited Ade and Ade derivatives by the elaborate surface hopping quantum dynamics calculations performed in the last few years.[83–90] For these reasons, our value of $\tau_2 = 0.45 \pm 0.5$ ps is assigned to the lifetime of the transient $^1n\pi^*$ intermediate state with respect to the eventual internal conversion of the photoexcited Ade molecules to the GS.

3.4.2.5 Hot ground-state absorption

A visual inspection of the shape of the DADS associated with time constant τ_2 in Fig. 3.6 also suggests a contribution by HGSA, in addition to the ESA contribution discussed in the preceding paragraph. In an attempt to separate both factors, Fig. 3.9 shows bi-exponential model fits to the DADS. The obtained qualitatively reasonable description suggests that the DADS component at $\lambda_{\text{probe}} \leq 400$ nm is due to HGSA, while the broad second component that ranges over the entire probe spectrum is caused by ESA. Since vibrationally highly excited molecules in the electronic GS generally exhibit substantially red-shifted electronic absorption spectra due to the Boltzmann tail of the vibrational state distribution, the transient absorption at $\lambda_{\text{probe}} \leq 400$ nm in the DADS is readily explained.

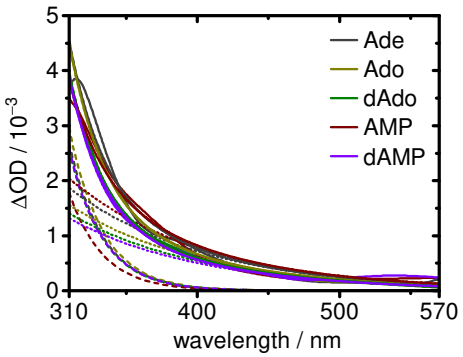

Figure 3.9: Bi-exponential model fits to the second DADS ($\tau_2 = 0.45$ ps) from the SVD analysis (solid lines) for the five Ade derivatives and (thin dashed and dotted lines) fitted exponential components.

3.4.2.6 Vibrational cooling

The time constant denoted as $\tau_c = 2.0 \pm 0.2$ ps above was found in the deep-UV measurements at $\lambda_{probe} = 255$ nm. The transient signal itself at this wavelength likely contains contributions from ESA too, but the negative net amplitude renders its assignment as "mostly GSB" unambiguous. As the data show the refilling of the GSB signal, the observed process is commonly referred to as ground-state recovery (GSR). This is the last step in the observed dynamics, which is practically over within $\Delta t \sim 6$ ps, as demonstrated by Fig. 3.7. As we argued for a lifetime of $\tau_2 = 0.45$ ps for the excited electronic state(s), the value of $\tau_c = 2.0$ ps is interpreted as the vibrational cooling time of the initially internally "hot" molecules returned to the GS by the internal conversion through the CI(s) from the excited state(s).

Interestingly, the vibrational energy dissipation in the investigated Ade derivatives appears to be independent of the sugar and sugar-phosphate substitutions at the N^9 position, although those modifications drastically increase the number of internal degrees of freedom and provide an extensive bath for the excess energy. This observation may be explained by the ultrafast electronic deactivation that leaves no time for intramolecular vibrational redistribution. Results of Nielsen et al.,[68] who found that the ultrafast deactivation of AMP leaves the vibrations of the phosphate group unexcited, support this interpretation. The fast vibrational cooling of the "hot" S_0 molecules resulting from the internal conversion from the photo-excited state(s) must be dominated by rapid intermolecular energy transfer to the solvent facilitated by hydrogen bonding of the nucleobase to surrounding water molecules,[93–96] as has been observed in studies of other DNA bases and building blocks.[7,57,69,77]

3.4.2.7 7H-Ade

Eventually, the minor 7H-Ade tautomer with its excited-state lifetime of $\tau_3 = 7.2 \pm 0.5$ ps was clearly identified by its well-separated third DADS component in the global SVD analysis for the measured 9H-/7H-Ade mixture in water (cf. Table 3.6). 7H- and 9H-Ade do not just differ by a simple substitution of the N^9–H atom by the ribose or deoxyribose sugars as in the N^9-derivatives Ado, dAdo, AMP and dAMP, but by a real tautomeric switch of the position of this H atom to the N^7–H position. Evidently, this small change affects the electronic structure of the molecules, including the excitation energies and orders of the states, as well as the topographies of the potential energy hypersurfaces quite substantially.[29,46,97] In 7H-Ade, the amino group is pyramidalized and rotated out of plane due to steric interactions with the N^7–H bond.[29] From the $^1\pi\pi^*$ (L_a) excited state of the molecule, a C^2–H

ring puckering motion is known to lead to a CI with the GS[29,46] in a similar way as in 9H-Ade. However, the $^1\pi\pi^*$ (L_a) excited PEHS first exhibits a shallow potential energy minimum,[29,98] where only CIs with the $^1\pi\pi^*$ (L_b) and $^1n\pi^*$ states, but not with the GS, are encountered. The cited CIs easily allow for mutual interconversion between the three states through C^2- or C^6-puckered structures. However, the critical CI with the electronic GS lies at or slightly above the energy of excitation,[46] so that extra internal energy is required to reach this CI.

Recent temperature-dependent fluorescence up-conversion measurements of the excited-state lifetimes of 7H-Ade in water indeed confirmed the existence of an activation energy for the electronic deactivation of about 0.1 eV.[99] The results of those measurements will be reported in a future paper.

3.5 Conclusions

The excited electronic state lifetimes of the free DNA base Ade, its nucleosides Ado and dAdo, and its nucleotides AMP and dAMP have been investigated by femtosecond time-resolved transient electronic absorption spectroscopy after excitation at $\lambda_{pump} = 260$ nm in buffered (pH 7.0) aqueous solution. Back-to-back measurements showed virtually identical temporal behavior for the five samples. This observation strongly indicates chromophore-governed excited-state dynamics with a common deactivation mechanism and without significant interaction with, or energy transfer to, the sugar-phosphate unit. A global analysis yielded excited-state lifetimes of $\tau_1 = 0.19 \pm 0.03$ ps and $\tau_2 = 0.45 \pm 0.05$ ps, which were assigned to stepwise ultrafast internal conversion to the electronic ground state. A main and prominent relaxation pathway (lifetime τ_1) is associated with a barrierless motion on the $^1\pi\pi^*$ (L_a) PEHS towards a conical intersection with the ground state involving a ring puckering movement of the C^2–H group to an almost perpendicular position of the H atom with respect to the ring. A second contribution to the electronic deactivation is connected with a C^6 puckering motion involving a nearly perpendicular NH_2 group. The slightly longer lifetime τ_2 is attributed to the $^1n\pi^*$ state as transient intermediate. The results demonstrate that an Ade monomer unit maintains its photophysical properties when connected to the DNA sugar-phosphate backbone groups.

Acknowledgments

The support of this work by the Deutsche Forschungsgemeinschaft is gratefully acknowledged. In addition, the authors thank Drs. Mayra C. Stuhldreier and Katharina Röttger for numerous discussions.

References and Notes

[1] J.-M. L. Pecourt, J. Peon, B. Kohler, 'Ultrafast Internal Conversion of Electronically Excited RNA and DNA Nucleosides in Water', *J. Am. Chem. Soc.* **2000**, *122*, 9348–9349.

[2] J.-M. L. Pecourt, J. Peon, B. Kohler, 'DNA Excited-State Dynamics: Ultrafast Internal Conversion and Vibrational Cooling in a Series of Nucleosides', *J. Am. Chem. Soc.* **2001**, *123*, 10370–10378.

[3] J. Peon, A. H. Zewail, 'DNA/RNA nucleotides and nucleosides: Direct measurement of excited-state lifetimes by femtosecond fluorescence up-conversion', *Chem. Phys. Lett.* **2001**, *348*, 255–262.

[4] T. Gustavsson, A. Sharonov, D. Onidas, D. Markovitsi, 'Adenine, deoxyadenosine and deoxyadenosine 5'-monophosphate studied by femtosecond fluorescence upconversion spectroscopy', *Chem. Phys. Lett.* **2002**, *356*, 49–54.

[5] D. Onidas, D. Markovitsi, S. Marguet, A. Sharonov, T. Gustavsson, 'Fluorescence Properties of DNA Nucleosides and Nucleotides: A Refined Steady-State and Femtosecond Investigation', *J. Phys. Chem. B* **2002**, *106*, 11367–11374.

[6] D. Markovitsi, A. Sharonov, D. Onidas, T. Gustavsson, 'The Effect of Molecular Organization in DNA Oligomers Studied by Femtosecond Fluorescence Spectroscopy', *ChemPhysChem* **2003**, *4*, 303–305.

[7] B. Cohen, P. M. Hare, B. Kohler, 'Ultrafast Excited-State Dynamics of Adenine and Monomethylated Adenines in Solution: Implications for the Nonradiative Decay Mechanism', *J. Am. Chem. Soc.* **2003**, *125*, 13594–13601.

[8] T. Pancur, N. K. Schwalb, F. Renth, F. Temps, 'Femtosecond fluorescence upconversion spectroscopy of adenine and adenosine: Experimental evidence for the $\pi\sigma^*$ state?', *Chem. Phys.* **2005**, *313*, 199–212.

[9] W.-M. Kwok, C. Ma, D. L. Phillips, 'Femtosecond Time- and Wavelength-Resolved Fluorescence and Absorption Spectroscopic Study of the Excited States of Adenosine and an Adenine Oligomer', *J. Am. Chem. Soc.* **2006**, *128*, 11894–11905.

[10] T. Gustavsson, N. Sarkar, I. Vayá, M. C. Jilménez, D. Markovitsi, R. Improta, 'A joint experimental/theoretical study of the ultrafast excited state deactivation of deoxyadenosine and 9-methyladenine in water and acetonitrile', *Photochem. Photobiol. Sci.* **2013**, *12*, 1375–1386.

[11] F. Buchner, H.-H. Ritze, J. Lahl, A. Lübcke, 'Time-resolved photoelectron spectroscopy of adenine and adenosine in aqueous solution', *Phys. Chem. Chem. Phys.* **2013**, *15*, 11402–11408.

[12] C. E. Crespo-Hernández, B. Cohen, P. M. Hare, B. Kohler, 'Ultrafast Excited-State Dynamics in Nucleic Acids', *Chem. Rev.* **2004**, *104*, 1977–2019.

[13] C. T. Middleton, K. de La Harpe, C. Su, Y. K. Law, C. E. Crespo-Hernández, B. Kohler, 'DNA Excited-State Dynamics: From Single Bases to the Double Helix', *Annu. Rev. Phys. Chem.* **2009**, *60*, 217–239.

[14] M. Barbatti, A. C. Borin, S. Ullrich, Eds., 'Photoinduced Phenomena in Nucleic Acids I. Nucleobases in the Gas Phase and in Solvents', *Topics in Current Chemistry, Vol. 355*, Springer, Heidelberg, Germany, **2015**.

[15] S. Alavi, 'Simple Ethers as Models of Sugar Molecules in Calculations of Vertical Excitation Energies of DNA and RNA Nucleosides', *J. Phys. Chem. A* **2005**, *109*, 9536–9541.

[16] R. So, S. Alavi, 'Vertical Excitation Energies for Ribose and Deoxyribose Nucleosides', *J. Comput. Chem.* **2007**, *28*, 1776–1782.

[17] F. Santoro, R. Improta, T. Fahleson, J. Kauczor, P. Norman, S. Coriani, 'Relative Stability of the L_a and L_b Excited States in Adenine and Guanine: Direct Evidence from TD-DFT Calculations of MCD Spectra', *J. Phys. Chem. Lett.* **2014**, *5*, 1806–1811.

[18] D. Tuna, A. L. Sobolewski, W. Domcke, 'Mechanisms of Ultrafast Excited-State Deactivation in Adenosine', *J. Phys. Chem. A* **2014**, *118*, 122–127.

[19] B. Marchetti, T. N. V. Karsili, M. N. R. Ashfold, W. Domcke, 'A 'bottom up' ab initio computational approach to understanding fundamental photophysical processes in nitrogen containing heterocycles, DNA bases and base pairs', *Phys. Chem. Chem. Phys.* **2016**, *18*, 20007–20027.

[20] B. A. West, J. M. Womick, A. M. Moran, 'Interplay between Vibrational Energy Transfer and Excited State Deactivation in DNA Components', *J. Phys. Chem.* **2013**, *117*, 5865–5874.

[21] M. Dreyfus, G. Dodin, O. Bensaude, J. E. Dubois, 'Tautomerism of Purines. I. N(7)H $\rightleftharpoons$ N(9)H Equilibrium in Adenine', *J. Am. Chem. Soc.* **1975**, *97*, 2369–2376.

[22] J. W. Eastman, 'Fluorescence and tautomerism of adenine', *Ber. Bunsenges. Phys. Chem.* **1969**, *73*, 407–412.

[23] S. Perun, A. L. Sobolewski, W. Domcke, 'Ab Initio Studies on the Radiationless Decay Mechanisms of the Lowest Excited Singlet States of 9H-Adenine', *J. Am. Chem. Soc.* **2005**, *127*, 6257–6265.

[24] S. Perun, A. L. Sobolewski, W. Domcke, 'Photostability of 9H-Adenine: Mechanisms of the Radiationless Deactivation of the Lowest Excited Singlet States', *Chem. Phys.* **2005**, *313*, 107–112.

[25] C. M. Marian, 'A new pathway for the rapid decay of electronically excited adenine', *J. Chem. Phys.* **2005**, *122*, 104314.

[26] S. Matsika, 'Three-State Conical Intersections in Nucleic Acid Bases', *J. Phys. Chem. A* **2005**, *109*, 7538–7545.

[27] H. Chen, S. Li, 'Theoretical Study toward Understanding Ultrafast Internal Conversion of Excited 9H-Adenine', *J. Phys. Chem. A* **2005**, *109*, 8443–8446.

[28] L. Blancafort, 'Excited-State Potential Energy Surface for the Photophysics of Adenine', *J. Am. Chem. Soc.* **2006**, *128*, 210–219.

[29] L. Serrano-Andrés, M. Merchán, A. C. Borin, 'A Three-State Model for the Photophysics of Adenine', *Chem. Eur. J.* **2006**, *12*, 6559–6571.

[30] S. Yamazaki, S. Kato, 'Solvent Effect on Conical Intersections in Excited-State 9H-Adenine: Radiationless Decay Mechanism in Polar Solvent', *J. Am. Chem. Soc.* **2007**, *129*, 2901–2909.

[31] M. Z. Zgierski, S. Patchkovski, E. Lim, 'Biradical radiationless decay channel in adenine and its derivatives', *Can. J. Chem.* **2007**, *85*, 124–134.

[32] I. Conti, M. Garavelli, G. Orlandi, 'Deciphering Low Energy Deactivation Channels in Adenine', *J. Am. Chem. Soc.* **2009**, *131*, 16108–16118.

[33] V. Ludwig, Z. M. da Costa, M. S. do Amaral, A. C. Borin, S. Canuto, L. Serrano-Andrés, 'Photophysics and photostability of adenine in aqueous solution: A theoretical study', *Chem. Phys. Lett.* **2010**, *492*, 164–169.

[34] W. M. I. Hassan, W. C. Chung, N. Shimakura, S. Koseki, H. Kono, Y. Fujimura, 'Ultrafast radiationless transition pathways through conical intersections in photoexcited 9H-adenine', *Phys. Chem. Chem. Phys.* **2010**, *12*, 5317–5328.

[35] Z. Benda, P. G. Szalay, 'Details of the Excited State Potential Energy Surfaces of Adenine by Coupled-Cluster Techniques', *J. Phys. Chem. A* **2014**, *118*, 6197–6207.

[36] V. Prokhorenko, A. Picchiotti, M. Pola, A. Dijkstra, R. Miller, 'New Insights into the Photophysics of DNA Nucleobases', *J. Phys. Chem. Lett.* **2016**, *7*, 4445–4450.

[37] H. Kang, K. T. Lee, B. Jung, Y. J. Ko, S. K. Kim, 'Intrinsic Lifetimes of the Excited State of DNA and RNA Bases', *J. Am. Chem. Soc.* **2002**, *124*, 12958–12959.

[38] S. Ullrich, T. Schultz, M. Z. Zgierski, A. Stolow, 'Direct Observation of Electronic Relaxation Dynamics in Adenine via Time-Resolved Photoelectron Spectroscopy', *J. Am. Chem. Soc.* **2004**, *126*, 2262–2263.

[39] C. Canuel, M. Mons, F. Piuzzi, B. Tardivel, I. Dimicoli, M. Elhanine, 'Excited States Dynamics of DNA and RNA Bases: Characterization of a Stepwise Deactivation Pathway in the Gas Phase', *J. Chem. Phys.* **2005**, *122*, 074316.

[40] H. Satzger, D. Townsend, M. Z. Zgierski, S. Patchkovski, S. Ullrich, A. Stolow, 'Primary processes underlying the photostability of isolated DNA bases: Adenine', *Proc. Natl. Acad. Sci. U. S. A.* **2006**, *103*, 10196–10201.

[41] C. Z. Bisgaard, H. Satzger, S. Ullrich, A. Stolow, 'Excited-State Dynamics of Isolated DNA Bases: A Case Study of Adenine', *ChemPhysChem* **2009**, *10*, 101–110.

[42] N. L. Evans, S. Ullrich, 'Wavelength Dependence of Electronic Relaxation in Isolated Adenine Using UV Femtosecond Time-Resolved Photoelectron Spectroscopy', *J. Phys. Chem. A* **2010**, *114*, 11225–11230.

[43] V. R. Smith, E. Samoylova, H.-H. Ritze, W. Radloff, T. Schultz, 'Excimer states in microhydrated adenine clusters', *Phys. Chem. Chem. Phys.* **2010**, *12*, 9632–9636.

[44] A. Chatterley, C. West, G. Roberts, V. Stavros, J. Verlet, 'Mapping the Ultrafast Dynamics of Adenine onto Its Nucleotide and Oligonucleotides by Time-Resolved Photoelectron Imaging', *J. Phys. Chem. Lett.* **2014**, *5*, 843–848.

[45] V. G. Stavros, J. R. Verlet, 'Gas-Phase Femtosecond Particle Spectroscopy: A Bottom-Up Approach to Nucleotide Dynamics', *Annu. Rev. Phys. Chem.* **2016**, *67*, 211–232.

[46] C. M. Marian, M. Kleinschmidt, J. Tatchen, 'The photophysics of 7H-adenine: A quantum chemical investigation including spin–orbit effects', *Chem. Phys.* **2008**, *347*, 346–359.

[47] C. E. Crespo-Hernández, B. Kohler, 'Influence of secondary structure on electronic energy relaxation in adenine homopolymers', *J. Phys. Chem. B* **2004**, *108*, 11182–11188.

[48] C. E. Crespo-Hernández, B. Cohen, B. Kohler, 'Base Stacking Controls Excited-State Dynamics in A·T DNA', *Nature* **2005**, *436*, 1141–1144.

[49] I. Buchvarov, Q. Wang, M. Raytchev, A. Trifonov, T. Fiebig, 'Electronic energy delocalization and dissipation in single- and double-stranded DNA', *Proc. Natl. Acad. Sci. U. S. A.* **2007**, *104*, 4794–4797.

[50] N. K. Schwalb, F. Temps, 'Base Sequence and Higher-Order Structure Induce the Complex Excited-State Dynamics in DNA', *Science* **2008**, *322*, 243–245.

[51] T. Takaya, C. Su, K. de La Harpe, C. E. Crespo-Hernández, B. Kohler, 'UV excitation of single DNA and RNA strands produces high yields of exciplex states between two stacked bases', *Proc. Natl. Acad. Sci. U. S. A.* **2008**, *105*, 10285–10290.

[52] B. Kohler, 'Nonradiative Decay Mechanisms in DNA Model Systems', *J. Phys. Chem. Lett.* **2010**, *1*, 2047–2053.

[53] M. C. Stuhldreier, C. Schüler, J. Kleber, F. Temps, 'Femtosecond Fluorescence Measurements of the Adenine Dinucleotide: Direct Observation of the Excimer State' in *Ultrafast Phenomena XVII*, (Eds.: M. Chergui, D. M. Jonas, E. Riedle, R. W. Schoenlein, A. J. Taylor), Oxford, **2011**, 553–555.

[54] C. Su, C. T. Middleton, B. Kohler, 'Base-Stacking Disorder and Excited-State Dynamics in Single-Stranded Adenine Homo-Oligonucleotides', *J. Phys. Chem. B* **2012**, *116*, 10266–10274.

[55] Á. Bányász, T. Gustavsson, D. Onidas, P. Changenet-Barret, D. Markovitsi, R. Improta, 'Multi-pathway excited state relaxation of adenine oligomers in aqueous solution: A joint theoretical and experimental study', *Chem. Eur. J.* **2013**, *19*, 3762–3774.

[56] X. Chen, W. Fang, H. Wang, 'Slow deactivation channels in UV-photoexcited adenine DNA', *Phys. Chem. Chem. Phys.* **2014**, *16*, 4210–4219.

[57] M. C. Stuhldreier, K. Röttger, F. Temps, 'Distinctive Spectral Features of Exciton and Excimer States in the Ultrafast Electronic Deactivation of the Adenine Dinucleotide' in *Ultrafast Phenomena XIX*, Vol. 162, (Eds.: K. Yamanouchi, S. Cundiff, R. de Vivie-Riedle, M. Kuwata-Gonokami, L. DiMauro), **2015**, 452–454.

[58] G. Olaso-González, M. Merchán, L. Serrano-Andrés, 'The Role of Adenine Excimers in the Photophysics of Oligonucleotides', *J. Am. Chem. Soc.* **2009**, *131*, 4368–4377.

[59] Y. Dou, Z. Liu, S. Yuan, W. Zhang, H. Tang, J. Zhao, W. Fang, G. V. Lo, 'Dynamics of laser-excited stacked adenines: Semiclassical simulations', *Int. J. Biol. Macromol.* **2012**, *52*, 358–367.

[60] Y. Dou, W. Zhao, S. Yuan, W. Zhang, H. Tang, 'Bonded excimer in stacked adenines: Semiclassical simulations', *Sci. China. Chem.* **2012**, *55*, 1377–1383.

[61] F. Plasser, H. Lischka, 'Electronic excitation and structural relaxation of the adenine dinucleotide in gas phase and solution', *Photochem. Photobiol.* **2013**, *12*, 1440–1452.

[62] F. Santoro, R. Improta, F. Avila, M. Segado, A. Lami, 'The interplay between neutral exciton and charge transfer states in single-strand polyadenine: A quantum dynamical investigation', *Photochem. Photobiol. Sci.* **2013**, *12*, 1527–1543.

[63] V. A. Spata, S. Matsika, 'Role of Excitonic Coupling and Charge-Transfer States in the Absorption and CD Spectra of Adenine-Based Oligonucleotides Investigated through QM/MM Simulations', *J. Phys. Chem. A* **2014**, *118*, 12021–12030.

[64] V. A. Spata, S. Matsika, 'Photophysical deactivation pathways in adenine oligonucleotides', *Phys. Chem. Chem. Phys.* **2015**, *17*, 31073–31083.

[65] I. Conti, A. Nenov, S. Höfinger, S. F. Altavilla, I. Rivalta, E. Dumont, G. Orlandi, M. Garavelli, 'Excited state evolution of DNA stacked adenines resolved at the CASPT2//CASSCF/Amber level: From the bright to the excimer state and back', *Phys. Chem. Chem. Phys.* **2015**, *17*, 7291–7302.

[66] J. J. Nogueira, F. Plasser, L. González, 'Electronic delocalization, charge transfer and hypochromism in the UV absorption spectrum of polyadenine unravelled by multiscale computations and quantitative wavefunction analysis', *Chem. Sci.* **2017**, *8*, 5682–5691.

[67] T. Gustavsson, A. Sharonov, D. Markovitsi, 'Thymine, Thymidine and Thymidine 5'-Monophosphate Studied by Femtosecond Fluorescence Upconversion', *Chem. Phys. Lett.* **2002**, *351*, 195–200.

[68] J. B. Nielsen, J. Thøgersen, S. K. Jensen, S. R. Keiding, 'Photo protection of RNA building blocks: Adenosine 5'-monophosphate, cytidine 5'-monophosphate and cytosine', *Chem. Phys. Lett.* **2013**, *567*, 50–54.

[69] K. Röttger, R. Siewertsen, F. Temps, 'Ultrafast Electronic Deactivation Dynamics of the Rare Natural Nucleobase Hypoxanthine', *Chem. Phys. Lett.* **2012**, *536*, 140–146.

[70] M. J. Tauber, R. A. Mathies, X. Chen, S. E. Bradforth, 'Flowing liquid sample jet for resonance Raman and ultrafast optical spectroscopy', *Rev. Sci. Instrum.* **2003**, *74*, 4958–4960.

[71] A. Picchiotti, V. I. Prokhorenko, R. J. D. Miller, 'A closed-loop pump-driven wire-guided flow jet for ultrafast spectroscopy of liquid samples', *Rev. Sci. Instrum.* **2015**, *86*, 093105.

[72] M. Lorenc, M. Ziolek, R. Naskrecki, J. Karolczak, J. Kubicki, A. Maciejewski, 'Artifacts in femtosecond transient absorption spectroscopy', *Appl. Phys. B* **2002**, *74*, 19–27.

[73] I. van Stokkum, D. S. Larsen, R. van Grondelle, 'Global and Target Analysis of Time-Resolved Spectra', *Biochim. Biophys. Acta* **2004**, *1657*, 82–104.

[74] N. Mouton, A. de Juan, M. Sliwa, C. Ruckebusch, 'Hybrid Hard- and Soft-Modeling Approach for the Resolution of Convoluted Femtosecond Spectrokinetic Data', *Chemom. Intell. Lab. Syst.* **2011**, *105*, 74–82.

[75] C. Ruckebusch, M. Sliwa, P. Pernot, A. de Juan, R. Tauler, 'Comprehensive data analysis of femtosecond transient absorption spectra: A review', *J. Photochem. Photobiol. C* **2012**, *13*, 1–27.

[76] Mathematica, Version 8.0, Wolfram Research, Inc., Champaign, IL, U.S.A. Champaign, Illinois, **2010**.

[77] M. C. Stuhldreier, F. Temps, 'Ultrafast photo-initiated molecular quantum dynamics in the DNA dinucleotide d(ApG) revealed by broadband transient absorption spectroscopy', *Faraday Discuss.* **2013**, *163*, 173–188.

[78] C. T. Middleton, B. Cohen, B. Kohler, 'Solvent and solvent isotope effects on the vibrational cooling dynamics of a DNA base derivative', *J. Phys. Chem. A* **2007**, *111*, 10460–10467.

[79] The high noise at negative delay times in the single-color pump–probe measurements at deep-UV wavelengths is due to an experimental artifact. Low-noise levels require that the probe and reference intensities on the photodiode detectors are comparable. In the present measurements, however, the single-color probe and reference intensities before time-zero differed substantially, because the reference was running horizontally displaced from the probe through air, where it experienced no absorption, whereas the probe was attenuated by the absorbing sample in the film. This led to high noise in the measured single-color time profiles before time-zero. At delay times after excitation of the sample (i. e., at $\Delta t > 0$), the probe was attenuated much less, because the ground state was bleached. Thus, the signal at $\Delta t > 0$ shows much less noise. This problem was noted only after conclusion of the present experiments, too late for a correction. It has since been fixed by displacing the reference beam vertically and steering it through the unexcited film above than the pump, rather than horizontally displaced through air.

[80] J. R. Platt, 'Classification of Spectra of Cata-Condensed Hydrocarbons', *J. Chem. Phys.* **1949**, *17*, 484–495.

[81] E. Nir, C. Plützer, K. Kleinermanns, M. de Vries, 'Properties of isolated DNA bases, base pairs and nucleosides examined by laser spectroscopy', *Eur. Phys. J. D* **2002**, *20*, 317–329.

[82] N. Kim, G. Jeong, Y. Kim, J. Sung, S. Kim, Y. Park, 'Resonant two-photon ionization and laser induced fluorescence spectroscopy of jet-cooled adenine', *J. Chem. Phys.* **2000**, *113*, 10051–10055.

[83] M. Barbatti, H. Lischka, 'Nonadiabatic Deactivation of 9H-Adenine: A Comprehensive Picture Based on Mixed Quantum-Classical Dynamics', *J. Am. Chem. Soc.* **2008**, *130*, 6831–6839.

[84] Y. Lei, S. Yuan, Y. Dou, Y. Wang, Z. Wen, 'Detailed Dynamics of the Nonradiative Deactivation of Adenine: A Semiclassical Dynamics Study', *J. Phys. Chem. A* **2008**, *112*, 8497–8504.

[85] E. Fabiano, W. Thiel, 'Nonradiative Deexcitation Dynamics of 9H-Adenine: An OM2 Surface Hopping Study', *J. Phys. Chem. A* **2008**, *112*, 6859–6863.

[86] M. Barbatti, A. J. A. Aquino, J. J. Szymczak, D. Nachtigallová, P. Hobza, H. Lischka, 'Relaxation mechanisms of UV-photoexcited DNA and RNA nucleobases', *Proc. Natl. Acad. Sci. U. S. A.* **2010**, *107*, 21453–21458.

[87] Z. Lan, Y. Lu, E. Fabiano, W. Thiel, 'QM/MM Nonadiabatic Decay Dynamics of 9H-Adenine in Aqueous Solution', *ChemPhysChem* **2011**, *12*, 1989–1998.

[88] M. Barbatti, Z. Lan, R. Crespo-Otero, J. J. Szymczak, H. Lischka, W. Thiel, 'Critical appraisal of excited state nonadiabatic dynamics simulations of 9H-adenine', *J. Chem. Phys.* **2012**, *137*, 22A503.

[89] F. Plasser, R. Crespo-Otero, M. Pederzoli, J. Pittner, H. Lischka, M. Barbatti, 'Surface Hopping Dynamics with Correlated Single-Reference Methods: 9H-Adenine as a Case Study', *J. Chem. Theory Comput.* **2014**, *10*, 1395–1405.

[90] J. W. Park, T. Shiozaki, 'On-the-Fly CASPT2 Surface-Hopping Dynamics', *J. Chem. Theory Comput.* **2017**, *13*, 3676–3683.

[91] M. Barbatti, 'Photorelaxation Induced by Water-Chromophore Electron Transfer', *J. Am. Chem. Soc.* **2014**, *136*, 10246–10249.

[92] L. Blancafort, B. Cohen, P. M. Hare, B. Kohler, M. A. Robb, 'Singlet Excited-State Dynamics of 5-Fluorocytosine and Cytosine: An Experimental and Computational Study', *J. Phys. Chem. A* **2005**, *109*, 4431–4436.

[93] X.-X. Zhang, M. Liang, N. P. Ernsting, M. Maroncelli, 'Complete Solvation Response of Coumarin 153 in Ionic Liquids', *J. Phys. Chem. B* **2013**, *117*, 4291–4304.

[94] J. Chen, B. Kohler, 'Ultrafast nonradiative decay by hypoxanthine and several methylxanthines in aqueous and acetonitrile solution', *Phys. Chem. Chem. Phys.* **2012**, *14*, 10677–10682.

[95] W. Liu, L. Tang, B. Oscar, Y. Wang., C. Chen, C. Fang, 'Tracking Ultrafast Vibrational Cooling during Excited-State Proton Transfer Reaction with Anti-Stokes and Stokes Femtosecond Stimulated Raman Spectroscopy', *J. Phys. Chem. Lett.* **2017**, *8*, 997–1003.

[96] P. Carbonniere, C. Pouchan, R. Improta, 'Intramolecular vibrational redistribution in the non-radiative excited state decay of uracil in the gas phase: an ab initio molecular dynamics study', *Phys. Chem. Chem. Phys.* **2015**, *17*, 11615–11626.

[97] L. Serrano-Andrés, M. Merchán, A. C. Borin, 'Adenine and 2-aminopurine: Paradigms of modern theoretical photochemistry', *Proc. Natl. Acad. Sci. U. S. A.* **2006**, *103*, 8691–8696.

[98] B. Mennucci, A. Toninolo, J. Tomasi, 'Theoretical Study of the Photophysics of Adenine in Solution: Tautomerism, Deactivation Mechanisms, and Comparison with the 2-Aminopurine Fluorescent Isomer', *J. Phys. Chem. A* **2001**, *105*, 4749–4757.

[99] U. C. Stange, G. Friedrichs, F. Temps, Unpublished work, CAU Kiel, **2018**.

4 Temperature-Dependent Electronic Deactivation of 7H-Adenine: Thermal Activation Matters even on the Sub-10-picoseconds Time Scale

Uta C. Stange, Gernot Friedrichs, and Friedrich Temps

Institut für Physikalische Chemie, Christian-Albrechts-Universität zu Kiel, Max-Eyth-Str. 1, D-24118 Kiel

manuscript

Own contributions:

- transient fluorescence measurements were performed during my Master's Thesis work
- complete re-analysis of the data
- master equation modeling
- writing the draft

Abstract

The ultrafast electronic deactivation of the DNA base adenine (Ade) in H_2O has been investigated by femtosecond fluorescence up-conversion spectroscopy following 260 nm excitation as function of temperature between 298 K $\leq T \leq$ 431 K. Whereas the observed fluorescence lifetime of the 9H-Ade tautomer remained constant ($\tau_{9H} = 0.21 \pm 0.01$ ps), the lifetime of the 7H-Ade tautomer was found to decrease with increasing temperature from $\tau_{7H} = 8.4 \pm 0.1$ ps to $\tau_{7H} = 2.4 \pm 0.1$ ps. Assuming that this unusual temperature dependence can be attributed to an underlying thermal activation process, an Arrhenius analysis yielded an activation energy of $E_{A,exp} = 10.1 \pm 0.5$ kJ/mol (0.105 ± 0.005 eV). In order to assess the feasibility of such a thermally controlled process in contrast to a purely dynamically controlled deactivation on the underlying potential energy hypersurfaces, the observed kinetics was simulated by master equation modeling. The consistent modeling of the experiments and the extracted energy transfer parameters that are within the expected range for collision-induced activation processes reveal that thermal excitation can indeed play an important role in photo-induced molecular dynamics processes even on timescales as short as several picoseconds. In particular, the kinetic simulations confirm the existence of a significant potential energy barrier along the electronic deactivation pathway of excited 7H-Ade to the conical intersection with the ground state.

4.1 Introduction

Pump–probe femtosecond spectroscopy is the method of choice for monitoring ultrafast molecular photochemical and photophysical processes. In most cases, the results cannot be understood on a molecular level without quantum chemical calculations of the underlying potential energy hypersurfaces (PEHS). However, in order to compare predicted values of potential energy barriers with the experimental data, it is essential to extract quantitative data from measurements.

Here, we investigate the ultrafast deactivation dynamics of electronically excited DNA building blocks using adenine (Ade) as a model system. The molecule is one of the five natural nucleic acid bases which form the DNA and build up the code of life. All of them were found to have very low fluorescence quantum yields ($\phi_{fl} \approx 10^{-4}$)[1,2] which has been attributed to to ultrafast deactivation processes often involving

conical intersections (CIs).[3]

In aqueous solution, Ade is present in two tautomeric forms, the biologically relevant 9H-Ade and the non-canonical 7H-Ade, depicted in Fig. 4.1. At room temperature, the equilibrium ratio of the tautomers is 3:1 (9H:7H),[4] but the 7H-species dominates the fluorescence spectrum.[5] The tautomers were found to exhibit different fluorescence lifetimes, a fast sub-picosecond component of 0.23 ± 0.05 ps corresponding to 9H-Ade, and a slow picosecond component of 8.0 ± 0.3 ps corresponding to 7H-Ade.[6] These values have been confirmed in several studies including time-resolved fluorescence,[7,8] transient absorption[9] and photo electron spectroscopy.[10,11]

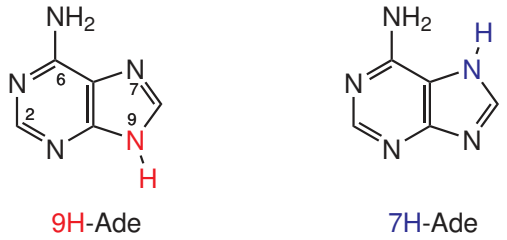

Figure 4.1: Molecular structures of adenine in its prevalent tautomer 9H and the minor 7H form.

Several quantum chemical investigations on both structures have been performed to explain the different experimental behavior of the two tautomers.[12–16] The three lowest singlet states (two $\pi\pi^*$ states and one $n\pi^*$ state) were found to be strongly coupled resulting in competing electronic deactivation pathways with effective population transfer via CIs right after leaving the Franck–Condon region.[12,14,17–25] Nevertheless, despite the extensive experimental and theoretical work, the pathways of deactivation are still subject of discussion.[22,26–29] Previous studies on 9H-Ade have shown a decrease of the excited-state lifetime with increasing excitation energy, i. e. the initial excess energy deposited in the sample.[7,10,30] The interpretation of this finding, as opening or closing of possible deactivation pathways, sensitively depends on the exact positions of the predicted CIs.

In order to clarify if the currently preferred view of a purely dynamical control of the ongoing deactivation process holds true, we performed a temperature-dependent study of the fluorescence lifetime. While the initial excitation energy distribution in the excited states slightly changes with temperature, for such a dynamical picture where collisions are nonrelevant the impact on the measured fluorescence lifetime is expected to be minor. In contrast, we found a distinct temperature dependence that indicate the importance of thermal activation for the overall deactivation process.

The extracted activation energy of 7H-Ade is consistent with a barrier deduced from detailed master equation (ME) modeling of the collision-controlled energy transfer process. To the best of our knowledge, our conclusion that thermal activation even matters on the sub-10-picoseconds time scale, supported by temperature-dependent experiments and master equation modeling, is new.

4.2 Experimental Methods

The home-built fluorescence up-conversion experiment has already been described in detail before.[7,31] The sample was diluted in ultrapure water and set to an absorbance of OD ≈ 0.5 at $\lambda_{exc} = 260$ nm. The sample solution was excited with 50 – 100 µW at $\lambda_{pump} = 260$ nm. The resulting fluorescence was up-converted and detected at the probe wavelengths $\lambda_{probe} = 320$ nm, 350 nm and 430 nm. The measured fluorescence time profiles were fitted with a sum of two decaying exponential functions convoluted with the instrumental response function as described elsewhere.[31] For the measurements at $T = 295$ K, 323 K and 363 K a flow cell with suprasil quartz windows (⌀ 15 mm × 0.2 mm) was enclosed into a heatable aluminum body. The sample reservoir was maintained at the desired temperature with a water thermostat leading to an estimated error of temperature of $\Delta T \pm 2$ K in the sample cell.

For the measurements at $T = 403$ K and 431 K a heatable pressure resistant cell was used in order to prevent the sample solution from vaporizing. This cell was made up of a stainless steel body with directly attached sapphire windows (⌀ 10 mm × 1.25 mm). The pressure in the cell was set to $p = 12$ bar at $T = 403$ K and $p = 16$ bar at $T = 431$ K. The experimental errors of the pressure resistant cell were estimated to be $\Delta T = \pm 4$ K and $\Delta p = \pm 2$ bar.

4.3 Results and Discussion

4.3.1 Experimental Results

Fluorescence time profiles for Ade in water were recorded after excitation in the absorption maximum at $\lambda_{pump} = 260$ nm. The curves are shown in Fig. 4.2 for the fluorescence detected at $\lambda_{probe} = 320$ nm at five different temperatures between $T = 295 - 431$ K. The time profiles clearly demonstrate a higher decay rate with increasing temperature.

All experimental curves can be described nicely by Gaussian-convoluted biexponential functions, the components of which are exemplarily shown for the data at $T = 295$ K in Fig. 4.2. The results of this analysis are summarized in Table 4.1.

Data measured at $\lambda_{probe} = 350$ nm and 430 nm yielded very similar results

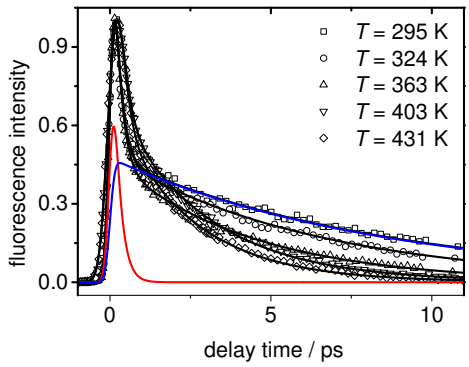

Figure 4.2: Time-resolved fluorescence decay curves of adenine in water measured at $\lambda_{\text{probe}} = 320$ nm as function of temperature. Data points are shown as open symbols, fitted biexponential model functions are represented by solid curves. The contributions for the data at $T = 295$ K are shown in red (9H-Ade) and blue (7H-Ade).

Table 4.1: Experimental results for the fluorescence decay times of 9H- and 7H-Ade at $\lambda_{\text{probe}} = 320$ nm in the range 298 K $\leq T \leq$ 431 K. Numbers in parentheses represent the 2σ standard error.

T/K	a_{9H}	τ_{9H}/ps	a_{7H}	τ_{7H}/ps
295	0.74(1)	0.21(1)	0.26(1)	8.4(2)
323	0.74(1)	0.21(1)	0.26(1)	6.3(1)
363	0.75(1)	0.21(1)	0.25(1)	4.3(1)
403	0.69(2)	0.21(1)	0.31(1)	2.8(1)
431	0.71(2)	0.21(1)	0.29(1)	2.4(1)

(see Additional Information). Due to the good agreement with literature values,[6–9] the measured fluorescence lifetimes $\tau_{9H} = 0.21$ ps and $\tau_{7H} = 8.4$ ps can directly be assigned to the two tautomers 9H- and 7H-Ade, respectively. The amplitudes of the exponential components at $\lambda_{\text{probe}} = 320$ nm approximately reflect the ratio of the tautomers. The amplitude for 7H-Ade, a_{7H}, showed no significant change with temperature but decreased to $a_{7H} = 0.07$ at $\lambda_{\text{probe}} = 430$ nm exposing a comparatively narrow emission band for the 7H species. The 9H-Ade species thus accounts for the broad fluorescence spectrum between $\lambda_{\text{fluo}} = 290 - 470$ nm (not shown).

The measurements reveal that 9H-Ade exhibits a temperature-independent fluorescence lifetime, whereas the fluorescence lifetime of 7H-Ade in water clearly decreases with increasing temperature. This temperature-dependent behavior was further investigated by an Arrhenius analysis yielding a linear plot (Fig. 4.3). The

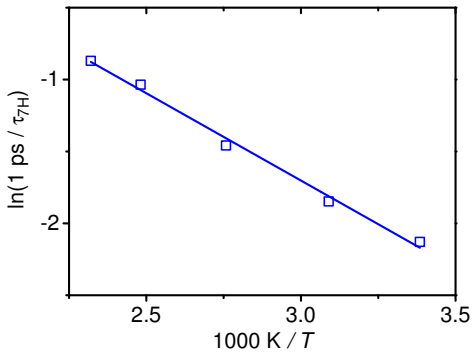

Figure 4.3: Arrhenius analysis of the fluorescence lifetimes of 7H-Ade at $\lambda_{\text{probe}} = 320$ nm. The solid line represents the Arrhenius expression.

resulting Arrhenius parameters are a frequency factor of

$$A = 7 \pm 1 \cdot 10^{12}\ \text{s}^{-1},$$

corresponding to a limiting excited-state lifetime of $\tau_\infty = 0.14 \pm 0.01$ ps at infinitely high temperatures, and an activation energy of

$$E_{\text{A,exp}} = 10.1 \pm 0.5\ \text{kJ/mol}\ (\widehat{=}0.105 \pm 0.005\ \text{eV}).$$

It is reasonable to suggest that this effective activation energy $E_{\text{A,exp}}$ reflects a potential energy barrier on the deactivation pathway.

4.3.2 Electronic Deactivation Mechanisms

Quantum chemical data on the PEHS of the excited states of 7H-Ade reveal different possible electronic deactivation pathways. A sketch of the PEHS model is shown in Fig. 4.4. In 9H-Ade, the optically bright and barrierless $\pi\pi^*$ L_a excited state was found to be initially populated at $\lambda_{\text{pump}} = 260$ nm.[14,18,22,23,32,33] Relaxation on this state's hypersurface is characterized by a ring puckering mode involving an out-of-plane bending of the C^2–H bond (see Fig. 4.1 for numbering) leading to a CI with the ground-state PEHS.[12,16,34–36] Relaxation on the optically forbidden $n\pi^*$ excited-state PEHS involves a ring puckering and an out-of-plane bending of the amino group at the C^6 position.[34,37,38] This deactivation is hindered by a potential energy barrier before reaching the CI with the ground state. In water, the $n\pi^*$ excited state was found to be destabilized, thus this deactivation path is less likely to be populated in aqueous phase experiments.[3,20,22,38–40] The $\pi\pi^*$ L_b excited-state PEHS forms a minimum with planar molecular structure and has CIs with both deactivation pathways but none with the ground state.[14,17,18,20,23,32] Including a

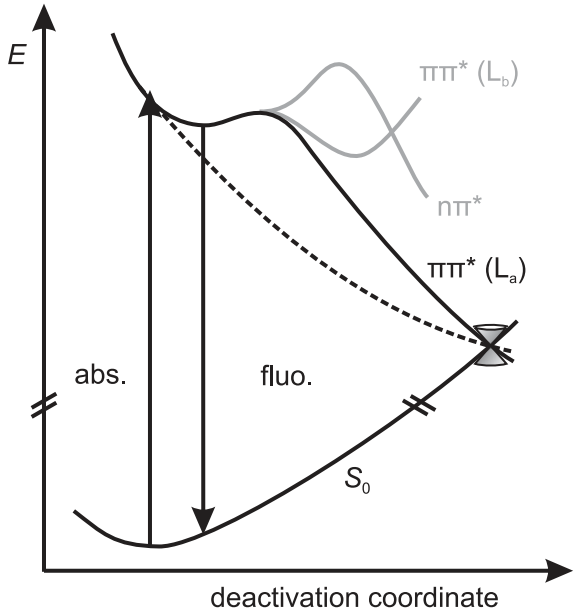

Figure 4.4: Schematic representation of the PEHS of adenine based on calculations by Serrano-Andrés et al. (Ref. 14), see text. Absorption and emission of radiation are indicated as arrows. The electronic deactivation pathway towards the CI with the ground state is hindered by an energy barrier in 7H-Ade (upper solid black curve). The barrierless relaxation pathway of 9H-Ade leading to the CI with the ground state S_0 is shown by the lower dashed curve.

water shell, Barbatti[16] found the ring puckering at the C^2 position to make up for 90 % of the calculated dynamics trajectories. The temperature-independent excited-state behavior of 9H-Ade can be assigned to the relaxation on the barrierless $\pi\pi^*$ L_a excited PEHS between the Franck–Condon region and the CI with the ground state. The fast unhampered deactivation accounts for the low fluorescence quantum yield and most likely impedes the population of the bright $\pi\pi^*$ L_b excited state. The broad emission band of 9H-Ade thus results from the continuous fluorescence during relaxation.

For the minor tautomer much less theoretical work can be found. In 7H-Ade, similar excited states and molecular structures are involved in the relaxation process, i. e. the deactivation on the $\pi\pi^*$ L_a excited PEHS also involves a ring puckering and an out-of-plane bending of the C^2–H bond.[13] The main difference between the electronic properties of the tautomers results from a rotation of the amino group around the C^6–N^{10} bond in the excited state of 7H-Ade.[13,14] This deformation creates a plateau on the $\pi\pi^*$ L_a excited PEHS close to the CIs with the $n\pi^*$ and $\pi\pi^*$ L_b excited PEHS.[14,41] The $\pi\pi^*$ L_b excited PEHS forms a local minimum and

has CIs with the $n\pi^*$ and $\pi\pi^*$ L_a excited PEHS.[14] The $n\pi^*$ excited state was found to exhibit a very low oscillator strength and to be destabilized in water.[13] It should again not be observable in our experiments. The relaxation of 7H-Ade is thought to proceed on the $\pi\pi^*$ L_a excited-state PEHS along a similar C^2-puckering coordinate as in 9H-Ade. However, the CI with the ground state is not as easily reached by out-of-plane motion of the C^2–H bond.[13] We assume the excited-state population to go through a shallow minimum on this surface en route to the CI with the ground state (see Fig. 4.4) resulting in an emission spectrum that is comparatively narrow. Expensive quantum chemical calculations are necessary to locate such small energy barriers.

4.3.3 Master Equation Modeling

We further assess our conclusion of a thermally activated process by detailed master equation modeling and by applying the standard toolset from statistical rate theory (RRKM). The aim of this approach was to test if an approximate treatment of the overall deactivation as a thermally activated process yields a consistent energy barrier and reasonable collisional energy transfer parameters. Calculations were performed with the MultiWell program suite[42–44] to generate sums and densities of states, specific rate constants, and to solve the master equation based on Gillespie's stochastic simulation algorithm.

A schematic representation of the thermal reaction model is depicted on the left-hand side in Fig. 4.5 and essentially corresponds to an assumed potential energy well on the excited-state PEHS of 7H-Ade. Vibrational frequencies and the moments of inertia of ground-state 7H-Ade were calculated by CC2 calculations for the isolated molecule starting with the equilibrium geometry from Ref. 14. As an estimate, these were taken as model parameters for the first excited state of 7H-Ade as well. The transition state (TS) was set at ΔE_0 above the reaction well minimum roughly matching the experimentally observed value of $E_{A,exp}$. It was used as an adjustable input parameter. The vibrations of the transition state and the electronically excited 7H-Ade were set equal, except for the C^2-puckering mode at $\tilde{\nu} = 605$ cm^{-1} which was assumed to be the reaction coordinate.

The photo-activated thermal reaction was started by assuming an initial energy of $E^*_{start} = E_{h\nu} - \Delta E_{S_1-S_0} = 30.88$ kJ/mol accounting for the laser excitation above the electronic origin of S_1. Unfortunately, the S_1-S_0 transition has not been precisely determined as yet. A transition was found at $\Delta E_{S_1-S_0} = 35824$ cm^{-1} but may not reflect the electronic origin.[45,46] Since no other value is available, this number was

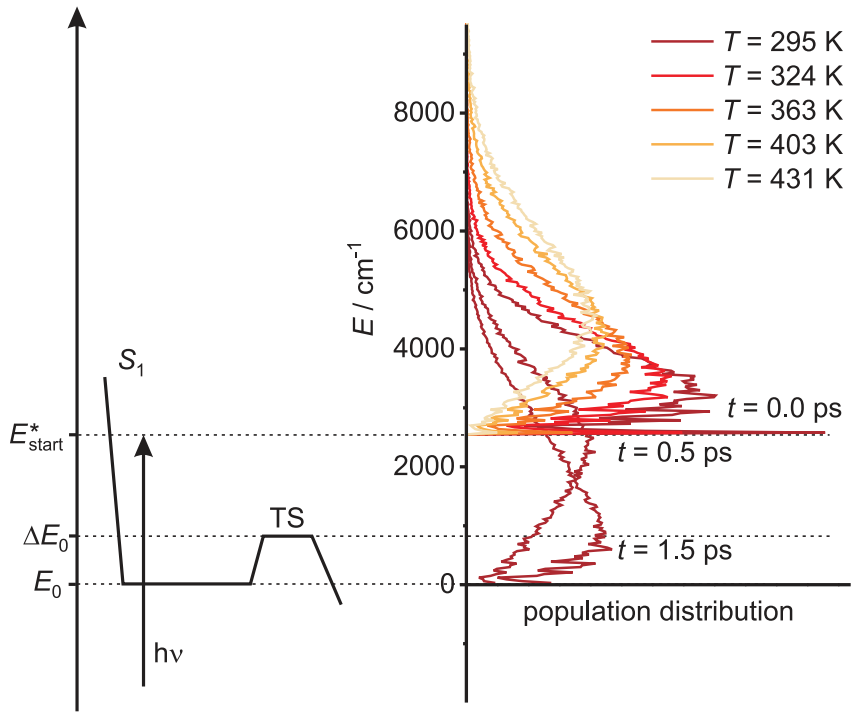

Figure 4.5: Model for the time-dependent master equation simulations of the electronic deactivation of 7H-Ade. Left: Potential energy diagram for the first excited state in 7H-Ade with a small barrier of ΔE_0 separating the well from the CI with the ground state (see also Fig. 4.4). The system is excited with a UV pulse leading to an excess energy in the excited state corresponding to E^*_{start}. Right: The simulated initial population distributions in the excited state of 7H-Ade at five temperatures. Exemplarily shown are the simulated population distributions after $t = 0.5$ ps and $t = 1.5$ ps at $T = 295$ K, respectively. Input parameters of the simulations are given in Table 4.2.

nevertheless used in the simulations leading to a lower bound for the excess energy in the excited state.

The collisional energy transfer is calculated within the MultiWell program package according to Barker's new approach, which is based on the Lennard–Jones expression for the collision frequency (Eq. 4.1) but allows for an energy-dependent attenuation.[44]

$$Z_{\text{LJ}} = \frac{\pi\sigma^2}{V_m}\sqrt{\frac{8NkT}{\pi\mu}}\Omega^{(2,2)} \tag{4.1}$$

σ is the collision diameter, V_m is the molar volume, μ is the reduced mass. The collision integral $\Omega^{(2,2)}$ is calculated using the empirical expression from Ref. 47 and depends on the reduced temperature kT/ϵ. The Lennard–Jones parameters for

water are $\sigma_{H_2O} = 2.71 \cdot 10^{-10}$ m and $\epsilon_{H_2O}/k = 506$ K.[48] In the calculations, 7H-Ade was approximated with the parameters of naphthalene, $\sigma_{naph.} = 6.299 \cdot 10^{-10}$ m and $\epsilon_{naph.}/k = 550$ K.[49]

In order to simulate a liquid collision bath, the effective particle densities in the (gas phase) simulations were set to values corresponding to the temperature-dependent density of liquid water. For example, a particle density of $[M] = 3.34 \cdot 10^{22}$ cm^{-3} at $T = 295$ K results in a collision frequency of $Z = 2.88 \cdot 10^{13}$ s^{-1} and slowly decreases with temperature (see Table 4.2).

The collision frequencies are in rough agreement with $Z \approx 10^{14}$ s^{-1} gained by scaling up gas-phase Lennard–Jones collision frequencies with the ratio of the diffusion coefficients in the liquid and in the gas phase according to Ref. 50, and with an estimate of $Z \approx 8 \cdot 10^{13}$ s^{-1} based on the kinetics theory of diffusion using the concept of persistence of velocity as described by Eq. (5) in Ref. 51. Apparently, the used gas phase collision frequencies somewhat underestimate collision frequencies in the liquid phase. Other treatments, such as the isolated binary collision model (IBC)[52] or centroid molecular dynamics simulations[53] are available, but resemble an excessive effort for the purpose of this work as the effect of collision frequency and energy transfer partially cancel out anyway.

The energy transfer parameter ΔE_{down} is indeed a key parameter for master equation modeling and specifies the averaged transferred energy in a collision causing energy loss of the reactant molecule. The corresponding ΔE_{up} value was automatically calculated from detailed balancing assuming an exponential-down model. Finally, $\Delta E_{all}(E)$ is the averaged transferred energy in all collisions. It strongly depends on the excitation energy E and is reported here as the initial change of the average energy of the population distribution function per collision.

Energy transfer parameters between $\Delta E_{down} = 100 - 500$ cm^{-1} were tested and found to directly influence the simulated reaction rate and its temperature dependence. Using ΔE_{down} and ΔE_0 as the sole adjustable parameters, we tried to match the simulated reactant loss profiles and the simulated Arrhenius activation energy to the experimental fluorescence time profiles and the experimental Arrhenius activation energy. Table 4.C1 and Fig. 4.C1 in the Additional Information show simulation results with varying values for ΔE_{down} and ΔE_0. The data demonstrate that a value of $\Delta E_{down} = 250$ cm^{-1}, corresponding to $\Delta E_{all} \approx -105$ cm^{-1} at E^*_{start} at $T = 295$ K, in combination with $\Delta E_0 = 9.62$ kJ/mol yielded excellent agreement between the experimental and the simulation results.

Although experimental data on collisional energy transfer at overall low excita-

tion energies are scarce, the obtained values can be compared with some literature values. Miller and Barker[54] (see Table II in that reference) reported energy transfer parameters for vibrationally excited pyrazine down to energies of 5000 cm^{-1}, resulting in extrapolated values of $\Delta E_{down}(Ar, E_{exc} + \langle E \rangle_{therm} = 3640\ cm^{-1}) = 54\ cm^{-1}$. Corresponding ΔE_{down} values for H_2O are expected to be about a factor of 2 – 3 times higher,[55] hence a value of $\Delta E_{down}(H_2O) \approx 140\ cm^{-1}$ can be estimated, which is comparable to the value of ΔE_{down} obtained in this work. Another extrapolation of data reported by Hippler et al.[56] for azulene-water collisions (Table 2 in their publication) yields $-\Delta E_{all} \lessapprox 100\ cm^{-1}$, again comparable to the ΔE_{all} reported here. Taking into account the uncertainties of such comparisons and of the data reduction scheme used by us, we conclude that the energy parameters extracted from the Ade experiments are reasonable and hence support the applied thermal activation model.

A summary of the input parameters used for the master equation modeling can be found in Table 4.2. The modeled thermal reaction yielded temperature-

Table 4.2: Input parameters used for master equation modeling of the electronic deactivation of excited-state 7H-Ade. The particle density $[M]$ corresponds to the density of liquid water.

T/K	$[M]/10^{22} cm^{-3}$	$Z_{LJ}/10^{13} s^{-1}$	general
295	3.34	2.88	
323	3.30	2.84	$E^*_{start} = 30.88$ kJ/mol
363	3.23	2.78	$\Delta E_0 = 9.62$ kJ/mol
403	3.16	2.71	$\Delta E_{down} = 250\ cm^{-1}$
431	3.11	2.66	

dependent reactant loss within a few picoseconds as depicted in Fig. 4.6 together with biexponential best fit curves. The simulated curves are in excellent agreement with the experimental time profiles as shown in Fig. 4.C2 in the Additional Information. Analysis of the simulated data revealed biexponential behavior with a fast $\tau_1 = 0.40$ ps component at $T = 295$ K, slightly increasing with temperature, and a slower component of $\tau_2 = 9.5$ ps at $T = 295$ K and $\tau_2 = 2.5$ ps at $T = 431$ K (see Table 4.3). The short component can be assigned to direct product formation of vibrationally hot molecules while the long component characterizes the thermally activated reactant flux over the barrier. An Arrhenius analysis of τ_2 yielded a simulated activation energy of $E_{A,sim} = 10.6$ kJ/mol fully consistent with the experimental activation energy as demonstrated in Fig. 4.7.

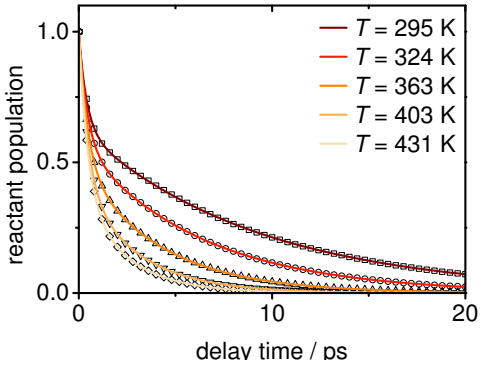

Figure 4.6: Simulated reactant population of excited-state 7H-Ade as function of temperature together with biexponential best fit curves. Input parameters of the simulations are given in Table 4.2.

Table 4.3: Results from master equation modeling of the electronic deactivation of excited-state 7H-Ade. Input parameters of the simulations are given in Table 4.2.

T/K	a_1	τ_1/ps	a_2	τ_2/ps
295	0.37	0.40	0.63	9.2
323	0.42	0.43	0.58	6.2
363	0.50	0.46	0.50	4.1
403	0.57	0.47	0.43	2.9
431	0.61	0.46	0.39	2.4

Actually, the fast initial reaction of hot molecules has no match in the experimental data, yet it may be overlain by the short-lived signal of 9H-Ade. However, transient absorption measurements on 7-methyl-Ade also show monoexponential decay of the electronic excited state with a lifetime of several picoseconds.[9,57] This indicates that, in the experiment, the excess energy from the pump pulse is rapidly dissipated and that a stationary, near-thermal equilibrium is established in the excited state potential well before the reaction over the potential energy barrier takes place. In this case, the intramolecular vibrational redistribution rate is slightly overestimated in the simulations and RRKM theory can only satisfactorily describe the experimentally observed processes after ultrafast vibrational energy transfer took place within the potential well.

The right-hand side of Fig. 4.5 illustrates the evolution of the simulated population distribution function following photoexcitation. The initial population distributions at five different temperatures were prepared by offsetting the ground state

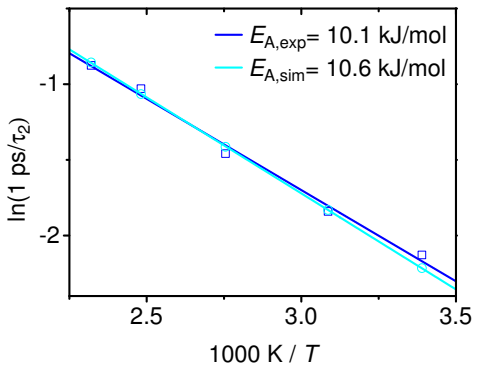

Figure 4.7: Arrhenius plot for the time constants resulting from the master equation modeling of the electronic deactivation of excited-state 7H-Ade (cyan) in comparison with the experimental data (blue). The input barrier height was $\Delta E_0 = 9.62$ kJ/mol.

distributions of 7H-Ade by E^*_{start}. Also shown are the population distributions after $t = 0.5$ ps and $t = 1.5$ ps for the simulation at $T = 295$ K resulting from pure thermal relaxation within a closed potential well ($\Delta E_0 = 30.88$ kJ/mol). Already the population distribution at $t = 1.5$ ps is essentially identical to the thermally equilibrated distribution, hence indicating a thermally activated reaction towards longer reaction times, but allowing for an unimpeded reaction at short reaction times. The time scale for pure thermal relaxation of the population distribution within the closed potential well was calculated to be $\tau_{\text{TR}} = 0.7$ ps at $T = 295$ K. Note that this is in good agreement with the ground state dynamics of nucleobases which usually yield vibrational cooling times of $\tau_{\text{vc}} \approx 2$ ps.[58–61]

The overall consistent modeling of the experiments, as well as the extracted energy transfer parameters that are within the expected range for collision-induced activation strongly indicate that ultrafast vibrational and collisional energy transfer in the electronic excited state controls the electronic deactivation dynamics of 7H-Ade on the sub-10-picosecond time scale.

4.4 Conclusion

The temperature-dependent electronic deactivation of 7H-Ade in water was investigated by femtosecond-resolved fluorescence up-conversion spectroscopy. The fluorescence lifetime of 7H-Ade decreased from $\tau_{7\text{H}} = 8.4 \pm 0.1$ ps at $T = 295$ K to $\tau_{7\text{H}} = 2.4 \pm 0.1$ ps at $T = 431$ K. Arrhenius analysis yielded an activation energy of $E_{\text{A,exp}} = 10.1 \pm 0.5$ kJ/mol which was assigned to a potential energy barrier along the pathway of ultrafast electronic deactivation with the help of time-dependent

master equation modeling. Presumably, the transition state barrier is located on the C^2-puckering coordinate on the $\pi\pi^*$ L_a excited-state PEHS.

With this work, we could identify experimentally and for the first time the potential energy barrier encountered during electronic deactivation of 7H-Ade in water. In contrast, the fluorescence lifetime of 9H-Ade ($\tau_{9H} = 0.21 \pm 0.01$ ps) was independent of temperature and, thus, the electronic deactivation process was concluded to follow a barrierless pathway.

The fact that master equation modeling yields a consistent energy barrier in combination with reasonable energy transfer parameters strongly supports our conclusion that thermal activation plays an important role even on the sub-10-picosecond time scale. Our findings also demonstrate that interpreting experimental findings of ultrafast experiments by employing purely dynamical arguments may actually lead to misguided conclusions. Temperature-dependent measurements of ultrafast processes as performed in this work may prove useful in other systems as well to elucidate new and validate predicted electronic deactivation pathways.

Acknowledgement

We kindly thank Dirk Schwarzer (Göttingen) for providing the pressure resistant sample cell and Ole Hüter for the frequency calculations of 7H-Ade.

Additional Information available: experimental details, additional fluorescence data and fitting results, MultiWell input file example

References

[1] M. Daniels, W. W. Hauswirth, 'Fluorescence of the purine and pyrimidine bases of the nucleic acids in neutral aqueous solution at 300° K.', *Science* **1971**, *171*, 675–677.

[2] P. R. Callis, 'Electronic States and Luminescence of Nucleic Acid Systems', *Annu. Rev. Phys. Chem.* **1983**, *34*, 329–352.

[3] C. E. Crespo-Hernández, B. Cohen, P. M. Hare, B. Kohler, 'Ultrafast Excited-State Dynamics in Nucleic Acids', *Chem. Rev.* **2004**, *104*, 1977–2019.

[4] M. Dreyfus, G. Dodin, O. Bensaude, J. E. Dubois, 'Tautomerism of Purines. I. N(7)H ⇌ N(9)H Equilibrium in Adenine', *J. Am. Chem. Soc.* **1975**, *97*, 2369–2376.

[5] J. W. Eastman, 'Fluorescence and tautomerism of adenine', *Ber. Bunsenges. Phys. Chem.* **1969**, *73*, 407–412.

[6] T. Gustavsson, A. Sharonov, D. Onidas, D. Markovitsi, 'Adenine, deoxyadenosine and deoxyadenosine 5'-monophosphate studied by femtosecond fluorescence upconversion spectroscopy', *Chem. Phys. Lett.* **2002**, *356*, 49–54.

[7] T. Pancur, N. K. Schwalb, F. Renth, F. Temps, 'Femtosecond fluorescence upconversion spectroscopy of adenine and adenosine: Experimental evidence for the $\pi\sigma^*$ state?', *Chem. Phys.* **2005**, *313*, 199–212.

[8] T. Häupl, C. Windolph, T. Jochum, O. Brede, R. Hermann, 'Picosecond fluorescence of nucleic acid bases', *Chem. Phys. Lett.* **1997**, *280*, 520–524.

[9] B. Cohen, P. M. Hare, B. Kohler, 'Ultrafast Excited-State Dynamics of Adenine and Monomethylated Adenines in Solution: Implications for the Nonradiative Decay Mechanism', *J. Am. Chem. Soc.* **2003**, *125*, 13594–13601.

[10] N. L. Evans, S. Ullrich, 'Wavelength Dependence of Electronic Relaxation in Isolated Adenine Using UV Femtosecond Time-Resolved Photoelectron Spectroscopy', *J. Phys. Chem. A* **2010**, *114*, 11225–11230.

[11] F. Buchner, H.-H. Ritze, J. Lahl, A. Lübcke, 'Time-resolved photoelectron spectroscopy of adenine and adenosine in aqueous solution', *Phys. Chem. Chem. Phys.* **2013**, *15*, 11402–11408.

[12] C. M. Marian, 'A new pathway for the rapid decay of electronically excited adenine', *J. Chem. Phys.* **2005**, *122*, 104314.

[13] C. M. Marian, M. Kleinschmidt, J. Tatchen, 'The photophysics of 7H-adenine: A quantum chemical investigation including spin–orbit effects', *Chem. Phys.* **2008**, *347*, 346–359.

[14] L. Serrano-Andrés, M. Merchán, A. C. Borin, 'A Three-State Model for the Photophysics of Adenine', *Chem. Eur. J.* **2006**, *12*, 6559–6571.

[15] L. Serrano-Andrés, M. Merchán, A. C. Borin, 'Adenine and 2-aminopurine: Paradigms of modern theoretical photochemistry', *Proc. Natl. Acad. Sci. U. S. A.* **2006**, *103*, 8691–8696.

[16] M. Barbatti, 'Photorelaxation Induced by Water-Chromophore Electron Transfer', *J. Am. Chem. Soc.* **2014**, *136*, 10246–10249.

[17] H. Chen, S. Li, 'Theoretical Study toward Understanding Ultrafast Internal Conversion of Excited 9H-Adenine', *J. Phys. Chem. A* **2005**, *109*, 8443–8446.

[18] L. Blancafort, 'Excited-State Potential Energy Surface for the Photophysics of Adenine', *J. Am. Chem. Soc.* **2006**, *128*, 210–219.

[19] L. Blancafort, A. A. Voityuk, 'CASSCF/CAS-PT2 Study of Hole Transfer in Stacked DNA Nucleobases', *J. Phys. Chem. A* **2006**, *110*, 6426–6432.

[20] S. Yamazaki, S. Kato, 'Solvent Effect on Conical Intersections in Excited-State 9H-Adenine: Radiationless Decay Mechanism in Polar Solvent', *J. Am. Chem. Soc.* **2007**, *129*, 2901–2909.

[21] R. Mitrić, U. Werner, M. Wohlgemuth, G. Seifert, V. Bonačić-Koutecký, 'Nonadiabatic Dynamics within Time-Dependent Density Functional Tight Binding Method.', *J. Phys. Chem. A* **2009**, *113*, 12700–12705.

[22] Z. Lan, Y. Lu, E. Fabiano, W. Thiel, 'QM/MM Nonadiabatic Decay Dynamics of 9H-Adenine in Aqueous Solution', *ChemPhysChem* **2011**, *12*, 1989–1998.

[23] T. Gustavsson, N. Sarkar, I. Vayá, M. C. Jilménez, D. Markovitsi, R. Improta, 'A joint experimental/theoretical study of the ultrafast excited state deactivation of deoxyadenosine and 9-methyladenine in water and acetonitrile', *Photochem. Photobiol. Sci.* **2013**, *12*, 1375–1386.

[24] Z. Benda, P. G. Szalay, 'Details of the Excited State Potential Energy Surfaces of Adenine by Coupled-Cluster Techniques', *J. Phys. Chem. A* **2014**, *118*, 6197–6207.

[25] X. Chen, W. Fang, H. Wang, 'Slow deactivation channels in UV-photoexcited adenine DNA', *Phys. Chem. Chem. Phys.* **2014**, *16*, 4210–4219.

[26] M. Barbatti, Z. Lan, R. Crespo-Otero, J. J. Szymczak, H. Lischka, W. Thiel, 'Critical appraisal of excited state nonadiabatic dynamics simulations of 9H-adenine', *J. Chem. Phys.* **2012**, *137*, 22A503.

[27] I. Conti, M. Garavelli, G. Orlandi, 'Deciphering Low Energy Deactivation Channels in Adenine', *J. Am. Chem. Soc.* **2009**, *131*, 16108–16118.

[28] E. Fabiano, W. Thiel, 'Nonradiative Deexcitation Dynamics of 9H-Adenine: An OM2 Surface Hopping Study', *J. Phys. Chem. A* **2008**, *112*, 6859–6863.

[29] F. Plasser, R. Crespo-Otero, M. Pederzoli, J. Pittner, H. Lischka, M. Barbatti, 'Surface Hopping Dynamics with Correlated Single-Reference Methods: 9H-Adenine as a Case Study', *J. Chem. Theory Comput.* **2014**, *10*, 1395–1405.

[30] S. Ullrich, T. Schultz, M. Z. Zgierski, A. Stolow, 'Direct Observation of Electronic Relaxation Dynamics in Adenine via Time-Resolved Photoelectron Spectroscopy', *J. Am. Chem. Soc.* **2004**, *126*, 2262–2263.

[31] N. K. Schwalb, F. Temps, 'A Modified Four-State Model for the "Dual Fluorescence" of N^6,N^6-Dimethyladenine derived from Femtosecond Fluorescence Spectroscopy', *J. Phys. Chem. A* **2009**, *113*, 13113–13123.

[32] S. Perun, A. L. Sobolewski, W. Domcke, 'Ab Initio Studies on the Radiationless Decay Mechanisms of the Lowest Excited Singlet States of 9H-Adenine', *J. Am. Chem. Soc.* **2005**, *127*, 6257–6265.

[33] M. Z. Zgierski, S. Patchkovski, E. Lim, 'Biradical radiationless decay channel in adenine and its derivatives', *Can. J. Chem.* **2007**, *85*, 124–134.

[34] Y. Lei, S. Yuan, Y. Dou, Y. Wang, Z. Wen, 'Detailed Dynamics of the Nonradiative Deactivation of Adenine: A Semiclassical Dynamics Study', *J. Phys. Chem. A* **2008**, *112*, 8497–8504.

[35] S. Mai, M. Richter, P. Marquetand, L. González, 'Excitation of Nucleobases from a Computational Perspective II: Dynamics' in *Photoinduced Phenomena in Nucleic Acids I. Nucleobases in the Gas Phase and in Solvents*, (Eds.: M. Barbatti, A. C. Borin, S. Ullrich), *Topics in Current Chemistry, Vol. 355*, Springer, Heidelberg, Germany, **2014**, 99–153.

[36] J. W. Park, T. Shiozaki, 'On-the-Fly CASPT2 Surface-Hopping Dynamics', *J. Chem. Theory Comput.* **2017**, *13*, 3676–3683.

[37] A. Broo, 'A Theoretical Investigation of the Physical Reason for the Very Different Luminescence Properties of the Two Isomers Adenine and 2-Aminopurine', *J. Phys. Chem. A* **1998**, *102*, 526–531.

[38] V. Ludwig, Z. M. da Costa, M. S. do Amaral, A. C. Borin, S. Canuto, L. Serrano-Andrés, 'Photophysics and photostability of adenine in aqueous solution: A theoretical study', *Chem. Phys. Lett.* **2010**, *492*, 164–169.

[39] S. K. Mishra, M. K. Shukla, P. Mishra, 'Electronic spectra of adenine and 2-aminopurine: an ab initio study of energy level diagrams of different tautomers in gas phase and aqueous solution', *Spectrochim. Acta Part A* **2000**, *56*, 1355–1384.

[40] F. Plasser, H. Lischka, 'Electronic excitation and structural relaxation of the adenine dinucleotide in gas phase and solution', *Photochem. Photobiol.* **2013**, *12*, 1440–1452.

[41] B. Mennucci, A. Toninolo, J. Tomasi, 'Theoretical Study of the Photophysics of Adenine in Solution: Tautomerism, Deactivation Mechanisms, and Comparison with the 2-Aminopurine Fluorescent Isomer', *J. Phys. Chem. A* **2001**, *105*, 4749–4757.

[42] J. R. Barker, T. L. Nguyen, J. F. Stanton, C. Aieta, M. Ceotto, F. Gabas, T. J. D. Kumar, C. G. L. Li, L. L. Lohr, A. Maranzana, N. F. Ortiz, J. M. Preses, J. M. Simmie, J. A. Sonk, P. J. Stimac, MultiWell-2017 Software Suite, J. R. Barker, University of Michigan, Ann Arbor, Michigan, USA, **2017**.

[43] J. R. Barker, 'Multiple-Well, Multiple-Path Unimolecular Reaction Systems. I. MultiWell Computer Program Suite', *Int. J. Chem. Kinetics* **2001**, *33*, 232–245.

[44] J. R. Barker, 'Energy transfer in master equation simulations: A new approach', *Int. J. Chem. Kinetics* **2009**, *41*, 748–763.

[45] E. Nir, C. Plützer, K. Kleinermanns, M. de Vries, 'Properties of isolated DNA bases, base pairs and nucleosides examined by laser spectroscopy', *Eur. Phys. J. D* **2002**, *20*, 317–329.

[46] C. Plützer, K. Kleinermanns, 'Tautomers and Electronic States of Jet-Cooled Adenine Investigated by Double Resonance Spectroscopy', *Phys. Chem. Chem. Phys.* **2002**, *4*, 4877–4882.

[47] P. D. Neufeld, J. A. R., R. A. Aziz, 'Empirical Equations to Calculate 16 of the Transport Collision Integrals $\Omega^{(l,s)^*}$ for the Lennard-Jones (12–6) Potential', *J. Chem. Phys.* **1972**, *57*, 1100–1102.

[48] H. Hippler, J. Troe, H. J. Wendelken, 'Collisional deactivation of vibrationally highly excited polyatomic molecules. II. Direct observations for excited toluene', *J. Chem. Phys.* **1983**, *78*, 6709–6717.

[49] C. M. Silva, H. Liu, E. A. Macedo, 'Models for self-diffusion coeffcients of dense fluids, including hydrogen-bonding substances', *Chem. Eng. Sci.* **1998**, *53*, 2423–2429.

[50] J. Troe, 'Elementary Reactions in Compressed Gases and Liquids: From Collisional Energy Transfer to Diffusion Control', *J. Phys. Chem.* **1986**, *90*, 357–365.

[51] M. Jowett, 'CIX. The rate of molecular collisions in liquid systems', *The London Edinburgh and Dublin Philosophical Magazine and Journal of Science* **1929**, *8*, 1059–1072.

[52] J. Chesnoy, G. M. Gale, 'Vibrational energy relaxation in liquids', *Ann. Phys. Fr.* **1984**, *9*, 893–949.

[53] G. Shi, E. Geva, 'On the calculation of vibrational energy relaxation rate constants from centroid molecular dynamics simulations', *J. Chem. Phys.* **2003**, *119*, 9030–9046.

[54] L. A. Miller, J. R. Barker, 'Collisional deactivation of highly vibrationally excited pyrazine', *J. Chem. Phys.* **1996**, *105*, 1383–1391.

[55] I. Oref, D. C. Tardy, 'Energy Transfer in Highly Excited Large Polyatomic Molecules', *Chem. Rev.* **1990**, *90*, 1407–1445.

[56] H. Hippler, B. Otto, J. Troe, 'Collisional Energy Transfer of Vibrational Highly Excited Molecules. VI. Energy Dependence of ΔE in Azulene', *Ber. Bunsenges. Phys. Chem.* **1989**, *93*, 428–434.

[57] P. M. Hare, B. Cohen, B. Kohler, 'Excited state lifetimes of the N(7)H and N(9)H tautomers of adenine and their methyl derivatives' in *Abstracts of Papers, 226th ACS National Meeting*, New York, NY, United States, **2003**, PHYS–403.

[58] C. T. Middleton, B. Cohen, B. Kohler, 'Solvent and solvent isotope effects on the vibrational cooling dynamics of a DNA base derivative', *J. Phys. Chem. A* **2007**, *111*, 10460–10467.

[59] B. Kohler, 'Nonradiative Decay Mechanisms in DNA Model Systems', *J. Phys. Chem. Lett.* **2010**, *1*, 2047–2053.

[60] J. Chen, B. Kohler, 'Ultrafast nonradiative decay by hypoxanthine and several methylxanthines in aqueous and acetonitrile solution', *Phys. Chem. Chem. Phys.* **2012**, *14*, 10677–10682.

[61] Y. Zhang, J. Chen, B. Kohler, 'Hydrogen Bond Donors Accelerate Vibrational Cooling of Hot Purine Derivatives in Heavy Water', *J. Phys. Chem. A* **2013**, *117*, 6771–6780.

Additional Information of Chapter 4

4.A Additional Experimental Details

Adenine (99 % purity) was obtained from Sigma-Aldrich and used without further purification. Sample solutions were prepared with bidistilled water and degassed by sonication. The sample concentration was set to 0.5 OD at 260 nm and 1 mm cell length which corresponds to 0.355 mM. The heated flow cell was pumped by a peristaltic pump at a flow rate of 21 mL/min. The temporal resolution of the experiment using this sample cell was around $\sigma_{\mathrm{IRF}} \approx 0.12$ ps.

The two halves of the body of the pressure resistant sample cell were held together by one-piece steel screws. The cell was connected to a high precision flow pump to establish a continuous flow of 4.99 mL/min. The pressure in the cell was manually adjusted using a needle valve at the outlet of the cell. The temporal resolution of the experiment using this sample cell was around $\sigma_{\mathrm{IRF}} \approx 0.23$ ps, hence lower than for the other cell due to the thicker windows.

4.B Additional Experimental Data

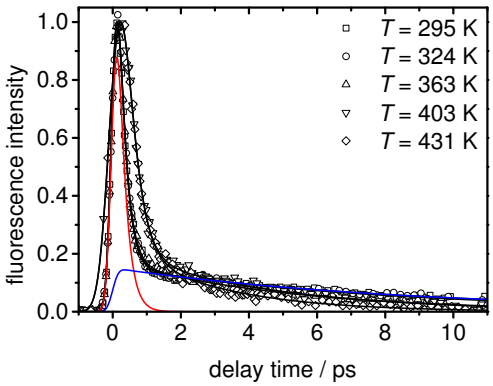

Figure 4.B1: Time-resolved fluorescence decay curves of adenine in water measured at $\lambda_{\mathrm{probe}} = 430$ nm as function of temperature. Data points are shown as open symbols, fitted biexponential model functions are represented by solid lines. The contributions for the data at $T = 295$ K are shown in red (9H-Ade) and blue (7H-Ade).

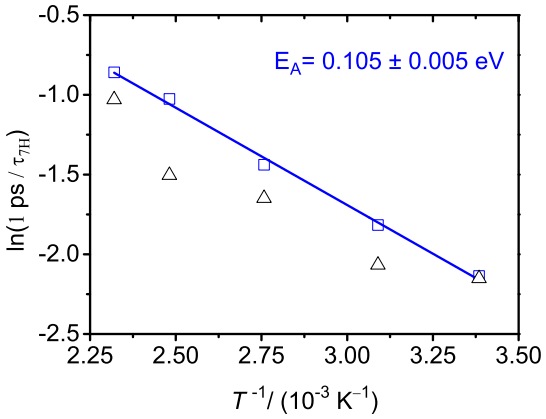

Figure 4.B2: Arrhenius plot from main text, added are the results for $\lambda_{\text{probe}} = 430$ nm in open triangles.

Table 4.B1: Additional experimental results for the fluorescence decay times of 9H- and 7H-Ade at $\lambda_{\text{probe}} = 350$ nm and 430 nm in the range 298 K $\leq T \leq$ 431 K. Numbers in parentheses represent the 2σ standard error.

T/K	a_{9H}	τ_{9H}/ps	a_{7H}	τ_{7H}/ps
$\lambda_{\text{probe}} = 350$ nm				
295	0.76(1)	0.21(1)	0.24(1)	8.4(2)
323	0.75(1)	0.21(1)	0.25(1)	6.3(1)
363	0.73(1)	0.21(1)	0.27(1)	4.3(1)
403	0.71(2)	0.21(1)	0.29(1)	2.8(1)
431	0.73(2)	0.21(1)	0.27(1)	2.4(1)
$\lambda_{\text{probe}} = 430$ nm				
295	0.93(1)	0.21(1)	0.07(1)	8.6(3)
323	0.93(1)	0.21(1)	0.07(1)	7.9(3)
363	0.92(1)	0.31(1)	0.08(1)	5.2(3)
403	0.92(3)	0.31(1)	0.08(3)	4.5(2)
431	0.91(3)	0.31(1)	0.09(3)	2.8(2)

4.C Additional Master Equation Modeling Details and Results

Table 4.C1: Overview of MultiWell simulation results for the electronic dynamics 7H-Ade for $E^*_{\text{start}} = 30.88$ kJ/mol and different parameters ΔE_{down} and ΔE_0. The simulated values are the exponential decay time components τ_1 and τ_2 of the reactant loss time profiles shown exemplarily in Fig. 4.6, and the simulated activation energy $E_{\text{A,sim}}$ obtained by Arrhenius analysis of τ_2.

ΔE_{down}	$\Delta E_0 = 9.20$ kJ/mol	$\Delta E_0 = 9.62$ kJ/mol	$\Delta E_0 = 10.0$ kJ/mol
500 cm^{-1}	$\tau_1 = 0.20$ ps $\tau_2(295\text{ K}) = 7.3$ ps $\tau_2(431\text{ K}) = 1.8$ ps $E_{\text{A,sim}} = 10.9$ kJ/mol	$\tau_1 = 0.14$ ps $\tau_2(295\text{ K}) = 8.9$ ps $\tau_2(431\text{ K}) = 2.0$ ps $E_{\text{A,sim}} = 11.3$ kJ/mol	$\tau_1 = 0.22$ ps $\tau_2(295\text{ K}) = 10.4$ ps $\tau_2(431\text{ K}) = 2.2$ ps $E_{\text{A,sim}} = 11.8$ kJ/mol
250 cm^{-1}	$\tau_1 = 0.43$ ps $\tau_2(295\text{ K}) = 7.7$ ps $\tau_2(431\text{ K}) = 2.1$ ps $E_{\text{A,sim}} = 10.3$ kJ/mol	$\tau_1 = 0.45$ ps $\tau_2(295\text{ K}) = 9.2$ ps $\tau_2(431\text{ K}) = 2.4$ ps $E_{\text{A,sim}} = 10.6$ kJ/mol	$\tau_1 = 0.47$ ps $\tau_2(295\text{ K}) = 10.6$ ps $\tau_2(431\text{ K}) = 2.6$ ps $E_{\text{A,sim}} = 10.8$ kJ/mol
205 cm^{-1}	$\tau_1 = 0.49$ ps $\tau_2(295\text{ K}) = 7.6$ ps $\tau_2(431\text{ K}) = 2.1$ ps $E_{\text{A,sim}} = 9.86$ kJ/mol	$\tau_1 = 0.53$ ps $\tau_2(295\text{ K}) = 9.5$ ps $\tau_2(431\text{ K}) = 2.5$ ps $E_{\text{A,sim}} = 10.25$ kJ/mol	$\tau_1 = 0.55$ ps $\tau_2(295\text{ K}) = 10.9$ ps $\tau_2(431\text{ K}) = 2.8$ ps $E_{\text{A,sim}} = 10.5$ kJ/mol
100 cm^{-1}	$\tau_1 = 0.70$ ps $\tau_2(295\text{ K}) = 9.5$ ps $\tau_2(431\text{ K}) = 2.0$ ps $E_{\text{A,sim}} = 12.0$ kcal/mol	$\tau_1 = 0.78$ ps $\tau_2(295\text{ K}) = 11.6$ ps $\tau_2(431\text{ K}) = 2.6$ ps $E_{\text{A,sim}} = 11.5$ kcal/mol	$\tau_1 = 0.83$ ps $\tau_2(295\text{ K}) = 13.0$ ps $\tau_2(431\text{ K}) = 3.2$ ps $E_{\text{A,sim}} = 11.5$ kJ/mol

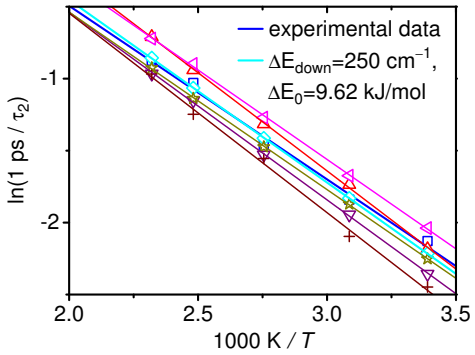

Figure 4.C1: Arrhenius plot for the simulated time constants in comparison with the experimental data (blue). $E^*_{\text{start}} = 7.38$ kcal/mol for all.
Red: $\Delta E_{\text{down}} = 500$ cm^{-1} and $\Delta E_0 = 9.62$ kJ/mol.
Purple: $\Delta E_{\text{down}} = 250$ cm^{-1} and $\Delta E_0 = 10.0$ kJ/mol.
Cyan: $\Delta E_{\text{down}} = 250$ cm^{-1} and $\Delta E_0 = 9.62$ kJ/mol.
Magenta: $\Delta E_{\text{down}} = 250$ cm^{-1} and $\Delta E_0 = 9.20$ kJ/mol.
Dark Yellow: $\Delta E_{\text{down}} = 205$ cm^{-1} and $\Delta E_0 = 9.62$ kJ/mol.
Wine: $\Delta E_{\text{down}} = 100$ cm^{-1} and $\Delta E_0 = 9.62$ kJ/mol.

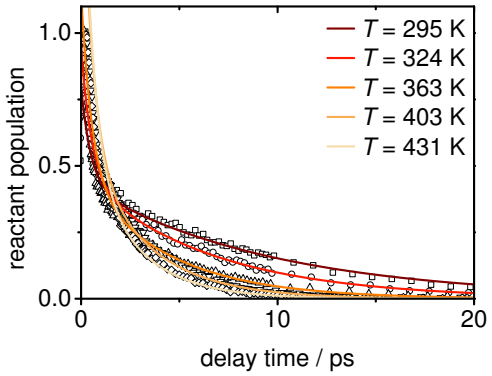

Figure 4.C2: Simulated reactant population as function of temperature. Shown are the biexponential best fit curves (solid lines) in comparison to the experimental data (open symbols). The amplitudes of the simulated curves were scaled to meet the experimental data. Input parameters of the simulations are given in Table 4.2 in the main text.

```
7H-Ade thermal reaction
10. 1000 1500 25000. 2113989022
'BAR' 'KCAL' 'AMUA'
295. 295.
1
1360. !pressure adjusted to meet the liquid particle density
1 1
1 'Ade1frq_____' 0. 269.065 1 1 1
2 'Ade2frq_____' 0.
2.71 506. 18.0153 135.127 !H2O collider
1 6.299 550. 1 250. 0.0 0.0 0.0 0.0 0.0 0.0 0.0 !naphthalene parameters
'LJ'
1
1 2 'TSfrq________' 269.065 1 1 1 1.0e+14 2.3 'NOREV' 'FAST' 'NOTUN' 'NOCENT'
'SUM'
100000 'TIME' 4.0E-11 'THERMAL' 1 3 7.38
```

Figure 4.C3: Example input file for simulations using MultiWell.

5 Electronic Deactivation Dynamics of the Adenine Dinucleotide

Abstract

Stacking interactions between nucleobases stabilize the helical structure of DNA strands, but change their electronic structure. Electronic excitation of well-stacked systems generates states of exciton and excimer character that show distinctly different excited-state dynamics than single excited nucleobases. The adenine dinucleotide d(ApA) was investigated as a model system by femtosecond time-resolved transient electronic absorption spectroscopy after excitation at $\lambda_{\mathrm{pump}} = 260$ nm in aqueous solution in the temperature range 278 K $\leq T \leq$ 295 K and in D_2O at room temperature. The results were directly compared to measurements of the adenine monomer dAMP. The experimental data are assigned to critical steps in the evolution of the excited state via proposed exciton- and excimer-like states en route towards the electronic ground state and give insight into the molecular mechanisms of electronic relaxation. Two sub-picosecond decay components, independent of temperature and deuteration, were assigned to relaxation within the exciton stack in $\tau_1 \approx 0.16$ ps and to "perturbed-monomer-like" decay in $\tau_2 \approx 0.48$ ps by a C^2-puckering deformation of one of the Ade units. Two long-lived excited-state lifetime components showed temperature dependence indicating potential energy barriers on the electronic deactivation pathway. The time constants were assigned to relaxation within $\tau_3 \approx 6$ ps from an intermediate excimer to a stabilized excimer, and to subsequent conversion to the ground state within $\tau_4 \approx 360$ ps. The states were found to be separated by a barrier and to lie at similar energy levels. A pronounced kinetic isotope effect demonstrated involvement of at least one of the fully deuterated amino groups in the deactivation mechanism of the stabilized excimer which is discussed in context of recent quantum chemical calculations.

5.1 Introduction and Motivation

Three phenomena influence the reliability of the biologically most relevant DNA molecule. These are the vertical stacking of nucleobases within DNA strands, the base pairing between two DNA single strands and the nucleobase sequence of these strands. While the sequence encodes the genomic information and the base pairing facilitates molecular recognition and replication, all three were found to directly influence UV-induced processes in the DNA molecules.[1–8] Stacking results from weak interactions between the π-orbitals of aromatic molecules and can be observed even between free nucleobases in sufficiently concentrated aqueous solutions.[9–11] The interactions stabilize the helical structure of DNA strands, but change their electronic structure. In particular, the ultrafast dynamics known for single photo-excited nucleobases are heavily influenced and new excited-state features appear.

The dinucleotide d(ApA) acts as a bridge between the model systems dAMP and polydA that are frequently investigated with the goal to understanding the electronic deactivation dynamics of natural DNA. Due to the outstanding stacking ability of adenine (Ade), d(ApA) adopts B-DNA conformation with an interbase distance of $d = 3.4$ Å and a twist angle of $\alpha = 36°$ between the chromophores as shown in Fig. 5.1. The molecular structure is readily formed upon dissolving in

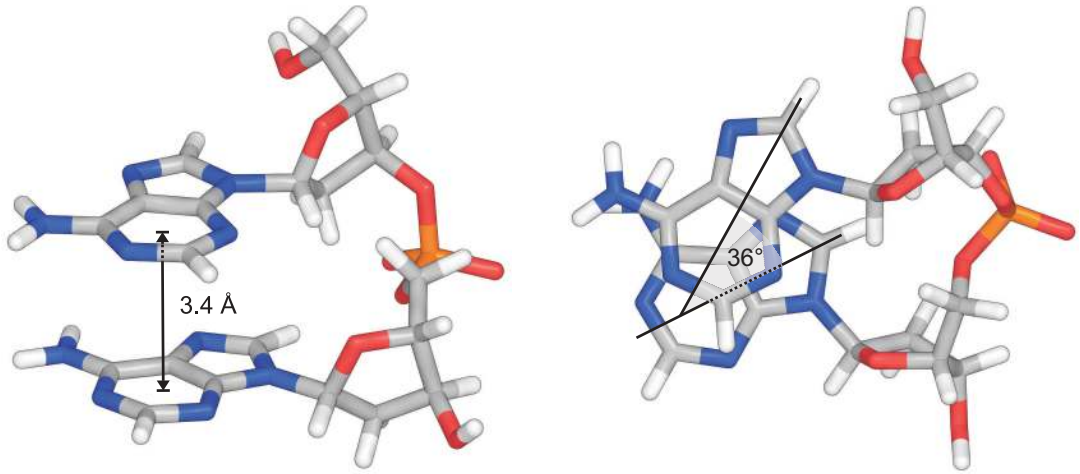

Figure 5.1: Molecular structure of the stacked Ade dinucleotide d(ApA) in B-DNA conformation in side view (left) and top view (right). Under physiological conditions, the phosphate group is deprotonated and the charge is compensated by a Na^+ counterion.

water as was confirmed by NMR[12] and CD[13,14] spectroscopy and consistent with DFT calculations.[15] The Ade dinucleotide is the smallest possible model structure to study DNA single strands. However, the stacked structure was described as highly

dynamic and the stacking fraction depends on temperature.[13] In the excited state, this flexibility allows for rearrangement to a face-to-back conformation with enhanced nucleobase overlap.[16–20]

Pronounced characteristics for exciton and excimer formation were observed for excited-state d(ApA). Recent calculations could show that in an Ade polynucleotide the excitation energy is mostly delocalized over two adjacent bases[21] giving the dinucleotide the opportunity to form similar delocalized states as the polymer. The delocalization is a result of excitonic coupling between the transition dipole moments of the adenine units[22,23] which causes band splitting and hypochromism of the lowest $\pi\pi^*$ transitions in the Ade units.[21,24–29] The static absorption spectrum of the dinucleotide d(ApA) is shown in Fig. 5.2 next to its fluorescence spectrum. The spectra of the monomer dAMP and the polynucleotide dA_{20} are given in direct comparison for they represent the unstacked unit and the extended Ade stack. The

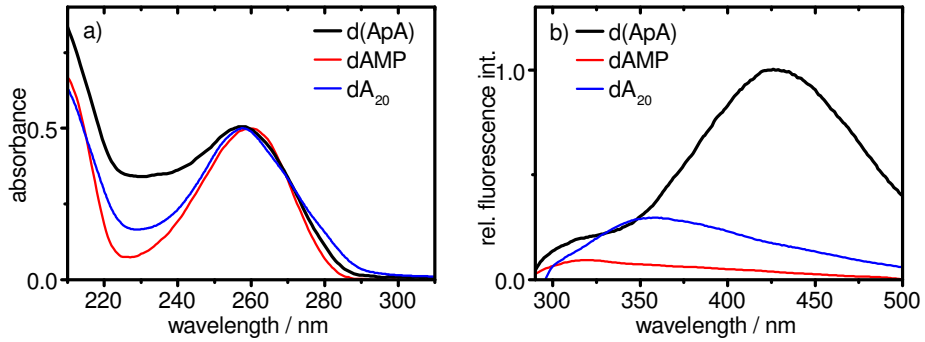

Figure 5.2: Static UV absorption (b) and static fluorescence (b) spectra of d(ApA) (black) measured after excitation at $\lambda_{exc} = 260$ nm in buffered aqueous solution (pH 7.0) in comparison to the spectra of dAMP (red) and dA_{20} (blue, taken by J. Kleber[30]). The solutions were normalized to an absorbance of $OD_{260\,nm} = 0.5$ for better comparison. The fluorescence spectra were scaled to $OD_{260\,nm} = 0.5$ and normalized relative to the emission maximum of d(ApA).

absorption spectra show small blue-shifts of the maxima for d(ApA) and dA_{20} due to exciton coupling in vertically stacked chromophores. A weakly increased absorption in the red wing indicates helical structures with a twist angle between the interacting transition dipole moments.[27] Direct absorption to charge transfer (CT) states is predicted for the red wing of the absorption spectrum and the transition probability increases with the wavelength.[18,31,32]

The fluorescence spectrum of d(ApA) shows a weak band similar to that of the

monomer at $\lambda = 320$ nm and a strongly red-shifted emission band at $\lambda = 425$ nm with a nearly three times higher quantum yield ($\phi_f(\text{ApA}) \approx 1.6 \cdot 10^{-4}$ compared to $\phi_f(\text{dAMP}) \approx 0.5 \cdot 10^{-4}$).[33,34] The strong band is a signature of excimer formation[35] with an energetic stabilization of about $\Delta E = 1$ eV. In this context, an excimer is an energetically favorable excited state featuring significant electron density between the interacting units. It is only accessible in well-stacked molecules with delocalized π-electron systems. Interestingly, the oligomer emission intensity and position lies between those of the monomer and the dimer (see Fig. 5.2 and also Chapter 6 of this Thesis). The strong stabilization by excimer formation thus seems to be unique for the Ade dinucleotide.

The increased fluorescence intensity of d(ApA) indicates prolonged excited-state lifetimes. Four electronic lifetime components spanning nearly three orders of magnitude, 0.1 ps, 0.3 ps, $5 - 10$ ps and 360 ps, were determined for d(ApA) in aqueous solution by transient electronic absorption and transient fluorescence spectroscopy.[4–6,36] In fact, d(ApA) not only shows the strongest fluorescence shift but also the longest excited-state lifetime among other hetero- and homodinucleotides.[37–39] The longest electronic lifetime component was only found at fluorescence wavelengths at $\lambda_{\text{fluo}} \geq 360$ nm and its amplitude increases towards the red side of the emission spectrum.[4,5] This lifetime-increase with the emission wavelength is also known for longer Ade oligonucleotide strands[40–42] which will be investigated and discussed in Chapter 6.

In transient electronic absorption, the long lifetime of d(ApA) is accompanied by a narrow transient excited-state absorption band in the near UV probe range[4,6,43] which seems to be characteristic also for heterodinucleotides containing Ade.[37–39] The spectral evolution and temporal sequence of the transient signals leading to the formation of this signature were interpreted as stepwise evolution of electronic character from excitons to excimer-like states.[4–6] Accoring to this interpretation, the evolution starts with the ultrafast relaxation within the exciton stack and is followed either by decay to localized states on a single base leading to monomer-like relaxation, or by transfer to excimer-like states with shared excitation energy between both bases. Only then, a stabilized excimer is formed which shows hindered decay to the ground state.

While the ultrafast monomer-like excited-state deactivation is reasonably well described,[16,18,19,44–48] the transition to and the deactivation from the excimer-like state(s) are not at all conclusively understood. A number of molecular decay mechanisms were proposed from theoretical calculations, among which are shortening

of the interbase distance,[4,16–20,49] intermediate bond-formation,[47,50–53] and decay by monomer-like puckering motions after relocalization to one of the monomer units.[16,19,31,44–46,48,54] Complicating matters further, several types of excimer-like states were identified with various degrees of charge transfer character, delocalization of electron density between the bases, and conformation and ring puckering of the molecular units.[55–57]

Thus, in spite of detailed experimental observations and theoretical predictions, the exact sequence of molecular mechanisms for the formation and decay of the stabilized excimer needs further investigations.

This work presents a comprehensive experimental approach to tackle the complex electronic deactivation mechanisms of the dinucleotide d(ApA) by comparing time-resolved measurements in H_2O, at lowered temperature, and in D_2O. For this purpose, transient electronic absorption spectroscopy with a broad UV-vis probe range was applied. Temperature-dependent measurements showed clear trends for excited-state lifetimes of $\tau > 1$ ps. As was shown in Chapter 4, temperature change affects thermally activated processes and can quantify energy barriers for electronic deactivation processes. Measurements in D_2O were expected to separate solvent-mediated relaxation from intramolecular relaxation, i. e. vibrational cooling from excited-state absorption. However, deuteration effects were also observed for excited-state signals. These will be discussed in view of the participation of deuterated molecular moieties in the electronic deactivation mechanisms.

In the following, after giving experimental details, the experimental results and the data analysis will be described in three Sections. The first shows the data for d(ApA) which were measured at room temperature in H_2O back to back to measurements of dAMP as reference sample. The second shows the data measured at lowered temperature in H_2O and the third shows the data measured at room temperature in D_2O. Again, the results for d(ApA) will be shown in detail and compared to the results for dAMP. A discussion of the temperature- and solvent-dependent electronic deactivation of dAMP can be found in the Additional Information.

5.2 Experimental Details

2'-Deoxyadenosine 5'-Monophosphate ($98 - 100\,\%$, dAMP) was purchased from Sigma-Aldrich and used as received. d(ApA) was synthesized, purified by HPLC and checked by ESI mass spectrometry by metabion international AG. The sample was delivered lyophilized and used as received. Solutions with an optical density of OD ≈ 0.5 at 260 nm at an optical path length of 100 µm were prepared with

ultra-pure water and set to pH 7.0 using phosphate buffer (16 mM NaH_2PO_4, 34 mM Na_2HPO_4, 117 mM NaCl). Solutions in D_2O (99.9 %, Deutero) were set to pD 7.4 with the same buffer. The concentrations of the samples were c(dAMP) = 3.7 mM and c(d(ApA)) = 1.6 mM.

Time-resolved measurements were performed using the femtosecond transient electronic absorption spectrometer for simultaneous broadband and single-color detection described before (Chapter 2 and Ref. 58). The excitation pulses were generated in a Ti:Sa-pumped home-built frequency-doubled NOPA at $\lambda_{pump} = 260$ nm with pulse durations of 35 fs (fwhm) and focused into the sample under magic angle polarization. The pulse energy was attenuated to 100 nJ for the measurements at room temperature in H_2O and D_2O. The samples were excited with 220 nJ pulse energy at lowered temperature. Broadband detection pulses were generated in CaF_2 by careful adjustment of the Ti:Sa fundamental pump pulse energy to yield a spectrum between $\lambda_{probe} = 315-600$ nm. Single-color detection pulses were generated in a second frequency-doubled NOPA at $\lambda_{probe} = 255$ nm with pulse durations of 40 fs(fwhm).

The sample solutions were flowed through a home-built wire-guided gravity-driven liquid film device described in Section 2.1.2 providing a film thickness of 100 µm and a constant sample temperature. Samples were measured at $T = 278$ K, $T = 288$ K and $T = 295$ K. Sample volume and flow speed ensured an exchange of probed molecules between two excitation pulses and an overall excitation of the sample below 1 %. The measurement time was adjusted to avoid evaporation of water to ensure constant sample concentrations during one measurement. All samples were measured back-to-back with measurements of the neat solvent. For each sample, three successive runs were checked for consistency and averaged for final analysis. After each run, the static UV absorption spectrum was checked for sample integrity. The recorded transient electronic absorption maps and the single color curves were corrected for solvent contributions, noise and white light chirp as described in the literature[59,60] and earlier PhD Theses.[4,61,62] The spectra were cut off at the maximum of the solvent signal in the UV part of the probe spectrum due to the white light break-off.

The data were analyzed using a nonlinear least-squares routine based on the Levenberg–Marquardt algorithm for fitting of time profiles or transient spectra. For a global analysis, the method of singular value decomposition (SVD)[63–65] was applied that separated the temporal from the spectral information and allowed for independent analyses. All given errors for the fitting results correspond to 2σ

standard deviations.

5.3 Results in H_2O at Room Temperature

5.3.1 Transient Electronic Absorption

Femtosecond time-resolved transient electronic absorption spectroscopy of d(ApA) in H_2O at $T = 295$ K in the probe wavelength range $\lambda_{probe} = 315 - 600$ nm after excitation at $\lambda_{pump} = 260$ nm yielded the two-dimensional map presented in Fig. 5.3 shown in direct comparison to the map for dAMP. The electronic absorption change

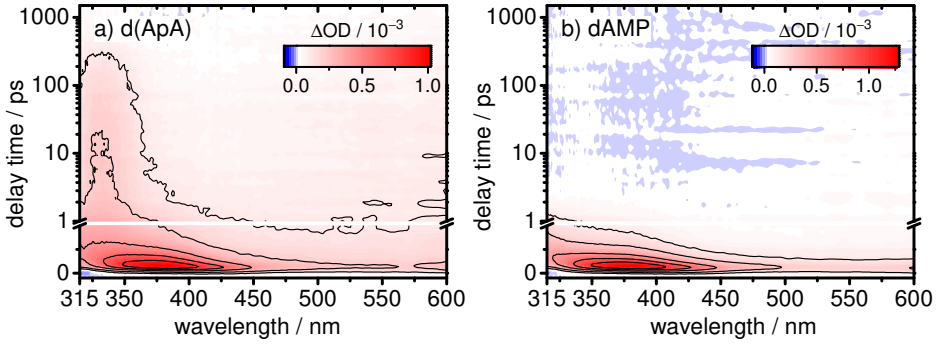

Figure 5.3: Two-dimensional spectro-temporal transient electronic absorption maps of d(ApA) (a) and dAMP (b) recorded in H_2O at $T = 295$ K after excitation at $\lambda_{pump} = 260$ nm shown on a linear scale up to $\Delta t = 1$ ps and on a logarithmic timescale for delay times up to $\Delta t = 1500$ ps.

ΔOD after photoexcitation is plotted against probe wavelength and time delay in a bipolar color map. Delay times are shown on a logarithmic timescale up to $\Delta t = 1000$ ps, but were measured up to $\Delta t = 1700$ ps.

The spectro-temporal signal for d(ApA) shows a spectrally broad initial excited-state absorption (ESA) expanding over the entire probe wavelength range. It shifts towards the UV edge of the probe spectrum within a few hundred femtoseconds and decays on the same timescale. Between $\lambda_{probe} = 315 - 370$ nm, an additional narrow and long-lived ESA signal can be seen that decays within several hundred picoseconds. A weak ESA band with a similar lifetime is observed at $\lambda_{probe} = 500 - 600$ nm. The spectro-temporal signal of dAMP shows a broad ESA band which shifts towards the UV edge of the probe spectrum and decays within $\Delta t = 2$ ps. For both samples, the transient signal around $\lambda_{probe} = 315$ nm has a negative sign at short delay times and rises delayed. This is assigned to an overlay of stimulated emission (SE), yielding a negative signal contribution, and hot ground state absorption (HGSA), giving

a positive signal. The latter can only be observed after internal conversion of the excited state to the ground state, and, thus, shows delayed rise.

5.3.1.1 Spectro-Temporal Evolution of the Transient Absorption Bands

In order to expose the excited-state behavior, selected transient electronic absorption spectra were cut out from the spectro-temporal transient electronic absorption map of d(ApA) measured at $T = 295$ K in H_2O. The spectra are shown in Fig. 5.4 for delay times up to $\Delta t = 600$ ps in direct comparison to selected transient spectra of dAMP for delay times up to $\Delta t = 1.9$ ps. The broad initial the transient electronic

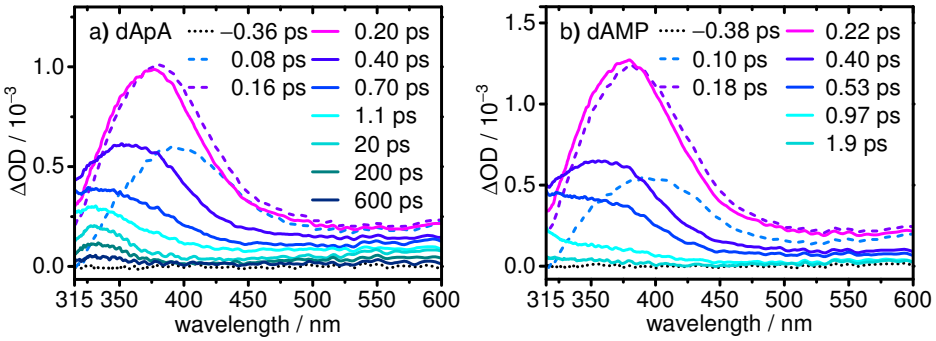

Figure 5.4: Selected transient electronic absorption spectra of d(ApA) (a) and dAMP (b) measured at $T = 295$ K in H_2O after excitation at $\lambda_{pump} = 260$ nm. Dashed lines indicate delay times during the rise of the signal.

absorption band of d(ApA) rises to a maximum at $\lambda_{probe} = 380$ nm and evolves to a narrow ESA structure with a maximum at $\lambda_{probe} = 330$ nm after $\Delta t \approx 1$ ps that is clearly visible for delay times $\Delta t \geq 600$ ps. The transient spectra of dAMP also show an ESA band shift between the rise of the signal with a maximum at $\lambda_{probe} > 400$ nm and its decay around $\lambda_{probe} \approx 350$ nm. The shift is completed after $\Delta t \approx 1$ ps and the signal fully decays within $\Delta t = 2$ ps.

At first glance, the ESA bands of both samples appear to be similar in shape and in their temporal blue-shift. For further analysis of the fast spectro-temporal dynamics, all transient electronic absorption spectra were modeled by a sum of three log-normal functions. Selected transient spectra and best fit curves for d(ApA) are shown in Fig. 5.5 together with the individual spectral bands. The three spectral bands represent i) the negative contribution of SE and the ensuing positive contribution of HGSA around $\lambda_{probe} = 315$ nm, ii) the most prominent, long-lived ESA band with its maximum shifting between $\lambda_{probe} = 420 - 330$ nm, and iii) the

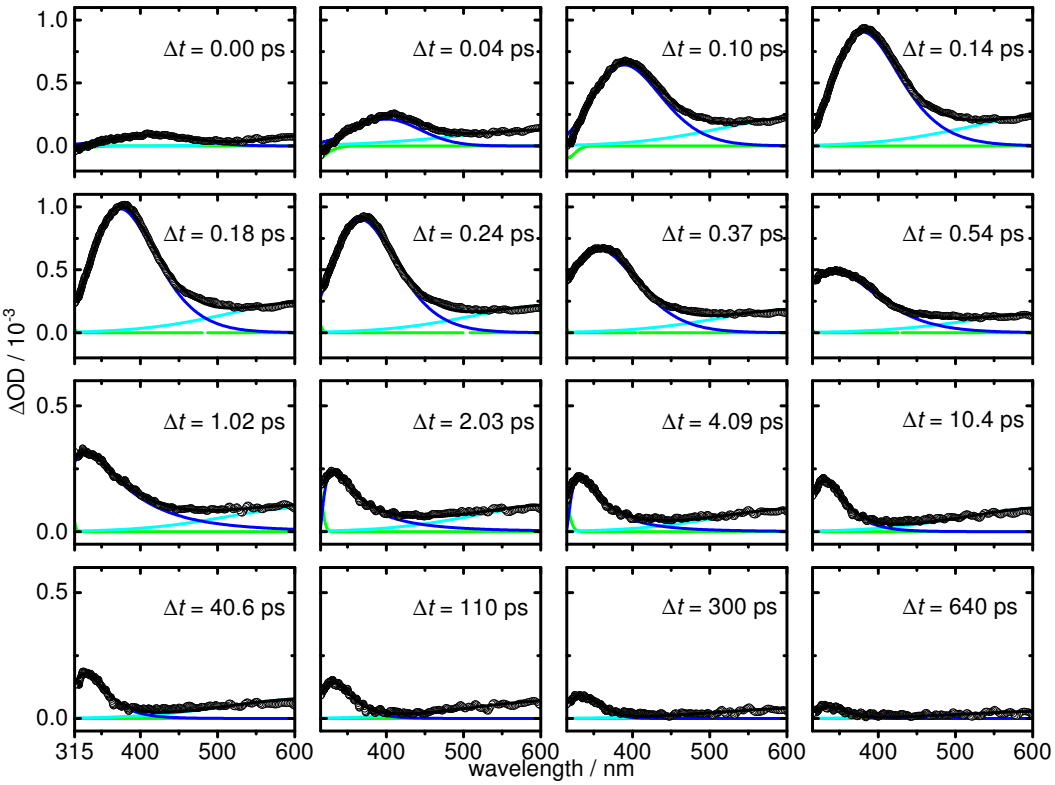

Figure 5.5: Expanded views of the transient electronic absorption spectra of d(ApA) at selected delay times up to $\Delta t = 640$ ps after excitation at $\lambda_{pump} = 260$ nm measured at $T = 295$ K in H_2O. The experimental data (open circles) were described by a sum of three log-normal functions (black line) each representing an individual spectral band (green, blue, cyan).

weak and broad long-lived ESA band with maximum at $\lambda_{probe} > 600$ nm. The correesponding results for dAMP can be found in the Additional Information.

5.3.1.2 Time-Profile Analysis

A set of decay time constants was determined to describe the temporal evolution of the transient electronic absorption signal of d(ApA). For this purpose, a time profile was extracted from the spectro-temporal data of d(ApA) by spectral integration over the probe wavelength range $\lambda_{probe} = 315 - 450$ nm. This range comprises most of the initial broad and blue-shifting ESA band, the full long-lived narrow ESA band and the SE/HGSA signals. Thus, it contains the full temporal information of the measured data. A second time profile was obtained by the single-color probe measurement at $\lambda_{probe} = 255$ nm where the ground state population was monitored. The bleach of the signal directly after excitation is followed by the recovery of the

ground state population (GSR) due to internal conversion from the first excited state. The GSR signal of d(ApA) did not completely decay to zero within the measured time window of $\Delta t = 600$ ps.

The two data sets were modeled with Gaussian-convoluted multi-exponential decay functions with simultaneously fitted time constants. The data and the best fit curves are shown in Fig. 5.6 together with the respective time profiles and best fit curves for dAMP for comparison. The direct comparison emphasizes the dinucleotide-specific decay dynamics that are nearly three orders of magnitude longer than in the monomer.

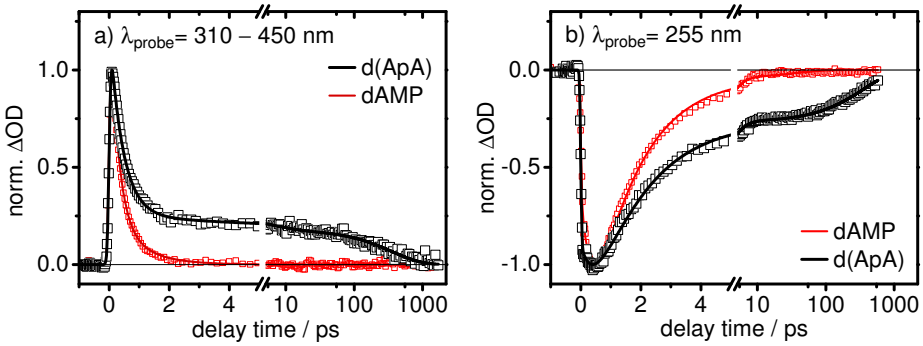

Figure 5.6: Transient absorption-time profiles of d(ApA) (black) in direct comparison to the time profiles of dAMP (red) measured after excitation at $\lambda_{\mathrm{pump}} = 260$ nm at $T = 295$ K in H_2O. Time profiles in a) were extracted by wavelength integration of the measured spectro-temporal data between $\lambda_{\mathrm{probe}} = 315 - 450$ nm. Time profiles in b) were recorded with a single-color probe beam at $\lambda_{\mathrm{probe}} = 255$ nm. Open symbols represent the data points, solid lines show the best fit curves from a simultaneous multi-exponential fit. Note the linear timescale for the first 5 ps and the logarithmic timescale thereafter.

For d(ApA), the fit yielded

$\tau_2 = 0.44 \pm 0.06$ ps,

$\tau_3 = 6 \pm 4$ ps

$\tau_4 = 360 \pm 40$ ps,

with an amplitude ratio of $\approx 13 : 1 : 2$ and a temporal resolution of $\sigma_{\mathrm{IRF}} = 0.052 \pm 0.001$ ps (width parameter of the Gaussian describing the instrumental response function) determined by deconvolution. The time constants were numbered according to their magnitude for better comparison, with τ_1 and τ_2 reserved for

sub-picosecond components. An additional time component,

$$\tau_{vc} = 1.7 \pm 0.3 \text{ ps},$$

necessary to describe the GSR time profile characterizes the overall timescale for vibrational cooling of hot ground state molecules, which are generated upon internal conversion from the excited state. The determined values are in excellent agreement with previous work at room temperature.[4–6]

For dAMP, the simultaneous fit of the wavelength-integrated and the GSR signal yielded

$$\tau_1 = 0.27 \pm 0.01 \text{ ps},$$
$$\tau_2 = 0.9 \pm 0.1 \text{ ps}$$

with an amplitude ratio of $\approx 4 : 1$ and a temporal resolution of $\sigma_{IRF} = 0.056 \pm 0.001$ ps, and

$$\tau_{vc} = 1.5 \pm 0.2 \text{ ps}$$

for the GSR signal. The probe wavelength range for integration, $\lambda_{probe} = 315-450$ nm, is known to contain signal contributions from SE, HGSA and ESA. In the case of dAMP, the transient signal is so short-lived that HGSA and ESA contribute equally to the wavelength-integrated time profile. The time constant for HGSA decay, which can be rationalized as an early sign of vibrational cooling, has been seen to increase with decreasing wavelength and can be extrapolated to be $\tau_{HGSA} \approx 1.0$ ps around $\lambda_{probe} = 300$ nm.[4,58,66] This explains that the here observed time constants for dAMP are longer than those found in Chapter 3.

5.3.1.3 Global Analysis

Global analyses of the full spectro-temporal transient electronic absorption maps for d(ApA) and dAMP were performed by singular value decomposition. The method separates the spectral from the temporal information and allows for a global description of the transient signals over the complete probe wavelength range.

The SVD time traces are multi-peak functions that converged to zero within $\Delta t = 1000$ ps for the dinucleotide and within $\Delta t = 3$ ps for the monomer (see Fig. 5.7). They could be described by Gaussian-convoluted multi-exponential functions so that every maximum or minimum yielded a new time constant. Small-amplitude oscillations were observed in traces 3 and 4 that were assumed to be a residue from the chirp correction and experimental noise. These were not modeled. The time

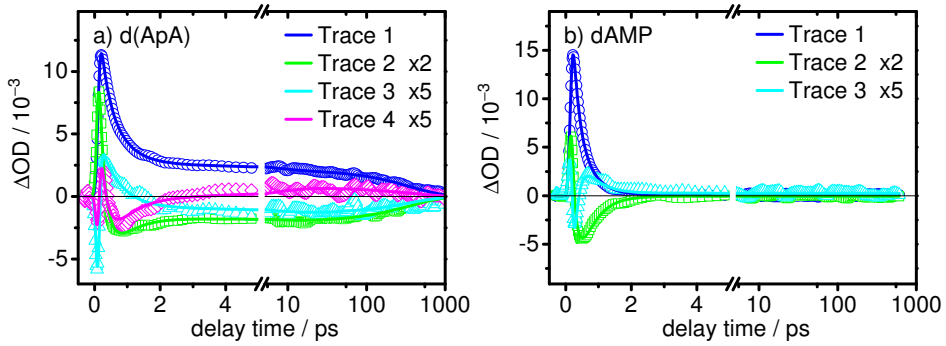

Figure 5.7: Time traces from the global SVD analysis of the spectro-temporal transient electronic absorption data of d(ApA) (a) and dAMP (b) measured after excitation at $\lambda_{pump} = 260$ nm at $T = 295$ K in H_2O. Time traces 2 – 4 were scaled by the given factors for better visibility. Note the linear timescale for the first 5 ps and the logarithmic timescale thereafter.

constants derived from this global analysis are in reasonable agreement with the above given time constants from the simultaneous analysis of the time profiles.

For d(ApA), the analysis yielded

$\tau_1 = 0.23 \pm 0.02$ ps,

$\tau_2 = 0.56 \pm 0.04$ ps,

$\tau_3 = 6$ ps (fixed),

$\tau_4 = 360 \pm 14$ ps.

Here, two sub-picosecond components were found. The third time constant, τ_3, had to be fixed at the value found in the time-profile analysis due to its low amplitude. It was considered essential because of previous results from transient fluorescence spectroscopy.[4,5,36]

For dAMP, the analysis yielded

$\tau_1 = 0.16 \pm 0.01$ ps,

$\tau_2 = 0.45 \pm 0.01$ ps.

The differences between the two methods of analysis will be discussed for dAMP in the Additional Information.

The decay-associated difference spectra (DADS) calculated from the SVD results to visualize the spectral contributions of the time components are shown in Fig. 5.8. These demonstrate that time constant τ_2, as it was found in the time-profile analysis,

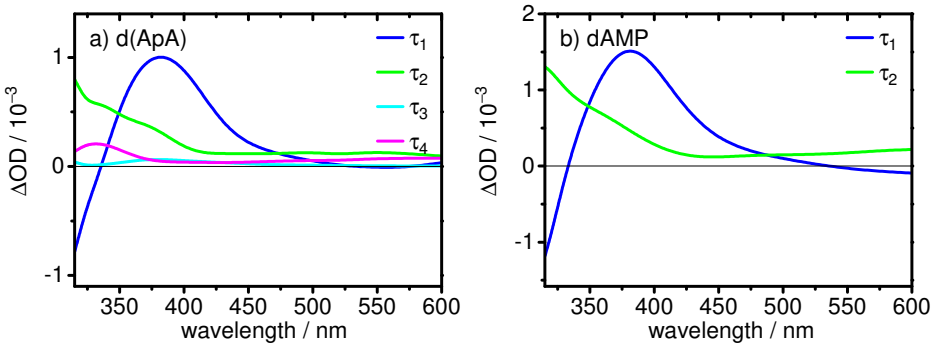

Figure 5.8: Decay-associated difference spectra from the global SVD analysis of the spectro-temporal transient electronic absorption data of d(ApA) (a) and dAMP (b) measured after excitation at $\lambda_{pump} = 260$ nm at $T = 295$ K in H_2O. The spectra each represent the spectral contribution of the time components τ_1 (blue), τ_2 (green), τ_3 (cyan) and τ_4 (magenta) given in the text.

is in fact a mixture of two sub-picosecond time components. They were separated in the SVD analysis to τ_1 and τ_2 and show DADS that are very similar for d(ApA) and dAMP. The DADS of the first time component shows a negative contribution in the range 315 nm $\leq \lambda_{probe} \leq$ 335 nm, where it is attributed to SE and the delayed rise of the signal. The spectrum shows a positive value with a maximum at $\lambda_{probe} = 380$ nm corresponding to the initial ESA decay. The negative amplitude at $\lambda_{probe} \geq 530$ nm is likely due to an overdone solvent subtraction. The second time component has a maximum DADS amplitude at $\lambda_{probe} = 315$ nm that decreases steadily with the wavelength and seems to decay to a constant at $\lambda_{probe} = 430$ nm. This hints at HGSA at the UV edge of the probe spectrum, but is assigned to ESA at visible probe wavelengths (see Chapter 3). The value of time constant τ_2 from the SVD analysis thus is a mixture of ESA and HSGA decay. The third and fourth lifetime components yield shallow spectra with maxima at $\lambda_{probe} = 380$ nm and $\lambda_{probe} = 330$ nm, respectively, that are assigned to ESA.

A direct comparison with previously measured transient absorption data for d(ApA) from this work group can be found in the Additional Information.

5.4 Results in H_2O at Lowered Temperature

5.4.1 Static Absorption and Static Fluorescence

The static UV absorption spectra and the fluorescence spectra after excitation of d(ApA) in H_2O at $\lambda_{exc} = 260$ nm at three temperatures in the range $T = 278 - 295$ K

are depicted in Fig. 5.9. While the absorption is independent from temperature

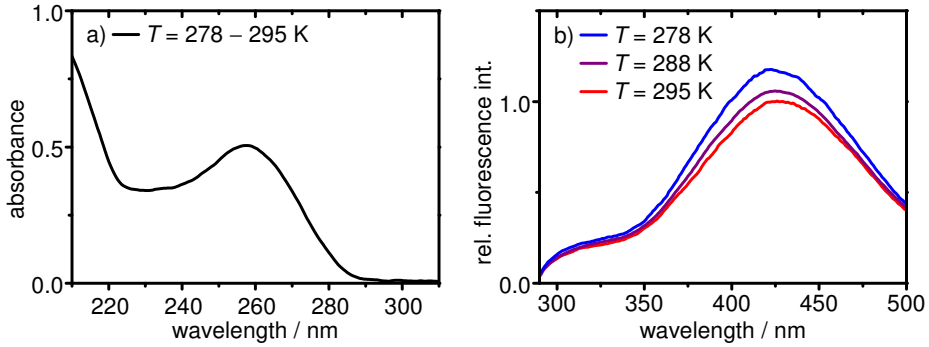

Figure 5.9: Static UV absorption (a) and static fluorescence (b) of d(ApA) measured at $T = 278$ K, $T = 288$ K and $T = 295$ K after excitation at $\lambda_{exc} = 260$ nm in H_2O. The fluorescence spectra were normalized relative to the emisson maximum of d(ApA) at room temperature.

within experimental errors, the fluorescence shows significant changes. The static fluorescence of the dinucleotide d(ApA) showed an increase by 25 % and a blue-shift of the maxiumum at $\lambda = 430$ nm by 3 nm at $T = 278$ K compared to room temperature. This effect is known from literature and was attributed to an increase of the stacking fraction at lowered temperature.[67,68]

5.4.2 Transient Electronic Absorption

Femtosecond time-resolved transient electronic absorption spectroscopy of the dinucleotide d(ApA) in the probe wavelength range $\lambda_{probe} = 315 - 600$ nm after excitation at $\lambda_{pump} = 260$ nm at $T = 278$ K and $T = 288$ K yielded the two-dimensional maps presented in Fig. 5.10. At first glance, the spectro-temporal maps seem to be highly similar to each other and in good agreement with the measurement at room temperature. A temperature effect on the signal is hardly distinguishable by eye due to the bipolar color representation and the broad range of signal intensities. It is clearly revealed, however, by the temporal analysis in the following.

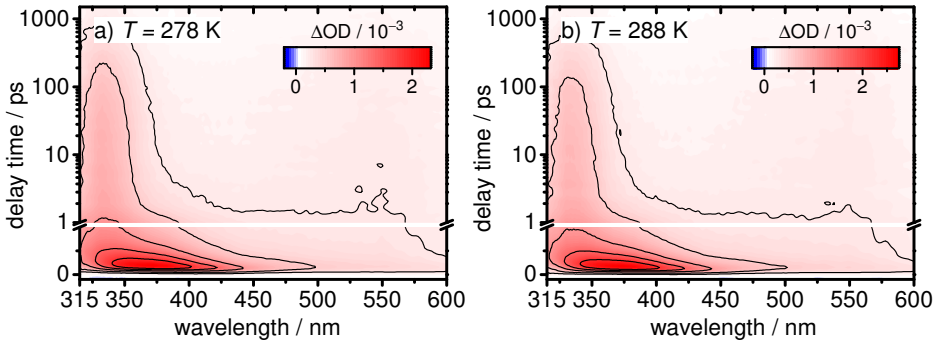

Figure 5.10: Two-dimensional spectro-temporal transient electronic absorption maps of d(ApA) recorded at $T = 278$ K (a) and $T = 288$ K (b) after excitation at $\lambda_{pump} = 260$ nm in H_2O shown on a linear scale up to $\Delta t = 1$ ps and on a logarithmic timescale for delay times up to $\Delta t = 1500$ ps.

5.4.2.1 Time-Profile Analysis

In order to expose the temperature dependence of the electronic deactivation dynamics of d(ApA), time profiles were extracted from the spectro-temporal absorption data by spectral integration over the probe wavelength range $\lambda_{probe} = 315 - 450$ nm as above for room temperature. Also here, this range contains the full temporal information of the measured data. Another set of time profiles was obtained by single-color probe measurements of the GSR signals at $\lambda_{probe} = 255$ nm. The ground state was not fully recovered within the measured time window of $\Delta t = 600$ ps (Fig. 5.11).

The data sets were modeled with Gaussian-convoluted multi-exponential decay functions with simultaneously fitted time constants. The data and the best fit curves for the measurements at $T = 278$ K and $T = 288$ K are shown in Fig. 5.11 together with the time profiles and best fit curves of the measurements at $T = 295$ K for direct comparison. The time profiles exhibit a gradual overall acceleration of the dynamics with increasing temperature.

For $T = 278$ K, the fit yielded

$\tau_2 = 0.44 \pm 0.01$ ps,

$\tau_3 = 8 \pm 2$ ps,

$\tau_4 = 690 \pm 30$ ps,

$\tau_{vc} = 2.0 \pm 0.1$ ps,

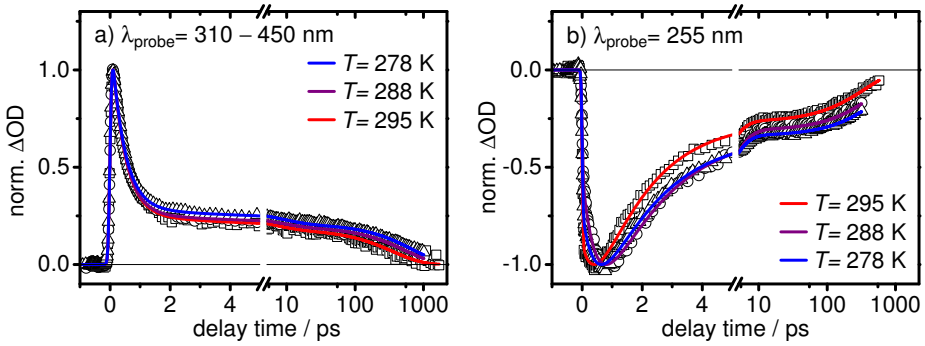

Figure 5.11: Transient absorption-time profiles of d(ApA) recorded at $T = 278$ K (blue), $T = 288$ K (purple) and $T = 295$ K (red) after excitation at $\lambda_{\text{pump}} = 260$ nm in H_2O. Time profiles in a) were extracted by wavelength integration of the measured spectro-temporal data between $\lambda_{\text{probe}} = 315 - 450$ nm. Time profiles in b) were recorded with a single-color probe beam at $\lambda_{\text{probe}} = 255$ nm. Open symbols represent the data points, solid lines show the best fit curves from multi-exponential fits. Note the linear timescale for the first 5 ps and the logarithmic timescale thereafter.

and for $T = 288$ K

$$\tau_2 = 0.44 \pm 0.01 \text{ ps},$$
$$\tau_3 = 7 \pm 2 \text{ ps},$$
$$\tau_4 = 550 \pm 20 \text{ ps},$$
$$\tau_{\text{vc}} = 2.1 \pm 0.1 \text{ ps},$$

with an amplitude ratio of $\approx 13 : 1 : 3$ and a temporal resolution of $\sigma_{\text{IRF}} = 0.052 \pm 0.001$ ps (width parameter of the Gaussian describing the instrumental response function). The time constants τ_1 and τ_2 were again reserved for sub-picosecond components. Both the longer components were found to decrease with increasing temperature which is consistent with the above seen decrease of the fluorescence quantum yield.

The additional time component, τ_{vc}, stems from the GSR time profiles. The vibrational cooling time seems to be increased at lower temperatures in comparison to room temperature, which can be attributed to a lower vibrational energy transfer rate to the solvent.

5.4.2.2 Global Analysis

Global analyses of the full spectro-temporal transient electronic absorption maps of d(ApA) at lowered temperature were performed by singular value decomposition. The

SVD time traces did not fully converge to zero within $\Delta t = 1000$ ps (see Fig. 5.12). They were described by Gaussian-convoluted multi-exponential functions.

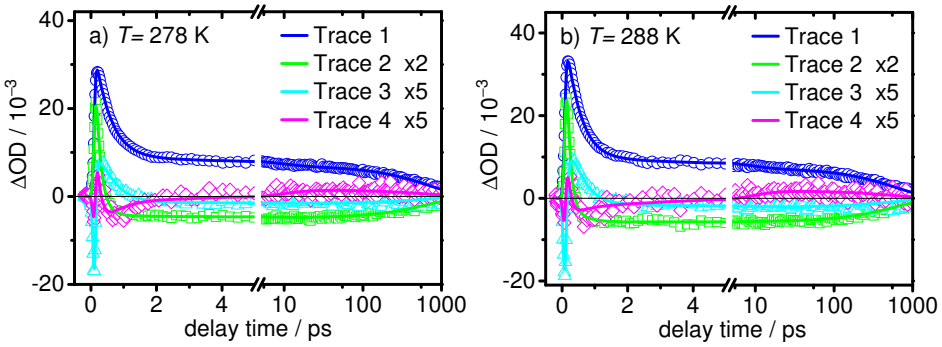

Figure 5.12: Time traces from the global SVD analysis of the spectro-temporal transient electronic absorption data of d(ApA) at $T = 278$ K (a) and $T = 288$ K (b) measured after excitation at $\lambda_{pump} = 260$ nm in H_2O. Time traces 2 – 4 were scaled by the given factors for better visibility. Note the linear timescale for the first 5 ps and the logarithmic timescale thereafter.

For $T = 278$ K, the analysis yielded

$$\tau_1 = 0.15 \pm 0.02 \text{ ps},$$
$$\tau_2 = 0.47 \pm 0.02 \text{ ps},$$
$$\tau_3 = 8 \text{ ps (fixed)},$$
$$\tau_4 = 680 \pm 25 \text{ ps}.$$

and for $T = 288$ K:

$$\tau_1 = 0.11 \pm 0.01 \text{ ps},$$
$$\tau_2 = 0.42 \pm 0.02 \text{ ps},$$
$$\tau_3 = 7 \text{ ps (fixed)},$$
$$\tau_4 = 600 \pm 25 \text{ ps}.$$

Again, two sub-picosecond components were found. The third time constant, τ_3, had to be fixed at the values found in the time-profile analysis due to their low amplitudes.

The decay-associated difference spectra calculated from the SVD results to visualize the spectral contributions of the time components are shown in Fig. 5.13. The DADS of the measurements of d(ApA) at lowered temperature are similar to those from the measurements at room temperature (Fig. 5.8 on page 125) except for

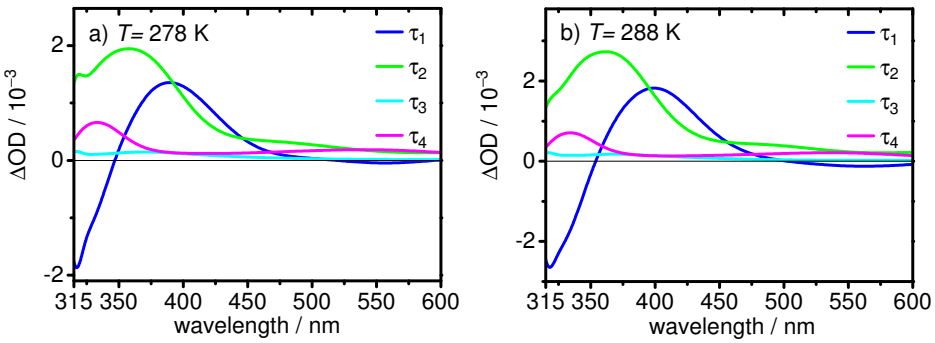

Figure 5.13: Decay-associated difference spectra from the global SVD analysis of the spectro-temporal transient electronic absorption data of d(ApA) at $T = 278$ K (a) and $T = 288$ K (b) measured after excitation at $\lambda_{pump} = 260$ nm in H_2O. The spectra each represent the spectral contribution of the time components τ_1 (blue), τ_2 (green), τ_3 (cyan) and τ_4 (magenta) given in the text.

the amplitude ratio of the first two time components at wavelengths $\lambda_{probe} < 420$ nm. This is attributed to the higher pump pulse energy that was used for the experiments at lowered temperature. The effect was also seen in the data for dAMP (see 5.C.5 in the Additional Information). The negative value of the DADS of the first component in the range 315 nm $\leq \lambda_{probe} \leq$ 335 nm is again attributed to SE and the delayed rise of the signal. The positive value with a maximum at $\lambda_{probe} = 380$ nm corresponds to the initial ESA decay. The second time component has a new maximum DADS amplitude at $\lambda_{probe} = 360$ nm. Contribution from HGSA is assigned to the UV edge of the spectrum. The third and fourth lifetime components yield shallow spectra with maxima at $\lambda_{probe} \approx 370$ nm and $\lambda_{probe} = 333 - 334$ nm, respectively, that are assigned to ESA. At the maximum, the relative amplitude of component τ_4 decreases with increasing temperature.

5.5 Results in D_2O at Room Temperature

Upon dissolving in D_2O, it is known that the hydrogen atoms of the amino group of Ade are fully exchanged by deuterium.[69] The same happens in the dinucleotide d(ApA) as was confirmed experimentally by a small blue-shift of the static absorption spectrum (not shown).

5.5.1 Transient Electronic Absorption

Femtosecond time-resolved transient electronic absorption spectra of d(ApA) were recorded in buffered D_2O solution (pD 7.4) at $T = 295$ K after excitation at

$\lambda_{pump} = 260$ nm. The two-dimensional spectro-temporal absorption map is presented in Fig. 5.14 and shows a similar excited-state decay behavior as in H_2O.

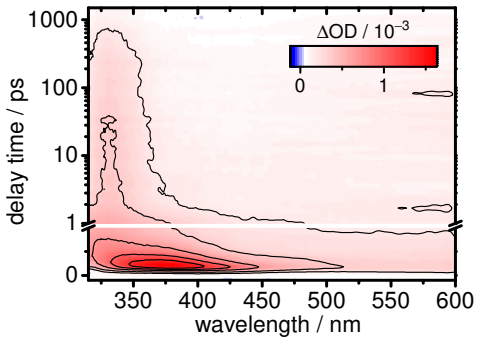

Figure 5.14: Two-dimensional spectro-temporal transient electronic absorption map of d(ApA) measured in D_2O at $T = 295$ K after excitation at $\lambda_{pump} = 260$ nm shown on a linear scale up to $\Delta t = 1$ ps and on a logarithmic timescale for delay times up to $\Delta t = 1500$ ps.

5.5.1.1 Time-Profile Analysis

The effect of deuteration on the electronic deactivation dynamics of d(ApA) becomes evident in the time profiles which were generated as described before. The data sets were modeled with Gaussian-convoluted multi-exponential decay functions with simultaneously fitted time constants. The data and the best fit curves for the measurements of d(ApA) in D_2O are shown in Fig. 5.15 together with the time profiles and best fit curves of the measurements of d(ApA) in H_2O for direct comparison. It can be seen that the long-time signal of d(ApA) extends to even longer times in D_2O. The fit yielded

$$\tau_2 = 0.44 \pm 0.01 \text{ ps},$$
$$\tau_3 = 6 \text{ ps (fixed)},$$
$$\tau_4 = 980 \pm 80 \text{ ps},$$
$$\tau_{vc} = 2.5 \pm 0.3 \text{ ps},$$

with an amplitude ratio of $\approx 9 : 1 : 2$ and a temporal resolution of $\sigma_{IRF} = 0.052 \pm 0.001$ ps (width parameter of the Gaussian describing the instrumental response function). The time constants τ_1 and τ_2 were again reserved for sub-picosecond components. The third time constant, τ_3, was fixed at the value found in H_2O. The additional time component, τ_{vc}, stems from the GSR time profiles. The longest time

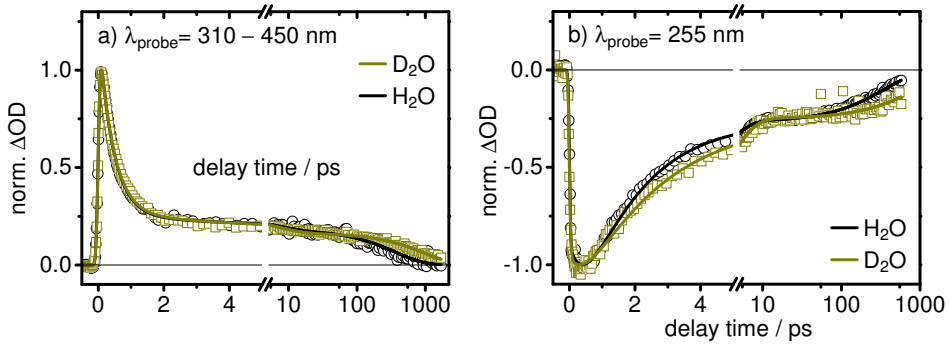

Figure 5.15: Transient absorption-time profiles of d(ApA) in D_2O (dark yellow) in direct comparison to the time profiles in H_2O (black) measured at $T = 295$ K after excitation at $\lambda_{pump} = 260$ nm. Time profiles in a) were extracted by wavelength integration of the measured spectro-temporal data between $\lambda_{probe} = 315 - 450$ nm. Time profiles in b) were recorded with a single-color probe beam at $\lambda_{probe} = 255$ nm. Open symbols represent the data points, solid lines show the best fit curves from multi-exponential fits. Note the linear timescale for the first 5 ps and the logarithmic timescale thereafter.

component, τ_4, and the vibrational cooling time, τ_{vc}, were found to be slightly higher in D_2O compared to the measurements in H_2O.

5.5.1.2 Global Analysis

The results from a global SVD analysis of the full spectro-temporal transient electronic absorption map of d(ApA) in D_2O confirm the observations. The SVD time traces are shown in Fig. 5.16 and were described by Gaussian-convoluted multi-exponential functions. The time constants derived from this global analysis are in reasonable agreement with the above given time constants from the simultaneous analysis of the time profiles. The fit yielded

$$\tau_1 = 0.23 \pm 0.02 \text{ ps},$$
$$\tau_2 = 0.59 \pm 0.05 \text{ ps},$$
$$\tau_3 = 6 \text{ ps (fixed)},$$
$$\tau_4 = 820 \pm 40 \text{ ps}.$$

Again, two sub-picosecond components were found and τ_3 had to be fixed at the value found in H_2O due to its low amplitude.

The decay-associated difference spectra calculated from the SVD results to visualize the spectral contributions of the time components are shown in Fig. 5.17.

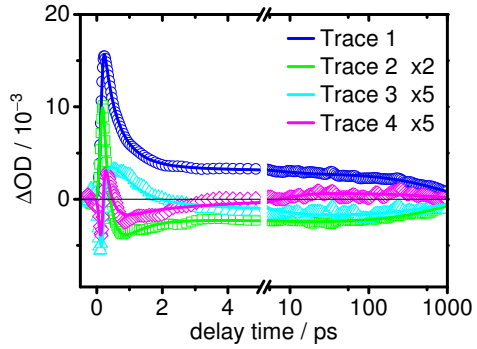

Figure 5.16: Time traces from the global SVD analysis of the spectro-temporal transient electronic absorption data of d(ApA) in D_2O measured at $T = 295$ K after excitation at $\lambda_{pump} = 260$ nm. Time traces 2 – 4 were scaled by the given factors for better visibility. Note the linear timescale for the first 5 ps and the logarithmic timescale thereafter.

The DADS of the measurement of d(ApA) in D_2O are highly similar to those from

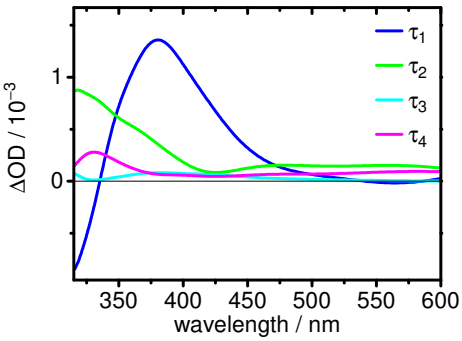

Figure 5.17: Decay-associated difference spectra from the global SVD analysis of the spectro-temporal transient electronic absorption data of d(ApA) in D_2O measured at $T = 295$ K after excitation at $\lambda_{pump} = 260$ nm. The spectra each represent the spectral contribution of the time components τ_1 (blue), τ_2 (green), τ_3 (cyan) and τ_4 (magenta) given in the text.

the measurement in H_2O (Fig. 5.8 on page 125) and reflect SE, HGSA and ESA contributions as described before.

5.6 Discussion

The investigation of the transient electronic absorption of the dinucleotide d(ApA) in direct comparison to dAMP, as a function of temperature and affected by deuterium

exchange yielded a large data set for the effects of stacking on the electronic dynamics of the nucleobase Ade under different environmental conditions. Five individual time constants were determined for the excited-state relaxation of d(ApA) after excitation at $\lambda_{pump} = 260$ nm spanning more than three orders of magnitude. The results from time-profile and SVD analysis are summarized in Table 5.1.

Table 5.1: Experimental results for the electronic dynamics of d(ApA) in dependence of temperature and measured in H_2O (H) or D_2O (D) and in comparison to dAMP. The values were rounded to significant digits.

sample, solvent, T	τ_1/ps	a_2	τ_2/ps	a_3	τ_3/ps	a_4	τ_4/ps	τ_{vc}/ps
time-profile analyses								
d(ApA), H, 278 K		0.76[a]	0.44[b]	0.06	8	0.17	690	2.0
d(ApA), H, 288 K		0.79	0.44	0.05	7	0.16	550	2.1
d(ApA), H, 295 K		0.79	0.44	0.06	6	0.15	360	1.7
d(ApA), D, 295 K		0.78	0.44	0.08	6	0.13	980	2.5
dAMP[c]	0.27	[d]	0.9					≈ 2
global analyses								
d(ApA), H, 278 K	0.15		0.47		8		680	
d(ApA), H, 288 K	0.11		0.42		7		600	
d(ApA), H, 295 K	0.23		0.56		6		360	
d(ApA), D, 295 K	0.23		0.59		6		820	
dAMP[c]	$\langle 0.16 \rangle$[e]		$\langle 0.46 \rangle$[e]					
averaged results								
d(ApA), H	$\langle 0.18 \rangle$		$\langle 0.50 \rangle$		$\langle 6-8 \rangle$		$\langle 360-690 \rangle$	$\langle 1.7-2.0 \rangle$
d(ApA), D	$\langle 0.18 \rangle$		$\langle 0.50 \rangle$		$\langle 6 \rangle$		$\langle 900 \rangle$	$\langle 2.5 \rangle$

[a] The error limits of the amplitudes are < 10 % for a_2 and a_4, and < 20 % for a_3.
[b] The error limits of the time constants are given in the text.
[c] In H_2O at $T = 278 - 295$ K and in D_2O at $T = 295$ K.
[d] Amplitudes vary with solvent and temperature between $a_1 = 0.75 - 0.89$ and $a_2 = 0.11 - 0.25$.
[e] Time constants were averaged.

5.6.1 Comparison to dAMP

The unique and long-lived excited-state relaxation behavior of the dinucleotide d(ApA) becomes most obvious in direct comparison to the short-lived monomer dAMP. While the first two sub-picosecond decay components are quite similar for the two samples, the two long-lived components are only found in the dinucleotide, each set apart by at least one order of magnitude. These long excited-state lifetime are consistent with the increased fluorescence quantum yield of d(ApA) compared to dAMP[67,68] and are matched by time-resolved fluorescence spectroscopy results.[4,5,36] In the latter, especially the red wing of the fluorescence band shows these long

lifetimes. This is mirrored in the present results by a blue-shifting of the transient spectra and a long-lived narrow transient absorption band at the UV edge of the probe-light spectrum. The observed time components and the corresponding complex spectro-temporal behavior of d(ApA) will be discussed in order of appearance.

The Short Time Components

The spectral blue-shift of the initial transient signal is further quantified by plotting the peak wavenumber of the strong ESA band against the delay time for d(ApA) and dAMP shown in Fig. 5.18. The transient spectra were observed to be highly similar

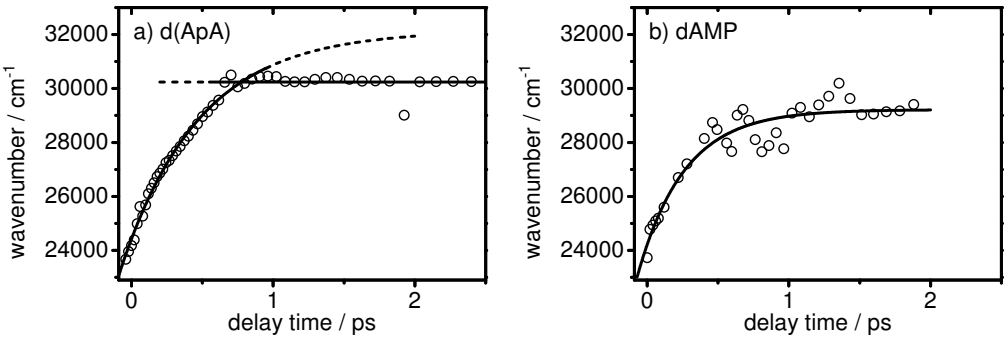

Figure 5.18: Peak wavenumber vs. time profiles of the broad initial ESA band measured after excitation at $\lambda_{\text{pump}} = 260$ nm at $T = 295$ K in H_2O between $\lambda_{\text{probe}} = 315 - 450$ nm for dApA (a) and dAMP (b) for delay times up to $\Delta t = 2.5$ ps. The transient signal of dAMP had already decayed at $\Delta t = 2.0$ ps.

to the eye, but these peak wavenumber-time profiles reveal subtle differences. For d(ApA), the data are described with an exponential growing function with a time constant of $\tau_{\text{shift}} = 0.32 \pm 0.02$ ps that abruptly changes to a constant at $\Delta t = 0.6$ ps indicating two independent processes. The overall blue-shift covers $\Delta E = 6568$ cm^{-1} ($\widehat{=}$ 0.81 eV). In the monomer dAMP, the shift covers an energy range of $\Delta E = 5489$ cm^{-1} ($\widehat{=}$ 0.68 eV). The time profile for dAMP is described by an exponentially growing function with nearly the same time constant, $\tau_{\text{shift}} = 0.3 \pm 0.1$ ps, but the data points show higher noise.

This band-shift analysis allows us to take a close look into the particular dynamics of the Franck–Condon (FC) region of the electronic excited state. We observe that the excited-state wavepackets relax on the same timescale for d(ApA) and dAMP, but that in d(ApA) the relaxation is completed earlier and that a greater energy difference is covered. The abrupt change of the slope of the peak wavenumber

vs. time profile for d(ApA) indicates overlap with a second, independent process, which is assigned to the rise of the long-lived narrow band at $\lambda_{probe} = 330$ nm. The great temporal and structural similarity between the initial signals of d(ApA) and dAMP hint at wavepacket motion that is not yet influenced by the particular potential energy hypersurface (PEHS) topography, namely the gradients and the shape of the pathway towards conical intersections (CIs), or the exact amount of excess energy, or the temperature. Thus, the PEHS appears to be very steep in this region leading to fast and unimpeded energetic relaxation, most likely without significant nuclear motions.[18,46]

Also, the first two decay-associated difference spectra from SVD analysis of d(ApA) and dAMP (a direct comparison is shown in Fig 5.19) and the corresponding time constants, $\tau_1 \approx 0.18$ ps and $\tau_2 \approx 0.50$ ps, show high similarity. They seem to be characteristic for monomer deactivation.

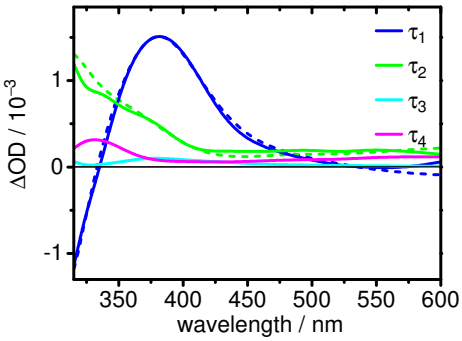

Figure 5.19: Direct comparison of the decay-associated difference spectra from the global SVD analysis of the spectro-temporal transient electronic absorption data of the dinucleotide d(ApA) (solid) and the monomer dAMP (dashed) measured at $T = 295$ K after excitation at $\lambda_{pump} = 260$ nm. The spectra each represent the spectral contribution of the time components $\tau_1 \approx 0.18$ ps (blue), $\tau_2 \approx 0.50$ ps (green), $\tau_3 \approx 6$ ps (cyan) and $\tau_4 \approx 360$ ps (magenta).

We may assume that the sub-picosecond excited-state decay of d(ApA) is composed of two processes for which three distinct possibilities can be conceived: i) real "monomer-like" deactivation of dynamically unstacked bases by FC relaxation and internal conversion via a CI, ii) "perturbed-monomer-like" deactivation of stacked bases by relaxation within the exciton stack and internal conversion via a CI, iii) "exciton-to-excimer" deactivation of stacked bases by relaxation within the exciton stack and transfer towards another PEHS region, likely a minimum. In any

case, the relaxation can be assumed to be facilitated by a C^2-puckering motion of one of the Ade bases as it is often predicted for stacked systems of Ade units[16,18,19,44–48,54] as well as for Ade monomers.[70–81] According to the present data, the out-of-plane motion is not hindered by the stacking interactions.

Although the first suggested possibility (i) is widely accepted,[4,19,32,38,43,47,55,82–86] these short decay times were also found for end-linked polydA·polydT double strands that show little unstacking,[87] and in dynamics calculations of well-stacked adenines.[16] Thus, the amplitudes of the sub-picosecond decay components should not be a measure of the unstacked fraction ($\approx 30\,\%$ at room temperature[13,88]) as previously thought. The DADS show high amplitudes for the first two decay components in comparison with the long-lived components. This indicates an independent deactivation process with a direct internal conversion mechanism as proposed in the second possibility (ii). Also, if only the third possibility (iii) was in place, relaxation steps three and four would gain more intensity. In conclusion, the second proposed deactivation process (ii), i. e. relaxation within the exciton stack followed by internal conversion to the ground state, becomes most plausible to explain the sub-picosecond excited-state decay of d(ApA), but the signal possibly is an overlay of all three proposed processes.

The Long Time Components

The two long-lived signal contributions reveal the formation and decay of excimer states in the dinucleotide d(ApA). A stepwise relaxation to a stabilized excimer state via an intermediate state is proposed, which supports previous experimental work[4–6] as well as postulations derived from quantum chemical studies.[16–19,44,46] After relaxation to the intermediate state within $\Delta t = 1$ ps, the intermediate decays to the stabilized excimer with time constant $\tau_3 \approx 6$ ps. Time constant $\tau_4 \approx 360$ ps is then assigned to internal conversion from the stabilized excimer to the ground state.

The intermediate time constant was also seen in time-resolved fluorescence experiments[4,5,36,89] and is in agreement with other transient absorption experiments.[4,6,43] The DADS of components three and four (Fig. 5.19 on page 136), and earlier broadband time-resolved fluorescence measurements of d(pApA)[4,5] show spectral separation of the intermediate from the stabilized excimer signature. The lack of the intermediate time constant in the ground state refilling signal also indicates a process that does not directly lead to internal conversion to the ground state but that connects different PEHS regions. Thus, the assignment is plausible although an intermediate should show itself as a rise time in the transient signal of

the stabilized excimer. This was not seen in the experiment, because it is obscured by the close-lying signal of the intermediate excimer itself and HGSA.

In d(ApA), three excited states are supposed to be in in dynamic equilibrium, namely one of localized excitation, a neutral excimer and a CT excimer.[16,18,19,32,44,47,55,90] It is probable that one of the excimers acts as an intermediate during electronic deactivation since both show minimum structures.Note that in this context, the individual predicted potential energy minima can be understood as different "states". However, the assignment of the two longest observed lifetimes to these excimers is not unambiguous. An excimer with CT character was predicted to be formed within 1 ps and to persist for 10 ps[91] in good agreement with the intermediate experimental lifetime. In fact, several observations are in favor of a strong CT character of excimer states. The long-lived states in base multimers have around three times the fluorescence quantum yields of their monomers (ϕ_{fl}(ApA)[33,34] $\approx 1.6 \cdot 10^{-4}$ ϕ_{fl}(dAMP)[33] $\approx 0.5 \cdot 10^{-4}$) in spite of a 1000-fold lifetime. The emissive state thus must be comparatively dark which is the case for states with CT character.[92] Different Ade dimers with varying backbones were found to exhibit nearly the same lifetime. This was attributed to formation of CT excimers rather than neutral excimers[93] since CT coupling is strong and only moderately sensitive to stacking fluctuations.[94] The coupling is predicted to leave the interbase distance unchanged in comparison with the ground state structure.[18] Quantum dynamics calculations on Ade oligomers could show that the energetic position of CT states at the FC geometry is not as essential for the fate of the population as coupling and oscillator strength. Thus, CT excimer states are likely to be populated although they are predicted to lie above the $\pi\pi^*$ excited states in the FC region.[18,28,44,90,95] CT excimers are said to act as trap states, especially in polar solvents,[48,90] and to have lifetimes of more than 100 ps.[32,44] In view of this information, both the experimentally observed excimer with the intermediate lifetime and the stabilized and long-lived excimer may have CT character.

5.6.2 Effect of Temperature

The sub-picosecond excited-state decay components of d(ApA) were found to be independent of temperature within experimental errors. The monomer dAMP also exhibits temperature-independent dynamics as is shown in the Additional Information. In contrast, the third and fourth decay components of d(ApA) were slowed down considerably at $T = 278$ K compared to $T = 295$ K although this range is comparatively small. The fourth decay component was prolonged nearly by a

factor of two. To the best of our knowledge, this marked temperature-effect was not observed before. On the contrary, excimer lifetimes of large Ade oligonucleotides were so far reported as constant against a temperature change.[39,87,96]

The gradual decrease of the amplitude of τ_4 with increasing the temperature lies barely above errors, but could be assigned to the known decrease of the stacking fraction. The stacking fraction is not expected to have an effect on the lifetimes. Remember that for the measurements at $T = 278$ K and 288 K a higher pump pulse energy was used than in the experiment at $T = 295$ K. This seems to result in an increased amplitude of decay component τ_2 at $\lambda_{probe} < 420$ nm (also seen for dAMP). Fortunately though, according to the present data, increasing the pump pulse energy leaves the experimental decay times unchanged.

The temperature-dependent excited-state lifetimes of d(ApA) were analyzed by application of the Arrhenius equation in Fig. 5.20 and yielded activation energies $E_A[\tau_3] = 0.11 \pm 0.04$ eV ($\widehat{=}10.6 \pm 3.7$ kJ/mol) and $E_A[\tau_4] = 0.25 \pm 0.06$ eV ($\widehat{=}24.1 \pm 5.8$ kJ/mol). These can be interpreted as potential energy barriers on

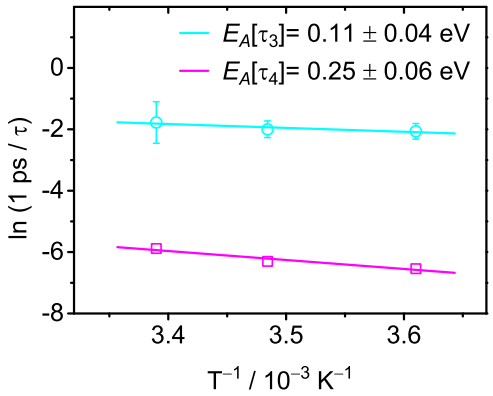

Figure 5.20: Arrhenius analysis of the excited-state lifetimes τ_3 and τ_4 of d(ApA) in H_2O. The solid lines represent the fitted Arrhenius expression. The error limits for τ_3 are included. The error limits of τ_4 are smaller than the height of the symbol.

the deactivation pathway on the excited-state PEHS which may result from the electronic or steric hindrance of out-of-plane movements or other large-amplitude motions ultimately breaking the excimer bond energy. The existence of potential energy barriers on the deactivation pathway of excimers is consistent with quantum chemical calculations that predict minimum structures for excimers in stacked Ade systems.[16,18,19,38,47,48,90,97]

The small potential barrier $E_A[\tau_3]$ is derived from the decay times of the intermediate excimer and thus lies between the two proposed excimers. The potential

barrier results in a low transient population of the intermediate excimer which is consistent with the low amplitudes of τ_3. The potential barrier $E_A[\tau_4]$ is thought to inhibit the ground state decay of the stabilized excimer. This gives rise to the observed narrow transient absorption band. Since the enthalpy change for unstacking of ApA was determined to be significantly larger ($\Delta H_{\text{unstack}} = 0.35$ eV $\widehat{=}33.8$ kJ/mol)[98,99] the stack is likely not disrupted by the deactivation mechanism.

In this way, temperature-dependent femtosecond time-resolved spectroscopy could identify for the first time the potential energy barriers on the electronic deactivation pathway of the dinucleotide d(ApA) that impede excimer formation and deactivation.

5.6.3 Effect of D_2O

The transient electronic absorption signal of d(ApA) in D_2O was found to be similar with the one in H_2O only for delay times up to $\Delta t \approx 50$ ps, just as the measurements of dAMP in D_2O and H_2O were highly similar as is shown in the Additional Information. For the long-time electronic dynamics of d(ApA), however, a drastic lifetime-increase was observed from $\tau_4 \approx 360$ ps in H_2O to $\tau_4 \approx 900$ ps in D_2O (averaged results). The kinetic isotope effect can by quantified by calculating KIE $= \tau_D/\tau_H = 2.5$. To the best of our knowledge, this astoundingly huge deuteration effect on the dynamics of the dinucleotide d(ApA) was so far unknown.

In general, the occurrence of a KIE can be assigned either to interaction with solvent molecules, i. e. energy transfer to the solvent, or to the involvement of a deuterated functional group in the relaxation mechanism. The effect of solvent interactions can best be seen in the vibrational cooling times determined in this work from measurements at $\lambda_{\text{probe}} = 255$ nm. The ratio of the vibrational cooling times in D_2O and H_2O was found to be KIE ≈ 1.4 for both d(ApA) and dAMP in excellent agreement with literature.[60,85,94,100,101] It was shown that a KIE can also reveal the participation of deuterated molecular moieties in electronic deactivation processes. For example, the electronic dynamics of an alternating GC oligonucleotide double strand were observed to be subject to a pronounced KIE. This was interpreted as an electron driven proton transfer[94] that was proven later to take place in GC base pairs.[3]

Along these lines, since no KIE was seen for decay component τ_3, conversion from the proposed intermediate to the stabilized excimer seems to follow a deactivation mechanism involving neither one of the deuterated amino groups nor solvent interactions. Admittedly, a small deuteration effect could be disguised by

the experimental errors for this time constant. It would, however, be weaker than the KIE for vibrational cooling. Since no significant effect of D_2O was found for HGSA signals either, the suggested intermediate might also be a hot excimer that relaxes to the stabilized excimer by vibrational energy transfer as suggested by Kohler and co-workers.[92,93] Solvation times are known to be on that order magnitude for molecules embedded in DNA.[102,103] Despite the above seen temperature-effect for τ_3, a solvent-mediated process cannot be fully excluded.

In this regard, one could also argue that the strong KIE of the fourth decay component of d(ApA) were induced by the change in solvent frequencies when going form H_2O to D_2O, particularly because energy transfer rates directly influence relaxation times (a connection observed during work on Chapter 4). However, vibrational cooling was changed by a factor of 1.4, but τ_4 was increased by a factor of 2.5. This pronounced KIE clearly indicates an additional effect and hints at a deactivation mechanism involving significant nuclear motion of at least one of the fully deuterated amino groups in the Ade dinucleotide.

In this way, femtosecond time-resolved transient electronic absorption spectroscopy can competently contribute to identifying molecular deactivation mechanisms.

5.6.4 Electronic Deactivation Mechanisms

The observed multi-exponential electronic decay dynamics of d(ApA) showed distinct dependencies on the experimental conditions which shed light on the proposed stepwise exciton-to-excimer deactivation mechanism.

The ultrafast relaxation with time constants $\tau_1 \approx 0.18$ ps and $\tau_2 \approx 0.50$ ps (averaged SVD result) is assigned to "perturbed-monomer-like" deactivation. In the schematic potential energy model depicted in Fig. 5.21 the exciton states are indicated by short horizontal lines while the deactivation pathways are depicted as solid curves. Time component τ_1 is assigned to the initial decay within the exciton stack $(AA)^*_{Exciton}$ in stacked conformations, but can also be assigned to FC relaxation in dynamically unstacked bases. As was discussed, the PEHS must be steep in this region and the molecule probably still has B-DNA conformation after the initial relaxation. Component τ_2 is assigned to the internal conversion of a locally excited state A^*A to the ground state.

With the term "perturbed-monomer-like", we suggest that indeed the same deactivation mechanism takes place in the dinucleotide as was found for the monomer, namely a ring puckering centered at the C^2 position leading to an out-of-plane

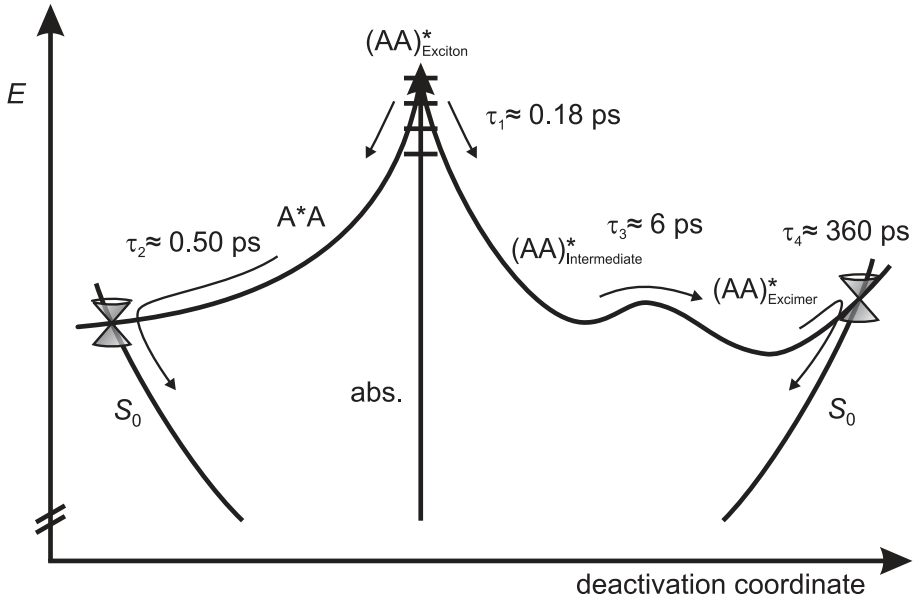

Figure 5.21: Potential energy model curve for the electronic deactivation of d(ApA) after excitation at $\lambda_{pump} = 260$ nm. Relaxation within the initially excited exciton stack $(AA)^*_{Exciton}$ in $\tau_1 \approx 0.18$ ps either leads to a locally excited state A^*A and deactivation via a "perturbed-monomer-like" deactivation pathway within $\tau_2 \approx 0.50$ ps, or to a stepwise excimer formation. An intermediate structure $(AA)^*_{Intermediate}$ is populated directly from the FC region and decays to a stabilized excimer $(AA)^*_{Excimer}$ within $\tau_3 \approx 6$ ps at $T = 295$ K. $(AA)^*_{Excimer}$ decays to the ground state within $\tau_4 \approx 360$ ps at $T = 295$ K.

motion of the C^2–H bond.[16,18,19,44,47,48,50,54,55,104] According to the present data, steric hindrance by the stacking interaction of the bases does not influence this decay mechanism which was also found to be independent of temperature and deuteration. However, the internal conversion of the locally excited state A^*A probably is overlain by direct passage of the wavepacket towards different PEHS regions. In the dinucleotide, the rapid initial electronic relaxation causing departure from the FC region and arrival at an excimer-like state was observed to be completed after $\Delta t = 0.6$ ps and to cover an energy range of $\Delta E \approx 0.8$ eV (as was concluded from the band shift dynamics shown in Fig. 5.5).

This other PEHS region is thought to be a set of PEHS minima with excimer character that trap the excited-state wavepacket and induce the long-lived excited-state decay times. The formation of excimers is a consequence of the stacking interaction of the adjacent bases and the delocalization of excitation energy. It can compete with the "perturbed-monomer-like" deactivation due to the rapid initial energetic relaxation. A transiently populated intermediate excimer $(AA)^*_{Intermediate}$ is

assumed to be directly formed from the exciton stack and to evolve within $\tau_3 \approx 6$ ps to an energetically stabilized excimer $(AA)^*_{Excimer}$. The intermediate probably shows CT character[18,19,44,46,83,105] and an unchanged interbase distance.[18,46] Both excimers have a similar energy level and are separated by a potential energy barrier of $E_A[\tau_3] \approx 0.11$ eV. Internal conversion from $(AA)^*_{Excimer}$ to the ground state takes place within $\tau_4 \approx 360$ ps due to inhibition by a potential energy barrier of $E_A[\tau_4] \approx 0.25$ eV.

The stabilized excimer is often assumed to be a neutral state with a stable minimum and the structure is described with high orbital overlap in a face-to-back conformation and with a shortened interbase distance of ≈ 3.0 Å or even closer.[16–19,46,49,106,107] Other interpretations feature intermediate bond-formation,[47,50–53] or states with pronounced CT character.[18,44,48,90] The deactivation mechanism occurs then via relocalization to monomers followed by monomer-like out-of-plane deformations.[19,31,44–46,54]

However, none of these descriptions can explain the present observations satisfactorily. Especially the drastic KIE = 2.5 that was attributed to internal conversion from the stabilized excimer can only be rationalized by involvement of at least one of the deuterated amino groups in the mechanism. Two relevant theoretical studies are quoted in the following. Conti et al.[48] predicted a barrier of $\Delta E \leq 0.28$ eV for the transition to a relaxed CT state which can decay by an excited-state proton transfer (ESPT) between the amino groups over a barrier of $\Delta E = 0.9$ eV to the ground state. This mechanism would explain the observed temperature-dependent lifetime of the excimers and the lifetime-increase in D_2O, although the barriers seem to be too high. The authors state that the stability of the CT state may be overestimated in their QM/MM (quantum mechanics/molecular mechanics) approach. Plasser et al.[16] also chose a QM/MM framework and saw a deactivation mechanism in aqueous solution that features an excimer with a short interbase distance of 2.0 Å in a delocalized excited state of d(ApA). Consistent with the initial transient absorption band-shift, the excimer was found to have an excitation energy about $\Delta E = 1.1$ eV below the FC geometry and a relatively high oscillator strength. The stabilized structure is predicted to decay by ring puckering centered at the C^6 position and an out-of-plane motion of the amino group. It is likely that the rearrangement processes, i. e. overcoming the orbital interaction during approaching and distancing of the bases and the strong molecular deformation, need activation energies.[16] This mechanism would indicate that the well-known C^6-puckering deformation becomes more accessible for the Ade units as the system is relaxed into the excimer structure. Thus, this deactivation pathway would not be relevant in Ade monomers due to the

ultrafast decay described above and in Chapter 3 of this Thesis.

Interestingly, both presented mechanisms can explain the observed decay behavior of the long-lived excited-state decay of d(ApA). A stabilizing electronic effect traps the excited-state population in a minimum structure. Both a CT state and increased orbital interaction at lowered interbase distances are plausible origins for this effect.

5.7 Conclusion

The adenine dinucleotide d(ApA) was investigated by femtosecond time-resolved transient electronic absorption spectroscopy after excitation at $\lambda_{\text{pump}} = 260$ nm in H_2O in the temperature range 278 K $\leq T \leq$ 295 K and in D_2O at room temperature. The results were directly compared to measurements for the monomer dAMP. The comprehensive experimental results shed light on the detailed mechanisms of electronic relaxation and allow for assignment of the observations to critical steps in the evolution of the electronic excited-state character from excitons to excimer-like states en route towards the electronic ground state.

For d(ApA), the two sub-picosecond decay components were independent of temperature and deuteration. These were assigned to relaxation within the exciton stack within $\tau_1 \approx 0.18$ ps and to "perturbed-monomer-like" decay within $\tau_2 \approx 0.50$ ps by a C^2-puckering deformation of one of the Ade units. The two long-lived excited-state lifetime components showed temperature dependence indicating potential energy barriers on the deactivation pathway. The time constants were assigned to relaxation from an intermediate excimer within $\tau_3 \approx 6$ ps to a stabilized excimer, and to subsequent conversion to the ground state within $\tau_4 \approx 360$ ps. The states were found to be separated by a barrier and to lie at similar energy levels. For τ_4, a pronounced KIE demonstrated involvement of at least one of the fully deuterated amino groups in the deactivation mechanism. A ring puckering accompanied by an out-of-plane motion of the amino group on one of the Ade units is most probably responsible for the deactivation of the dinucleotide.[16] An ESPT mechanism between both amino groups is also thinkable.[48]

For dAMP, neither a temperature nor a deuteration effect was observed for the sub-picosecond excited-state lifetimes. This is assigned to an ultrafast barrierless deactivation to the ground state within $\Delta t < 1$ ps that does not involve significant nuclear motions of the deuterated amino groups but is promoted by the well-known C^2-puckering deformation.

In conclusion, this work demonstrates that temperature- and solvent-dependent

femtosecond time-resolved spectroscopy can give direct insights into electronic deactivation and narrows down the scope of interpretation.

References

[1] N. K. Schwalb, F. Temps, 'Base Sequence and Higher-Order Structure Induce the Complex Excited-State Dynamics in DNA', *Science* **2008**, *322*, 243–245.

[2] N. K. Schwalb, T. Michalak, F. Temps, 'Ultrashort Fluorescence Lifetimes of Hydrogen-Bonded Base Pairs of Guanosine and Cytidine in Solution', *J. Phys. Chem. B* **2009**, *113*, 16365–16376.

[3] K. Röttger, H. Marroux, M. Grubb, P. Coulter, H. Böhnke, A. Henderson, M. Galan, F. Temps, A. Orr-Ewing, G. Roberts, 'Ultraviolet Absorption Induces Hydrogen-Atom Transfer in G·C Watson–Crick DNA Base Pairs in Solution', *Angew. Chem.* **2015**, *127*, 14932–14935.

[4] M. C. Stuhldreier, 'Electronic Deactivation Dynamics of DNA Model Systems and Solvation Dynamics of a Natural Antioxidant by Femtosecond Fluorescence and Absorption Spectroscopy', Dissertation, Christian-Albrechts-Universität zu Kiel, **2013**.

[5] M. C. Stuhldreier, C. Schüler, J. Kleber, F. Temps, 'Femtosecond Fluorescence Measurements of the Adenine Dinucleotide: Direct Observation of the Excimer State' in *Ultrafast Phenomena XVII*, (Eds.: M. Chergui, D. M. Jonas, E. Riedle, R. W. Schoenlein, A. J. Taylor), Oxford, **2011**, 553–555.

[6] M. C. Stuhldreier, K. Röttger, F. Temps, 'Distinctive Spectral Features of Exciton and Excimer States in the Ultrafast Electronic Deactivation of the Adenine Dinucleotide' in *Ultrafast Phenomena XIX*, Vol. 162, (Eds.: K. Yamanouchi, S. Cundiff, R. de Vivie-Riedle, M. Kuwata-Gonokami, L. DiMauro), **2015**, 452–454.

[7] C. E. Crespo-Hernández, B. Cohen, P. M. Hare, B. Kohler, 'Ultrafast Excited-State Dynamics in Nucleic Acids', *Chem. Rev.* **2004**, *104*, 1977–2019.

[8] C. T. Middleton, K. de La Harpe, C. Su, Y. K. Law, C. E. Crespo-Hernández, B. Kohler, 'DNA Excited-State Dynamics: From Single Bases to the Double Helix', *Annu. Rev. Phys. Chem.* **2009**, *60*, 217–239.

[9] V. L. Rapoport, B. M. Malkin, S. V. Zorina, 'Luminescence Detection of Tightly Bound Stacking Aggregates of Adenine and Adenosine in Aqueous Solutions—the Candidates for the Role of the First Genetic Templates', *Dokl. Biochem. Biophys.* **2006**, *406*, 23–26.

[10] V. L. Rapoport, V. M. Malkin, A. V. Savina, E. A. Safargaleyeva, V. V. Goryuchko, 'Luminescence of Stable Stacking Aggregates of Adenine and Uracil in Water', *Biophysics* **2012**, *57*, 9–13.

[11] R. Tribolet, H. Sigel, 'Self-association of adenosine 5'-monophosphate (5'-AMP) as a function of pH and in comparison with adenosine, 2'-AMP and 3'-AMP', *Biophys. Chem.* **1987**, *27*, 119–130.

[12] C.-H. Lee, F. S. Ezra, N. S. Kondo, R. H. Sarma, S. S. Danyluk, 'Conformational Properties of Dinucleoside Monophosphates in Solution: Dipurines and Dipyrimidines', *Biochemistry* **1976**, *15*, 3627–3639.

[13] C. S. M. Olsthoorn, L. J. Bostelaar, J. F. M. de Rooij, J. H. van Boom, C. Altona, 'Circular Dichroism Study of Stacking Properties of Oligodeoxyadenylates and Polydeoxyadenylate—A Three-State Conformational Model', *Eur. J. Biochem.* **1981**, *115*, 309–321.

[14] C. R. Cantor, M. M. Warshaw, H. Shapiro, 'Oligonucleotide Interactions. III. Circular Dichroism Studies of the Conformation of Deoxyoligonucleotides', *Biopolymers* **1970**, *9*, 1059–1077.

[15] P. Norman, J. Parello, L. Polavarapu, M. Linares, 'Predicting near-UV electronic circular dichroism in nucleosomal DNA by means of DFT response theory', *Phys. Chem. Chem. Phys.* **2015**, *17*, 21866–21879.

[16] F. Plasser, H. Lischka, 'Electronic excitation and structural relaxation of the adenine dinucleotide in gas phase and solution', *Photochem. Photobiol.* **2013**, *12*, 1440–1452.

[17] W. Zhang, S. Yuan, Z. Wang, Z. Qi, J. Zhao, Y. Dou, G. V. Lo, 'A Semiclassical Dynamics Simulation for a Long-Lived Excimer State of π-Stacked Adenines', *Chem. Phys. Lett.* **2011**, *506*, 303–308.

[18] R. Improta, V. Barone, 'Interplay between "Neutral" and "Charge-Transfer" Excimers Rules the Excited State Decay in Adenine-Rich Polynucleotides', *Angew. Chem. Int. Ed.* **2011**, *50*, 12016–12019.

[19] G. Olaso-González, M. Merchán, L. Serrano-Andrés, 'The Role of Adenine Excimers in the Photophysics of Oligonucleotides', *J. Am. Chem. Soc.* **2009**, *131*, 4368–4377.

[20] T. Zelený, M. Ruckenbauer, A. J. Aquino, T. Müller, F. Lankaš, T. Dršata, W. L. Hase, D. Nachtigallova, H. Lischka, 'Strikingly Different Effects of Hydrogen Bonding on the Photodynamics of Individual Nucleobases in DNA: Comparison of Guanine and Cytosine', *J. Am. Chem. Soc.* **2012**, *134*, 13662–13669.

[21] J. J. Nogueira, F. Plasser, L. González, 'Electronic delocalization, charge transfer and hypochromism in the UV absorption spectrum of polyadenine unravelled by multiscale computations and quantitative wavefunction analysis', *Chem. Sci.* **2017**, *8*, 5682–5691.

[22] M. Kasha, H. R. Rawls, M. Ashraf El-Bayoumi, 'The Exciton Model in Molecular Spectroscopy', *Pure Appl. Chem.* **1965**, *11*, 371–392.

[23] M. Kasha, 'Molecular Excitons in Small Aggregates' in *Spectroscopy of the Excited State*, (Eds.: B. Di Bartolo, D. Pacheco, V. Goldberg), *Nato Advanced Study Institutes Series: Series B, Physics, Vol. 12*, Plenum Press, New York and London, **1976**, 337–380.

[24] I. Tinoco jr., 'Hypochromism in Polynucleotides', *J. Am. Chem. Soc.* **1960**, *82*, 4785–4790.

[25] B. Bouvier, T. Gustavsson, D. Markovitsi, P. Millié, 'Dipolar Coupling Between Electronic Transitions of the DNA Bases and its Relevance to Exciton States in Double Helices', *Chem. Phys.* **2002**, *275*, 75–92.

[26] B. Bouvier, J.-P. Dognon, R. Lavery, D. Markovitsi, P. Millié, D. Onidas, K. Zakrzewska, 'Influence of Conformational Dynamics on the Exciton States of DNA Oligomers Benjamin Bouvier', *J. Phys. Chem. B* **2003**, *107*, 13512–13522.

[27] L. M. Nielsen, S. Ø. Pedersen, M.-B. S. Kirketerp, S. Brøndsted Nielsen, 'Absorption by DNA single strands of adenine isolated in vacuo: The role of multiple chromophores', *J. Chem. Phys.* **2012**, *136*, 064302.

[28] A. W. Lange, J. M. Herbert, 'Both Intra- and Interstrand Charge-Transfer Excited States in Aqueous B-DNA Are Present at Energies Comparable To, or Just Above, the $^1\pi\pi^*$ Excitonic Bright States', *J. Am. Chem. Soc.* **2009**, *131*, 3913–3922.

[29] D. Nachtigallová, P. Hobza, H.-H. Ritze, 'Electronic splitting in the excited states of DNA base homodimers and -trimers: an evaluation of short-range and Coulombic interactions', *Phys. Chem. Chem. Phys.* **2008**, *10*, 5689–5697.

[30] J. Kleber, 'Statische Absorptions- und Fluoreszenzspektroskopische Untersuchungen von kooperativen Effekten zwischen DNA-Chromophoren im Einzelstrang', Diplomarbeit, Christian-Albrechts-Universität zu Kiel, **2009**.

[31] Á. Bányász, I. Vayá, P. Changenet-Barret, T. Gustavsson, T. Douki, D. Markovitsi, 'Base Pairing Enhances Fluorescence and Favors Cyclobutane Dimer Formation Induced upon Absorption of UVA Radiation by DNA', *J. Am. Chem. Soc.* **2011**, *133*, 5163–5165.

[32] D. Markovitsi, 'UV-induced DNA Damage: The Role of Electronic Excited States', *Photochem. Photobiol.* **2016**, *92*, 45–51.

[33] P. Vigny, M. Duquesne, *Organic Molecular Photophysics*, (Ed.: J. B. Birks), Wiley, New York, **1976**, 167–177.

[34] J. P. Morgan, M. Daniels, 'Excited states of DNA and its components at room temperature. III. Spectra polarization, and quantum yields of emissions from ApA and poly rA.', *Photochem. Photobiol.* **1979**, *31*, 101–113.

[35] J. Eisinger, M. Guéron, R. G. Shulman, T. Yamane, 'Excimer fluorescence of dinucleotides, polynucleotides, and DNA.', *Proc. Natl. Acad. Sci. U. S. A.* **1966**, *55*, 1015–1020.

[36] U. C. Stange, 'Untersuchung der Temperaturabhängigkeit der ultraschnellen elektronischen Desaktivierung von Adenin und dem Adenindinukleotid', Masterarbeit, Christian-Albrechts-Universität zu Kiel, **2012**.

[37] M. C. Stuhldreier, F. Temps, 'Ultrafast photo-initiated molecular quantum dynamics in the DNA dinucleotide d(ApG) revealed by broadband transient absorption spectroscopy', *Faraday Discuss.* **2013**, *163*, 173–188.

[38] T. Takaya, C. Su, K. de La Harpe, C. E. Crespo-Hernández, B. Kohler, 'UV excitation of single DNA and RNA strands produces high yields of exciplex states between two stacked bases', *Proc. Natl. Acad. Sci. U. S. A.* **2008**, *105*, 10285–10290.

[39] C. Su, 'Femtosecond Transient Absorption Study of the Excited-State Dynamics of Single-Stranded Adenine-Containing Multinucleotides and Steady-State Absorption Spectroscopy of Mononucleotides in Cryogenic Water/Ethylene Glycol Matrices', Dissertation, Graduate School of The Ohio State University, **2010**.

[40] S. Kobayashi, M. Yamashita, T. Sato, S. Muramatsu, 'A single-photon sensitive synchroscan streak camera for room temperature picosecond emission dynamics of adenine and polyadenylic acid', *IEEE J. Quantum Electron.* **1984**, *QE-20*, 1383–1385.

[41] R. Plessow, A. Brockhinke, W. Eimer, K. Kohse-Höinghaus, 'Intrinsic Time- and Wavelength-Resolved Fluorescence of Oligonucleotides: A Systematic Investigation Using a Novel Picosecond Laser Approach', *J. Phys. Chem. B* **2000**, *104*, 3695–3704.

[42] D. Onidas, T. Gustavsson, E. Lazzarotto, D. Markovitsi, 'Fluorescence of the DNA Double Helix $(dA)_{20}\cdot(dT)_{20}$ Studied by Femtosecond Spectroscopy—Effect of the Duplex Size on the Properties of the Excited States', *J. Phys. Chem. B* **2007**, *111*, 9644–9650.

[43] I. Buchvarov, Q. Wang, M. Raytchev, A. Trifonov, T. Fiebig, 'Electronic energy delocalization and dissipation in single- and double-stranded DNA', *Proc. Natl. Acad. Sci. U. S. A.* **2007**, *104*, 4794–4797.

[44] F. Santoro, V. V. Barone, R. Improta, 'Influence of base stacking on excited-state behavior of polyadenine in water, based on time-dependent density functional calculations', *Proc. Natl. Acad. Sci. U.S.A.* **2007**, *104*, 9931–9936.

[45] Y. Lu, Z.-G. Lan, W. Thiel, 'Hydrogen Bonding Regulates the Monomeric Nonradiative Decay of Adenine in DNA Strands', *Angew. Chem.* **2011**, *123*, 6996–6999.

[46] X. Chen, W. Fang, H. Wang, 'Slow deactivation channels in UV-photoexcited adenine DNA', *Phys. Chem. Chem. Phys.* **2014**, *16*, 4210–4219.

[47] V. A. Spata, S. Matsika, 'Photophysical deactivation pathways in adenine oligonucleotides', *Phys. Chem. Chem. Phys.* **2015**, *17*, 31073–31083.

[48] I. Conti, A. Nenov, S. Höfinger, S. F. Altavilla, I. Rivalta, E. Dumont, G. Orlandi, M. Garavelli, 'Excited state evolution of DNA stacked adenines resolved at the CASPT2//CASSCF/Amber level: From the bright to the excimer state and back', *Phys. Chem. Chem. Phys.* **2015**, *17*, 7291–7302.

[49] Á. Bányász, T. Gustavsson, D. Onidas, P. Changenet-Barret, D. Markovitsi, R. Improta, 'Multi-pathway excited state relaxation of adenine oligomers in aqueous solution: A joint theoretical and experimental study', *Chem. Eur. J.* **2013**, *19*, 3762–3774.

[50] Y. Dou, W. Zhao, S. Yuan, W. Zhang, H. Tang, 'Bonded excimer in stacked adenines: Semiclassical simulations', *Sci. China. Chem.* **2012**, *55*, 1377–1383.

[51] Y. Dou, Z. Liu, S. Yuan, W. Zhang, H. Tang, J. Zhao, W. Fang, G. V. Lo, 'Dynamics of laser-excited stacked adenines: Semiclassical simulations', *Int. J. Biol. Macromol.* **2012**, *52*, 358–367.

[52] V. A. Spata, S. Matsika, 'Role of Excitonic Coupling and Charge-Transfer States in the Absorption and CD Spectra of Adenine-Based Oligonucleotides Investigated through QM/MM Simulations', *J. Phys. Chem. A* **2014**, *118*, 12021–12030.

[53] V. A. Spata, W. Lee, S. Matsika, 'Excimers and Exciplexes in Photoinitiated Processes of Oligonucleotides', *J. Phys. Chem. Lett.* **2016**, *7*, 976–984.

[54] I. Conti, P. Altoé, M. Stenta, M. Garavelli, G. Orlandi, 'Adenine deactivation in DNA resolved at the CASPT2//CASSCF/AMBER level', *Phys. Chem. Chem. Phys.* **2010**, *12*, 5016–5023.

[55] R. Improta, F. Santoro, L. Blancafort, 'Quantum Mechanical Studies on the Photophysics and the Photochemistry of Nucleic Acids and Nucleobases', *Chem. Rev.* **2016**, *116*, 3540–3593.

[56] M. Barbatti, A. C. Borin, S. Ullrich, Eds., 'Photoinduced Phenomena in Nucleic Acids I. Nucleobases in the Gas Phase and in Solvents', *Topics in Current Chemistry, Vol. 355*, Springer, Heidelberg, Germany, **2015**.

[57] M. Barbatti, A. C. Borin, S. Ullrich, Eds., 'Photoinduced Phenomena in Nucleic Acids II. DNA Fragments and Phenomenological Aspects', *Topics in Current Chemistry, Vol. 356*, Springer, Heidelberg, Germany, **2014**.

[58] K. Röttger, R. Siewertsen, F. Temps, 'Ultrafast Electronic Deactivation Dynamics of the Rare Natural Nucleobase Hypoxanthine', *Chem. Phys. Lett.* **2012**, *536*, 140–146.

[59] M. Lorenc, M. Ziolek, R. Naskrecki, J. Karolczak, J. Kubicki, A. Maciejewski, 'Artifacts in femtosecond transient absorption spectroscopy', *Appl. Phys. B* **2002**, *74*, 19–27.

[60] B. Cohen, P. M. Hare, B. Kohler, 'Ultrafast Excited-State Dynamics of Adenine and Monomethylated Adenines in Solution: Implications for the Nonradiative Decay Mechanism', *J. Am. Chem. Soc.* **2003**, *125*, 13594–13601.

[61] K. Röttger, 'Ultrafast Deactivation Dynamics of Structurally Modified and Hydrogen-Bonded DNA and RNA Building Blocks', Dissertation, Christian-Albrechts-Universität zu Kiel, **2013**.

[62] R. Siewertsen, 'Ultrafast Photochromic Reactions of Structurally Modified Furylfulgides and a Bridged Azobenzene', Dissertation, Christian-Albrechts-Universität zu Kiel, **2011**.

[63] I. van Stokkum, D. S. Larsen, R. van Grondelle, 'Global and Target Analysis of Time-Resolved Spectra', *Biochim. Biophys. Acta* **2004**, *1657*, 82–104.

[64] N. Mouton, A. de Juan, M. Sliwa, C. Ruckebusch, 'Hybrid Hard- and Soft-Modeling Approach for the Resolution of Convoluted Femtosecond Spectrokinetic Data', *Chemom. Intell. Lab. Syst.* **2011**, *105*, 74–82.

[65] C. Ruckebusch, M. Sliwa, P. Pernot, A. de Juan, R. Tauler, 'Comprehensive data analysis of femtosecond transient absorption spectra: A review', *J. Photochem. Photobiol. C* **2012**, *13*, 1–27.

[66] J.-M. L. Pecourt, J. Peon, B. Kohler, 'Ultrafast Internal Conversion of Electronically Excited RNA and DNA Nucleosides in Water', *J. Am. Chem. Soc.* **2000**, *122*, 9348–9349.

[67] P. Vigny, J. P. Ballini, 'Excited states of nucleic acids at 300 K and electronic energy transfer' in *Excited States in Organic Chemistry and Biochemistry*, (Eds.: B. Pullman, N. Goldblum), Reidel, Dordrecht, Holland, **1977**, 1–13.

[68] P. R. Callis, 'Electronic States and Luminescence of Nucleic Acid Systems', *Annu. Rev. Phys. Chem.* **1983**, *34*, 329–352.

[69] D. G. Cross, 'Hydrogen Exchange in Nucleosides and Nucleotides. Measurement of Hydrogen Exchange by Stopped-Flow and Ultraviolet Difference Spectroscopy', *Biochemistry* **1975**, *14*, 357–362.

[70] S. Perun, A. L. Sobolewski, W. Domcke, 'Ab Initio Studies on the Radiationless Decay Mechanisms of the Lowest Excited Singlet States of 9H-Adenine', *J. Am. Chem. Soc.* **2005**, *127*, 6257–6265.

[71] H. Chen, S. Li, 'Theoretical Study toward Understanding Ultrafast Internal Conversion of Excited 9H-Adenine', *J. Phys. Chem. A* **2005**, *109*, 8443–8446.

[72] C. M. Marian, 'A new pathway for the rapid decay of electronically excited adenine', *J. Chem. Phys.* **2005**, *122*, 104314.

[73] L. Blancafort, 'Excited-State Potential Energy Surface for the Photophysics of Adenine', *J. Am. Chem. Soc.* **2006**, *128*, 210–219.

[74] L. Serrano-Andrés, M. Merchán, A. C. Borin, 'A Three-State Model for the Photophysics of Adenine', *Chem. Eur. J.* **2006**, *12*, 6559–6571.

[75] Y. Lei, S. Yuan, Y. Dou, Y. Wang, Z. Wen, 'Detailed Dynamics of the Nonradiative Deactivation of Adenine: A Semiclassical Dynamics Study', *J. Phys. Chem. A* **2008**, *112*, 8497–8504.

[76] I. Conti, M. Garavelli, G. Orlandi, 'Deciphering Low Energy Deactivation Channels in Adenine', *J. Am. Chem. Soc.* **2009**, *131*, 16108–16118.

[77] W. M. I. Hassan, W. C. Chung, N. Shimakura, S. Koseki, H. Kono, Y. Fujimura, 'Ultrafast radiationless transition pathways through conical intersections in photoexcited 9H-adenine', *Phys. Chem. Chem. Phys.* **2010**, *12*, 5317–5328.

[78] Z. Lan, Y. Lu, E. Fabiano, W. Thiel, 'QM/MM Nonadiabatic Decay Dynamics of 9H-Adenine in Aqueous Solution', *ChemPhysChem* **2011**, *12*, 1989–1998.

[79] M. Barbatti, 'Photorelaxation Induced by Water-Chromophore Electron Transfer', *J. Am. Chem. Soc.* **2014**, *136*, 10246–10249.

[80] J. W. Park, T. Shiozaki, 'On-the-Fly CASPT2 Surface-Hopping Dynamics', *J. Chem. Theory Comput.* **2017**, *13*, 3676–3683.

[81] S. Mai, M. Richter, P. Marquetand, L. González, 'Excitation of Nucleobases from a Computational Perspective II: Dynamics' in *Photoinduced Phenomena in Nucleic Acids I. Nucleobases in the Gas Phase and in Solvents*, (Eds.: M. Barbatti, A. C. Borin, S. Ullrich), *Topics in Current Chemistry, Vol. 355*, Springer, Heidelberg, Germany, **2014**, 99–153.

[82] C. E. Crespo-Hernández, B. Cohen, B. Kohler, 'Base Stacking Controls Excited-State Dynamics in A·T DNA', *Nature* **2005**, *436*, 1141–1144.

[83] R. Improta, 'The excited states of π-stacked 9-methyladenine oligomers: a TD-DFT study in aqueous solution', *Phys. Chem. Chem. Phys.* **2008**, *10*, 2656–2664.

[84] I. Vayá, T. Gustavsson, F.-A. Miannay, T. Douki, D. Markovitsi, 'Fluorescence of Natural DNA: From the Femtosecond to the Nanosecond Time Scales', *J. Am. Chem. Soc.* **2010**, *132*, 11834–11835.

[85] C. Su, C. T. Middleton, B. Kohler, 'Base-Stacking Disorder and Excited-State Dynamics in Single-Stranded Adenine Homo-Oligonucleotides', *J. Phys. Chem. B* **2012**, *116*, 10266–10274.

[86] A. Chatterley, C. West, G. Roberts, V. Stavros, J. Verlet, 'Mapping the Ultrafast Dynamics of Adenine onto Its Nucleotide and Oligonucleotides by Time-Resolved Photoelectron Imaging', *J. Phys. Chem. Lett.* **2014**, *5*, 843–848.

[87] J. Chen, A. K. Thazhathveetil, F. D. Lewis, B. Kohler, 'Ultrafast Excited-State Dynamics in Hexaethyleneglycol-Linked DNA Homoduplexes Made of A·T Base Pairs', *J. Am. Chem. Soc.* **2013**, *135*, 10290–10293.

[88] H. Kang, P.-J. Chou, W. C. Johnson jr., D. Weller, S.-B. Huang, J. E. Summerton, 'Stacking Interactions of ApA Analogues with Modified Backbones', *Biopolymers* **1992**, *32*, 1351–1363.

[89] W.-M. Kwok, C. Ma, D. L. Phillips, 'Femtosecond Time- and Wavelength-Resolved Fluorescence and Absorption Spectroscopic Study of the Excited States of Adenosine and an Adenine Oligomer', *J. Am. Chem. Soc.* **2006**, *128*, 11894–11905.

[90] F. Santoro, R. Improta, F. Avila, M. Segado, A. Lami, 'The interplay between neutral exciton and charge transfer states in single-strand polyadenine: A quantum dynamical investigation', *Photochem. Photobiol. Sci.* **2013**, *12*, 1527–1543.

[91] R. R. Ramazanov, D. A. Maksimov, A. I. Kononov, 'Noncanonical Stacking Geometries of Nucleobases as a Preferred Target for Solar Radiation', *J. Am. Chem. Soc.* **2015**, *137*, 11656–11665.

[92] J. Chen, Y. Zhang, B. Kohler, 'Excited States in DNA Strands Investigated by Ultrafast Laser Spectroscopy' in *Photoinduced Phenomena in Nucleic Acids II. DNA Fragments and Phenomenological Aspects*, (Eds.: M. Barbatti, A. C. Borin, S. Ullrich), *Topics in Current Chemistry, Vol. 356*, Springer, Heidelberg, Germany, **2014**, 39–87.

[93] J. Chen, B. Kohler, 'Base Stacking in Adenosine Dimers Revealed by Femtosecond Transient Absorption Spectroscopy', *J. Am. Chem. Soc.* **2014**, *136*, 6362–6372.

[94] K. de La Harpe, C. E. Crespo-Hernández, B. Kohler, 'Deuterium Isotope Effect on Excited-State Dynamics in an Alternating GC Oligonucleotide', *J. Am. Chem. Soc.* **2009**, *131*, 17557–17559.

[95] A. W. Lange, M. A. Rohrdanz, J. M. Herbert, 'Charge-Transfer Excited States in a π-Stacked Adenine Dimer, As Predicted Using Long-Range-Corrected Time-Dependent Density Functional Theory', *J. Phys. Chem. B* **2008**, *112*, 6304–6306.

[96] C. E. Crespo-Hernández, B. Kohler, 'Influence of secondary structure on electronic energy relaxation in adenine homopolymers', *J. Phys. Chem. B* **2004**, *108*, 11182–11188.

[97] S. O. Konorov, H. G. Schulze, C. J. Addison, C. A. Haynes, M. W. Blades, R. F. B. Turner, 'Base stacking configuration is a major determinant of excited state dynamics in A·T DNA and LNA.', *Open Spectrosc. J.* **2009**, *3*, 9–20.

[98] K. E. van Holde, J. Brahms, A. M. Michelson, 'Base Interactions of Nucleotide Polymers in Aqueous Solution', *J. Mol. Biol.* **1965**, *12*, 726–739.

[99] F. E. Hruska, S. S. Danyluk, 'A Nuclear Magnetic Resonance Study of Thermal Effects upon Base Stacking in Oligonucleotides: ApA>p', *Biochim. Biophys. Acta* **1968**, *157*, 238–241.

[100] C. T. Middleton, B. Cohen, B. Kohler, 'Solvent and solvent isotope effects on the vibrational cooling dynamics of a DNA base derivative', *J. Phys. Chem. A* **2007**, *111*, 10460–10467.

[101] C. Cheng, C. Ma, C. Chan, K. Ho, W. Kwok, 'The solvent effect and identification of a weakly emissive state in nonradiative dynamics of guanine nucleosides and nucleotides—a combined femtosecond broadband time-resolved fluorescence and transient absorption study', *Photochem. Photobiol. Sci.* **2013**, *12*, 1351–1365.

[102] D. Andreatta, J. L. P. Lustres, S. A. Kovalenko, N. P. Ernsting, C. J. Murphy, R. S. Coleman, M. A. Berg, 'Power-law solvation dynamics in DNA over six decades in time.', *J. Am. Chem. Soc.* **2005**, *127*, 7270–7271.

[103] K. E. Furse, S. A. Corcelli, 'Molecular Dynamics Simulations of DNA Solvation Dynamics', *J. Phys. Chem. Lett.* **2010**, *1*, 1813–1820.

[104] Y. Lu, Z. Lan, W. Thiel, 'Monomeric adenine decay dynamics influenced by the DNA environment.', *J. Comput. Chem.* **2012**, *33*, 1225–1235.

[105] R. Improta, F. Santoro, V. Barone, A. Lami, 'Vibronic Model for the Quantum Dynamical Study of the Competition between Bright and Charge-Transfer Excited States in Single-Strand Polynucleotides: The Adenine Dimer Case', *J. Phys. Chem. A* **2009**, *113*, 15346–15354.

[106] J. Norberg, L. Nilsson, 'Influence of Adjacent Bases on the Stacking-Unstacking Process of Single-Stranded Oligonucleotides', *Biopolymers* **1996**, *39*, 765–768.

[107] S. Jafilan, L. Klein, C. Hyun, J. Florián, 'Intramolecular Base Stacking of Dinucleoside Monophosphate Anions in Aqueous Solution', *J. Chem. Phys. B* **2012**, *116*, 3613–3618.

Additional Information of Chapter 5

5.B Comparison with Previous Results for d(ApA) in H_2O

Global Analysis

The transient electronic absorption of d(ApA) was previously measured in the probe wavelength range $\lambda_{probe} = 315 - 600$ nm at $T = 295$ K after excitation at $\lambda_{pump} = 260$ nm in buffered H_2O solution (pH 7.0) by M. C. Stuhldreier.[1] The exact measurement conditions and the resulting spectro-temporal map can be found in the corresponding Thesis. The data were analyzed in detail by time-profile analysis before. An additional global analysis by singular value decomposition (SVD) is presented in the following and will be compared to the present and the previous results.

The SVD time traces are multi-peak functions that converge to zero within $\Delta t = 1000$ ps (see Fig. 5.B1). They could be described by Gaussian-convoluted

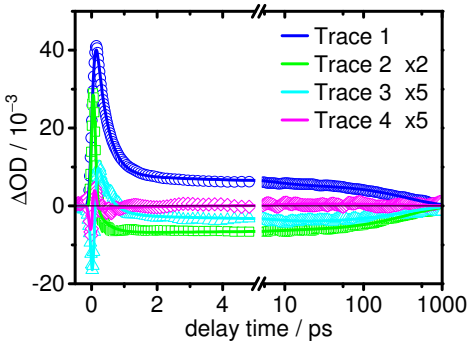

Figure 5.B1: Time traces from the global SVD analysis of the spectro-temporal transient electronic absorption data of d(ApA) measured by M. C. Stuhldreier after excitation at $\lambda_{pump} = 260$ nm at $T = 295$ K in H_2O. Time traces 2 – 4 were scaled by the given factors for better visibility. Note the linear timescale for the first 5 ps and the logarithmic timescale thereafter.

multi-exponential functions. Small-amplitude oscillations were observed in traces 3 and 4 but were not modeled. The analysis yielded

$\tau_1 = 0.03 \pm 0.01$ ps,

$\tau_2 = 0.34 \pm 0.01$ ps,

$\tau_3 = 6$ ps (fixed),

$\tau_4 = 370 \pm 15$ ps.

The decay-associated difference spectra (DADS) calculated from the SVD results to visualize the spectral contributions of the time components are shown in Fig. 5.B2. The DADS of the first time component shows a negative contribution in the range

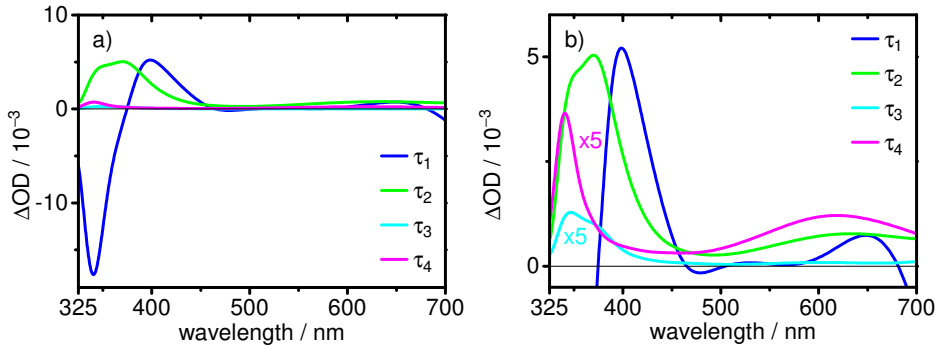

Figure 5.B2: Decay-associated difference spectra from the global SVD analysis of the spectro-temporal transient electronic absorption data of d(ApA) measured by M. C. Stuhldreier after excitation at $\lambda_{pump} = 260$ nm at $T = 295$ K in H_2O. The spectra each represent the spectral contribution of the time components τ_1 (blue), τ_2 (green), τ_3 (cyan) and τ_4 (magenta) given in the text. The spectra of the third and fourth component are shown enlarged in b).

325 nm $\leq \lambda_{probe} \leq$ 375 nm, where it is attributed to stimulated emission (SE) and the delayed rise of the signal. The spectrum shows a positive value with a maximum at $\lambda_{probe} = 398$ nm corresponding to the initial excited-state absorption (ESA) decay. The multiple changes of sign at $\lambda_{probe} \geq 464$ nm indicate an ill-defined time constant. The value is probably too small. The second time component has a maximum DADS amplitude at $\lambda_{probe} = 370$ nm with a shoulder at $\lambda_{probe} = 350$ nm and decreases to a constant at $\lambda_{probe} \approx 480$ nm. The third lifetime component of d(ApA) yielded a shallow spectrum with a maximum at $\lambda_{probe} = 345$ nm and a shoulder at $\lambda_{probe} = 375$ nm. The fourth component also shows a shallow DADS with two maxima at $\lambda_{probe} = 340$ nm and $\lambda_{probe} = 620$ nm. The shoulders in the DADS indicate that the excited-state species were less-than-well separated by the SVD procedure. The second maxima around $\lambda_{probe} \approx 370$ nm for components τ_2 and τ_3 may hint at mixing with τ_1 since the DADS of the latter component shows a much stronger negative amplitude in this spectral region than can be expected from

SE contributions.

Discussion

For direct comparison, the results from the previous and the present time-profile analyses were reprinted in Table 5.B1 in comparison to the new SVD results. The

Table 5.B1: Comparison of the present and previous experimental results for the temperature-dependent electronic dynamics of d(ApA). Values are given with 2σ standard deviation of the last decimal digit in parentheses.

species	τ_1/ps	τ_2/ps	τ_3/ps	τ_4/ps	analysis method	Ref.
d(pApA)[a]	0.10(5)	0.41(5)	8.3(6)	380(40)	time profiles[b]	1, 2
d(ApA)	-	0.34(3)	80(23)	380(40)	time profiles[c]	1
d(ApA)	0.03(1)	0.34(1)	6	370(15)	global SVD	1[d]
d(ApA)	-	0.44(6)	6(4)	360(40)	time profiles	this work
d(ApA)	0.23(2)	0.56(4)	6	360(14)	global SVD	this work

[a] d(pApA) differs from d(ApA) by the extra 5'-phosphate group
[b] results from transient fluorescence spectroscopy
[c] results from transient electronic absorption spectroscopy
[d] data reanalyzed in this work

time constants show slightly differing values for the sub-picosecond components but good agreement for τ_3 and τ_4, except for the analysis that found an intermediate time constant of ≈ 80 ps which cannot be rationalized in retrospect.

The higher values for τ_1 and τ_2 in the data measured in this work may be explained by the different probe wavelength range. It is known that transient electronic absorption spectra show contributions from hot ground state absorption (HGSA) in the near UV. HGSA decay can be extrapolated to have a lifetime of $\tau_{\mathrm{HGSA}} \approx 1.0$ ps around $\lambda_{\mathrm{probe}} = 300$ nm.[1,3,4] Since the probe wavelength range extended farther into the UV in this work, the data contain higher contribution from HGSA signal which mixes into the observed lifetimes.

The resulting DADS from the SVD analysis of the present and the previous data are compared in Fig. 5.B3. At this point, it must be noted that the previous measurements of d(ApA) were taken with a pump pulse energy of 300 nJ, which is three times the pump pulse energy used in the present work. Therefore, especially the sub-picosecond signals significantly gain in amplitude. The lifetimes seem not to be affected. The different probe wavelength range, i. e. the white light break-off at $\lambda_{\mathrm{probe}} \approx 330$ nm in the previous measurements causes the DADS to show closed bands at the UV edge of the probe spectrum. It becomes evident, that the transient

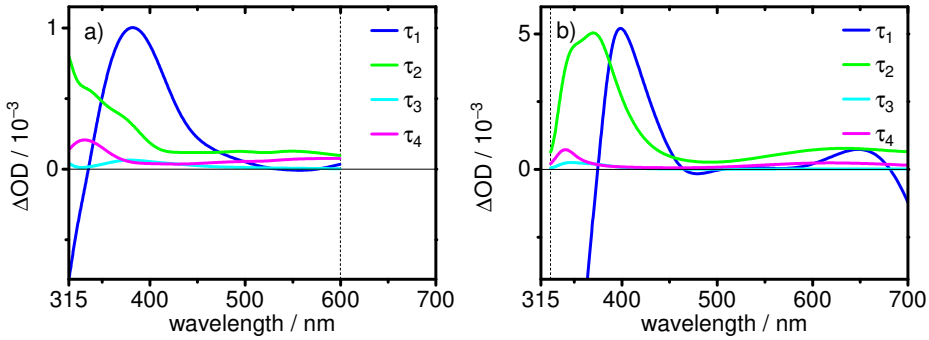

Figure 5.B3: Direct comparison of the decay-associated difference spectra from the global SVD analysis of the spectro-temporal transient electronic absorption data of the d(ApA) sample measured in this work (a) and the d(ApA) sample measured by M. C. Stuhldreier (b). The spectra each represent the spectral contribution of the time components τ_1 (blue), τ_2 (green), τ_3 (cyan) and τ_4 (magenta).

absorption signal at $\lambda_{probe} < 325$ nm is necessary to satisfactorily distinguish HGSA and SE contributions from ESA signals. Stuhldreier[1] discussed the rise and decay of two separate transient spectral bands in the near UV probe wavelength range, ESA_{345} and ESA_{375}. These could not be separated by the new SVD analysis and were both attributed to the third time constant, $\tau_3 \approx 6$ ps, as can be seen by the maximum and the shoulder of the third DADS. The DADS of the fourth component, $\tau_4 \approx 360$ ps, shows good agreement when comparing the two data sets.

All in all, the previous and the present results are consistent. It was seen that the probe wavelength range is a critical factor for analyzing and interpreting transient absorption data.

5.C Additional Results for dAMP in H_2O

5.C.1 Spectro-Temporal Evolution of the Transient Absorption Bands at Room Temperature

All transient electronic absorption spectra of dAMP measured at $T = 295$ K in H_2O after exctitation at $\lambda_{pump} = 260$ nm were modeled by a sum of three log-normal functions for further analysis of the fast spectro-temporal electronic dynamics. Selected transient spectra and best fit curves are shown in Fig. 5.C1 together with the individual spectral bands. The three spectral bands represent i) the negative contribution of SE and the ensuing positive contribution of HGSA around $\lambda_{probe} = 315$ nm, ii) the most prominent ESA band with its maximum shifting between $\lambda_{probe} = 420 - 350$ nm, and iii) the weak and broad ESA band with a

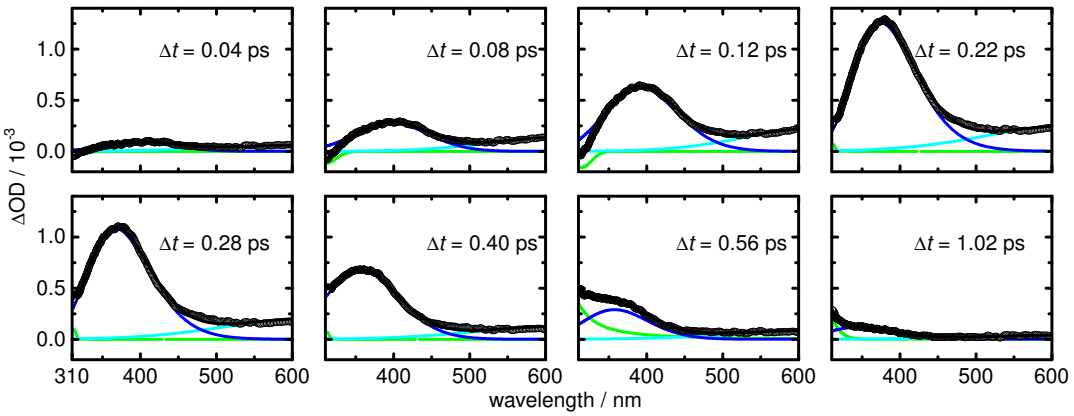

Figure 5.C1: Expanded views of the transient electronic absorption spectra of dAMP at selected delay times up to $\Delta t = 1$ ps after excitation at $\lambda_{\text{pump}} = 260$ nm measured at $T = 295$ K in H_2O. The experimental data (open circles) were described by a sum of three log-normal functions (black line) each representing individual spectral bands (green, blue, cyan).

maximum at $\lambda_{\text{probe}} > 600$ nm.

5.C.2 Static Absorption and Fluorescence Spectra at Lowered Temperature

The static UV absorption spectra and the fluorescence spectra after excitation at $\lambda_{exc} = 260$ nm of dAMP in H_2O at three temperatures in the range $T = 278 - 295$ K are depicted in Fig. 5.C2. The static absorption was independent from temperature.

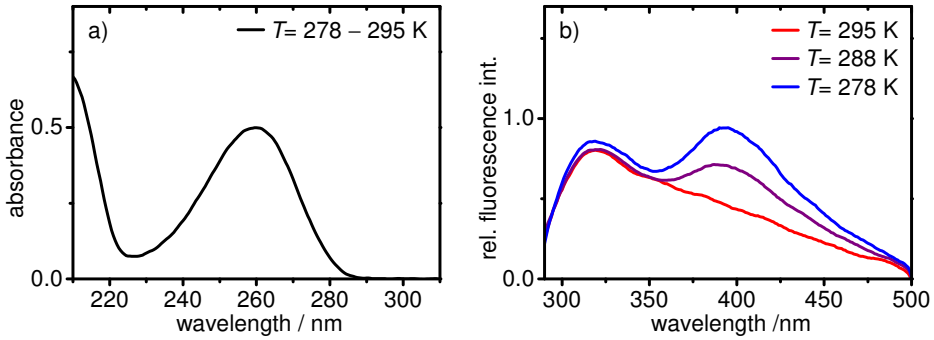

Figure 5.C2: Static UV absorption (a) and static fluorescence (b) of dAMP measured at $T = 278$ K (blue), $T = 288$ K (purple) and $T = 295$ K (red) after excitation at $\lambda_{exc} = 260$ nm in H_2O. The fluorescence spectra were normalized relative to the emisson maximum of dAMP at room temperature.

In the fluorescence spectrum, when reducing the temperature to $T = 278$ K, the emission maximum at $\lambda = 320$ nm gradually decreased and an additional fluorescence band emerged around $\lambda = 395$ nm.

This behavior was observed before for dAMP in glycol water glasses at $T = 77$ K. Rapoport et al.[5,6] detected increasingly red-shifted emission at concentrations between $c = 0.05 - 10$ mM and interpreted this as stacked aggregates. For AMP, a self-stacking constant of $K_{ass} = 2.1$ M^{-1} was determined at $T = 300$ K in D_2O (pD 8.9) for concentrations between $c = 2.6 - 400$ mM.[7] In this work, a concentration of $c = 3.7$ mM was used that lies within this domain. In analogy to the dinucleotide, the additional band seen in the present experimental fluorescence spectra of dAMP is assigned to excimer states that can form in loosely self-assembled stacks of Ade moieties in aqueous solution. Due to the lack of a connecting backbone the nucleobases have a high flexibility to form a variety of stacked structures which may explain that the fluorescence maximum lies to the blue of that of the dinucleotide. The stacking fraction, however, is probably be very low because the fluorescence quantum yield of Ade stacks is at least twice that of the monomers.[8–10]

5.C.3 Transient Electronic Absorption at Lowered Temperature

Femtosecond time-resolved transient electronic absorption spectroscopy of dAMP in the probe wavelength range $\lambda_{probe} = 315 - 600$ nm after excitation at $\lambda_{pump} = 260$ nm at $T = 278$ K and $T = 288$ K yielded the two-dimensional maps presented in Fig. 5.C3. The spectro-temporal signal of dAMP shows a broad and blue-shifting

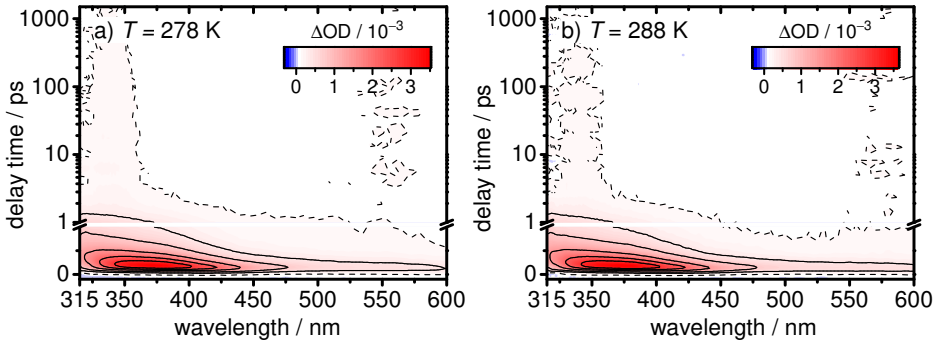

Figure 5.C3: Two-dimensional spectro-temporal transient electronic absorption maps of dAMP recorded at $T = 278$ K (a) and $T = 288$ K (b) after excitation at $\lambda_{pump} = 260$ nm in H_2O shown on a linear scale up to $\Delta t = 1$ ps and on a logarithmic timescale for delay times up to $\Delta t = 1500$ ps.

ESA band that decays within $\Delta t = 2$ ps similar to the one found at room temperature. However, a very weak and long-lived transient absorption band appears between $\lambda_{probe} = 315 - 360$ nm in the measurements at lowered temperature (see dashed contour lines).

Time-Profile Analysis

In order to investigate the temperature dependence of the electronic deactivation dynamics of dAMP, time profiles were extracted from the spectro-temporal absorption data by spectral integration over the probe wavelength range $\lambda_{probe} = 315 - 450$ nm. Another set of time profiles was obtained by single-color probe measurements of the GSR signals at $\lambda_{probe} = 255$ nm. The data sets were modeled with Gaussian-convoluted multi-exponential decay functions with simultaneously fitted time constants. The data and the best fit curves for the measurements at $T = 278$ K and $T = 288$ K are shown in Fig. 5.C4 together with the time profiles and best fit curves of the measurements at $T = 295$ K in direct comparison. The excited-state decay of dAMP is independent from temperature within experimental errors. The data were

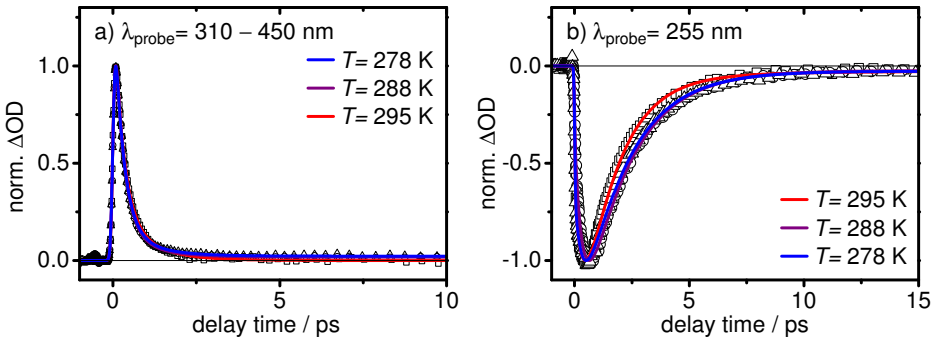

Figure 5.C4: Transient absorption-time profiles of dAMP recorded at $T = 278$ K (blue), $T = 288$ K (purple) and $T = 295$ K (red) after excitation at $\lambda_{\text{pump}} = 260$ nm in H_2O. Time profiles in a) were extracted by wavelength integration of the measured spectro-temporal data between $\lambda_{\text{probe}} = 315 - 450$ nm and are shown for delay times up to $\Delta t = 10$ ps. Time profiles in b) were recorded with a single-color probe beam at $\lambda_{\text{probe}} = 255$ nm and are shown for delay times up to $\Delta t = 15$ ps. Open symbols represent the data points, solid lines show the best fit curves from a simultaneous multi-exponential fit.

simultaneously fitted by biexponential functions with the time constants

$$\tau_1 = 0.27 \pm 0.01 \text{ ps and}$$
$$\tau_2 = 0.9 \pm 0.1 \text{ ps.}$$

with an amplitude ratio of $\approx 4 : 1$ and a temporal resolution of $\sigma_{\text{IRF}} = 0.056 \pm 0.001$ ps. The invariability of the decay components with temperature is consistent with studies of Ado, AMP and 9-methyl-Ade which all show constant excited-state lifetimes between $T = 100 - 340$ K.[11,12]

An additional long-time component with an amplitude $< 2\,\%$ can be seen at delay times $\Delta t > 3$ ps for the measurements below room temperature. This long-lived contribution is assigned to the small fraction of stacked Ade chromophores already seen in the static spectra.

The vibrational cooling time of dAMP was determined to $\tau_{\text{vc}} = 1.97 \pm 0.03$ ps at $T = 278$ K and $\tau_{\text{vc}} = 1.96 \pm 0.03$ ps at $T = 288$ K.

Global Analysis

Global analyses of the full spectro-temporal transient electronic absorption maps of dAMP at lowered temperature were performed by singular value decomposition. The

SVD time traces (Fig. 5.C5) were described by Gaussian-convoluted multi-exponential functions.

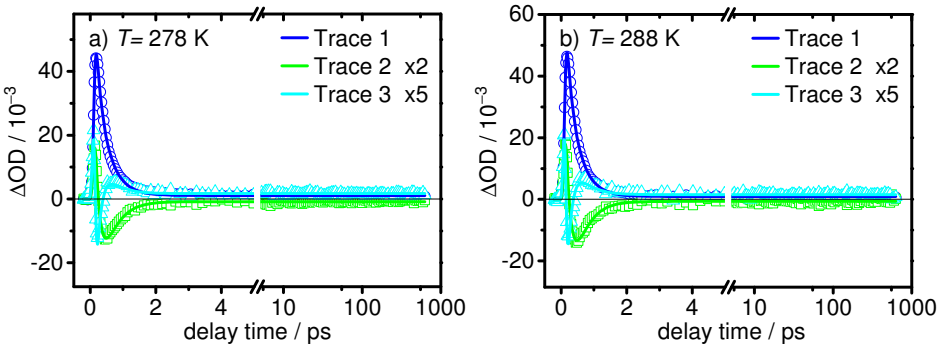

Figure 5.C5: Time traces from the global SVD analysis of the spectro-temporal transient electronic absorption data of dAMP at $T = 288$ K (a) and $T = 278$ K (b) measured after excitation at $\lambda_{pump} = 260$ nm in H_2O. Time traces 2 – 3 were scaled by the given factors for better visibility. Note the linear timescale for the first 5 ps and the logarithmic timescale thereafter.

For $T = 278$ K, the analysis yielded

$$\tau_1 = 0.16 \pm 0.01 \text{ ps},$$
$$\tau_2 = 0.39 \pm 0.02 \text{ ps}$$

and for $T = 288$ K:

$$\tau_1 = 0.15 \pm 0.01 \text{ ps},$$
$$\tau_2 = 0.40 \pm 0.01 \text{ ps}.$$

The time constants at these temperatures were mutually consistent within experimental errors and in good agreement with the above given time constants found at room temperature. The diminutive additional long-time component was approximated by an offset function.

The decay-associated difference spectra calculated from the SVD results to visualize the spectral contributions of the time components are shown in Fig. 5.C6. The first two DADS represent highly similar and characteristic decay dynamics of the monomer dAMP. The DADS of the first time component shows a negative contribution in the range 315 nm $\leq \lambda_{probe} \leq$ 340 nm, where it is attributed to SE and the delayed rise of the signal. The spectrum shows a positive value with a maximum at $\lambda_{probe} \approx 380$ nm corresponding to the initial ESA decay. The negative amplitude at

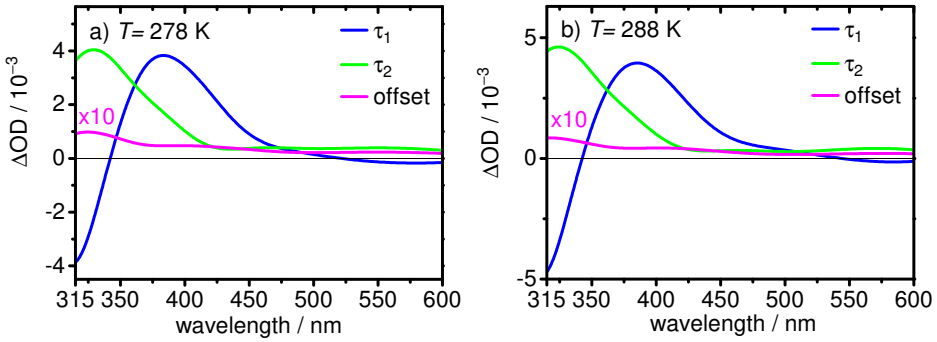

Figure 5.C6: Decay-associated difference spectra from the global SVD analysis of the spectro-temporal transient electronic absorption data of dAMP at $T = 288$ K (a) and $T = 278$ K (b) measured after excitation at $\lambda_{pump} = 260$ nm in H_2O. The spectra each represent the spectral contribution of the time components τ_1 (blue), τ_2 (green) and the offset (magenta, enlarged) given in the text.

$\lambda_{probe} \geq 520$ nm is likely due to an imperfect time-zero correction or overdone solvent subtraction and thus erroneous. The second time component has a maximum DADS amplitude at $\lambda_{probe} \approx 325$ nm and seems to decay to a constant at $\lambda_{probe} = 430$ nm. Contribution from HGSA is assigned to the UV edge of the DADS. The offset component yields a shallow spectrum with a maximum at $\lambda_{probe} = 318 - 325$ nm that is assigned to ESA. The relative amplitude of this component decreases with increasing temperature. It is again assigned to the small fraction of stacked Ade chromophores. Although this is a highly interesting phenomenon it was not aim of the study and will not be further discussed.

5.C.4 Hot Ground State Contribution

For dAMP, the time constants from the time-profile analyses were generally greater than the ones determined from SVD analyses.

The transient electronic absorption signal at the UV edge of the present probe wavelength spectrum can be assigned to absorption of highly vibrationally excited ground state molecules, called HGSA.[1,3,4,13,14] (See also Chapter 3 for a discussion of HGSA signals.) The time constant of HGSA decay has been seen to increase with decreasing wavelength and can be extrapolated to be $\tau_{HGSA} \approx 1.0$ ps around $\lambda_{probe} = 300$ nm.[1,3,4]

Wavelength-integration over $\lambda_{probe} = 310 - 450$ nm thus includes SE, HGSA and ESA signals and the time constants determined from these time-profiles show slightly greater values than those from SVD analysis. Most probably, the time profiles of

dAMP are positively dominated by HGSA decay with $\tau_2 \approx 0.9$ ps. While the overall vibrational cooling time, τ_{vc}, was found to be increased at lowered temperature, τ_2 was seen to be invariable towards temperature change. This demonstrates its direct dependency from the ultrafast excited-state deactivation and hints at an intramolecular energy redistribution process. The high excess energy contained in the molecule at the point of interconversion induces rapid redistribution independent from the temperature of the surroundings.

The global SVD analysis incorporates the whole probe wavelength range and the results thus give an average time constant of $\tau_2 \approx 0.45$ ps that is shorter than the one describing only the UV part of the probe spectrum. This value is in good agreement with the excited-state lifetime of dAMP found in time-resolved fluorescence measurements.[1] Thus, τ_2 probably changes its origin from HGSA to ESA when going from the UV to the visible probe wavelength range. The assignment of the second decay component of dAMP is therefore not unambiguous.

The full HGSA signal is subject to band-shifting and would be better visible at probe wavelengths $\lambda_{probe} < 315$ nm. An elaborate model function is needed for an improved SVD analysis to incorporate wavelength-dependent time constants and the complex kinetics including the excited state and the ground state.

5.C.5 Effect of Pump Pulse Energy

Close inspection of the DADS of dAMP at the three temperatures shows a different amplitude ratio of the two time components at wavelengths $\lambda_{probe} < 420$ nm for the data measured at lower temperatures in comparison with the one measured at room temperature. This effect was also in Section 5.B and is attributed to the higher pump pulse energy that was used for the experiments at lowered temperature. The lifetimes were found to be unaffected.

The band shape of the DADS of component τ_2 was seen to change due to the increased pump pulse energy. It yielded a new maximum at $\lambda_{probe} \approx 325$ nm. Whether this spectral band can be attributed to ESA or HGSA is unclear. A higher pump pulse energy increases the number of excited molecules and does not enhance the excited-state population. However, this should enhance all signal components to the same extent. Further studies are needed here, especially in the probe wavelength range $\lambda_{probe} = 260 - 315$ nm.

5.D Additional Results for dAMP in D_2O

Upon dissolving in D_2O, it is known that the hydrogen atoms of the amino group of Ade are fully exchanged by deuterium.[15] This was confirmed experimentally by a small blue-shift of the static absorption spectrum (not shown).

5.D.1 Transient Electronic Absorption

Femtosecond time-resolved transient electronic absorption spectra of dAMP were recorded in buffered D_2O solution (pD 7.4) at $T = 295$ K after excitation at $\lambda_{pump} = 260$ nm. The two-dimensional spectro-temporal absorption map is presented in Fig. 5.D1 and shows a similar excited-state decay behavior as in H_2O.

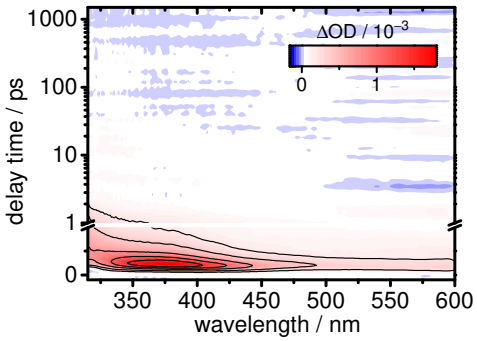

Figure 5.D1: Two-dimensional spectro-temporal transient electronic absorption maps of dAMP measured in D_2O at $T = 295$ K after excitation at $\lambda_{pump} = 260$ nm shown on a linear scale up to $\Delta t = 1$ ps and on a logarithmic timescale for delay times up to $\Delta t = 1500$ ps.

Time-Profile Analysis

The effect of deuteration on the electronic deactivation dynamics of dAMP was closely investigated in time profiles generated as described before. The data sets were modeled with Gaussian-convoluted multi-exponential decay functions with simultaneously fitted time constants. The data and the best fit curves are shown in Fig. 5.D2 together with the time profiles and best fit curves of the measurements of dAMP in H_2O in direct comparison. It can be seen that the transient signal of dAMP in D_2O is similar to that in H_2O. The fit yielded

$$\tau_1 = 0.27 \pm 0.01 \text{ ps},$$

$$\tau_2 = 0.9 \pm 0.1 \text{ ps},$$

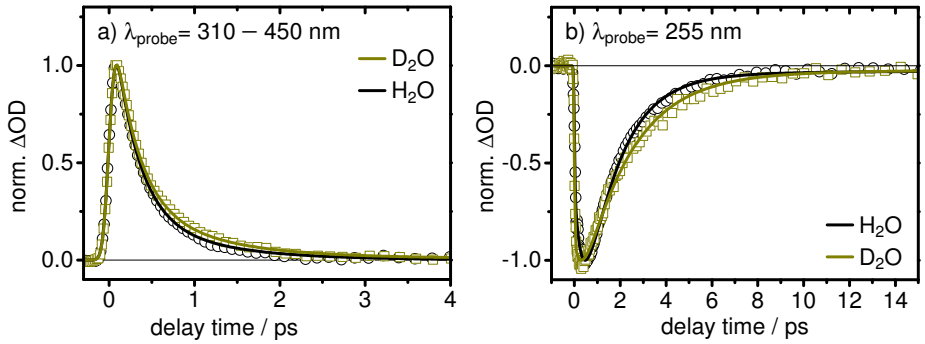

Figure 5.D2: Transient absorption-time profiles of dAMP in D_2O (dark yellow) in direct comparison to the time profiles in H_2O (black) measured at $T = 295$ K after excitation at $\lambda_{pump} = 260$ nm. Time profiles in a) were extracted by wavelength integration of the measured spectro-temporal data between $\lambda_{probe} = 315 - 450$ nm and are shown for delay times up to $\Delta = 4$ ps. Time profiles in b) were recorded with a single-color probe beam at $\lambda_{probe} = 255$ nm and are shown for delay times up to $\Delta = 15$ ps. Open symbols represent the data points, solid lines show the best fit curves from multi-exponential fits.

with a changed amplitude ratio of $\approx 3 : 1$ and a temporal resolution of $\sigma_{IRF} = 0.056 \pm 0.001$ ps, and

$$\tau_{vc} = 2.1 \pm 0.2 \text{ ps}$$

for the GSR signal. An additional long-time component with an amplitude $< 3\,\%$ can be seen at delay times $\Delta t > 8$ ps for the GSR signal.

Global Analysis

A global analysis of the full spectro-temporal transient electronic absorption map of dAMP in D_2O was performed by singular value decomposition. The SVD time traces (Fig. 5.D3) were described by Gaussian-convoluted multi-exponential functions.

The fit yielded

$$\tau_1 = 0.17 \pm 0.01 \text{ ps},$$

$$\tau_2 = 0.59 \pm 0.03 \text{ ps}.$$

The additional long-time component was neglected due to its low amplitude.

The decay-associated difference spectra calculated from the SVD results to visualize the spectral contributions of the time components are shown in Fig. 5.D4. The DADS of the measurements of dAMP in D_2O are highly similar to those from

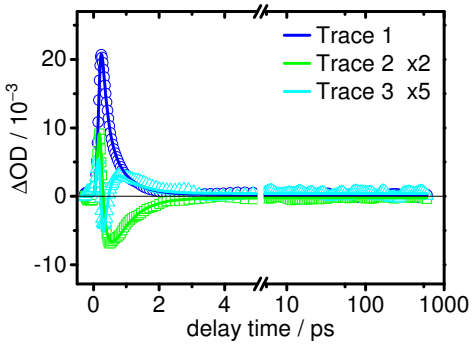

Figure 5.D3: Time traces from the global SVD analysis of the spectro-temporal transient electronic absorption data of dAMP in D_2O measured at $T = 295$ K after excitation at $\lambda_{pump} = 260$ nm. Time traces 2 – 3 were scaled by the given factors for better visibility. Note the linear timescale for the first 5 ps and the logarithmic timescale thereafter.

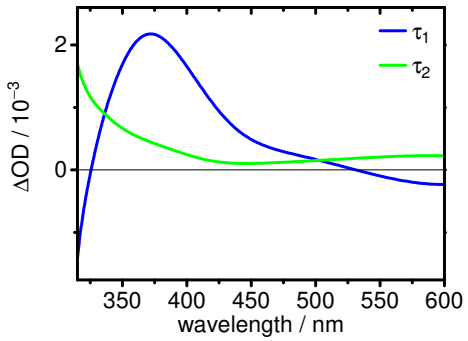

Figure 5.D4: Decay-associated difference spectra from the global SVD analysis of the spectro-temporal transient electronic absorption data of dAMP in D_2O measured at $T = 295$ K after excitation at $\lambda_{pump} = 260$ nm. The spectra each represent the spectral contribution of the time components τ_1 (blue) and τ_2 (green) given in the text.

the measurements in H_2O (Fig. 5.8 on page 125) and reflect contributions form SE, HGSA and ESA as described in the main text.

5.D.2 Effect of D_2O

In the time-profile analysis, no change of the time components was observed for the measurements in D_2O in comparison to H_2O, but an amplitude increase was found for τ_2. This hints at an increase of the HGSA contribution. The reason for this cannot be simply deduced from the experimental results. In the SVD analysis,

the second time component was slightly increased from $\tau_2 \approx 0.45$ ps in H_2O to $\tau_2 \approx 0.59$ ps in D_2O. Although this seems to be a marked change it can be explained by the amplitude increase of the HGSA signal which influences the SVD results because τ_2 is a mixture of HGSA and ESA signals.

A clear kinetic isotope effect was observed for the vibrational cooling time. This intermolecular energy transfer process is directly dependent on the vibrational frequencies of solvent. HGSA, on the other hand, is an intramolecular process that is independent from deuteration within experimental errors because the vibrational frequencies of the molecule hardly change upon deuteration.[16]

The fully deuterated amino group is expected to induce a significant KIE for the excited-state relaxation if it was involved in the decay mechanism. Thus, the excited-state relaxation of dAMP is concluded to not involve significant nuclear motion of the amino group.

5.E Electronic Deactivation Mechanism of dAMP

The experimental results for the electronic deactivation dynamics of dAMP in H_2O and D_2O and at lowered temperature can be found in Table 5.E1.

The two sub-picosecond lifetime components reflect the ultrafast electronic

Table 5.E1: Experimental results for the temperature-dependent electronic dynamics of dAMP in H_2O, and the effect of D_2O. Values were rounded to significant digits. The error limits of the amplitudes are typically < 5 %.

solvent, T	a_1	τ_1/ps	a_2	τ_2/ps	a_{offset}	τ_{vc}/ps
time-profile analyses						
H_2O, 278 K	0.86	0.27	0.12	0.9	0.02	1.97
H_2O, 288 K	0.88	0.27	0.11	0.9	0.01	1.96
H_2O, 295 K	0.80	0.27	0.20	0.9	-	1.5
D_2O, 295 K	0.74	0.27	0.25	0.9	0.01	2.1
global analyses						
H_2O, 278 K		0.15		0.40		
H_2O, 288 K		0.16		0.39		
H_2O, 295 K		0.16		0.45		
D_2O, 295 K		0.17		0.59		
averaged results						
H_2O		$\langle 0.16 \rangle$		$\langle 0.46 \rangle$		$\langle 1.5 - 2.0 \rangle$
D_2O		$\langle 0.16 \rangle$		$\langle 0.46 \rangle$		$\langle 2.1 \rangle$

deactivation of the excited molecule. In the time-profile analysis, the data could be described with the same time constants for all temperatures in the range $T = 278 - 295$ K and for the measurement in D_2O thanks to a simultaneous fit and exposes environment-independent dynamics. The individual SVD analyses of the data sets also yielded similar lifetimes that were mutually consistent within errors. A diminutive contribution from a long-lived component was necessary to model the data. The differences between the time-profile analyses and the SVD analyses were traced back to HGSA contribution in the ESA signal.

The vibrational cooling time was found to be slightly increased at lowered temperature and in D_2O compared to the measurement in H_2O at room temperature which is assigned to the change of the vibrational energy transfer rate determined by the solvent.

The first excited-state decay time constant, $\tau_1 \approx 0.16$ ps, can be assigned to the departure of the wavepacket from the Franck–Condon (FC) region. The second time constant, $\tau_2 \approx 0.46$ ps, describes the transfer time towards the point of internal conversion to the ground state. The temperature-independent ultrashort lifetimes expose a barrierless relaxation pathway and corroborate the results from Chapters 3 and 4.

At the excitation wavelength $\lambda_{\text{pump}} = 260$ nm, the Ade unit absorbs mainly in the $\pi\pi^*$ L_a excited state. Its potential energy hypersurface (PEHS) was predicted to steeply descend towards the region of conical intersections (CIs) with S_0. A CI is predicted to lie $\Delta E = 0.5 - 0.7$ eV below FC excitation.[17–21] In the present experimental data, an overall blue-shift of the transient spectra of $\Delta E = 0.68$ eV was observed within $\Delta t = 1$ ps after excitation. Due to the good agreement, the ultrafast transient signal decay is assigned to the electronic relaxation on the $\pi\pi^*$ L_a excited-state PEHS towards a CI with the ground-state PEHS. The two time components may be a result from the steadily decreasing slope of the PEHS on the deactivation pathway.

An unimpeded relaxation mechanism for the deactivation of the Ade monomer was predicted by various quantum chemical calculations. It is characterized by a puckering of the ring system centered at the C^2 position and leads to an out-of-plane motion of the C^2–H bond.[17–19,22–30] Another decay mechanism is often described to be nearly equally likely and involves a C^6-puckering and an out-of-plane bending of the amino group. The pathway connecting the FC region with such a CI, however, was predicted to be impeded by a small barrier.[17,19,22–27,30–32] This mechanism should be drastically decelerated by deuteration of the amino group. Only the first

mechanism is fully consistent with the present experimental data of the excited-state decay dynamics of dAMP.

References of Additional Information

[1] M. C. Stuhldreier, 'Electronic Deactivation Dynamics of DNA Model Systems and Solvation Dynamics of a Natural Antioxidant by Femtosecond Fluorescence and Absorption Spectroscopy', Dissertation, Christian-Albrechts-Universität zu Kiel, **2013**.

[2] M. C. Stuhldreier, C. Schüler, J. Kleber, F. Temps, 'Femtosecond Fluorescence Measurements of the Adenine Dinucleotide: Direct Observation of the Excimer State' in *Ultrafast Phenomena XVII*, (Eds.: M. Chergui, D. M. Jonas, E. Riedle, R. W. Schoenlein, A. J. Taylor), Oxford, **2011**, 553–555.

[3] J.-M. L. Pecourt, J. Peon, B. Kohler, 'Ultrafast Internal Conversion of Electronically Excited RNA and DNA Nucleosides in Water', *J. Am. Chem. Soc.* **2000**, *122*, 9348–9349.

[4] K. Röttger, R. Siewertsen, F. Temps, 'Ultrafast Electronic Deactivation Dynamics of the Rare Natural Nucleobase Hypoxanthine', *Chem. Phys. Lett.* **2012**, *536*, 140–146.

[5] V. L. Rapoport, B. M. Malkin, S. V. Zorina, 'Luminescence Detection of Tightly Bound Stacking Aggregates of Adenine and Adenosine in Aqueous Solutions—the Candidates for the Role of the First Genetic Templates', *Dokl. Biochem. Biophys.* **2006**, *406*, 23–26.

[6] V. L. Rapoport, V. M. Malkin, A. V. Savina, E. A. Safargaleyeva, V. V. Goryuchko, 'Luminescence of Stable Stacking Aggregates of Adenine and Uracil in Water', *Biophysics* **2012**, *57*, 9–13.

[7] R. Tribolet, H. Sigel, 'Self-association of adenosine 5'-monophosphate (5'-AMP) as a function of pH and in comparison with adenosine, 2'-AMP and 3'-AMP', *Biophys. Chem.* **1987**, *27*, 119–130.

[8] P. Vigny, J. P. Ballini, 'Excited states of nucleic acids at 300 K and electronic energy transfer' in *Excited States in Organic Chemistry and Biochemistry*, (Eds.: B. Pullman, N. Goldblum), Reidel, Dordrecht, Holland, **1977**, 1–13.

[9] J. P. Morgan, M. Daniels, 'Excited states of DNA and its components at room temperature. III. Spectra polarization, and quantum yields of emissions from ApA and poly rA.', *Photochem. Photobiol.* **1979**, *31*, 101–113.

[10] P. Vigny, M. Duquesne, *Organic Molecular Photophysics*, (Ed.: J. B. Birks), Wiley, New York, **1976**, 167–177.

[11] B. A. West, J. M. Womick, A. M. Moran, 'Interplay between Vibrational Energy Transfer and Excited State Deactivation in DNA Components', *J. Phys. Chem.* **2013**, *117*, 5865–5874.

[12] S. O. Konorov, H. G. Schulze, C. J. Addison, C. A. Haynes, M. W. Blades, R. F. B. Turner, 'Base stacking configuration is a major determinant of excited state dynamics in A·T DNA and LNA.', *Open Spectrosc. J.* **2009**, *3*, 9–20.

[13] J.-M. L. Pecourt, J. Peon, B. Kohler, 'DNA Excited-State Dynamics: Ultrafast Internal Conversion and Vibrational Cooling in a Series of Nucleosides', *J. Am. Chem. Soc.* **2001**, *123*, 10370–10378.

[14] I. Buchvarov, Q. Wang, M. Raytchev, A. Trifonov, T. Fiebig, 'Electronic energy delocalization and dissipation in single- and double-stranded DNA', *Proc. Natl. Acad. Sci. U. S. A.* **2007**, *104*, 4794–4797.

[15] D. G. Cross, 'Hydrogen Exchange in Nucleosides and Nucleotides. Measurement of Hydrogen Exchange by Stopped-Flow and Ultraviolet Difference Spectroscopy', *Biochemistry* **1975**, *14*, 357–362.

[16] C. T. Middleton, B. Cohen, B. Kohler, 'Solvent and solvent isotope effects on the vibrational cooling dynamics of a DNA base derivative', *J. Phys. Chem. A* **2007**, *111*, 10460–10467.

[17] S. Perun, A. L. Sobolewski, W. Domcke, 'Ab Initio Studies on the Radiationless Decay Mechanisms of the Lowest Excited Singlet States of 9H-Adenine', *J. Am. Chem. Soc.* **2005**, *127*, 6257–6265.

[18] C. M. Marian, 'A new pathway for the rapid decay of electronically excited adenine', *J. Chem. Phys.* **2005**, *122*, 104314.

[19] L. Serrano-Andrés, M. Merchán, A. C. Borin, 'A Three-State Model for the Photophysics of Adenine', *Chem. Eur. J.* **2006**, *12*, 6559–6571.

[20] E. Fabiano, W. Thiel, 'Nonradiative Deexcitation Dynamics of 9H-Adenine: An OM2 Surface Hopping Study', *J. Phys. Chem. A* **2008**, *112*, 6859–6863.

[21] M. Barbatti, Z. Lan, R. Crespo-Otero, J. J. Szymczak, H. Lischka, W. Thiel, 'Critical appraisal of excited state nonadiabatic dynamics simulations of 9H-adenine', *J. Chem. Phys.* **2012**, *137*, 22A503.

[22] H. Chen, S. Li, 'Theoretical Study toward Understanding Ultrafast Internal Conversion of Excited 9H-Adenine', *J. Phys. Chem. A* **2005**, *109*, 8443–8446.

[23] L. Blancafort, 'Excited-State Potential Energy Surface for the Photophysics of Adenine', *J. Am. Chem. Soc.* **2006**, *128*, 210–219.

[24] Y. Lei, S. Yuan, Y. Dou, Y. Wang, Z. Wen, 'Detailed Dynamics of the Nonradiative Deactivation of Adenine: A Semiclassical Dynamics Study', *J. Phys. Chem. A* **2008**, *112*, 8497–8504.

[25] I. Conti, M. Garavelli, G. Orlandi, 'Deciphering Low Energy Deactivation Channels in Adenine', *J. Am. Chem. Soc.* **2009**, *131*, 16108–16118.

[26] W. M. I. Hassan, W. C. Chung, N. Shimakura, S. Koseki, H. Kono, Y. Fujimura, 'Ultrafast radiationless transition pathways through conical intersections in photoexcited 9H-adenine', *Phys. Chem. Chem. Phys.* **2010**, *12*, 5317–5328.

[27] Z. Lan, Y. Lu, E. Fabiano, W. Thiel, 'QM/MM Nonadiabatic Decay Dynamics of 9H-Adenine in Aqueous Solution', *ChemPhysChem* **2011**, *12*, 1989–1998.

[28] M. Barbatti, 'Photorelaxation Induced by Water-Chromophore Electron Transfer', *J. Am. Chem. Soc.* **2014**, *136*, 10246–10249.

[29] J. W. Park, T. Shiozaki, 'On-the-Fly CASPT2 Surface-Hopping Dynamics', *J. Chem. Theory Comput.* **2017**, *13*, 3676–3683.

[30] S. Mai, M. Richter, P. Marquetand, L. González, 'Excitation of Nucleobases from a Computational Perspective II: Dynamics' in *Photoinduced Phenomena in Nucleic Acids I. Nucleobases in the Gas Phase and in Solvents*, (Eds.: M. Barbatti, A. C. Borin, S. Ullrich), *Topics in Current Chemistry, Vol. 355*, Springer, Heidelberg, Germany, **2014**, 99–153.

[31] A. Broo, 'A Theoretical Investigation of the Physical Reason for the Very Different Luminescence Properties of the Two Isomers Adenine and 2-Aminopurine', *J. Phys. Chem. A* **1998**, *102*, 526–531.

[32] V. Ludwig, Z. M. da Costa, M. S. do Amaral, A. C. Borin, S. Canuto, L. Serrano-Andrés, 'Photophysics and photostability of adenine in aqueous solution: A theoretical study', *Chem. Phys. Lett.* **2010**, *492*, 164–169.

6 Is the Electronic Deactivation Dynamics in the Adenine Tri- and Tetranucleotides Consistent with the Stepwise Excimer Formation in the Dinucleotide?

Abstract

Excitonic coupling and π-stacking directly influence the electronic deactivation processes of DNA building blocks and lead to the strikingly long electronic lifetimes of dinucleotides in contrast to the shorter lifetimes of longer DNA strands. For the adenine dinucleotide in aqueous solution, the initially excited excitonic states were observed to decay to an energetically relaxed state which has a lifetime of several hundred picoseconds. This decay is assigned to the stepwise evolution of the electronic character from excitons to excimer-like states as discussed in Chapter 5. In the present work, the longer trinucleotide dA_3 and the tetranucleotide dA_4 were investigated with static spectroscopy and femtosecond transient electronic absorption spectroscopy. The resulting time components $\tau_1 \approx 0.13$ ps and $\tau_2 \approx 0.47$ ps are assigned to "perturbed-monomer-like" deactivation. Components $\tau_3 \approx 6$ ps and $\tau_4 \approx 360$ ps are associated with excimer formation and decay. The observed electronic lifetimes of the oligonucleotides and their good overall agreement with the lifetimes of dA_2 suggest that the excited-state relaxation mechanism in all of these molecules is consistent with a stepwise excimer formation.

6.1 Introduction and Motivation

Excited electronic states of multi-chromophore systems are subject to excitonic coupling whose characteristics depend on the number of absorbing moieties and their spatial arrangement. In DNA, the adjacent nucleobases are stacked vertically due to π-orbital interaction which has an immense influence on the electronic structure and electronic deactivation processes of DNA building blocks.

In short model systems, particularly in homo- and heterodinucleotides containing

adenine (Ade), the mixed and initially excited excitonically coupled states were observed to decay to energetically relaxed states which show lifetimes of several hundred picoseconds.[1–7] For the dinucleotide dA_2 (or d(ApA)) in aqueous solution at room temperature, four electronic lifetime components spanning four orders of magnitude, 0.1 ps, 0.3 ps, 5−10 ps and 360 ps, were determined by transient electronic absorption and transient fluorescence spectroscopy (see also Chapter 5).[1,2,8,9] The spectral evolution and temporal sequence of the transient signals were interpreted as stepwise evolution of electronic character from excitons to excimer-like states.[1,2,5,8,10]

This Chapter focuses on the Ade homo-oligonucleotides shown in Fig. 6.1, namely the trinucleotide dA_3 and the tetranucleotide dA_4 are investigated in direct comparison with the dinucleotide dA_2 by means of static spectroscopy and transient electronic absorption spectroscopy. The central question is whether the electronic dynamics of the Ade tri- and tetranucleotide are consistent with the stepwise excimer-

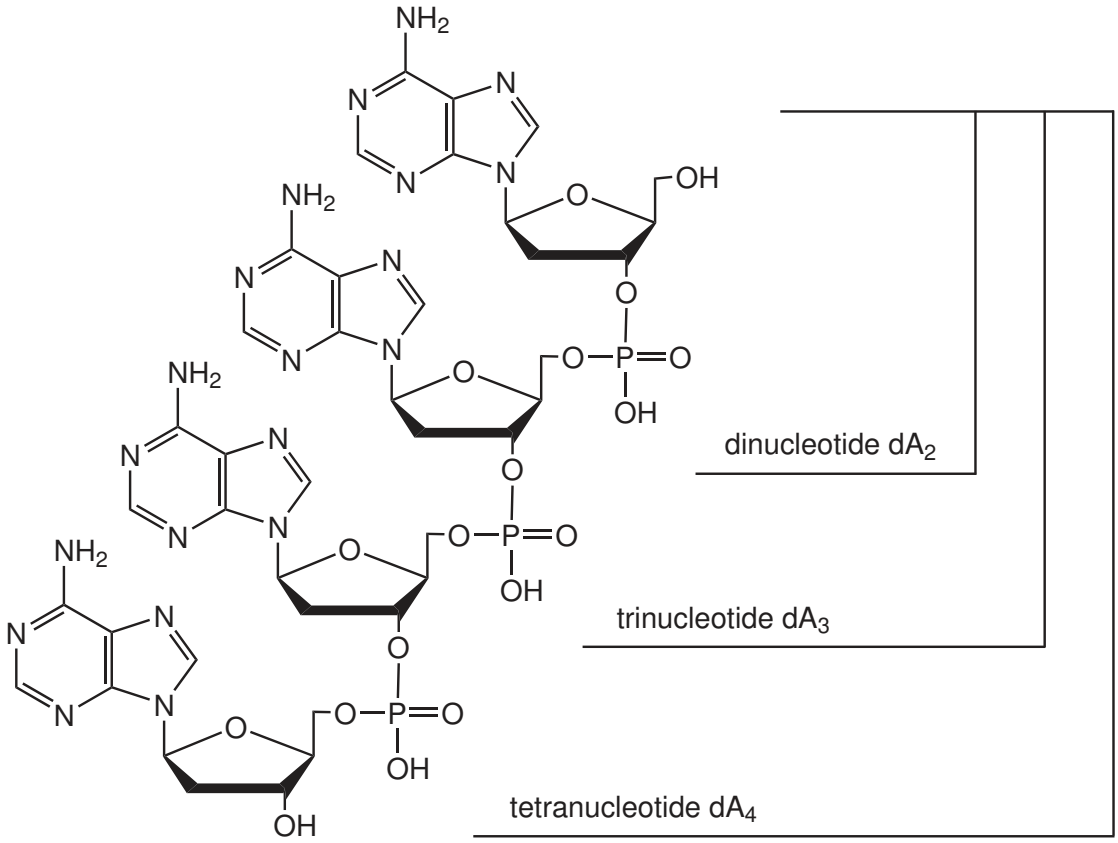

Figure 6.1: Molecular structure of the Ade tetranucleotide dA_4 and its subunits, the trinucleotide dA_3 and the dinucleotide dA_2. Under physiological conditions, the phosphate groups are deprotonated and their charge is compensated by Na^+ counterions.

formation mechanism, particularly the transition from an intermediate state to a stabilized excimer state as was proposed for the dinucleotide in Chapter 5. All three molecules build helically stacked structures which is known from circular dichroism spectroscopy in conjunction with density functional theory calculations.[11,12] The delocalization length of the excimer-like states observed in these stacked systems was determined to be only $\approx 2-3$ bases,[3,5,7,12] suggesting similar electronic structures. Also, excited-state lifetimes were found invariant to the number of bases in Ade oligonucleotides[5,7] and were assigned to common trapping states.[5] However, Ade polymers with 12 to 20 subunits show significantly shorter electronic lifetimes than the dinucleotide.[13–17] In the light of these results, special attention was payed to the influence of neighboring bases on the temporal and spectral characteristics of the long-lived electronic decay dynamics of the stacked Ade systems.

6.2 Experimental Details

The oligonucleotides dA_2, dA_3 and dA_4 were synthesized, purified by HPLC and checked by ESI mass spectrometry by metabion international AG. The samples were delivered as lyophilized products and used as received. Solutions with optical densities of OD ≈ 0.5 at 260 nm at an optical path length of 100 µm were prepared with ultra-pure water and set to pH 7.0 using phosphate buffer (16 mM NaH_2PO_4, 34 mM Na_2HPO_4, 117 mM NaCl). The concentrations of the samples were $c(dA_2) = 1.55$ mM, $c(dA_3) = 1.04$ mM and $c(dA_4) = 0.79$ mM.

Time-resolved measurements were performed using the femtosecond transient electronic absorption spectrometer for simultaneous broadband and single-color detection described before (Chapter 2 and Ref. 18). Excitation pulses were generated in a Ti:Sa-pumped home-built frequency-doubled NOPA at $\lambda_{pump} = 260$ nm with pulse durations of 35 fs (fwhm) and focused into the sample under magic angle polarization. The pulse energy was attenuated to 220 nJ for the measurements of the oligonucleotides. Only the sample of dA_2 at room temperature was measured with a pump pulse energy of 100 nJ. Broadband detection pulses were generated in CaF_2 by careful adjustment of the input Ti:Sa fundamental pulse energy to yield a spectrum between $\lambda_{probe} = 315-600$ nm. Single-color detection pulses were generated in a second frequency-doubled NOPA at $\lambda_{probe} = 255$ nm with pulse durations of 40 fs (fwhm).

The sample solutions were flowed through a home-built wire-guided gravity-driven liquid sample film described in Section 2.1.2 providing a film thickness of 100 µm. They were measured at $T = 295$ K and $T = 278$ K with help of a cryostatic

temperature regulator. The sample volume and flow speed ensured an exchange of probed molecules between two excitation pulses and an overall excitation of the sample below 1 %. The measurement time was adjusted to avoid evaporation of water to ensure constant concentrations during one measurement. All samples were measured back-to-back with measurements of the neat solvent. Each time, three successive runs were checked for consistency and averaged for final analysis. After every run, the static UV absorption spectrum was checked for sample integrity. The recorded transient electronic absorption maps and the single color curves were corrected for solvent contributions, noise and white light chirp as described in the literature[19,20] and earlier PhD Theses.[1,21,22] The spectra were cut off at the maximum of the solvent signal in the UV part of the probe spectrum due to the white light break-off.

The data were analyzed using a nonlinear least-squares routine based on the Levenberg–Marquardt algorithm for fitting of time profiles. For a global analysis, the method of singular value decomposition (SVD)[23–25] was applied that separated the temporal from the spectral information and allowed for independent analyses. All given errors for the fitting results correspond to 2σ standard deviations.

6.3 Results

6.3.1 Static Absorption and Static Fluorescence

The static UV absorption spectra and the fluorescence spectra after excitation at $\lambda_{exc} = 260$ nm of the three Ade oligonucleotides, dA_2, dA_3 and dA_4, in buffered aqueous solution (pH 7.0) at room temperature are depicted in Fig. 6.2. By increasing the number of bases, the absorption maximum of the Ade oligonucleotide shifts slightly to the blue, but its low-energy side extends more and more to the red. These are the characteristics of excitonic coupling[27–29] in helically stacked chromophores.[30] The gradual increase demonstrates that the coupling spans more than two bases and that an extended exciton stack is formed.

The fluorescence spectra show weak bands at $\lambda = 320$ nm, similar to the fluorescence of the monomer, and strong and red-shifted emission bands at $\lambda =$ 400 nm, 415 nm and 425 nm for the tetramer, the trimer and the dimer, respectively. The red-shift can be assigned to excimer formation[31] with an energetic stabilization of $\Delta E = 0.8 - 1.0$ eV. In this context, an excimer is an energetically favorable excited state that spans two or more stacked nucleobases. However, the fluorescence maximum is blue-shifted with the number of bases hinting at less stabilized states.

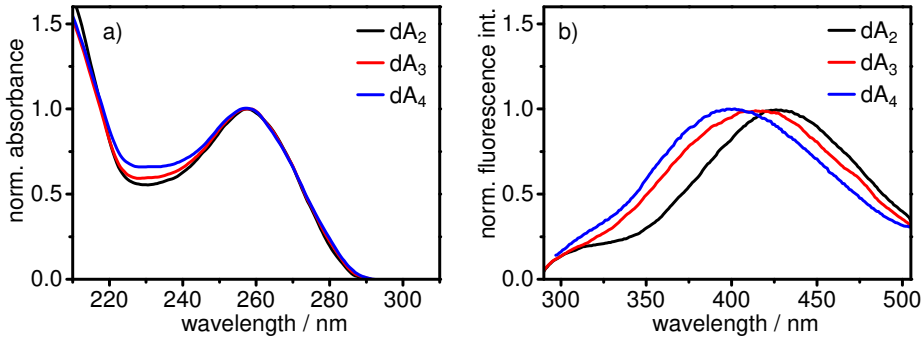

Figure 6.2: a) UV absorption and b) fluorescence spectra of the Ade oligonucleotides dA_2 (black), dA_3 (red) and dA_4 (blue) measured in buffered aqueous solution (pH 7.0) after excitation at $\lambda_{pump} = 260$ nm. The spectra were normalized for comparison. The fluorescence spectrum of dA_4 was taken by M. C. Stuhldreier.[26]

This trend was also seen for the fluorescence of dA_{20}.[8,32]

No temperature effect was found on the static spectra of dA_3 within experimental errors while the emission of dA_2 increased by 25 % between $T = 295$ K and $T = 278$ K (see Chapter 5). Unfortunately, no reliable data could be collected for dA_4.

6.3.2 Transient Electronic Absorption

Femtosecond time-resolved transient electronic absorption spectroscopy of dA_2, dA_3 and dA_4 after excitation at $\lambda_{pump} = 260$ nm at $T = 295$ K and $T = 278$ K yielded the two-dimensional maps shown in Fig. 6.3. The electronic absorption change (ΔOD) is plotted against probe wavelength and time delay in a bipolar color map. Delay times are shown on a linear scale up to $\Delta t = 1$ ps and on a logarithmic timescale up to $\Delta t = 1500$ ps.

The spectro-temporal signals of the Ade di-, tri- and tetranucleotide exhibit spectrally broad initial excited-state absorption (ESA) expanding over the entire probe wavelength range that shifts towards the UV edge of the probe spectrum within few hundred femtoseconds and decays on the same timescale. Between $\lambda_{probe} = 315 - 370$ nm, a narrow and long-lived ESA signal can be seen that decays within several hundred picoseconds. It is found at the same spectral position for all samples and temperatures. A weak ESA band with a similar lifetime is observed at $\lambda_{probe} = 450 - 600$ nm. The transient signal around $\lambda_{probe} = 315$ nm has a negative sign at short delay times and rises delayed. As already argued for dA_2 in Chapter 5, this is assigned to an overlay of stimulated emission (SE), yielding a negative signal

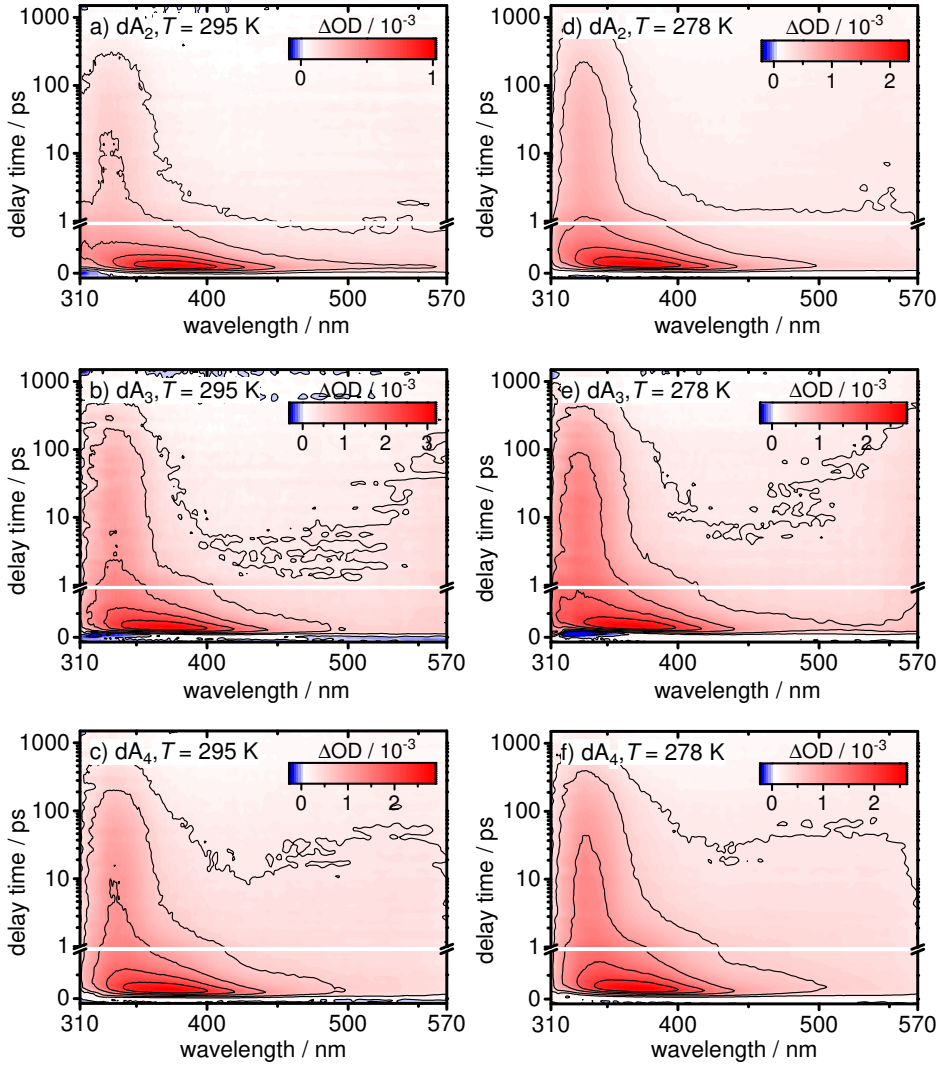

Figure 6.3: Two-dimensional transient absorption maps of dA_2 (a, d), dA_3 (b, e) and dA_4 (c, f) measured at $T = 295$ K (a – c) and $T = 278$ K (d – f) after excitation at $\lambda_{pump} = 260$ nm. Delay times are shown on a linear scale up to $\Delta t = 1$ ps and on a logarithmic timescale up to $\Delta t = 1500$ ps.

contribution, and hot ground state absorption (HGSA), giving a positive signal. The spectro-temporal signals are characteristic for excimer formation[1–4,8] and seem to be highly similar to each other.

At the first glance, the spectro-temporal maps measured at $T = 278$ K are in good agreement with the measurements at room temperature. A temperature effect for the signal is hardly distinguishable by eye due to the broad range of signal intensities. The temperature dependence of the electronic dynamics of the Ade

oligomers and the differences among each other were exposed in a two-step analysis.

6.3.2.1 Time-Profile Analysis

For better comparison of the electronic dynamics of the Ade oligomers, a set of two time profiles was analyzed for each sample. The first time profile was extracted from the spectro-temporal data by spectral integration over the probe wavelength range $\lambda_{\text{probe}} = 315 - 450$ nm. This range comprises most of the initial broad and blue-shifting ESA band, the full long-lived narrow ESA band and the SE/HGSA signals. Thus, it contains the full temporal information of the measured data. The second time profile was provided by the single-color probe measurement at $\lambda_{\text{probe}} = 255$ nm where the ground state population was monitored. The bleach of the signal directly after excitation is restored by the recovery of the ground state population (GSR) due to internal conversion from the first excited state. The GSR signals of the Ade di-, tri- and tetranucleotide did not fully decay to zero because of the too small measured time window of $\Delta t = 600$ ps. However, extrapolation of the data indicates full recovery of the ground state signal within $\Delta t = 2000$ ps.

The time profiles were modeled with Gaussian-convoluted multi-exponential decay functions with simultaneously fitted time constants. The data and the best fit curves are shown in Fig. 6.4 for $T = 295$ K and $T = 278$ K. It can be seen immediately that the amplitude of the long-lived signal increases with the number of bases and is even higher in the measurements at $T = 278$ K.

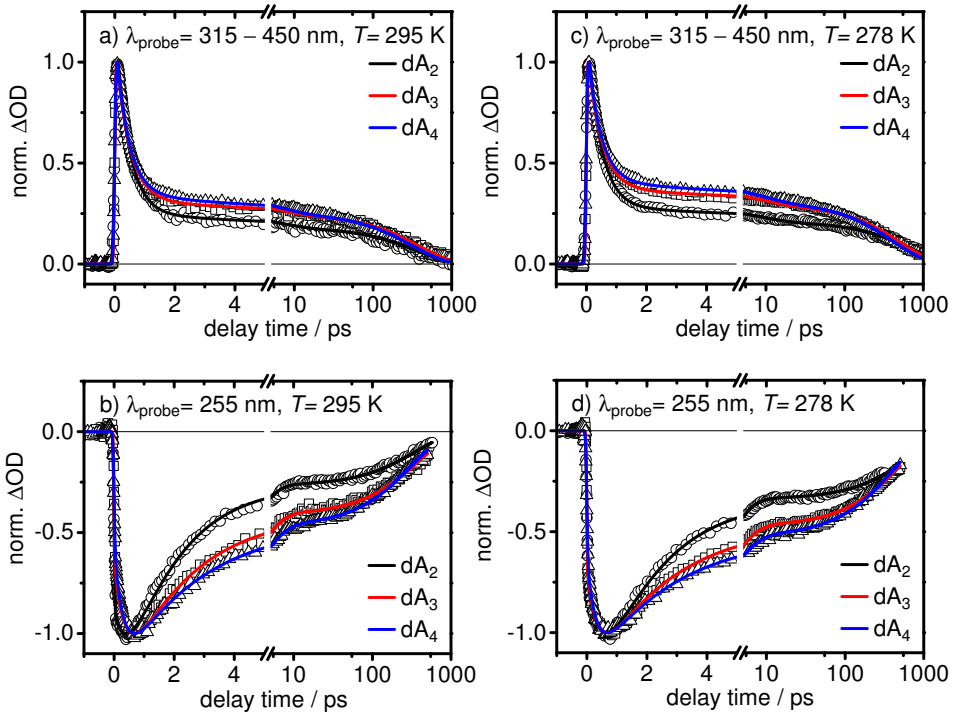

Figure 6.4: Transient absorption-time profiles of dA_2 (black), dA_3 (red) and dA_4 (blue) at $T = 295$ K (a, b) and at $T = 278$ K (c, d) after excitation at $\lambda_{pump} = 260$ nm. Time profiles in a and c were extracted by wavelength integration of the measured spectro-temporal data between $\lambda_{probe} = 315 - 450$ nm. Time profiles in b and d were recorded with a single-color probe beam at $\lambda_{probe} = 255$ nm. Open symbols represent measured data, solid lines multi-exponential fits. The data is shown on a linear timescale for the first 5 ps and on a logarithmic scale thereafter.

The resulting fit parameters are listed in Table 6.1. The time constants were numbered according to their magnitude for better comparison, with τ_1 and τ_2 reserved for sub-picosecond components. The third time constant, τ_3, was fixed at the value found for dA_2 in order to facilitate comparison. It is necessary for testing the proposed stepwise excimer formation mechanism. The values for the excited-state decay at $T = 295$ K are in reasonable agreement with each other. The lifetime-change with temperature seems to be less pronounced for dA_3 and dA_4 than for dA_2. An additional time component τ_{vc} was obtained from the GSR time profile and characterizes the overall timescale for vibrational cooling of hot ground state molecules which are generated upon internal conversion from the excited state. The vibrational cooling time increases with the number of bases which may relate to a reduced hydration of the single nucleobase due to shielding by the backbone

Table 6.1: Experimental results for the temperature-dependent electronic dynamics of the Ade oligomers dA_2, dA_3 and dA_4 from the time-profile analyses. The error limits of the amplitudes typically are < 10 % for a_2 and a_4, and < 20 % for a_3. The temporal resolution of $\sigma_{IRF} \approx 0.040$ ps was determined by deconvolution. τ_3 was fixed at the value found for dA_2.

species	T/K	a_2	τ_2/ps	a_3	τ_3/ps	a_4	τ_4/ps	τ_{vc}/ps
dA_2	295	0.79	0.44(6)	0.06	6	0.15	360(40)	1.7(3)
	278	0.76	0.44(6)	0.06	8	0.17	690(30)	2.0(1)
dA_3	295	0.71	0.45(5)	0.07	6	0.22	370(15)	2.2(1)
	278	0.66	0.45(5)	0.07	8	0.26	500(17)	2.5(1)
dA_4	295	0.70	0.42(3)	0.09	6	0.22	310(7)	2.6(1)
	278	0.64	0.42(3)	0.09	8	0.27	410(10)	2.7(1)

and the stacked bases.[7] This observation will not be further discussed because it does not contribute to the central question of this work. The vibrational cooling times are slightly increased at $T = 278$ K with respect to the measurements at room temperature. This can be attributed to a lower vibrational energy transfer rate to the solvent.

6.3.2.2 Global Analysis

Global analyses of the full spectro-temporal transient electronic absorption maps of the Ade di-, tri- and tetranucleotide measured at $T = 295$ K and $T = 278$ K were performed by singular value decomposition.

The SVD time traces are shown in Fig. 6.5. They could be described by Gaussian-convoluted multi-exponential functions. Small-amplitude oscillations were observed in traces 3 and 4 that were assumed to be a residue from the chirp correction and experimental noise and these were not modeled. For dA_4, only three time traces were included because the fourth did not contain any significant information.

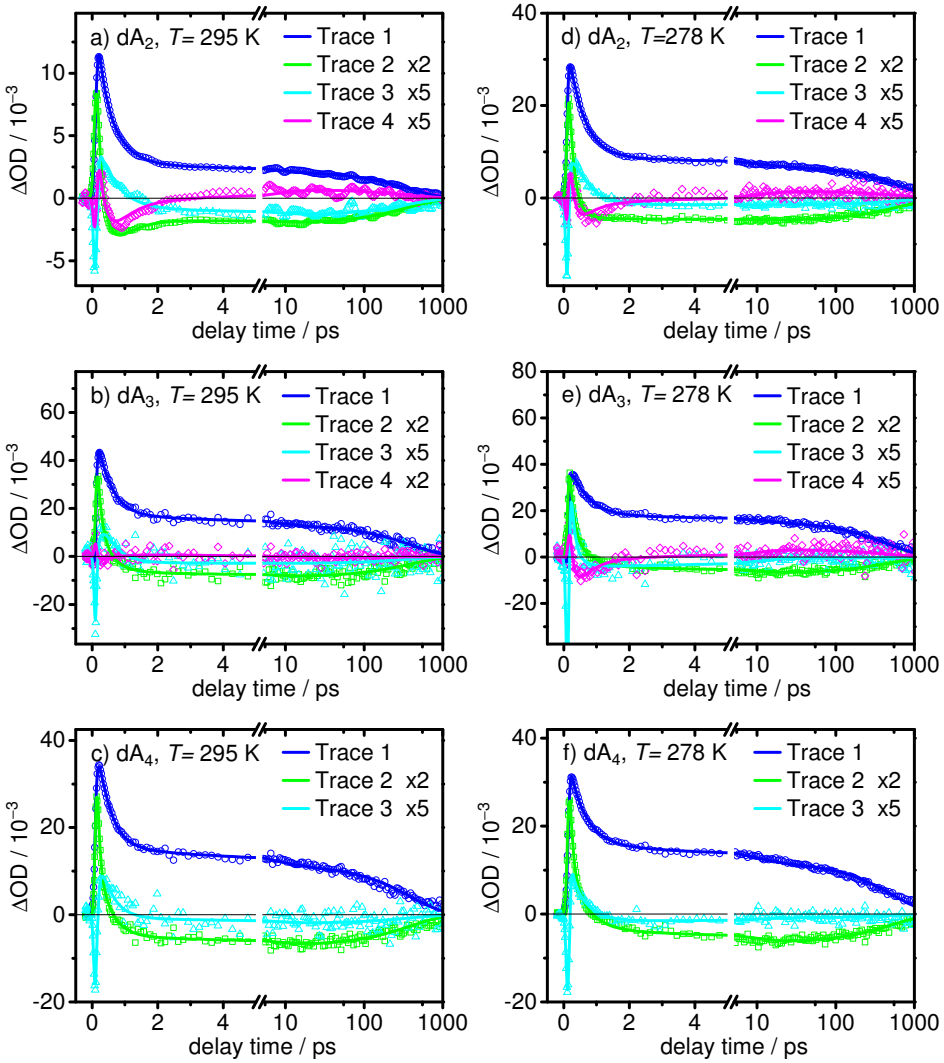

Figure 6.5: Time traces from the global SVD analysis of the spectro-temporal transient electronic absorption data of dA_2 (a, d), dA_3 (b, e) and dA_4 (c, f) at $T = 295$ K (a – c) and at $T = 295$ K (d – f) after excitation at $\lambda_{pump} = 260$ nm. Time traces 2 – 4 were scaled by the given factors for visibility. Note the linear timescale for the first 5 ps and the logarithmic timescale thereafter.

The results of the global analyses are listed in Table 6.2. Two sub-picosecond components were obtained. The third time constant, τ_3, was fixed at the value found in the time-profile analysis of dA_2. The time constants derived from this global analysis are in reasonable agreement with the above given time constants from the simultaneous analysis of the time profiles.

Table 6.2: Experimental results for the temperature-dependent electronic dynamics of the Ade oligomers dA_2, dA_3 and dA_4 from the global analyses. Values were rounded to significant digits. τ_3 was fixed at the value found for dA_2.

species	T/K	τ_1/ps	τ_2/ps	τ_3/ps	τ_4/ps
dA_2	295	0.23(2)	0.56(4)	6	360(14)
	278	0.15(2)	0.47(2)	8	680(25)
dA_3	295	0.13(6)	0.42(7)	6	390(35)
	278	0.12(3)	0.52(6)	8	470(25)
dA_4	295	0.07(2)	0.39(3)	6	390(20)
	278	0.09(2)	0.51(4)	8	530(20)

The decay-associated difference spectra (DADS) calculated from the SVD results to visualize the spectral contributions of the time components are shown in Fig. 6.6 for $T = 295$ K and $T = 278$ K. These demonstrate that time constant τ_2, as it was found in the time-profile analysis, is in fact a mixture of two sub-picosecond time components. They were separated in the SVD analysis and show DADS that are similar for all Ade oligonucleotide samples and all temperatures.

In each case, the DADS of the first time component shows a negative contribution at the UV edge of the probe wavelength range, where it is attributed to SE and the delayed rise of the signal. The spectrum shows a positive value with a maximum around $\lambda_{\text{probe}} = 380 - 410$ nm corresponding to the initial ESA decay. A negative amplitude at $\lambda_{\text{probe}} \geq 480$ nm is thought to be erroneous and to stem from an imperfect time-zero correction or overdone solvent subtraction.

The second time component has a maximum DADS amplitude at $\lambda_{\text{probe}} = 315$ nm for dA_2 at $T = 295$ K and at $\lambda_{\text{probe}} \approx 370$ nm for dA_2 at $T = 278$ K, for dA_3 and for dA_4. It decreases with the wavelength and seems to decay to a constant. The spectral differences between the measurements can be traced back to the different experimental conditions, i. e. the lower pump pulse energy for the measurement of dA_2 at $T = 295$ K. As was seen in Chapter 5, this does not affect the decay times. HGSA is expected at the UV edge of the probe spectrum, but at visible probe wavelengths the second time constant is assigned to ESA. The value of time constant τ_2 from the SVD analysis assumed to be a mixture of ESA and HSGA decay.

The third and fourth lifetime components yield shallow spectra with maxima at $\lambda_{\text{probe}} \approx 370$ nm and $\lambda_{\text{probe}} = 330 - 335$ nm, respectively, that are assigned to ESA.

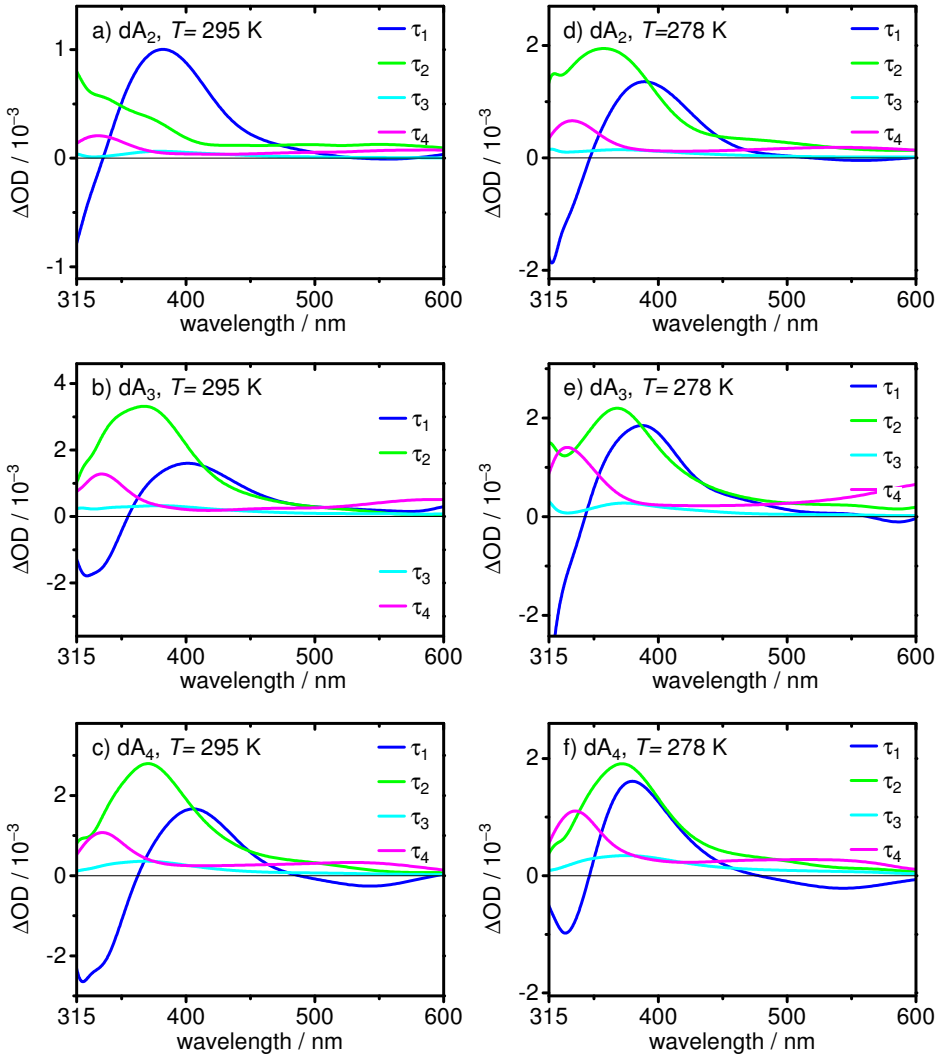

Figure 6.6: Decay-associated difference spectra from the global SVD analysis of the spectro-temporal transient electronic absorption data of dA_2 (a, d), dA_3 (b, e) and dA_4 (c, f) measured at $T = 295$ K (a – c) and at $T = 295$ K (d – f) after excitation at $\lambda_{pump} = 260$ nm. The spectra each represent the spectral contribution of the time components τ_1 (blue), τ_2 (green), τ_3 (cyan) and τ_4 (magenta) given in Table 6.2.

6.4 Discussion

The investigation of the transient electronic absorption of the Ade di-, tri- and tetranucleotides in direct comparison to each other and in dependence of temperature yielded five individual time constants spanning more than three orders of magnitude for the excited-state relaxation after excitation at $\lambda_{pump} = 260$ nm and the ensuing vibrational cooling in the ground state. The time constants from the time-profile

and the global analyses were averaged and the results are summarized in Table 6.3.

Table 6.3: Averaged results for the temperature-dependent electronic dynamics of the Ade oligomers dA_2, dA_3 and dA_4.

species	T/K	τ_1/ps	τ_2/ps	τ_3/ps	τ_4/ps	τ_{vc}/ps
dA_2	295	⟨0.18⟩	⟨0.50⟩	⟨6⟩	⟨360⟩	⟨1.7⟩
	278	⟨0.18⟩	⟨0.50⟩	⟨8⟩	⟨690⟩	⟨2.0⟩
dA_3	295	⟨0.13⟩	⟨0.46⟩	⟨6⟩	⟨380⟩	⟨2.2⟩
	278	⟨0.13⟩	⟨0.46⟩	⟨8⟩	⟨490⟩	⟨2.5⟩
dA_4	295	⟨0.08⟩	⟨0.44⟩	⟨6⟩	⟨350⟩	⟨2.6⟩
	278	⟨0.08⟩	⟨0.44⟩	⟨8⟩	⟨470⟩	⟨2.7⟩

The observed excited-state lifetimes of the oligonucleotides dA_3 and dA_4 closely resemble the excited-state lifetimes of dA_2 which suggests that the excited-state relaxation mechanism in all of these molecules is a stepwise excimer formation as it was discussed in Chapter 5 for the dinucleotide.

The sub-picosecond excited-state lifetime components, $\tau_1 \approx 0.13$ ps and $\tau_2 \approx 0.47$ ps (averaged results), are highly similar to the lifetimes of the Ade monomer discussed in all preceding Chapters. The underlying deactivation processes appear to be largely independent of the size of the molecules and the particular environment of the single nucleobase, and their assignment to monomer-like deactivation mechanisms is reasonable. However, in stacked systems these processes must also include relaxation within the exciton stack and transfer towards excimer-like structures. This overlay will be called "perturbed-monomer-like" deactivation.

For all investigated oligonucleotide samples, an intermediate excimer state is proposed that decays to a stabilized excimer within $\tau_3 \approx 6$ ps at $T = 295$ K. The stabilized structure is then converted to the ground state within $\tau_4 \approx 360$ ps at $T = 295$ K. An amplitude increase of the fourth component between the dimer and the tetramer is associated with a higher stacking yield in the oligomers and thus an increased excimer yield.[6,12] However, the energetics seem to be changed markedly by adding bases to the stack as follows. The blue-shifted fluorescence maxima of the trimer and the tetramer in comparison with the dimer may be explained by an energetically higher-lying excimer structure. Also, the temperature change of the long excited-state lifetime to $\tau_4 \approx 480$ ps in dA_3 and dA_4 (averaged result) is less pronounced than in dA_2, where $\tau_4 \approx 690$ ps was found at $T = 278$ K. Although quantification via Arrhenius analysis was not attempted due to the few data points

and their large errors, the effective potential energy barrier for electronic deactivation in the tri- and tetranucleotide must be significantly lower than in the dinucleotide. Evidently, interaction with the adjacent bases influences excimer formation and decay in Ade oligomers, most significantly so at low temperatures where the stacking fraction is increased.[33–37] One can speculate that the systems cannot relax into the stabilized structure because of the reduced ability for conformational change induced by the neighboring bases on both sides of the nucleobase stack.

A potential energy model curve of the proposed deactivation details is depicted in Fig. 6.7. The present experimental results indicate that the apparent excimer

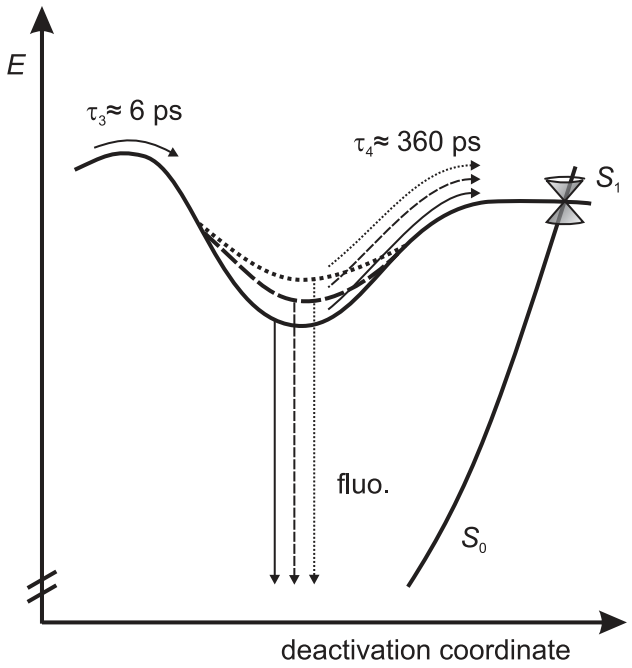

Figure 6.7: Cutout from the potential energy model curve for the proposed electronic deactivation of the investigated Ade oligonucleotides dA_2 (solid line), dA_3 (dashed line), dA_4 (dotted line). A stabilized excimer is formed within $\tau_3 \approx 6$ ps and is deactivated by internal conversion to the ground state via a conical intersection within $\tau_4 \approx 360$ ps at room temperature. The potential well of the stabilized excimer structure becomes shallower with the number of stacked nucleobases.

minimum grows increasingly shallow with the number of bases in the oligomer and that the potential energy barrier for deactivation is gradually lowered. This trend can be extrapolated to larger Ade polynucleotides where excimer lifetimes were reported as constant against temperature change.[6,17,38] Their fluorescence maxima were found much less red-shifted with respect to the monomer.[8,32] Both observations indicate the formation of less stabilized excited states in Ade polynucleotides.

At this point it must be noted that the analysis gave hints that the deactivation dynamics become more and more complex for the longer Ade oligonucleotides. The time profiles and time traces were increasingly unsatisfactorily described by multi-exponential model functions. Although the spectro-temporal transient electronic absorption maps of the di-, tri- and tetranucleotide are so similar to the eye, it is probable that they represent an overlay of diverse deactivation processes including two, three or four nucleobases that are probed in parallel.

6.5 Conclusion

The Ade oligonucleotides dA_2, dA_3 and dA_4 were investigated by static spectroscopy and by femtosecond time-resolved transient electronic absorption spectroscopy after excitation at $\lambda_{pump} = 260$ nm in buffered aqueous solution (pH 7.0). Direct comparison of the fluorescence spectra of the trimer and the tetramer with the dimer hints at the formation of less stabilized excimer states, i. e. located at higher energies compared to the ground state. The transient data yielded similar lifetimes for all three species indicating a common deactivation mechanism consistent with a stepwise excimer formation as proposed in Chapter 5. Two sub-picosecond components, $\tau_1 \approx 0.13$ ps and $\tau_2 \approx 0.47$ ps, were assigned to "perturbed-monomer-like" deactivation. Components $\tau_3 \approx 6$ ps and $\tau_4 \approx 360$ ps were associated with formation of a stabilized excimer from an intermediate state. Decreasing the temperature to $T = 278$ K, the fourth component was increased to $\tau_4 \approx 480$ ps for the trimer and the tetramer, revealing lower necessary thermal activation energy for the deactivation of dA_3 and dA_4 in comparison with dA_2. The results suggest that the increased π-stacking interaction in these systems destabilizes excimer formation and thus lowers the potential energy barrier for electronic deactivation.

References

[1] M. C. Stuhldreier, 'Electronic Deactivation Dynamics of DNA Model Systems and Solvation Dynamics of a Natural Antioxidant by Femtosecond Fluorescence and Absorption Spectroscopy', Dissertation, Christian-Albrechts-Universität zu Kiel, **2013**.

[2] M. C. Stuhldreier, K. Röttger, F. Temps, 'Distinctive Spectral Features of Exciton and Excimer States in the Ultrafast Electronic Deactivation of the Adenine Dinucleotide' in *Ultrafast Phenomena XIX*, Vol. 162, (Eds.: K. Yamanouchi, S. Cundiff, R. de Vivie-Riedle, M. Kuwata-Gonokami, L. DiMauro), **2015**, 452–454.

[3] I. Buchvarov, Q. Wang, M. Raytchev, A. Trifonov, T. Fiebig, 'Electronic energy delocalization and dissipation in single- and double-stranded DNA', *Proc. Natl. Acad. Sci. U. S. A.* **2007**, *104*, 4794–4797.

[4] M. C. Stuhldreier, F. Temps, 'Ultrafast photo-initiated molecular quantum dynamics in the DNA dinucleotide d(ApG) revealed by broadband transient absorption spectroscopy', *Faraday Discuss.* **2013**, *163*, 173–188.

[5] T. Takaya, C. Su, K. de La Harpe, C. E. Crespo-Hernández, B. Kohler, 'UV excitation of single DNA and RNA strands produces high yields of exciplex states between two stacked bases', *Proc. Natl. Acad. Sci. U. S. A.* **2008**, *105*, 10285–10290.

[6] C. Su, 'Femtosecond Transient Absorption Study of the Excited-State Dynamics of Single-Stranded Adenine-Containing Multinucleotides and Steady-State Absorption Spectroscopy of Mononucleotides in Cryogenic Water/Ethylene Glycol Matrices', Dissertation, Graduate School of The Ohio State University, **2010**.

[7] C. Su, C. T. Middleton, B. Kohler, 'Base-Stacking Disorder and Excited-State Dynamics in Single-Stranded Adenine Homo-Oligonucleotides', *J. Phys. Chem. B* **2012**, *116*, 10266–10274.

[8] M. C. Stuhldreier, C. Schüler, J. Kleber, F. Temps, 'Femtosecond Fluorescence Measurements of the Adenine Dinucleotide: Direct Observation of the Excimer State' in *Ultrafast Phenomena XVII*, (Eds.: M. Chergui, D. M. Jonas, E. Riedle, R. W. Schoenlein, A. J. Taylor), Oxford, **2011**, 553–555.

[9] U. C. Stange, 'Untersuchung der Temperaturabhängigkeit der ultraschnellen elektronischen Desaktivierung von Adenin und dem Adenindinukleotid', Masterarbeit, Christian-Albrechts-Universität zu Kiel, **2012**.

[10] J. Chen, B. Kohler, 'Base Stacking in Adenosine Dimers Revealed by Femtosecond Transient Absorption Spectroscopy', *J. Am. Chem. Soc.* **2014**, *136*, 6362–6372.

[11] C. S. M. Olsthoorn, L. J. Bostelaar, J. F. M. de Rooij, J. H. van Boom, C. Altona, 'Circular Dichroism Study of Stacking Properties of Oligodeoxyadenylates and Polydeoxyadenylate—A Three-State Conformational Model', *Eur. J. Biochem.* **1981**, *115*, 309–321.

[12] S. Tonzani, G. C. Schatz, 'Electronic Excitations and Spectra in Single-Stranded DNA', *J. Am. Chem. Soc.* **2008**, *130*, 7607–7612.

[13] W.-M. Kwok, C. Ma, D. L. Phillips, '"Bright" and "Dark" Excited States of an Alternating AT Oligomer Characterized by Femtosecond Broadband Spectroscopy', *J. Phys. Chem. B* **2009**, *113*, 11527–11534.

[14] C. E. Crespo-Hernández, B. Cohen, B. Kohler, 'Base Stacking Controls Excited-State Dynamics in A·T DNA', *Nature* **2005**, *436*, 1141–1144.

[15] N. K. Schwalb, F. Temps, 'Base Sequence and Higher-Order Structure Induce the Complex Excited-State Dynamics in DNA', *Science* **2008**, *322*, 243–245.

[16] W.-M. Kwok, C. Ma, D. L. Phillips, 'Femtosecond Time- and Wavelength-Resolved Fluorescence and Absorption Spectroscopic Study of the Excited States of Adenosine and an Adenine Oligomer', *J. Am. Chem. Soc.* **2006**, *128*, 11894–11905.

[17] C. E. Crespo-Hernández, B. Kohler, 'Influence of secondary structure on electronic energy relaxation in adenine homopolymers', *J. Phys. Chem. B* **2004**, *108*, 11182–11188.

[18] K. Röttger, R. Siewertsen, F. Temps, 'Ultrafast Electronic Deactivation Dynamics of the Rare Natural Nucleobase Hypoxanthine', *Chem. Phys. Lett.* **2012**, *536*, 140–146.

[19] M. Lorenc, M. Ziolek, R. Naskrecki, J. Karolczak, J. Kubicki, A. Maciejewski, 'Artifacts in femtosecond transient absorption spectroscopy', *Appl. Phys. B* **2002**, *74*, 19–27.

[20] B. Cohen, P. M. Hare, B. Kohler, 'Ultrafast Excited-State Dynamics of Adenine and Monomethylated Adenines in Solution: Implications for the Nonradiative Decay Mechanism', *J. Am. Chem. Soc.* **2003**, *125*, 13594–13601.

[21] K. Röttger, 'Ultrafast Deactivation Dynamics of Structurally Modified and Hydrogen-Bonded DNA and RNA Building Blocks', Dissertation, Christian-Albrechts-Universität zu Kiel, **2013**.

[22] R. Siewertsen, 'Ultrafast Photochromic Reactions of Structurally Modified Furylfulgides and a Bridged Azobenzene', Dissertation, Christian-Albrechts-Universität zu Kiel, **2011**.

[23] I. van Stokkum, D. S. Larsen, R. van Grondelle, 'Global and Target Analysis of Time-Resolved Spectra', *Biochim. Biophys. Acta* **2004**, *1657*, 82–104.

[24] N. Mouton, A. de Juan, M. Sliwa, C. Ruckebusch, 'Hybrid Hard- and Soft-Modeling Approach for the Resolution of Convoluted Femtosecond Spectrokinetic Data', *Chemom. Intell. Lab. Syst.* **2011**, *105*, 74–82.

[25] C. Ruckebusch, M. Sliwa, P. Pernot, A. de Juan, R. Tauler, 'Comprehensive data analysis of femtosecond transient absorption spectra: A review', *J. Photochem. Photobiol. C* **2012**, *13*, 1–27.

[26] M. C. Stuhldreier, Unpublished results.

[27] I. Tinoco jr., 'Hypochromism in Polynucleotides', *J. Am. Chem. Soc.* **1960**, *82*, 4785–4790.

[28] M. Kasha, H. R. Rawls, M. Ashraf El-Bayoumi, 'The Exciton Model in Molecular Spectroscopy', *Pure Appl. Chem.* **1965**, *11*, 371–392.

[29] M. Kasha, 'Molecular Excitons in Small Aggregates' in *Spectroscopy of the Excited State*, (Eds.: B. Di Bartolo, D. Pacheco, V. Goldberg), *Nato Advanced Study Institutes Series: Series B, Physics, Vol. 12*, Plenum Press, New York and London, **1976**, 337–380.

[30] L. M. Nielsen, S. Ø. Pedersen, M.-B. S. Kirketerp, S. Brøndsted Nielsen, 'Absorption by DNA single strands of adenine isolated in vacuo: The role of multiple chromophores', *J. Chem. Phys.* **2012**, *136*, 064302.

[31] J. Eisinger, M. Guéron, R. G. Shulman, T. Yamane, 'Excimer fluorescence of dinucleotides, polynucleotides, and DNA.', *Proc. Natl. Acad. Sci. U. S. A.* **1966**, *55*, 1015–1020.

[32] J. Kleber, 'Statische Absorptions- und Fluoreszenzspektroskopische Untersuchungen von kooperativen Effekten zwischen DNA-Chromophoren im Einzelstrang', Diplomarbeit, Christian-Albrechts-Universität zu Kiel, **2009**.

[33] H. Simpkins, E. G. Richards, 'Titration Properties of Some Dinucleotides', *Biochemistry* **1967**, *6*, 2513–2520.

[34] S. I. Chan, J. H. Nelson, 'Proton Magnetic Resonance Studies of Ribose Dinucleoside Monophosphates in Aqueous Solution. I. The Nature of the Base-Stacking Interaction in Adenylyl(3'–5')adenosine', *J. Am. Chem. Soc.* **1969**, *91*, 168–183.

[35] D. Frechet, R. Ehrlich, P. Remy, 'Thermal perturbation differential spectra of ribonudeic acids. II. Nearest neighbour interactions', *Nucleic Acids Res.* **1979**, *7*, 1981–2001.

[36] J. Norberg, L. Nilsson, 'Temperature Dependence of the Stacking Propensity of Adenylyl-3',5'-Adenosine', *J. Phys. Chem.* **1995**, *99*, 13056–13058.

[37] K. E. van Holde, J. Brahms, A. M. Michelson, 'Base Interactions of Nucleotide Polymers in Aqueous Solution', *J. Mol. Biol.* **1965**, *12*, 726–739.

[38] J. Chen, A. K. Thazhathveetil, F. D. Lewis, B. Kohler, 'Ultrafast Excited-State Dynamics in Hexaethyleneglycol-Linked DNA Homoduplexes Made of A·T Base Pairs', *J. Am. Chem. Soc.* **2013**, *135*, 10290–10293.

7 Nearly 10-fold Increase in Electronic Lifetime of the Stacked Guanine Dinucleotide in Comparison to dGMP

Abstract

Purine-purine dinucleotides show strong π-stacking interactions that stabilize their DNA-like conformation, but also affect their electronic properties. As a result, these molecules exhibit intense red-shifted fluorescence bands that are unknown for mononucleotides and for longer single- or double-stranded DNA. While the adenine dinucleotide is well-studied, the excited-state dynamics of guanine stacks remain unknown. We present the first experimental investigation of the guanine dinucleotide d(GpG) in comparison to its monomer dGMP by femtosecond time-resolved transient electronic absorption spectroscopy after excitation at $\lambda_{\mathrm{pump}} = 260$ nm in buffered aqueous solution (pH 7.0). Pronounced characteristics for excitonic coupling were observed in static spectra. The time-resolved measurements revealed triexponential decay dynamics that indicate complex coupled kinetics for the deactivation process. The longest excited-state lifetime component was determined to be $\tau_3 \approx 18$ ps, almost a factor of 10 longer than for dGMP. We assign the observed dynamics to a relaxation towards excimer-like states as were found for adenine dinucleotides. A temperature-effect on the excited-state dynamics of dGMP observed at $T = 278$ K hints at a potential energy barrier on the deactivation pathway as was discussed in light of theoretical work.

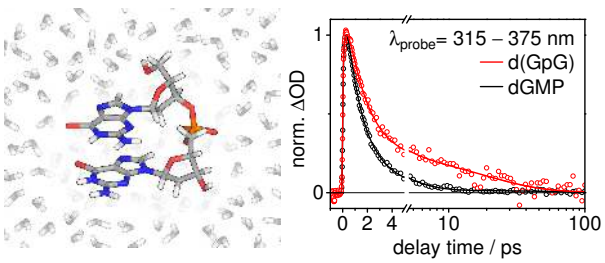

Table-of-contents graphic.

7.1 Introduction and Motivation

Dinucleotides offer the easiest insights into the stacking effects in DNA strands. Compared to large DNA molecules, they reduce the multiple intermolecular interactions to the vicinity of two nucleobases. Especially purine-purine dinucleotides show strong π-stacking interactions with stacking free energies between $2-8$ kJ/mol that stabilize their DNA like conformation.[1–5] Among these, adenine stacks are the most stable, while guanine stacks show only a slightly lower stacking stability.[6–11]

Stacked nucleobases are known to undergo excitonic coupling and the effect is seen as hypochromicity and exciton splitting of the absorption bands.[12–16] In dinucleotides, excited-state relaxation of excitons leads to the formation of energetically stabilized electronic states with quite long excited-state lifetimes[17–20] for which base stacking is thought to be the prerequisite.[21–23] These states are called excimers and are associated with the strong and red-shifted fluorescence observed for dinucleotides that are unknown for monomer DNA bases and for longer single or double stranded DNA.[24–28] Excimers are excited states with delocalized excitation energy between the loosely bound nucleobases.

In transient electronic absorption spectroscopy, Stuhldreier and Temps[29] identified a characteristic narrow excited-state absorption (ESA) band for the adenine dinucleotide and the adenine–guanine hetero-dinucleotide d(ApG). Both feature long excited-state lifetimes of 380 ps and 124 ps, respectively, that are unique for the stacked systems and were assigned to excimer formation occurring within $\Delta t = 5-10$ ps.[29] The authors concluded that the excimer is less stable in the d(ApG) sample due to the non-optimal orbital overlap.[29] Several more consistent studies are available on the electronic dynamics of the adenine dinucleotide[18,21,22,30–38] and few more for other stacked bases.[17,39] Studies on guanine-containing oligonucleotides and double strands also exhibit a prolongation of the excited-state lifetime in comparison to the monomer.[40–42] Interestingly, no preceding time-dependent measurements of the deactivation dynamics of the guanine dinucleotide can be found in literature and, thus, the excited-state dynamics of guanine–guanine stacks remain unknown.

In guanine, the two lowest $\pi\pi^*$ states (named L_a and L_b) are visibly separated in the absorption spectrum. Excitation in these bands will excite both states to varying extent. Time-resolved studies on the guanine nucleoside or nucleotide give three time constants between $0.2-2.5$ ps which are assigned to ultrafast internal conversion between the $\pi\pi^*$ states and decay to the electronic ground state.[19,29,43–50] The structural deformation that is predicted to facilitate conical intersections (CIs)

with the ground state is ring puckering centered at the C^2- or the C^6-position. In most cases it leads to out-of-plane bending of the respective amino or carbonyl group.[51–59]

This work presents the first experimental time-resolved study on the guanine dinucleotide d(GpG) in aqueous solution by transient electronic absorption spectroscopy. For comparison, the monomer dGMP was studied in parallel. Deeper insight into its electronic dynamics was gained by an additional measurement at lowered temperature.

7.2 Experimental Details

The guanine dinucleotide d(GpG) was synthesized, purified by HPLC and checked by ESI mass spectrometry by metabion international AG. The sample was delivered lyophilized and used as received. 2'-Deoxyguanosine 5'-monophosphate sodium salt hydrate (99 %) was purchased from Sigma-Aldrich and used as received. Solutions with a optical densities of OD $\approx$ 0.5 at 260 nm at an optical path length of 100 µm, corresponding to about 2 mM for d(GpG) and 4.1 mM for dGMP, were prepared with ultra-pure water and set to pH 7.0 using phosphate buffer. At these concentrations, significant aggregation at room temperature can be excluded.[60,61] The sample solutions were allowed to rest for 2 h after dissolution.

Time-resolved measurements were performed using the femtosecond transient electronic absorption spectrometer for simultaneous broadband and single-color detection described before (Chapter 2 and Ref. 62). The excitation pulses were generated in a frequency-doubled NOPA at 260 nm with pulse durations of 35 fs (fwhm) and focused onto the sample film under magic angle polarization to a diameter of 360 µm. The excitation energy was attenuated to 100 nJ per pulse. Broadband detection pulses were generated in CaF_2 by careful adjustment of the pump energy to extend the spectrum down to $\approx$ 310 nm. Single-color detection pulses were generated in a second frequency-doubled NOPA at 255 nm with pulse durations of 50 fs (fwhm).

The sample solutions were flowed through a home-built wire-guided gravity-driven liquid film device described in Section 2.1.2. For measurements at $T = 278$ K, the liquid-film housing was connected to a copper body that was cooled with a cryostat. Sample volumes of 20 mL and a high flow speed ensured an exchange of the probed molecules between two excitation pulses and an overall excitation of the sample below 1 %. The measurement time was adjusted to the rate of evaporation to ensure constant sample concentrations during one measurement.

All samples were measured back-to-back with measurements of the neat solvent.

For each sample, three successive runs were checked for consistency and averaged for final analysis. After every run the absorption and fluorescence spectra were checked for sample integrity. The recorded transient electronic absorption maps and the single color curves were corrected for solvent contributions, noise and white light chirp as described in the literature[63,64] and earlier PhD Theses.[34,65,66] The spectra were cut off at the maximum of the solvent signal in the ultraviolet (UV) part of the probe spectrum due to the white light break-off.

For analysis, the wavelength scale was cut into three regions and the time-dependent information over these regions was integrated. The resulting time profiles for each sample were then simultaneously modeled in a nonlinear least squares analysis based on the Levenberg–Marquardt algorithm with Gaussian-convoluted multi-exponential functions. A global analysis of the transient absorption maps was performed using the method of singular value decomposition (SVD).[67–69] All given errors are the 2σ standard deviation.

7.3 Results

7.3.1 Static Absorption and Static Fluorescence

The static UV absorption spectrum and the fluorescence spectrum after excitation at $\lambda_{exc} = 260$ nm of d(GpG) in buffered aqueous solution (pH 7.0) are shown in Fig. 7.1 in direct comparison to the spectra of dGMP.

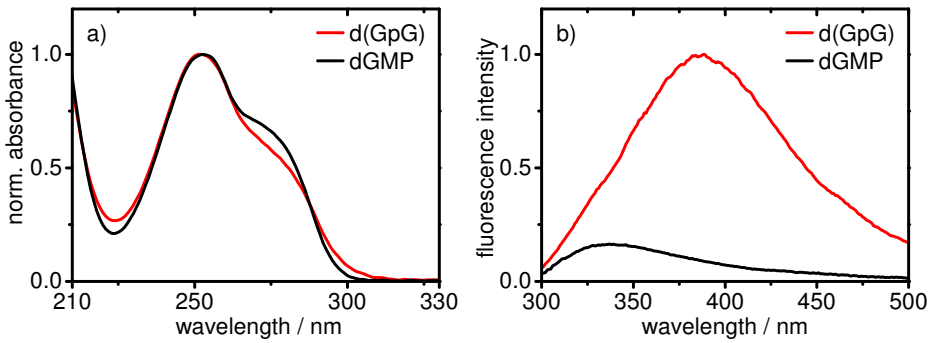

Figure 7.1: a) UV absorption and b) fluorescence spectra of the dinucleotide d(GpG) (red) in direct comparison to the monomer dGMP (black) measured after excitation at $\lambda_{exc} = 260$ nm in buffered aqueous solution (pH 7.0). The absorbances were normalized at the maxima for comparison. The fluorescence intensities were scaled to the same absorbances.

In the dinucleotide, due to excitonic interaction of the chromophores, the

absorption maximum at $\lambda = 252$ nm is blue-shifted by 1 nm in comparison to dGMP and the shoulder near 275 nm is less pronounced. Additionally, the red wing shows increased absorbance at $\lambda \geq 287$ nm. The extended red wing is characteristic for excitonic coupling in a helical structure.[15] In the UV spectrum of dGMP, the absorption maximum at $\lambda = 253$ nm and the shoulder at $\lambda = 273$ nm arise from the $\pi\pi^*$ L_b and L_a states of guanine, respectively.[54,70]

The fluorescence spectrum of the guanine dinucleotide shows an intense emission band at $\lambda = 390$ nm that is red-shifted in comparison to the monomer emission by $\Delta E = 0.26$ eV and that suggests strong base–base interactions in d(GpG). In fact, circular dichroism spectra of the guanine dinucleotide show characteristic features of a Z-DNA-like, significantly stacked structure.[4,71,72] Calculations predict an interbase distance of 3.3 Å[73] and a twist angle of about 30°[3,5] between the bases in the stacked dimer. The fluorescence spectrum is in agreement with the emission of a d(pGpG) sample measured earlier in this work group (not shown).[74] The fluorescence spectrum of dGMP shows a broad, but weak band with a maximum at $\lambda = 360$ nm.

Static Fluorescence of dGMP at $T = 278$ K

While the static absorption spectrum of dGMP was found to be independent of temperature within experimental uncertainty, the fluorescence intensity showed a small increase at a temperature of $T = 278$ K compared to room temperature (see Fig. 7.2).

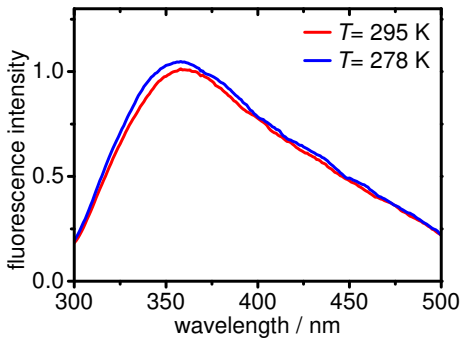

Figure 7.2: Fluorescence spectra of dGMP measured at $T = 295$ K (red) and $T = 278$ K (blue) after excitation at $\lambda_{exc} = 260$ nm in buffered aqueous solution (pH 7.0). The fluorescence intensities were normalized relative to the emission maximum at room temperature.

7.3.2 Transient Electronic Absorption of d(GpG) in comparison to dGMP

Femtosecond time-resolved transient electronic absorption spectra of d(GpG) and dGMP were recorded after excitation at $\lambda_{pump} = 260$ nm covering an overall time delay of $\Delta t = 1700$ ps. The two-dimensional spectro-temporal absorption maps are shown in Fig. 7.3 on a linear scale for up to $\Delta t = 1$ ps and on a logarithmic scale for delay times up to $\Delta t = 100$ ps together with selected transient spectra. The direct comparison shows a lower intensity and higher lifetime in the guanine

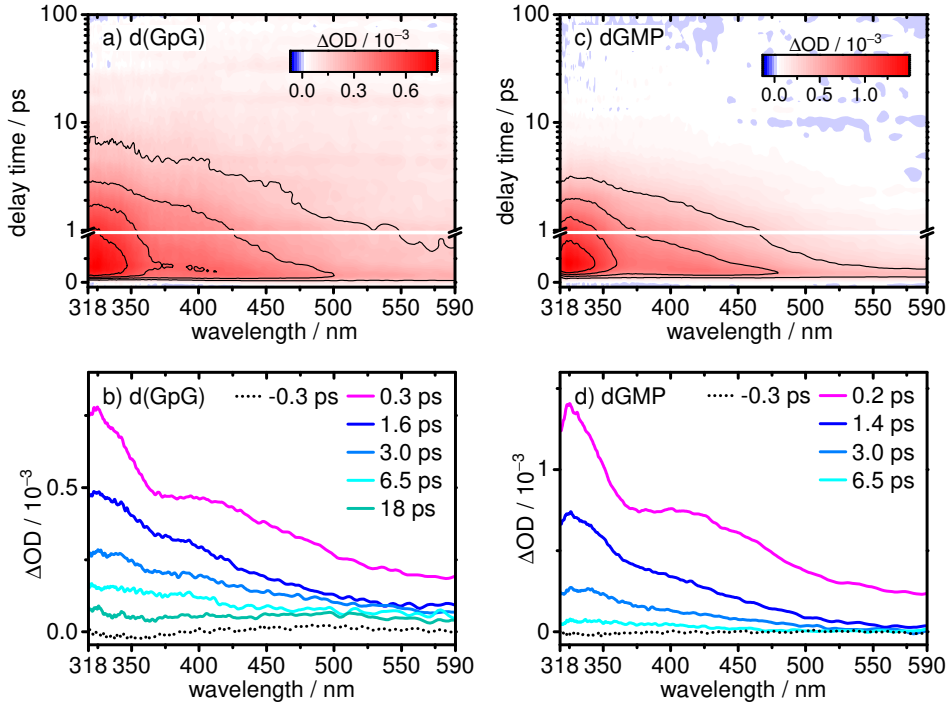

Figure 7.3: Two-dimensional transient absorption maps and selected transient spectra of d(GpG) (a, b) and dGMP (c, d) measured after excitation at $\lambda_{pump} = 260$ nm. Dashed lines indicate delay times during the rise of the signal.

dinucleotide compared to the mononucleotide. Both samples feature a broad excited-state absorption at short delay times with a narrow maximum at the UV edge of the probe-wavelength range and a second maximum around $\lambda_{probe} = 420$ nm that extends further into the visible presumably beyond $\lambda_{probe} = 600$ nm. The transient signal decays within $\Delta t = 7$ ps in the case of dGMP, but is distinguishable from the background noise for up to $\Delta t = 30$ ps in d(GpG). The transient data for dGMP is fully consistent with results from transient absorption studies in the literature.[47,49,75] Thus, also the transient data for d(GpG) is considered reliable.

7.3.2.1 Time-Profile Analysis

A set of decay time constants was determined to describe the temporal evolution of the transient electronic absorption signal of d(GpG) and dGMP measured at $T = 295$ K. For this purpose, three time profiles were extracted from the spectro-temporal data by spectral integration over the probe wavelength ranges $\lambda_{\text{probe}} = 605 - 500$ nm, $\lambda_{\text{probe}} = 500 - 375$ nm and $\lambda_{\text{probe}} = 375 - 315$ nm. A fourth time profile was obtained by the single-color probe measurement at $\lambda_{\text{probe}} = 255$ nm where the ground state population was monitored. The bleach of the signal directly after excitation is followed by the recovery of the ground state population (GSR) due to internal conversion from the first excited state.

The data sets were modeled with Gaussian-convoluted multi-exponential decay functions with simultaneously fitted time constants. Fig. 7.4 shows the data and the best fit curves for d(GpG) (a – d) and dGMP (e – h). The time profiles of d(GpG) are fully decayed within $\Delta t = 100$ ps, while they are back to zero after $\Delta t \approx 10$ ps in the dGMP case. The data sets were described by Gaussian-convoluted triexponential functions with simultaneously fitted time constants.

For d(GpG), the fit yielded

$$\tau_1 = 0.25 \pm 0.11 \text{ ps},$$
$$\tau_2 = 1.6 \pm 0.3 \text{ ps},$$
$$\tau_3 = 18 \pm 5 \text{ ps}$$

at a temporal resolution of $\sigma_{\text{IRF}} = 0.048 \pm 0.006$ ps (width parameter of the Gaussian describing the instrumental response function) determined by deconvolution. An additional time component,

$$\tau_{\text{vc}} = 2 \pm 1 \text{ ps},$$

necessary to describe the GSR time profile characterizes the overall timescale for vibrational cooling of hot ground state molecules, which are generated upon internal conversion from the excited state.

For dGMP, the simultaneous fit of the wavelength-integrated and the GSR signal yielded

$$\tau_1 = 0.20 \pm 0.02 \text{ ps},$$
$$\tau_2 = 0.9 \pm 0.2 \text{ ps},$$
$$\tau_3 = 2.3 \pm 0.4 \text{ ps},$$

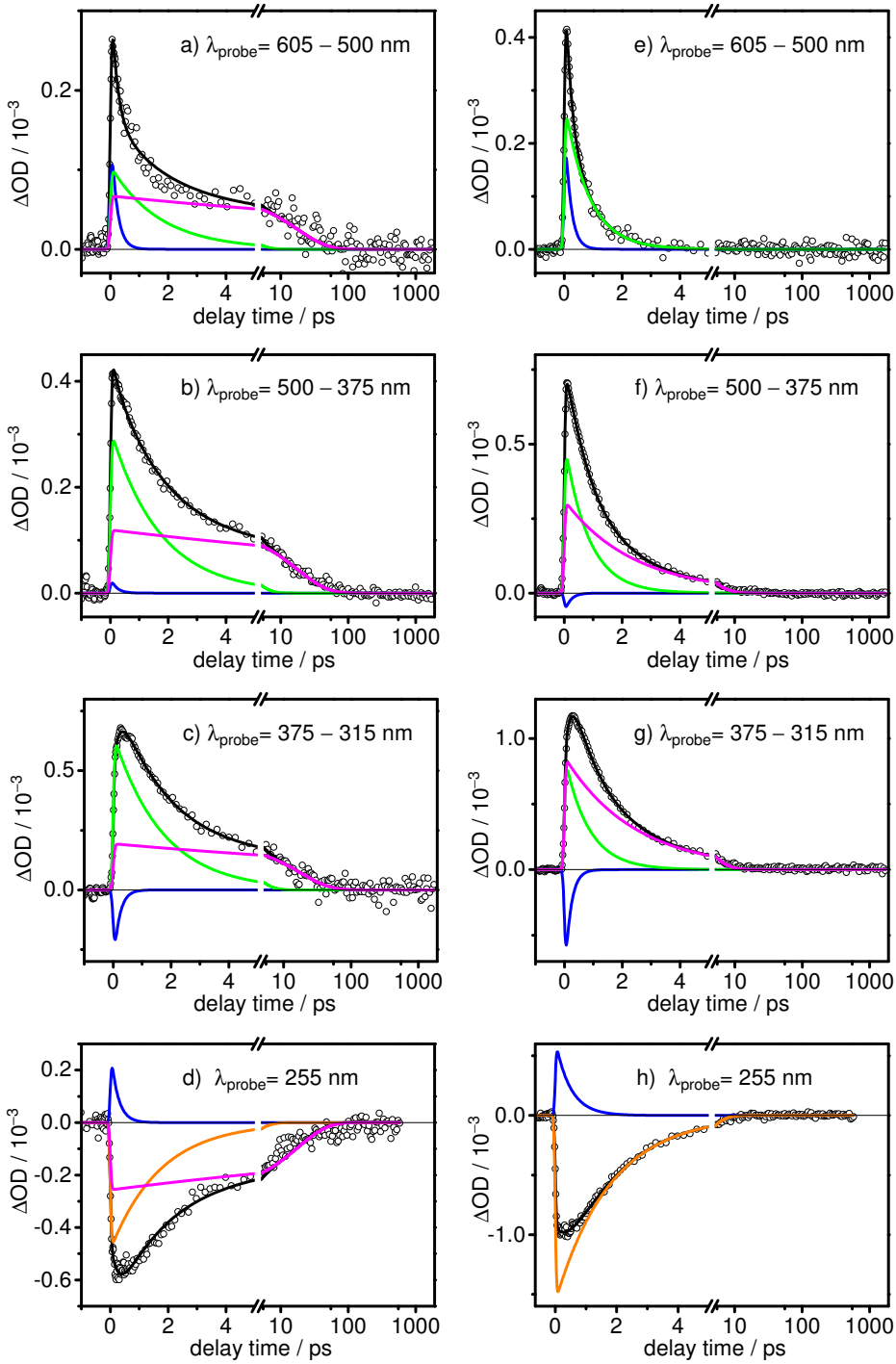

Figure 7.4: Transient absorption-time profiles of d(GpG) (a – d) and dGMP (e – h) at room temperature after excitation at $\lambda_{pump} = 260$ nm in the indicated spectral regions shown on a linear timescale for the first 5 ps and on a logarithmic scale thereafter. Open circles represent measured data, black lines multi-exponential fits, colored lines contributions of the global time constants τ_1 (blue), τ_2 (green), τ_3 (magenta) and τ_{vc} (orange).

$$\tau_{vc} = 1.8 \pm 0.1 \text{ ps}$$

at a temporal resolution of $\sigma_{IRF} = 0.046 \pm 0.003$ ps. The results from the two methods of analysis are in excellent agreement.

7.3.2.2 Global Analysis

Global analyses of the full spectro-temporal transient electronic absorption maps of d(GpG) and dGMP measured at $T = 295$ K were performed by singular value decomposition. The resulting time traces with the triexponential best fit curves and the corresponding decay-associated difference spectra (DADS) are shown in Fig. 7.5.

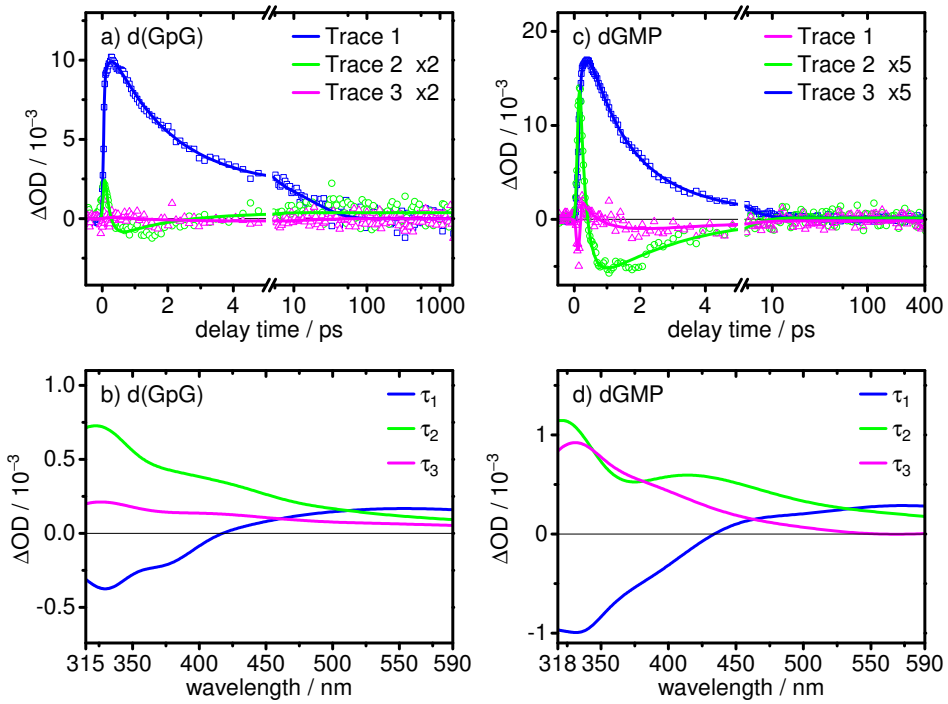

Figure 7.5: Results from the global SVD analysis of the spectro-temporal transient absorption data of d(GpG) (a, b) and dGMP (c, d) after excitation at $\lambda_{pump} = 260$ nm. Shown are the time traces (top) and decay-associated difference spectra (bottom). Traces 2 and 3 were scaled by the given factor for visibility.

The global time constants for d(GpG) were

$\tau_1 = 0.16 \pm 0.05$ ps,

$\tau_2 = 1.7 \pm 0.2$ ps,

$\tau_3 = 18 \pm 4$ ps.

at a temporal resolution of $\sigma_{\mathrm{IRF}} \approx 0.036$ ps.

For dGMP, the global time constants were

$$\tau_1 = 0.20 \pm 0.02 \text{ ps},$$
$$\tau_2 = 0.83 \pm 0.03 \text{ ps},$$
$$\tau_3 = 2.4 \pm 0.1 \text{ ps}.$$

at a temporal resolution of $\sigma_{\mathrm{IRF}} \approx 0.054$ ps.

The DADS for the guanine dinucleotide and its monomer are similar in shape. The first time component shows a negative amplitude at $\lambda_{\mathrm{probe}} \leq 430$ nm where it can be assigned to stimulated emission and/or to a delay of the rise of the signal. The positive signal in the visible region is assigned to ESA. The change in the sign of the amplitude of τ_1 is characteristic for a transient band shifting to the UV edge of the probe spectrum and can be assigned to fast initial relaxation in the Franck–Condon region. The second time component predominates in the UV probe range and has significant contribution at longer probe wavelengths, too. The third component shows a maximum at the UV edge of the probe spectrum and has a higher amplitude in dGMP than in d(GpG).

7.3.3 Transient Electronic Absorption of dGMP at $T = 278$ K

The time-resolved transient electronic absorption of a dGMP sample cooled down to $T = 278$ K in buffered aqueous solution (pH 7.0) was measured after excitation at $\lambda_{\mathrm{pump}} = 260$ nm. The two-dimensional map is shown in Fig. 7.6a. The transient data is similar to the measurement at room temperature, but the electronic lifetime of dGMP was found to be slightly increased at $T = 278$ K.

The data was analyzed as described above. Two exemplary time profiles are shown in Fig. 7.6b. The simultaneous fit of the wavelength-integrated and the GSR signal yielded

$$\tau_1 = 0.20 \pm 0.02 \text{ ps},$$
$$\tau_2 = 0.9 \pm 0.1 \text{ ps},$$
$$\tau_3 = 2.7 \pm 0.2 \text{ ps},$$
$$\tau_{\mathrm{vc}} = 2.3 \pm 0.1 \text{ ps}$$

at a temporal resolution of $\sigma_{\mathrm{IRF}} = 0.035 \pm 0.002$ ps.

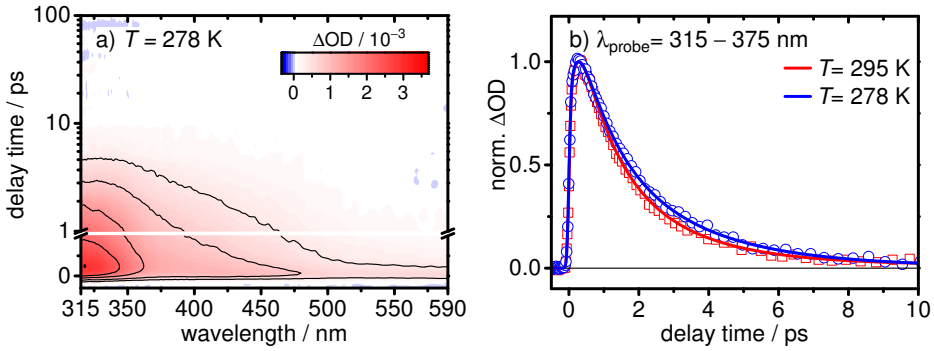

Figure 7.6: a) Two-dimensional transient absorption map of dGMP measured at $T = 278$ K after excitation at $\lambda_{\text{pump}} = 260$ nm in buffered aqueous solution shown on a linear scale for up to $\Delta t = 1$ ps and on a logarithmic scale for delay times up to $\Delta t = 100$ ps. b) Transient absorption time profiles of dGMP in the spectral range from $\lambda_{\text{probe}} = 315 - 375$ nm measured at $T = 295$ K (red) and $T = 278$ K (blue).

Fig. 7.7 shows the time traces and DADS resulting from the SVD analysis. The global time constants for dGMP at $T = 278$ K were

$$\tau_1 = 0.17 \pm 0.02 \text{ ps},$$

$$\tau_2 = 1.24 \pm 0.04 \text{ ps},$$

$$\tau_3 = 2.9 \pm 0.1 \text{ ps}.$$

at a temporal resolution of $\lambda_{\text{IRF}} = 0.064$ ps. The results from the two analysis

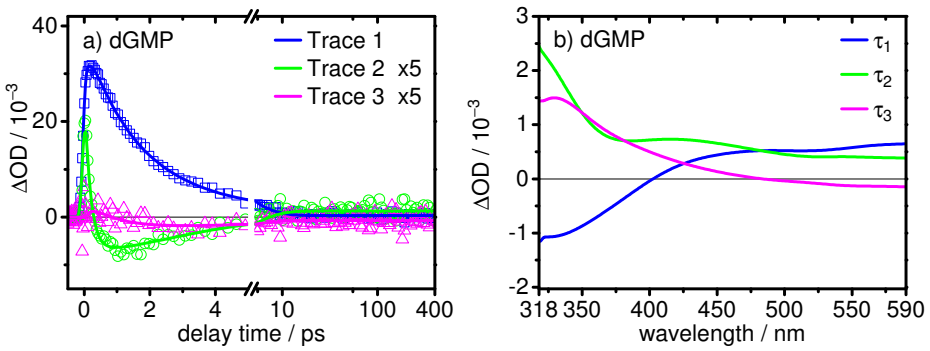

Figure 7.7: Results from the global SVD analysis of the spectro-temporal transient absorption data of dGMP measured at $T = 278$ K after excitation at $\lambda_{\text{pump}} = 260$ nm. Shown are the time traces (a) and decay-associated difference spectra (b). Traces 2 and 3 were scaled by the given factors for visibility.

methods are in good agreement. The DADS of dGMP at lowered temperature are very similar to the corresponding spectra at room temperature.

7.4 Discussion

7.4.1 Electronic Decay Dynamics of d(GpG)

The excited-state decay dynamics of d(GpG) in water exhibit three distinct time constants $\tau_1 \approx 0.21$ ps, $\tau_2 \approx 1.7$ ps and $\tau_3 \approx 18$ ps. The results from the two methods of analysis were in excellent agreement. Comparison to the excited-state lifetime of dGMP demonstrated a nearly 10-fold prolongation of the lifetime in the dinucleotide.

d(GpG) shows transient absorption spectra that are similar in shape, relative size and position to the transient spectra of the monomer. The high similarity to dGMP suggests that the same states take part in the deactivation. The interaction of the monomer states, however, induces the formation of excitons as demonstrated by the static absorption spectrum. From here, relaxation can lead to deeply stabilized excimers as was shown for d(ApA).[18,21,22,29,34,36,38]

Due to the overlap of two ESA bands, an initial shift of the transient bands could not be resolved in the present spectro-temporal data. However, the shape of the DADS of the first component hints at an overall blue-shift of the signal within the first picosecond. Thus, the short time component τ_1 reflects the initial relaxation in the molecule and can be assigned to the departure of the excited-state wavepacket from the FC region.

The intermediate time constant τ_2 was also found in a time-resolved fluorescence experiment on d(GpG)[76] making it clearly assignable to an excited-state process. Calculations of the guanine moiety embedded in a DNA environment predict H-bonds between adjacent nucleobases that may impede the necessary out-of-plane motions for the deactivation.[58] Thus, we propose assignment to a sterically hindered monomer-like deactivation process.

The prolongation of the excited-state lifetime seen in time component τ_3 and the red-shifted static fluorescence compared to the monomer hint at formation of an excimer between the guanine moieties after initial electronic relaxation. The electronic structure responsible for the τ_3-decay in d(GpG) may be similar to an excimer precursor state that is low in energy but not stable towards deactivation to the ground state, i. e. it only has a low barrier on the route towards the CI. Because of the broad transient spectra and their similarity to the data of dGMP, the transition

between the initially populated excitonic states and the relaxed and stabilized excimer appears to be smooth. The prolongation of the excited-state lifetime found here is unambiguous, but the effect of the stacking is much less pronounced than in the adenine dinucleotide where a stabilized excimer is formed and lives for several hundred picoseconds.[18,21,22,29,34,36,38] The fluorescence red-shift suggests a smaller stabilization energy of the excited-state potential energy hypersurface (PEHS) of d(GpG) compared to d(ApA) and, thus, less energy to be released in the overall relaxation process. This means, less time is lost for energy transfer processes and this may lead to overall shorter timescales than in d(ApA).

For a distinguished interpretation of the experimental data, quantum chemical calculations are necessary and contributions from fellow scientists will be warmly welcomed.

7.4.2 Electronic Decay Dynamics of dGMP

Three unique time constants, $\tau_1 \approx 0.2$ ps, $\tau_2 \approx 0.9$ ps and $\tau_3 \approx 2.4$ ps (averaged results), were found for the excited-state decay of dGMP in aqueous solution at $T = 295$ K. These are in excellent agreement with time-resolved fluorescence[43,45,48] and transient absorption experiments in aqueous solution,[29,47,49] and confirmed by gas phase experiments.[19,44,46,50] In agreement with these studies, the first component can be assigned to initial Franck–Condon relaxation and the other two to internal conversion to the ground state. The two observed transient absorption bands hint at a subsequent population of different energy levels on the excited-state PEHS of dGMP.

The third time component lies very close to the vibrational cooling time and was found in the UV probe range where the onset of hot ground state absorption (HGSA) can be expected[34,38,62,75] (cf. Chapter 3). However, it was found up to $\lambda_{\text{probe}} \approx 500$ nm with significant contribution. This abundance in the visible and its contribution to time-resolved fluorescence data[48,49] demonstrates a unique excited-state lifetime and makes it unlikely to result from hot ground state relaxation as was suggested before.[47] In a separate measurement, this time component was found to increase from $\tau_3 \approx 2.4$ ps at $T = 295$ K to $\tau_3 \approx 2.9$ ps at $T = 278$ K. The temperature dependence is mirrored in the static fluorescence intensity. A tentative Arrhenius analysis over the respective two data points yields an approximate activation energy of $E_{\text{A}} \approx 0.08$ eV for the excited-state decay of dGMP.

At $\lambda_{\text{pump}} = 260$ nm, guanine is excited to both the $\pi\pi^*$ L_a and L_b excited state. Fast internal conversion to the lower lying L_a state was described to take place

within 100 fs,[47,49,56] involving only slight changes of the molecular structure. The experimental value of $\tau_1 \approx 0.2$ ps, is consistent with this fast initial relaxation.

The $\pi\pi^*$ L_a excited PEHS was predicted to be barrierless[47,53–55,77,78] or to have a shallow minimum.[51,52,57] The spectrally broad transient signals observed in the experiments may be a sign of a widely spread wavepacket on this rather flat PEHS. Two structures for $\pi\pi^*$ L_a/S_0 CIs with the 6-membered ring puckered at the C^2-position, but with different degree of out-of-plane deformations of the amino group were predicted.[51–59,77–80] The barrier between the minimum and the CI region was calculated to be on the order of $\Delta E \approx 0.05$ eV.[51,52,57] The observed temperature dependence of τ_3 shows approximately the same amount of thermal activation necessary for the deactivation process and thus confirms the existence of the minimum on the $\pi\pi^*$ L_a excited PEHS. Already a shallow barrier is assumed to induce biexponential dynamics on an otherwise flat PEHS.[47] The deformation with (partial) out-of-plane motion of the amino group was found to dominate the calculated trajectories in the gas phase,[77] in water,[55,57] and in a DNA double strand.[58]

An $n_O\pi^*$ excited state is reached by excitation of a non-bonding orbital at the oxygen atom. Its CI with S_0 was predicted to form by ring puckering at the C^6-position and out-of-plane motion of the carbonyl bond.[52,54–57,77,80,81] The potential energy barrier for internal conversion was predicted to be 0.26 eV.[54] The out-of-plane motion of the carbonyl group was also predicted for the deactivation of the $\pi\pi^*$ L_a excited state.[56] Back-transfer to the $\pi\pi^*$ excited state was found possible and leads to a mixing of the states.[54]

In light of this information, $\tau_3 = 2.4 - 2.9$ ps in the range $T = 295 - 278$ K is assigned to the deactivation from a potential energy minimum on the $\pi\pi^*$ L_a state. Consequently, $\tau_2 \approx 0.9 - 1.1$ ps describes the preceding access to the minimum. In this picture, the mechanism for internal conversion is the C^2-puckering and the out-of-plane motion of the amino group. This interpretation is supported by the experimental observation of a kinetic isotope effect in D_2O[49] where the amino group is deuterated. Studies on NH_2-bridged guanine derivatives[82] and on guanine-containing base pairs[58] showed highly increased lifetimes due to constraining of the C^2-puckering. The deactivation of guanine slows down in MeOH and in glycerol[75] which also indicates that large-amplitude motions are required for the process. The non-canonical nucleobase hypoxanthine shows excellent agreement of lifetimes with guanine for the first two components, but lacks the third[83] which may be due to the missing amino group.

However, the two distinct time constants could also be assigned to two deactivation routes leading to differently puckered structures.[56,77] In this case, τ_2 would describe the out-of-plane motion of the carbonyl group and τ_3 the one of the amino group. The latter should be the slower process since the amino group is sterically more demanding.

The vibrational cooling time was found to increase from $\tau_{vc} = 1.8 \pm 0.1$ ps at $T = 295$ K to $\tau_{vc} = 2.3 \pm 0.1$ ps at $T = 278$ K. This is a solely dissipative process based on the detailed balance of up and down energy transfer. It is greatly influenced by solvent modes and the excess energy deposited in the molecule,[84] and the mechanism of energy transfer, i. e. formation of H-bonds,[85–88] excited-state proton transfer (ESPT)[87] and overall solvation dynamics.[89] Vibrational cooling should be studied separately.

7.5 Conclusion

The guanine dinucleotide d(GpG) was investigated in direct comparison to its monomer dGMP by femtosecond time-resolved transient electronic absorption spectroscopy after excitation at $\lambda_{pump} = 260$ nm in buffered aqueous solution (pH 7.0) at room temperature. Additional measurements were undertaken for dGMP at $T = 278$ K. To the best of our knowledge, the here measured transient electronic absorption of the guanine dinucleotide represents the first time-resolved study of this particular DNA building block. The observed triexponential decay dynamics showcase the complex coupled kinetics of the deactivation processes.

For d(GpG), the longest excited-state lifetime component was determined to $\tau_3 \approx 18$ ps, almost a factor of 10 longer than for dGMP. Direct comparison with dGMP shows high similarity of the transient spectra and suggests similar deactivation pathways to play a role. Nevertheless, the close vicinity of the chromophores induces excitonic coupling of the states and hindered out-of-plane motions. We assign the observed dynamics to a relaxation towards excimer states as they were found for other dinucleotides.

In the case of dGMP, the longest lifetime exhibits a weak temperature dependence indicating a deactivation pathway involving a small potential energy barrier of $E_A \approx 0.08$ eV. The longest time constant of dGMP $\tau_3 \approx 2.4$ ps is assigned to predicted internal conversion from a potential energy minimum on the $\pi\pi^*$ L_a PEHS that requires a ring puckering at the C^2-position and an out-of-plane motion of the sterically demanding amino group. The sub-picosecond lifetimes can be attributed to the FC relaxation and either the population of the mentioned minimum or a com-

peting deactivation channel characterized by an out-of-plane motion of the carbonyl group.

References

[1] S. Jafilan, L. Klein, C. Hyun, J. Florián, 'Intramolecular Base Stacking of Dinucleoside Monophosphate Anions in Aqueous Solution', *J. Chem. Phys. B* **2012**, *116*, 3613–3618.

[2] R. Brown, C. Andrews, A. Elock, 'Stacking Free Energies of All DNA and RNA Nucleoside Pairs and Dinucleoside-Monophosphates Computed Using Recently Revised AMBER Parameters and Compared with Experiment', *J. Chem. Theory Comput.* **2015**, *11*, 2315–2328.

[3] J. Florián, J. Šponer, A. Warshel, 'Thermodynamic Parameters for Stacking and Hydrogen Bonding of Nucleic Acid Bases in Aqueous Solution: Ab Initio/Langevin Dipoles Study', *J. Phys. Chem. B* **1999**, *103*, 884–892.

[4] C. R. Cantor, M. M. Warshaw, H. Shapiro, 'Oligonucleotide Interactions. III. Circular Dichroism Studies of the Conformation of Deoxyoligonucleotides', *Biopolymers* **1970**, *9*, 1059–1077.

[5] K. Murata, Y. Sugita, Y. Okamoto, 'Molecular dynamics simulations of DNA dimers based on replica-exchange umbrella sampling. II. Free Energy analysis', *J. Theor. Comput. Chem.* **2005**, *4*, 433–448.

[6] K. Murata, Y. Sugita, Y. Okamoto, 'Free energy calculations for DNA base stacking by replica-exchange umbrella sampling', *Chem. Phys. Lett.* **2004**, *385*, 1–7.

[7] K. Murata, Y. Sugita, Y. Okamoto, 'Molecular dynamics simulations of DNA dimers based on replica-exchange umbrella sampling. I. Test of sampling efficiency', *J. Theor. Comput. Chem.* **2005**, *4*, 411–432.

[8] J. Norberg, L. Nilsson, 'Stacking Free Energy Profiles for All 16 Natural Ribodinucleoside Monophosphates in Aqueous Solution', *J. Am. Chem. Soc.* **1995**, *117*, 10832–10840.

[9] J. Š. Jurečka, I. Marchan, F. J. Luque, M. Orosco, P. Hobza, 'Nature of Base Stacking: Reference Quantum-Chemical Stacking Energies in Ten Unique B-DNA Base-Pair Steps', *Chem. Eur. J.* **2006**, *12*, 2854–2865.

[10] J. Šponer, J. Leszczynski, V. Vetter, P. Hobza, 'Base Stacking and Hydrogen Bonding in Protonated Cytosine Dimer: The Role of Molecular Ion-Dipole and Induction Interactions', *J. Biomol. Struct. Dyn.* **1996**, *13*, 695–705.

[11] P. Cysewski, Ż. Czyżnikowska, R. Zaleśny, P. Czeleń, 'The post-SCF quantum chemistry characteristics of the guanine–guanine stacking in B-DNA', *Phys. Chem. Chem. Phys.* **2008**, *10*, 2665–2672.

[12] I. Tinoco jr., 'Hypochromism in Polynucleotides', *J. Am. Chem. Soc.* **1960**, *82*, 4785–4790.

[13] M. Kasha, H. R. Rawls, M. Ashraf El-Bayoumi, 'The Exciton Model in Molecular Spectroscopy', *Pure Appl. Chem.* **1965**, *11*, 371–392.

[14] M. Kasha, 'Molecular Excitons in Small Aggregates' in *Spectroscopy of the Excited State*, (Eds.: B. Di Bartolo, D. Pacheco, V. Goldberg), *Nato Advanced Study Institutes Series: Series B, Physics, Vol. 12*, Plenum Press, New York and London, **1976**, 337–380.

[15] L. M. Nielsen, S. Ø. Pedersen, M.-B. S. Kirketerp, S. Brøndsted Nielsen, 'Absorption by DNA single strands of adenine isolated in vacuo: The role of multiple chromophores', *J. Chem. Phys.* **2012**, *136*, 064302.

[16] L. Hu, Y. Zhao, F. Wang, G. Chen, C. Ma, W. Kwok, D. L. Phillips, 'Are Adenine Strands Helical H-Aggregates?', *J. Phys. Chem. B* **2007**, *111*, 11812–11816.

[17] C. T. Middleton, K. de La Harpe, C. Su, Y. K. Law, C. E. Crespo-Hernández, B. Kohler, 'DNA Excited-State Dynamics: From Single Bases to the Double Helix', *Annu. Rev. Phys. Chem.* **2009**, *60*, 217–239.

[18] T. Takaya, C. Su, K. de La Harpe, C. E. Crespo-Hernández, B. Kohler, 'UV excitation of single DNA and RNA strands produces high yields of exciplex states between two stacked bases', *Proc. Natl. Acad. Sci. U. S. A.* **2008**, *105*, 10285–10290.

[19] F. Buchner, B. Heggen, H. Ritze, W. Thiel, A. Lübcke, 'Excited-state dynamics of guanosine in aqueous solution revealed by time-resolved photoelectron spectroscopy: experiment and theory', *Phys. Chem. Chem. Phys.* **2015**, *17*, 31978–31987.

[20] G. Olaso-González, M. Merchán, L. Serrano-Andrés, 'The Role of Adenine Excimers in the Photophysics of Oligonucleotides', *J. Am. Chem. Soc.* **2009**, *131*, 4368–4377.

[21] C. Su, 'Femtosecond Transient Absorption Study of the Excited-State Dynamics of Single-Stranded Adenine-Containing Multinucleotides and Steady-State Absorption Spectroscopy of Mononucleotides in Cryogenic Water/Ethylene Glycol Matrices', Dissertation, Graduate School of The Ohio State University, **2010**.

[22] C. Su, C. T. Middleton, B. Kohler, 'Base-Stacking Disorder and Excited-State Dynamics in Single-Stranded Adenine Homo-Oligonucleotides', *J. Phys. Chem. B* **2012**, *116*, 10266–10274.

[23] F. Plasser, H. Lischka, 'Electronic excitation and structural relaxation of the adenine dinucleotide in gas phase and solution', *Photochem. Photobiol.* **2013**, *12*, 1440–1452.

[24] J. Eisinger, M. Guéron, R. G. Shulman, T. Yamane, 'Excimer fluorescence of dinucleotides, polynucleotides, and DNA.', *Proc. Natl. Acad. Sci. U. S. A.* **1966**, *55*, 1015–1020.

[25] P. Vigny, J. P. Ballini, 'Excited states of nucleic acids at 300 K and electronic energy transfer' in *Excited States in Organic Chemistry and Biochemistry*, (Eds.: B. Pullman, N. Goldblum), Reidel, Dordrecht, Holland, **1977**, 1–13.

[26] M. Daniels, J. P. Morgan, 'Polarization spectroscopy of homo-dinucleoside phosphate and homo-polynucleotides: evidence for excimer phosphorescence', *J. Luminescence* **1979**, *18/19*, 593–597.

[27] J. P. Morgan, M. Daniels, 'Excited states of DNA and its components at room temperature. III. Spectra polarization, and quantum yields of emissions from ApA and poly rA.', *Photochem. Photobiol.* **1979**, *31*, 101–113.

[28] P. R. Callis, 'Electronic States and Luminescence of Nucleic Acid Systems', *Annu. Rev. Phys. Chem.* **1983**, *34*, 329–352.

[29] M. C. Stuhldreier, F. Temps, 'Ultrafast photo-initiated molecular quantum dynamics in the DNA dinucleotide d(ApG) revealed by broadband transient absorption spectroscopy', *Faraday Discuss.* **2013**, *163*, 173–188.

[30] Á. Bányász, T. Gustavsson, D. Onidas, P. Changenet-Barret, D. Markovitsi, R. Improta, 'Multi-pathway excited state relaxation of adenine oligomers in aqueous solution: A joint theoretical and experimental study', *Chem. Eur. J.* **2013**, *19*, 3762–3774.

[31] J. Chen, B. Kohler, 'Base Stacking in Adenosine Dimers Revealed by Femtosecond Transient Absorption Spectroscopy', *J. Am. Chem. Soc.* **2014**, *136*, 6362–6372.

[32] C. E. Crespo-Hernández, B. Cohen, P. M. Hare, B. Kohler, 'Ultrafast Excited-State Dynamics in Nucleic Acids', *Chem. Rev.* **2004**, *104*, 1977–2019.

[33] V. R. Smith, E. Samoylova, H.-H. Ritze, W. Radloff, T. Schultz, 'Excimer states in microhydrated adenine clusters', *Phys. Chem. Chem. Phys.* **2010**, *12*, 9632–9636.

[34] M. C. Stuhldreier, 'Electronic Deactivation Dynamics of DNA Model Systems and Solvation Dynamics of a Natural Antioxidant by Femtosecond Fluorescence and Absorption Spectroscopy', Dissertation, Christian-Albrechts-Universität zu Kiel, **2013**.

[35] M. C. Stuhldreier, C. Schüler, J. Kleber, F. Temps, 'Femtosecond Fluorescence Measurements of the Adenine Dinucleotide: Direct Observation of the Excimer State' in *Ultrafast Phenomena XVII*, (Eds.: M. Chergui, D. M. Jonas, E. Riedle, R. W. Schoenlein, A. J. Taylor), Oxford, **2011**, 553–555.

[36] M. C. Stuhldreier, K. Röttger, F. Temps, 'Distinctive Spectral Features of Exciton and Excimer States in the Ultrafast Electronic Deactivation of the Adenine Dinucleotide' in *Ultrafast Phenomena XIX*, Vol. 162, (Eds.: K. Yamanouchi, S. Cundiff, R. de Vivie-Riedle, M. Kuwata-Gonokami, L. DiMauro), **2015**, 452–454.

[37] S. O. Konorov, H. G. Schulze, C. J. Addison, C. A. Haynes, R. F. Turner, M. W. Blades, 'Temperature-Dependent Excited State Absorption in DNA and LNA Oligomers Supports an Emerging Model of Excited State Dynamics in DNA', *Open Spectrosc. J.* **2009**, *3*, 43–51.

[38] I. Buchvarov, Q. Wang, M. Raytchev, A. Trifonov, T. Fiebig, 'Electronic energy delocalization and dissipation in single- and double-stranded DNA', *Proc. Natl. Acad. Sci. U. S. A.* **2007**, *104*, 4794–4797.

[39] G. W. Doorley, M. Wojdyla, G. W. Watson, M. Towrie, A. W. Parker, J. M. Kelly, S. Quinn, 'Tracking DNA Excited States by Picosecond-Time-Resolved Infrared Spectroscopy: Signature Band for a Charge-Transfer Excited State in Stacked Adenine–Thymine Systems', *J. Phys. Chem. Lett.* **2013**, *4*, 2739–2744.

[40] K. de La Harpe, C. E. Crespo-Hernández, B. Kohler, 'Deuterium Isotope Effect on Excited-State Dynamics in an Alternating GC Oligonucleotide', *J. Am. Chem. Soc.* **2009**, *131*, 17557–17559.

[41] M. K. Kuimova, J. Dyer, M. W. George, D. C. Grills, J. M. Kelly, P. Matousek, A. W. Parker, X. Z. Sun, M. Towrie, A. M. Whelan, 'Monitoring the effect of ultrafast deactivation of the electronic excited states of DNA bases and polynucleotides following 267 nm laser excitation using picosecond time-resolved infrared spectroscopy', *Chem. Comm.* **2005**, 1182–1184.

[42] G. W. Doorley, D. A. McGovern, M. W. George, M. Towrie, A. W. Parker, J. M. Kelly, S. J. Quinn, 'Picosecond Transient Infrared Study of the Ultrafast Deactivation Processes of Electronically Excited B-DNA and Z-DNA Forms of [poly(dG–dC)]$_2$', *Angew. Chem.* **2009**, *121*, 129–133.

[43] J. Peon, A. H. Zewail, 'DNA/RNA nucleotides and nucleosides: Direct measurement of excited-state lifetimes by femtosecond fluorescence up-conversion', *Chem. Phys. Lett.* **2001**, *348*, 255–262.

[44] H. Kang, K. T. Lee, B. Jung, Y. J. Ko, S. K. Kim, 'Intrinsic Lifetimes of the Excited State of DNA and RNA Bases', *J. Am. Chem. Soc.* **2002**, *124*, 12958–12959.

[45] D. Onidas, D. Markovitsi, S. Marguet, A. Sharonov, T. Gustavsson, 'Fluorescence Properties of DNA Nucleosides and Nucleotides: A Refined Steady-State and Femtosecond Investigation', *J. Phys. Chem. B* **2002**, *106*, 11367–11374.

[46] A. Chatterley, C. West, V. Stavros, J. Verlet, 'Time-resolved photoelectron imaging of the isolated deprotonated nucleotides', *Chem. Sci.* **2014**, *5*, 3963–3975.

[47] V. Karunakaran, K. Kleinermanns, R. Improta, S. A. Kovalenko, 'Photoinduced Dynamics of Guanosine Monophosphate in Water from Broad-Band Transient Absorption Spectroscopy and Quantum-Chemical Calculations', *J. Am. Chem. Soc.* **2009**, *131*, 5839–5850.

[48] F.-A. Miannay, T. Gustavsson, A. Bányász, D. Markovitsi, 'Excited-State Dynamics of dGMP Measured by Steady-State and Femtosecond Fluorescence Spectroscopy', *J. Phys. Chem. A* **2010**, *114*, 3256–3263.

[49] C. Cheng, C. Ma, C. Chan, K. Ho, W. Kwok, 'The solvent effect and identification of a weakly emissive state in nonradiative dynamics of guanine nucleosides and nucleotides—a combined femtosecond broadband time-resolved fluorescence and transient absorption study', *Photochem. Photobiol. Sci.* **2013**, *12*, 1351–1365.

[50] S. D. Camillis, J. Miles, G. Alexander, O. Ghafur, I. Williams, D. Townsend, J. Greenwood, 'Ultrafast non-radiative decay of gas-phase nucleosides', *Phys. Chem. Chem. Phys.* **2015**, *17*, 23643–23650.

[51] H. Chen, S. Lia, 'Ab initio study on deactivation pathways of excited 9H-guanine', *J. Chem. Phys.* **2006**, *124*, 154315.

[52] C. M. Marian, 'The Guanine Tautomer Puzzle: Quantum Chemical Investigation of Ground and Excited States', *J. Phys. Chem. A* **2007**, *111*, 1545–1553.

[53] S. Yamazaki, W. Domcke, A. L. Sobolewski, 'Nonradiative Decay Mechanisms of the Biologically Relevant Tautomer of Guanine', *J. Phys. Chem. A* **2008**, *112*, 11965–11968.

[54] L. Serrano-Andrés, M. Merchán, A. C. Borin, 'A Three-State Model for the Photophysics of Guanine', *J. Am. Chem. Soc.* **2008**, *130*, 2473–2484.

[55] M. Barbatti, J. J. Szymczak, A. J. A. Aquino, D. Nachtigallová, H. Lischka, 'The decay mechanism of photoexcited guanine—A nonadiabatic dynamics study', *J. Chem. Phys.* **2011**, *134*, 014304.

[56] B. Heggen, Z. Lan, W. Thiel, 'Nonadiabatic decay dynamics of 9H-guanine in aqueous solution', *Phys. Chem. Chem. Phys.* **2012**, *14*, 8137–8146.

[57] S. F. Altavilla, J. Segarra-Martí, A. Nenov, I. Conti, I. Rivalta, M. Garavelli, 'Deciphering the photochemical mechanisms describing the UV-induced processes occurring in solvated guanine monophosphate', *Front. Chem.* **2015**, *3*, 29.

[58] T. Zelený, M. Ruckenbauer, A. J. Aquino, T. Müller, F. Lankaš, T. Dršata, W. L. Hase, D. Nachtigallova, H. Lischka, 'Strikingly Different Effects of Hydrogen Bonding on the Photodynamics of Individual Nucleobases in DNA: Comparison of Guanine and Cytosine', *J. Am. Chem. Soc.* **2012**, *134*, 13662–13669.

[59] M. K. Shukla, J. Leszczynski, 'Effect of Hydration on the Lowest Singlet $\pi\pi^*$ Excited-State Geometry of Guanine: A Theoretical Study', *J. Phys. Chem. B* **2005**, *109*, 17333–17339.

[60] J. T. Davis, 'G-quartets 40 years later: From 5'-GMP to molecular biology and supramolecular chemistry.', *Angew. Chem. Int. Ed.* **2004**, *43*, 668–698.

[61] D. M. Gray, F. J. Bollum, 'A Circular Dichroism Study of Poly dG, Poly dC, and Poly dG:dC', *Biopolymers* **1974**, *13*, 2087–2102.

[62] K. Röttger, R. Siewertsen, F. Temps, 'Ultrafast Electronic Deactivation Dynamics of the Rare Natural Nucleobase Hypoxanthine', *Chem. Phys. Lett.* **2012**, *536*, 140–146.

[63] M. Lorenc, M. Ziolek, R. Naskrecki, J. Karolczak, J. Kubicki, A. Maciejewski, 'Artifacts in femtosecond transient absorption spectroscopy', *Appl. Phys. B* **2002**, *74*, 19–27.

[64] B. Cohen, P. M. Hare, B. Kohler, 'Ultrafast Excited-State Dynamics of Adenine and Monomethylated Adenines in Solution: Implications for the Nonradiative Decay Mechanism', *J. Am. Chem. Soc.* **2003**, *125*, 13594–13601.

[65] K. Röttger, 'Ultrafast Deactivation Dynamics of Structurally Modified and Hydrogen-Bonded DNA and RNA Building Blocks', Dissertation, Christian-Albrechts-Universität zu Kiel, **2013**.

[66] R. Siewertsen, 'Ultrafast Photochromic Reactions of Structurally Modified Furylfulgides and a Bridged Azobenzene', Dissertation, Christian-Albrechts-Universität zu Kiel, **2011**.

[67] I. van Stokkum, D. S. Larsen, R. van Grondelle, 'Global and Target Analysis of Time-Resolved Spectra', *Biochim. Biophys. Acta* **2004**, *1657*, 82–104.

[68] N. Mouton, A. de Juan, M. Sliwa, C. Ruckebusch, 'Hybrid Hard- and Soft-Modeling Approach for the Resolution of Convoluted Femtosecond Spectrokinetic Data', *Chemom. Intell. Lab. Syst.* **2011**, *105*, 74–82.

[69] C. Ruckebusch, M. Sliwa, P. Pernot, A. de Juan, R. Tauler, 'Comprehensive data analysis of femtosecond transient absorption spectra: A review', *J. Photochem. Photobiol. C* **2012**, *13*, 1–27.

[70] P. R. Callis, E. J. Rosa, W. T. Simpson, 'Search For Accidental Degeneracy in Purines', *J. Am. Chem. Soc.* **1964**, *86*, 2292–2294.

[71] M. M. Warshaw, C. R. Cantor, 'Oligonucleotide Interactions. IV. Conformational Differences between Deoxy- and Ribodinucleoside Phosphates', *Biopolymers* **1970**, *9*, 1079–1103.

[72] A. I. S. Holm, L. M. Nielsen, S. V. Hoffmann, S. B. Nielsen, 'Vacuum-ultraviolet circular dichroism spectroscopy of DNA: a valuable tool to elucidate topology and electronic coupling in DNA', *Phys. Chem. Chem. Phys.* **2010**, *12*, 9581–9596.

[73] R. Di Felice, A. Calzolari, E. Molinari, 'Ab initio study of model guanine assemblies: The role of $\pi - \pi$ coupling and band transport', *Phys. Rev. B* **2001**, *65*, 045404.

[74] J. Kleber, 'Statische Absorptions- und Fluoreszenzspektroskopische Untersuchungen von kooperativen Effekten zwischen DNA-Chromophoren im Einzelstrang', Diplomarbeit, Christian-Albrechts-Universität zu Kiel, **2009**.

[75] J. Lee, J. R. Challa, D. W. McCamant, 'Ultraviolet Light Makes dGMP Floppy: Femtosecond Stimulated Raman Spectroscopy of 2'-Deoxyguanosine 5'-Monophosphate', *J. Phys. Chem. B* **2017**, *121*, 4722–4732.

[76] U. C. Stange, Unpublished results.

[77] Z. Lan, E. Fabiano, W. Thiel, 'Photoinduced Nonadiabatic Dynamics of 9H-Guanine.', *ChemPhysChem* **2009**, *10*, 1225–1229.

[78] M. Barbatti, A. J. A. Aquino, J. J. Szymczak, D. Nachtigallová, P. Hobza, H. Lischka, 'Relaxation mechanisms of UV-photoexcited DNA and RNA nucleobases', *Proc. Natl. Acad. Sci. U. S. A.* **2010**, *107*, 21453–21458.

[79] I. Pugliesi, K. Müller-Dethlefs, 'Excited-State Ab Initio Calculations and Multidimensional Franck-Condon Simulations on Guanine', *J. Phys. Chem. A* **2006**, *110*, 13045–13057.

[80] S. Mai, M. Richter, P. Marquetand, L. González, 'Excitation of Nucleobases from a Computational Perspective II: Dynamics' in *Photoinduced Phenomena in Nucleic Acids I. Nucleobases in the Gas Phase and in Solvents*, (Eds.: M. Barbatti, A. C. Borin, S. Ullrich), *Topics in Current Chemistry, Vol. 355*, Springer, Heidelberg, Germany, **2014**, 99–153.

[81] R. Improta, F. Santoro, L. Blancafort, 'Quantum Mechanical Studies on the Photophysics and the Photochemistry of Nucleic Acids and Nucleobases', *Chem. Rev.* **2016**, *116*, 3540–3593.

[82] M. Zgierski, S. Patchkovskii, T. Fujiwara, E. C. Lim, 'The Role of Out-of-Plane Deformations in Subpicosecond Internal Conversion of Photoexcited Purine Bases: Absence of the Ultrafast Decay Channel in Propanodeoxyguanosine', *Chem. Phys. Lett.* **2007**, *440*, 145–149.

[83] K. Röttger, R. Stellmacher, M. Stuhldreier, F. Temps, 'Ultrafast Electronic Deactivation Dynamics of Xanthosine Monophosphate', *Molecules* **2017**, *22*, 160.

[84] T. Lenzer, K. Luther, J. Troe, R. Gilbert, K. Lim, 'Trajectory simulations of collisional energy transfer in highly excited benzene and hexafluorobenzene', *J. Chem. Phys.* **1995**, *103*, 626–641.

[85] X.-X. Zhang, M. Liang, N. P. Ernsting, M. Maroncelli, 'Complete Solvation Response of Coumarin 153 in Ionic Liquids', *J. Phys. Chem. B* **2013**, *117*, 4291–4304.

[86] J. Chen, B. Kohler, 'Ultrafast nonradiative decay by hypoxanthine and several methylxanthines in aqueous and acetonitrile solution', *Phys. Chem. Chem. Phys.* **2012**, *14*, 10677–10682.

[87] W. Liu, L. Tang, B. Oscar, Y. Wang., C. Chen, C. Fang, 'Tracking Ultrafast Vibrational Cooling during Excited-State Proton Transfer Reaction with Anti-Stokes and Stokes Femtosecond Stimulated Raman Spectroscopy', *J. Phys. Chem. Lett.* **2017**, *8*, 997–1003.

[88] P. Carbonniere, C. Pouchan, R. Improta, 'Intramolecular vibrational redistribution in the non-radiative excited state decay of uracil in the gas phase: an ab initio molecular dynamics study', *Phys. Chem. Chem. Phys.* **2015**, *17*, 11615–11626.

[89] R. Jimenez, G. Fleming, P. Kumar, M. Maroncelli, 'Femtosecond solvation dynamics of water', *Nature* **1994**, *369*, 471–473.

8 Summary and Outlook

The electronic deactivation dynamics of selected DNA mono-, di- and oligonucleotides of adenine and guanine were studied by aqueous-phase femtosecond time-resolved electronic absorption spectroscopy (TEAS) and fluorescence spectroscopy (TFLS) in order to assign deactivation pathways and to characterize deactivation mechanisms. Processes of barrierless relaxation were discerned from decay impeded by barriers. Temperature-dependent measurements as well as deuteration experiments proved extremely insightful to sort through the multiple deactivation pathways predicted by quantum chemical calculations. The results will be summarized across chapters with regard to the investigated molecules.

8.1 Electronic Deactivation Dynamics of Single Purine Nucleobases

8.1.1 9H-Adenine

The electronic deactivation of the canonical nucleobase 9H-adenine (9H-Ade) was characterized by two excited-state decay components with $\tau_{1,\mathrm{abs}} = 0.17 \pm 0.01$ ps and $\tau_{2,\mathrm{abs}} = 0.50 \pm 0.05$ ps (averaged results from TEAS) and a fluorescence lifetime of $\tau_{\mathrm{fluo}} = 0.21 \pm 0.01$ ps in mutual consistency. The two time scales were assigned to the initial relaxation in the Franck–Condon (FC) region and to ultrafast internal conversion to the ground state, respectively. The dynamics were found to be invariant to substitution with a sugar or a sugar-phosphate moiety from the DNA backbone demonstrating that the excited-state deactivation is governed only by the chromophore and excluding significant energy transfer towards the backbone. The excited-state lifetimes were independent from temperature within $T = 278 - 431$ K which shows that no thermal activation is necessary in the excited state and that no substantial potential energy barrier is encountered on the deactivation route. The electronic decay was also virtually identical in H_2O and D_2O. Therefore, no significant nuclear motion of the deuterated amino groups is expected in the molecular deactivation mechanism.

It was concluded that in the 9H-Ade chromophore the main relaxation pathway is located on a barrierless pathway on the $\pi\pi^*$ L_a excited-state potential energy hypersurface (PEHS). Internal conversion via a conical intersection (CI) with the

ground state PEHS is facilitated by a puckering centered at the C^2 position and an out-of-plane motion of the C^2–H bond. A minor contribution from electronic deactivation by C^6-puckering and out-of-plane motion of the NH_2 group cannot be excluded since both mechanisms were predicted in various quantum chemical studies. However, we suggest that the latter is less probable and that the observation of two time constants for the electronic deactivation of 9H-Ade rather indicates the participation of two areas of one excited-state PEHS with differing gradients.

8.1.2 7H-Adenine

The time-resolved fluorescence of the non-canonical nucleobase 7H-adenine (7H-Ade) was measured in the temperature range $T = 295 - 431$ K. The lifetime decreased from $\tau_{\text{fluo}} = 8.4 \pm 0.1$ ps to $\tau_{\text{fluo}} = 2.4 \pm 0.1$ ps and revealed a thermal activation process in the excited state. An Arrhenius analysis yielded an activation energy of $E_{\text{A}} = 0.105 \pm 0.005$ eV ($\widehat{=} 10.1 \pm 0.5$ kJ/mol) which was interpreted as a potential energy barrier on the deactivation route towards a CI with the ground state. Simulations of the kinetics by master equation modeling supported the interpretation and showed that vibrational relaxation controls the electronic deactivation of nucleobases. It competes with the excited-state decay and influences how strongly barriers and shallow PEHS affect excited-state lifetimes. The deactivation presumably takes place along the C^2-puckering coordinate on the $\pi\pi^*$ L_a excited-state PEHS. With this procedure, we could identify experimentally and for the first time the energy barrier encountered during electronic deactivation of 7H-Ade.

So far it is unclear which of the present $\pi\pi^*$ excited states is the emitting state in 7H-Ade since both were predicted to have PEHS minima. Since the transition dipole moments of $\pi\pi^*$ L_a and L_b are perpendicular to each other, a fluorescence anisotropy study would help to distinguish between them.

8.1.3 Guanine

For the guanine mononucleotide dGMP, three literature-consistent excited-state lifetimes of $\tau_1 = 0.20 \pm 0.02$ ps, $\tau_2 = 0.83 \pm 0.03$ ps and $\tau_3 = 2.4 \pm 0.1$ ps were determined from TEAS. The time scales were assigned to FC relaxation and to internal conversion. A slight lifetime increase was observed for measurements at $T = 278$ K yielding an approximate activation energy of $E_{\text{A}} \approx 0.08$ eV.

The longest time constant of dGMP was assigned to the predicted internal conversion from a potential energy minimum on the $\pi\pi^*$ L_a PEHS that requires a ring puckering at the C^2 position and an out-of-plane motion of the sterically

demanding amino group. A small potential energy barrier on this deactivation route is consistent with several quantum chemical investigations. The second lifetime can be attributed either to the population of the mentioned minimum or a competing deactivation channel characterized by an out-of-plane motion of the carbonyl group.

8.2 Electronic Deactivation Dynamics of Stacked Purine Nucleobases

8.2.1 Adenine Dinucleotide

The adenine dinucleotide d(ApA) was investigated by TEAS towards the assignment of critical steps in the evolution of the electronic excited-state character from excitons to excimer-like states en route towards the electronic ground state. The deactivation dynamics were characterized with a total of four decay time constants which were assigned to stepwise excimer formation in agreement with previous results of the workgroup.

The two sub-picosecond decay components were independent of temperature and deuteration. These were assigned to relaxation within the exciton stack within $\tau_1 = 0.16 \pm 0.02$ ps and to "perturbed-monomer-like" decay within $\tau_2 = 0.48 \pm 0.05$ ps by a C^2-puckering deformation of one of the Ade units. An intermediate excimer was proposed to be formed directly by FC relaxation and to decay to a stabilized excimer within $\tau_3 \approx 6$ ps. Time constant $\tau_4 = 360 \pm 14$ ps was assigned to the subsequent internal conversion of the stabilized excimer to the ground state. The states were found to lie at similar energy levels. The two long-lived excited-state lifetime components showed a temperature-increase to $\tau_3 \approx 8$ ps and $\tau_4 = 680 \pm 25$ ps at $T = 278$ K indicating potential energy barriers on the deactivation pathway. Via Arrhenius analysis, the activation energies were determined to $E_A[\tau_3] = 0.11 \pm 0.04$ eV and $E_A[\tau_4] = 0.25 \pm 0.06$ eV. The former was assigned to lie in-between the two excimer structures and the latter to hinder the electronic decay of the stabilized excimer. A pronounced kinetic isotope effect was observed for the lifetime of the stabilized excimer which increased to $\tau_4 \approx 900$ ps in D_2O. As discussed, this indicates the involvement of the fully deuterated amino group in the deactivation mechanism for which a ring puckering accompanied by an out-of-plane motion of the amino group on one of the Ade units may be responsible, but an excited-state proton transfer between both amino groups is also thinkable.

With this extensive experimental study, we contribute to identifying the potential energy barriers impeding excimer formation and decay in the dinucleotide d(ApA) and the corresponding molecular deactivation mechanisms.

8.2.2 Adenine Tri- and Tetranucleotide

Measurements of the Ade di-, tri- and tetranucleotide yielded similar excited-state lifetimes for all three samples indicating a common deactivation mechanism consistent with the above-described stepwise excimer formation.

Two sub-picosecond components, $\tau_1 \approx 0.15$ ps and $\tau_2 \approx 0.45$ ps, were again assigned to relaxation within the exciton stack and to "perturbed-monomer-like" deactivation. Components $\tau_3 \approx 6$ ps and $\tau_4 \approx 360$ ps were associated with formation of a stabilized excimer from an intermediate state. Decreasing the temperature to $T = 278$ K, the fourth component was increased to $\tau_4 \approx 480$ ps for the trimer and the tetramer, revealing a lower necessary thermal activation energy for the deactivation of dA_3 and dA_4 in comparison with d(ApA). From the blue-shift of the static fluorescence spectra of the oligonucleotides compared to the dinucleotide, the excimer structure was assumed to be less stabilized. The results suggest that the increased stacking interaction in these systems destabilizes excimer formation and thus lowers the potential energy barrier for electronic deactivation.

8.2.3 Guanine Dinucleotide

Three-exponential decay dynamics were obtained for the electronic deactivation of the guanine dinucleotide d(GpG) and showcase complex deactivation processes. To the best of our knowledge, this work represent the first time-resolved study of this particular DNA building block. Excited-state lifetimes of $\tau_1 = 0.2 \pm 0.1$ ps, $\tau_2 = 1.7 \pm 0.2$ ps, and $\tau_3 = 18 \pm 4$ ps demonstrate a nearly 10-fold increase compared to the guanine monomer.

The results hint at formation of an excimer between the guanine moieties in the dinucleotide after absorption of UV light. The lifetimes were assigned to FC relaxation, sterically hindered monomer-like deactivation, and excimer relaxation, respectively. The excimer is thought to be comparatively high in energy but to have a low potential energy barrier for deactivation, especially in contrast to the one found for d(ApA). Temperature-dependent time-resolved measurements of d(GpG) could provide a barrier height for direct comparison.

8.3 Concluding Remarks

The present results demonstrate that it is neither possible to predict electronic deactivation dynamics from molecular structures by mere chemical intuition nor to extrapolate from measurements of related structures. It is the delicate interplay of excited states, potential energy barriers and the shape of CIs, influenced by steric

and electronic restraints and the multifold effects of substituents and environment that determines which relaxation pathways are accessed and which CIs play the big roles in electronic deactivation processes.

In order to fully understand the experimentally observed molecular excited-state dynamics, specific decay models need to be constructed and applied to the measured time profiles. Especially in the analysis by the singular value decomposition (SVD) method, a more sophisticated model function would allow to draw species-associated spectra. The model needs to allow for wavelength-dependent time constants and has to incorporate the complex kinetics of the excited state as well as the ground state. To this end, the nuclear dynamics simulation method MCTDH is able to predict transient spectra on the basis of a PEHS and decay model and could also give the necessary decay functions. The SVD results could be additionally enhanced by simultaneous–global modeling of SVD time traces from the different measurements.

To some extent, short decay components were difficult to assign when their transient electronic absorption spectra overlapped with those of other processes. The signal of hot ground-state absorption is found at probe wavelengths $\lambda_{\text{probe}} < 330$ nm where also excited-state absorption occurs. These signals could be better distinguished by extending the probe spectrum further below $\lambda_{\text{probe}} = 310$ nm. To this end, a broadband UV-probe experiment was devised in cooperation with Entwicklungsbüro Stresing, Berlin. Pumping a CaF_2 crystal with the third harmonic of the laser fundamental yields a broad UV spectrum between 220 nm $\leq \lambda \leq$ 320 nm and was proved feasible in our lab.[1]

A sensitive time-resolved broadband fluorescence experiment with a high temporal resolution would give complementary results for the decay dynamics of the bright states. A band-shift of the fluorescence spectrum within $\Delta t = 1$ ps is expected for adenine nucleotide samples and could help to characterize the monomer-like decay. In the past, the necessary setup proved to be very difficult to realize.

8.4 Ongoing Studies

In time-resolved spectroscopy, low-amplitude nanosecond components are often observed as an offset in the measured time profiles.[2–4] These are usually not interpreted since they have contributions $< 5\,\%$ and cannot be quantified satisfactorily with a delay stage covering $\Delta t = 1 - 2$ ns. To investigate these decay components, time-correlated single photon counting (TCSPC) can be used. A combined transient electronic absorption and TCSPC study is currently conducted by M. M. Bohnsack and concerns stacked dimers of Ade that are connected by a simple alkyl chain.[5] It

is known that the linker length influences the conformation and thus the quality of the stack.[6] It will be seen how these parameters influence the particular deactivation dynamics and what role the so far overlooked decay components play.

In general, studies on electronic dynamics of DNA building blocks show that neither a long-lived excited state is always harmful nor that a quickly reached ground state is always safe when it comes to UV-induced photolesions. The shape of the CI is decisive in this context because here the wavepacket can either be funneled back to the original ground state or relax towards product configurations. Internal conversion to the ground state generates highly vibrationally excited and distorted ground-state molecules and, thus, barriers on the ground-state PEHS can be overcome more easily. Hot ground state molecules are prone to reactions, e. g. ring opening reactions.[7] It would be instructive to study the fate of the wavepacket when it has just reached the the ground state. A UV-pump–IR-probe transient vibrational absorption spectroscopy (TVAS) experiment was constructed in our lab by X. Ma, K. Röttger and H. Böhnke. It can monitor the molecular structure in the excited state and in the ground state and may thus help to discover the molecular deformations leading the wavepacket through CIs and facilitating the subsequent relaxation.

TVAS will also be helpful to study environmental effects such as vibrational cooling with the solvent. This work showed peculiar temperature effects for the vibrational cooling of nucleobases which also seemed to depend on the size of nucleotide. Both observations could not yet be fully explained.

The unsubstituted purine molecule was recently under investigation by TVAS.[8] In aqueous solution, a tautomeric mixture is present and 7H- and 9H-purine yielded mutual lifetimes. An IR spectroscopic method is extremely advantageous here because the species can be distinguished by their specific absorption bands which could also be helpful for further studies of 9H- and 7H-adenine.

References

[1] C. Schröder, 'Erzeugung spektral breitbandiger UV-Laserpulse in Calciumfluorid', F3-Praktikumsprotokoll, Christian-Albrechts-Universität zu Kiel, **2016**.

[2] M. C. Stuhldreier, 'Electronic Deactivation Dynamics of DNA Model Systems and Solvation Dynamics of a Natural Antioxidant by Femtosecond Fluorescence and Absorption Spectroscopy', Dissertation, Christian-Albrechts-Universität zu Kiel, **2013**.

[3] C. E. Crespo-Hernández, B. Kohler, 'Influence of secondary structure on electronic energy relaxation in adenine homopolymers', *J. Phys. Chem. B* **2004**, *108*, 11182–11188.

[4] C. Su, C. T. Middleton, B. Kohler, 'Base-Stacking Disorder and Excited-State Dynamics in Single-Stranded Adenine Homo-Oligonucleotides', *J. Phys. Chem. B* **2012**, *116*, 10266–10274.

[5] M. M. Bohnsack, 'Dissertation Studies', Unpublished results.

[6] J. Chen, B. Kohler, 'Base Stacking in Adenosine Dimers Revealed by Femtosecond Transient Absorption Spectroscopy', *J. Am. Chem. Soc.* **2014**, *136*, 6362–6372.

[7] M. Barbatti, B. Sellner, A. Aquino, H. Lischka, 'Nonadiabatic Excited-State Dynamics of Aromatic Heterocycles: Toward the Time-Resolved Simulation of Nucleobases' in *Radiation Induced Molecular Phenomena in Nucleic Acids*, (Eds.: M. Shukla, J. Leszczynski), Springer Science+Business Media B.V., **2008**, 209–235.

[8] A. Nimmrich, 'Time-resolved vibrational spectroscopy of the nucleic acid chromophore purine in excited singlet and triplet states', MA thesis, Christian-Albrechts-Universität zu Kiel, **2018**.

List of Figures

1.1 Molecular Structure of DNA 4
1.2 Conical Intersection 7
1.3 Molecular Structure of 9H-Ade 9
1.4 Molecular Structure of 9H-Ade at Relevant CIs 10
1.5 Molecular Structure of 7H-Ade 12
1.6 Molecular Structure of Gua 12
1.7 Molecular Structure of Gua at Relevant CIs 14
1.8 Energy Scheme of Excitons in a Dimer 17
1.9 Exciton Splitting of H and J Aggregates 18
1.10 Exciton Energy Twist Angle Dependence in H Aggregates 19
1.11 Energy Scheme of Excitons in Polymers 20
1.12 Energy Scheme of Excimers 22
1.13 Natural Transition Orbitals and Difference Dipole Moments for Excimers in Ade Stacks 24

2.1 Setup of the Transient Electronic Absorption Spectrometer 47
2.2 Pump and Probe Beam Positions at the Sample 48
2.3 Wire-Guided Liquid Sample Film Device 51
2.4 Sample Film Thickness 52
2.5 Wire-Guided Liquid Sample Film Device for Measurements at Lowered Temperature 53

3.1 Molecular Structures of the Ade Monomers 63
3.2 Static Absorption Spectra of the Ade Monomers 64
3.3 Transient Electronic Absorption Maps of the Ade Monomers 67
3.4 Transient Electronic Absorption Spectra of the Ade Monomers 68
3.5 Transient Absorption-Time Profiles at $\lambda_{\mathrm{probe}} = 380$ nm for the Ade Monomers 70
3.6 Time Traces and DADS from the SVD Analysis of the Ade Monomers 71
3.7 Transient Absorption-Time Profiles at $\lambda_{\mathrm{probe}} = 255$ nm for the Ade Monomers 73
3.8 Direct Comparison of Time Profiles and DADS for the Ade Monomers 74
3.9 Exponential Model of the Second DAS for the Ade Monomers 78

4.1 Molecular Structures of 9H- and 7H-Ade 91
4.2 Analysis of the Fluorescence Data of Ade 93
4.3 Arrhenius Plot for the Fluorescence Data of 7H-Ade 94
4.4 PEHS Scheme for Ade 95
4.5 MultiWell Model and Start Energy Distributions at Five Temperatures 97

4.6 Simulated Reactant Population of 7H-Ade at Five Temperatures . . . 100
4.7 Arrhenius Plot for Simulated Time Constants of 7H-Ade 101
4.B1 Fluorescence Data of Ade at $\lambda_{probe} = 430$ nm 107
4.B2 Arrhenius Plot for 7H-Ade at $\lambda_{probe} = 430$ nm 108
4.C1 Arrhenius Plot for Simulated Time Constants of 7H-Ade 110
4.C2 Simulated Reactant Population of 7H-Ade at Five Temperatures in Comparison to Experimental Data 110
4.C3 Example Input File for MultiWell 111

5.1 Molecular Structure of d(ApA) in B-DNA Conformation 114
5.2 Static Absorption and Static Fluorescence of d(ApA) and dAMP in H_2O at Room Temperature 115
5.3 Transient Absorption Maps of d(ApA) and dAMP at $T = 295$ K in H_2O 119
5.4 Transient Absorption Spectra of d(ApA) and dAMP at $T = 295$ K in H_2O 120
5.5 Expanded Views of the Transient Absorption Spectra of d(ApA) at $T = 295$ K in H_2O 121
5.6 Transient Absorption-Time Profiles of d(ApA) and dAMP at $T =$ 295 K in H_2O 122
5.7 Time Traces from the SVD Analysis of the Transient Absorption of d(ApA) and dAMP at $T = 295$ K in H_2O 124
5.8 DADS from the SVD Analysis of the Transient Absorption of d(ApA) and dAMP at $T = 295$ K in H_2O 125
5.9 Static Absorption and Static Fluorescence of d(ApA) at Lowered Temperature in H_2O 126
5.10 Transient Absorption Maps of d(ApA) at Lowered Temperature in H_2O 127
5.11 Transient Absorption-Time Profiles of d(ApA) at Lowered Temperature in H_2O 128
5.12 Time Traces from the SVD Analysis of the Transient Absorption of d(ApA) at Lowered Temperature in H_2O 129
5.13 DADS from the SVD Analysis of the Transient Absorption of d(ApA) at Lowered Temperature in H_2O 130
5.14 Transient Absorption Map of d(ApA) at $T = 295$ K in D_2O 131
5.15 Transient Absorption-Time Profiles of d(ApA) at $T = 295$ K in H_2O and D_2O 132
5.16 Time Traces from the SVD Analysis of the Transient Absorption of d(ApA) at $T = 295$ K in D_2O 133
5.17 DADS from the SVD Analysis of the Transient Absorption of d(ApA) at $T = 295$ K in D_2O 133
5.18 Peak Wavenumber-Time Profiles of d(ApA)and dAMP at $T = 295$ K in H_2O 135
5.19 Direct Comparison of the Decay-Associated Difference Spectra for d(ApA) and dAMP 136

5.20 Arrhenius Plot for the Lifetimes of d(ApA) . . . 139
5.21 Potential Energy Model Curve for the Electronic Deactivation of d(ApA) . . . 142
5.B1 Time Traces from the SVD Analysis of the Transient Absorption of d(ApA) at $T = 295$ K in H_2O . . . 153
5.B2 DADS from the SVD Analysis of the Transient Absorption of d(ApA) at $T = 295$ K in H_2O . . . 154
5.B3 Direct Comparison of the Decay-Associated Difference Spectra for the Present and Previous Measurements of d(ApA) . . . 156
5.C1 Expanded Views of the Transient Absorption Spectra of dAMP at $T = 295$ K in H_2O . . . 157
5.C2 Static Absorption and Static Fluorescence of dAMP in H_2O at Lowered Temperature . . . 158
5.C3 Transient Absorption Maps of dAMP at Lowered Temperature in H_2O 159
5.C4 Transient Absorption-Time Profiles of dAMP at Lowered Temperature in H_2O . . . 160
5.C5 Time Traces from the SVD Analysis of the Transient Absorption of dAMP at Lowered Temperature in H_2O . . . 161
5.C6 DADS from the SVD Analysis of the Transient Absorption of dAMP at Lowered Temperature in H_2O . . . 162
5.D1 Transient Absorption Map of dAMP at $T = 295$ K in D_2O . . . 164
5.D2 Transient Absorption-Time Profiles of dAMP at $T = 295$ K in H_2O and D_2O . . . 165
5.D3 Time Traces from the SVD Analysis of the Transient Absorption of dAMP at $T = 295$ K in D_2O . . . 166
5.D4 DADS from the SVD Analysis of the Transient Absorption of dAMP at $T = 295$ K in D_2O . . . 166

6.1 Molecular Structure of the Ade Tetranucleotide . . . 174
6.2 Static Absorption and Fluorescence Spectra of dA_2, dA_3 and dA_4 . . 177
6.3 Transient Absorption Maps of dA_2, dA_3 and dA_4 . . . 178
6.4 Transient Absorption-Time Profiles of dA_2, dA_3 and dA_4 . . . 180
6.5 Time Traces from the SVD Analysis of the Transient Absorption of dA_2, dA_3 and dA_4 . . . 182
6.6 DADS from the SVD Analysis of the Transient Absorption of dA_2, dA_3 and dA_4 . . . 184
6.7 Potential Energy Model Curve for Excimer Deactivation in Ade Oligonucleotides . . . 186

7.1 Static Absorption and Fluorescence Spectra of d(GpG) and dGMP . 194
7.2 Static Fluorescence Spectra of dGMP at $T = 295$ K and $T = 278$ K . 195
7.3 Transient Absorption Maps and Transient Spectra of d(GpG) and dGMP . . . 196
7.4 Transient Absorption-Time Profiles of d(GpG) and dGMP . . . 198
7.5 Results of the SVD Analysis of d(GpG) and dGMP . . . 199

7.6 Electronic Dynamics of dGMP at $T = 278$ K 201
7.7 Results of the SVD Analysis of dGMP at $T = 278$ K 201

List of Tables

3.1 Experimental Results for the Electronic Dynamics of the Ade Monomers 72

4.1 Experimental Results for the Electronic Dynamics of Ade 93
4.2 Input Parameters used for Master Equation Modeling 99
4.3 Exemplary MultiWell Simulation Results for 7H-Ade 100
4.B1 Additional Experimental Results for the Electronic Dynamics of Ade 108
4.C1 Overview of MultiWell Simulation Results for 7H-Ade 109

5.1 Experimental Results for the Electronic Dynamics of d(ApA) 134
5.B1 Comparison of the Present and Previous Experimental Results for d(ApA) 155
5.E1 Experimental Results for the Electronic Dynamics of dAMP 167

6.1 Experimental Results for the Electronic Dynamics of Ade Dimer, Trimer and Tetramer 181
6.2 Experimental Results for the Electronic Dynamics of Ade Dimer, Trimer and Tetramer 183
6.3 Averaged Experimental Results for the Electronic Dynamics of Ade Dimer, Trimer and Tetramer 185

Danksagung

Mein größter Dank gilt meinem Doktorvater Prof. Dr. Friedrich Temps. Ihre tiefe und ehrliche Begeisterung für die Femtochemie hat sich schnell auf mich übertragen und ich bin stolz, an diesem anspruchsvollen und spannenden Forschungsgebiet mitwirken zu dürfen. Sie hatten mich bereits durch das gesamte Chemiestudium begleitet und haben mich in den letzten Jahren über verschiedene lebensverändernde Ereignisse hinweg betreut. Danke für Ihre langjährige Unterstützung!

Herrn Prof. Dr. Gernot Friedrichs danke ich aufrichtig für die ausführlichen Telefonate und die Hilfe und die Mitarbeit bei der Interpretation der Ergebnisse von Kapitel 4.

Ich danke allen aktuellen und ehemaligen Mitgliedern der Arbeitsgruppe Temps für ihre andauernde intensive und hochwertige Arbeit, für die Entwicklung von experimentellen Techniken und der Auswertesoftware, für die kollegiale Zusammenarbeit, für die Offenheit und Hilfsbereitschaft und für den Spaß bei der Arbeit.

Julia Frej, geb. Bahrenburg, und Katharina Röttger danke ich für die kompetente Einarbeitung und die engagierte Betreuung und dafür, dass sie so ein gutes Vorbild waren. Mayra Stuhldreier danke ich für ihre ausführliche Arbeit am d(ApA).

Ole Hüter danke ich vielmals für die vielen Abbildungen und Rechnungen, alle fachlichen und moralischen Hilfen, für seinen kritischen Blick und für die Freundschaft. Mats Bohnsack danke ich für seine äußerst kritischen Hinweise und für das gegenseitige Interesse an der Forschungsarbeit. Meinem Büro 305 danke ich für den Zusammenhalt und die lustige Zeit.

Tanja Stojšić danke ich herzlich für die freundschaftliche Begegnung, für die mitfühlenden Worte und für die organisatorischen Dinge.

Den aktuellen und ehemaligen Mitarbeitern der Feinmechanik- und der Elektronikwerkstatt danke ich für die vielen funktionierenden Prototypen und die fachmännische Unterstützung bei deren Optimierung.

Ich danke Michael Pospiech für die LaTeXVorlage.

Vielen lieben Dank an Katharina Holz für die Arschtritte und die Eröffnung anderer Blickwinkel, für das Umschiffen brenzlicher Themen und für die gegenseitige Toleranz.

Herzlichen Dank an alle Freunde, die mich außerdem begleitet, gefordert und mir gut zugeredet haben: Svenja Fischmann, Boris Pinchuk, Benjamin Lachmann, Gunda Brandenburg.

Meiner Ursprungsfamilie danke ich von Herzen für die immerwährende, bedingungslose Unterstützung, unser gegenseitiges Interesse, unsere gemeinsamen lebensverändernden Erlebnisse und für das Zuhause. Meiner Schwiegerfamilie danke ich ebenfalls für euer Interesse und eure guten Gedanken.

Meinem besten Freund, meinem Partner und dem Vater meiner Kinder, Birk Stange, geb. Thiedemann, bin ich unendlich dankbar – dafür, dass du mich aus dem Haus holst, dass du uns alles zutraust, dass wir gemeinsame Träume haben und dass wir sie tatsächlich verfolgen. Das Beste ist noch nicht vorbei!

Liebe Runa, danke, dass du das ganze Adrenalin so gut vertragen hast, dass du aufgeschlossen und aktiv bist und dass wir uns so gut verstehen.